Title
Geometrical Frameworks for Wireless Access in Large Scale Multi-Antenna Networks

Author
Feres, Carlos José

Publication Date
2021

Peer reviewed|Thesis/dissertation

Geometrical Frameworks for Wireless Access in Large Scale Multi-Antenna Networks

By

CARLOS FERES

DISSERTATION

Submitted in partial satisfaction of the requirements for the degree of

DOCTOR OF PHILOSOPHY

in

Electrical and Computer Engineering

in the

OFFICE OF GRADUATE STUDIES

of the

UNIVERSITY OF CALIFORNIA

DAVIS

Approved:

_____

Zhi Ding, Chair

_____

Bernard C. Levy

_____

Khaled Abdel-Ghaffar

Committee in Charge

2021

Abstract

Geometrical Frameworks for Wireless Access in Large Scale Multi-Antenna Networks

Explosive growth of mobile networking and IoT demands efficient and reliable service for massive wireless systems. With limited radio resources, multi-input-multi-output (MIMO) technologies are successfully utilizing spatial diversity to substantially improve spectral efficiency. When considering large scale deployments, managing radio resource is more important than ever to service all these devices with appropriate quality of service. Moreover, in the context of performance-constrained, low-complexity devices, there is a clear need for new approaches that yield good performance with appropriate computational complexity. In this dissertation, we study such large scale networks from a geometric perspective, in order to better manage the networks' limited resources and mitigate co-channel interference in two key scenarios: when the multi-antenna servicing node is unaware of which devices are active (uplink access control); and when it does know all active devices (user scheduling).

In the first part of this dissertation, we tackle the problem of uplink grant-based access via blind signal recovery. Different from traditional grant-free access mechanisms that use pilot signals for signal separation, we propose two blind approaches based on the Constant Modulus Algorithm (CMA) for simultaneous multiple signal recovery: a regularized CMA cost function, and a Riemannian manifold optimization framework. By characterizing the underlying geometry of these formulations, we provide theoretical convergence guarantees for CMA-based signal recovery with limited data samples. The resulting algorithms provide successful signal recovery with high probability and reasonable computational load.

On the other hand, user scheduling is a combinatorial, NP-hard problem that has been long eluded optimal solutions. In MIMO networks, users groups with low co-channel interference correspond to groups that show high spatial channel diversity. In the second part of this dissertation, we propose a new two-step paradigm for MIMO user scheduling. First,

unsupervised learning identifies which devices experience similar channel conditions (i.e., low spatial diversity) and would incur high co-channel interference if they were to share resources. By clustering in the Grassmannian manifold, spatial similarity is inherent to the geometry and is easily computed in a global sense. We then leverage these learned features to assign users into low CCI groups that avoid pairings of users from the same cluster. The resulting similarity-assisted scheduling yields increased spectral efficiency and better user quality of service across design parameters for large number of users, compared to a direct scheduling mechanism.

Acknowledgments

This dissertation along with the work invested into it would not have been possible without the kind support of many people.

First of all, I would like to express my most sincere gratitude to my advisor, Prof. Zhi Ding, for his continuous guidance and encouragement throughout my Ph.D. studies and research, for his patience, motivation, inspiration and endless support. I am truly thankful for all his help in selecting research topics, suggesting technical insights, proofreading manuscripts, offering teaching opportunities, providing financial support, and overall, for his immense knowledge and wisdom. From him I have not only learned an effective approach for academic research, but also how to engage with others while doing so, in an encouraging and profoundly motivating manner. He is the best mentor I could ever have in this endeavor, and I deeply appreciate all these years under his tutelage.

I am also indebted to the members of my dissertation committee, Prof. Bernard Levy and Prof. Khaled Abdel-Ghaffar, for the time they spent in evaluating my dissertation. I have taken classes with both of them, which sparked my interest and allowed me to dive deeper in my research. I am also thankful to Prof. Lifeng Lai and Prof. Xin Liu for their service on my qualifying exam.

I would also like to thank all my friends and colleagues at the Broadband Radio Access Technology Lab (BRAT-Lab), especially (in no particular order), Wenhao Wu, Chen Jiang, Kun Wang, Taha Bouchoucha, Mohammadamin Farajzadehjalali, Hesham Mostafa Elsayed Elmaghraby, Xintong Ling, Pei-Rong Li, Songyang Zhang, Qinwen Deng, Lahiru D. Chamain Hewa Gamage, Siyu Qi, Mason del Rosario, GE Yao, Zhenyu Liu, Hui-Ying Siao, Dylan Shadduck, Jonathan Tivald, Kuangang Fan, and Qing Wei, for their great support, technical advice and stimulating discussions.

I would also like to acknowledge all my friends in Davis who have supported me throughout the last five years, and made my Ph.D. experience even better.

None of my accomplishments would have been possible without the everlasting love, encouragement and support of my family. The caring and guidance of my beloved parents, Carlos and Carolina, have been the foundation of who I am today, and even after their passing they continue to be my guides. My son Carlos León has been a shining light during these years.

And above all, I would like to thank my wife Constanza for her constant love and support, and for keeping me sane over the past few years. Thank you for being my best friend. I owe you everything.

The work invested into this dissertation was supported in part by the National Science Foundation under Grants No. 1711823, No. 1824553, No. 2009001, and No. 2029027. My Ph.D. studies and research were also supported by the National Agency for Research and Development (ANID) / Scholarship Program / DOCTORADO BECAS CHILE / 2016 72170648.

Contents

List of Figures

List of Tables

Chapter 1

Introduction

Recent advances in next generation networking technologies are poised to ubiquitously connect the full spectrum of sensors, devices, and computers to facilitate future development of smart cities and smart agriculture, among other applications [1]. These exciting developments, known collectively as Internet of Things (IoT), promise significant benefits in a plethora of fields including health care, farming, environmental science, infrastructure, energy efficiency, transportation, safety and sustainability. Such applications envision the deployment of a massive number of wireless devices, with billions being connected globally [2, 3], and demand ever higher spectrum efficiency over the limited bandwidth resources.

A typical IoT application involves sporadic communications between a significant number of transceivers, triggered by external events, in order to save energy. This prompts the need for low-latency communications and the ability to support these links with performance-constrained transceivers, in particular in terms of bandwidth efficiency. Multiple-input-multiple-output (MIMO) technologies have been playing a central role in achieving high network throughput and spectrum efficiency [4] for both uplink and downlink links. In uplink multiple access channel (MAC), classical multi-user detection (MUD) receivers such as the maximum-likelihood, decorrelator, MMSE receivers and variants support simultaneous recovery of multiple signals sharing the same physical resource [5–13]. Similarly, broadcast

(BC) enables shared spectrum and high efficiency in downlink [14].

The rapid growth of data applications worldwide continues to fuel the tremendous growth rate of wireless communication networks in areas such as transportation, environmental monitoring, robotics, and smart cities. In the Internet-of-Things (IoT) era, tens of billion wireless communication devices will be connected around the globe [2,3]. The massive deployment of wireless devices and the accompanied data traffic eruption shall pose important technological challenges, such as ubiquitous connectivity and ultra-high spectral utilization.

In this dissertation, we focus on the problem of servicing devices efficiently in such large scale networks, tackling their inherent challenges. We consider centralized networks where one base station (BS) with multiple antennas provides services to a large number of single-antenna devices. Here, we recognize two scenarios depending on the activity level of the devices.

In the case of low-activity devices, they attempt to communicate with the BS sporadically, without a set timing, and thus the BS does not know which devices are active at any given time. In this scenario, the BS attempts *access control* to detect and recover the unknown transmitted signals. Conversely, when we consider very active devices, network coordination is a must, and the BS is aware of all the active devices with grant-based access. Here, the BS performs *user scheduling* to service the active devices with its limited resources.

1.1 Access Control

First and foremost, in order to transmit information to users (downlink), the BS would "ping" the users to know which users are able to receive a message. Hence, in this operation mode the BS is always aware of the active users, and there is no need for access control. In other words, the problem of access control is only relevant in uplink operation, i.e., an unknown number of users transmitting signals simultaneously to the BS.

Generally, access control in wireless networks is based on either random access (e.g.,

WiFi) or centralized access (e.g., cellular). Contention based random access schemes, such as the CSMA-CA protocol adopted in IEEE 802.11a/g/n/ac, possess the advantage of simplicity but suffer from lower spectrum efficiency due to access collision when the number of active devices is large. Centralized access can achieve high spectrum efficiency but requires elaborate network-user interaction and higher energy consumption. As a typical IoT application involves sporadic communications of small amounts of data between a significant number of transceivers, triggered by external events, such systems are better served by low-latency and grant-free communications.

In grant-free access, multiple unscheduled signal transmissions could collide at receivers [15]. Traditional solutions use training or pilot sequences that allow the recovery of multiple signals at the BS with minimal interference, by either exploiting spread-spectrum or joint multi-user detection [16,17]. However, these approaches require accurate CSI to mitigate co-channel interference, and thereby require significant pilot overhead for synchronization and channel estimation. Such extra overhead can be significantly expensive in terms of energy consumption and bandwidth resources when data packets are short, as in IoT applications. Furthermore, as the number of devices increases, so does the pilot sequence length, exacerbating the pilot overhead problem. Clearly, for IoT applications involving large number of devices in grant-free applications, the burden on both spectrum and power [18] strongly motivates the investigation and deployment of blind signal receivers, which do not require known pilot or pilots for channel probing and rather exploit high-order statistics and known characteristics of source signals.

In the first part of this dissertation, we focus on the technical challenge of enabling grant-free access in massive wireless networks via blind signal recovery. Usually posed as (non-convex) optimization problems, we leverage recent advances in non-convex optimization from a geometrical perspective and provide convergence guarantees for blind source recovery in a finite-sample regime. Furthermore, we extend this approach to guarantee multiple signal recovery without regularization by means of redefining the search space as a Riemannian

manifold. Our findings show that these problems enjoy a benign geometry and are mathematically well-conditioned, and as such are an attractive option to enable grant-free access in large-scale deployments.

1.2 User Scheduling

In a different scenario, now the BS is aware of the active users and knows their channel state information (CSI). Hence, the BS will exploit CSI with MIMO techniques to improve spectrum efficiency. However, their performance depend critically on which users are allocated into resource-sharing user groups (RSGs). The ultimate goal of *user scheduling* is to assign users into RSGs such that more users can share resources with little mutual interference [19] without sacrificing performance in terms of e.g., sum-rate, capacity, outage probability, among others. In other words, user scheduling aims to identify co-channel users with minimal or controlled co-channel interference (CCI).

In MIMO systems, CCI depends directly on spatial channel diversity among users [20, 21], i.e., on CSI similarities. In other words, the co-channel user CSI vectors must exhibit sufficient linear independence [22,23]. To effectively mitigate CCI within MIMO user groups, one needs to assess for each possible co-channel MIMO user group their spatial diversity based on updated user CSIs. Given a large number of serviced devices N and increasingly large number of base-station antennas M, the number of user scheduling options is of combinatorial order and grows exponentially. Thus, to optimally schedule users in resource-sharing groups, one needs to examine the CSIs of each possible user grouping among potentially very large number of users in e.g., the thousands.

To this end, we develop a new dual-step approach based on unsupervised learning for user scheduling. We *first* leverage unsupervised learning to identify users with highly *similar* CSIs. To properly identify spatial CSIs that lead to large co-channel interference (CCI), we map user CSIs to a complex Grassmannian manifold during learning. On this manifold,

distances between CSIs relate directly to their spatial correlation, i.e. spatial diversity. We can apply *any solid* clustering algorithm over this geometry to cluster users that can generate high mutual interference. Our *second step* schedule co-channel diversity users in MAC or BC systems by barring user groups with highly similar CSIs from Grassmannian manifold clustering. Applicable to any well established performance metrics such as maximum sum-rate or maximum signal-to-interference-and-noise ratio (SINR), our proposed MIMO user scheduling can improve spatial diversity and effectively mitigate co-channel interference.

1.3 Notations

In the following, vectors and matrices will be denoted with small and capital boldface letters, such as $\boldsymbol{z}$ and $\boldsymbol{Z}$ respectively. Sets are denoted with calligraphic capital letters. For a complex scalar a, we use $\mathrm{Re}(a)$, $\mathrm{Im}(a)$, $\overline{a}$, $|a|$ and $\angle(a)$ to denote its real part, imaginary part, complex conjugate, magnitude and angle, respectively. The transpose, element-wise complex conjugation and conjugate transpose are denoted by $(\cdot)^{\mathsf{T}}$, $\overline{(\cdot)}$ and $(\cdot)^{\mathsf{H}}$, respectively. The Hermitian and skew-Hermitian parts of a matrix $\boldsymbol{Z}$ are denoted as $\mathrm{herm}(\boldsymbol{Z}) = 0.5(\boldsymbol{Z} + \boldsymbol{Z}^{\mathsf{H}})$ and $\mathrm{skew}(\boldsymbol{Z}) = 0.5(\boldsymbol{Z} - \boldsymbol{Z}^{\mathsf{H}})$. The Euclidean norm of vectors and spectral norm of matrices is denoted by $\|\cdot\|$, and the Frobenius norm of matrices is denoted by $\|\cdot\|_F$. $\mathrm{diag}(\boldsymbol{z})$ represents a diagonal matrix that uses elements of vector $\boldsymbol{z}$ on its diagonal.The Kronecker product and the Hadamard (element-wise) product are denoted as $\otimes$ and $\circ$, respectively. $\mathbf{0}_k$ and $\boldsymbol{I}_k$ represent the zero vector and the identity matrix of size k, respectively. We use $\boldsymbol{A} \preceq \boldsymbol{B}$ and $\boldsymbol{C} \succeq \boldsymbol{D}$ to denote that $\boldsymbol{B} - \boldsymbol{A}$ and $\boldsymbol{C} - \boldsymbol{D}$ are positive semidefinite matrices, respectively. $|\mathcal{S}|$ denotes the size or cardinality of a set $\mathcal{S}$. $\mathcal{O}(\cdot)$ denotes the order of complexity of an algorithm or problem. The abbreviation "i.i.d." stands for independent and identical distributed random variables, and $\mathbb{E}\{\cdot\}$ denotes expectation. Finally, $\mathbf{1}[expr]$ is the indicator function, that is equal to 1 if *expr* is true, and 0 otherwise.

Chapter 2

A General Model for Large-Scale Networks

In this chapter, we develop the system model that will be used for the rest of this dissertation. We first present a general framework describing large-scale networks in the context of our investigation, and then address particular details and the state of the art for both access control and user scheduling.

2.1 System Model

Figure 2.1 depicts a wireless system with a single BS with M receiver antennas and N single-antenna users, that could be operating in either uplink (MAC) or downlink (BC). In the context of large-scale MIMO networks, we assume $N \gg M$. We further assume a single-carrier system throughout this dissertation, although the extension to multi-carrier systems is well-known and fairly straightforward.

Part of this chapter is reprinted, with permission, from [C. Feres and Z. Ding, "Wirtinger Flow Meets Constant Modulus Algorithm: Revisiting Signal Recovery for Grant-Free Access" in *IEEE Transactions on Signal Processing (Early Access)*, Aug. 2021] and followup modifications for final publication. Notations may have changed for consistency throughout this dissertation. Other parts have been previously submitted in different works to *IEEE Transactions on Signal Processing* and *IEEE Transactions on Wireless Communications*.

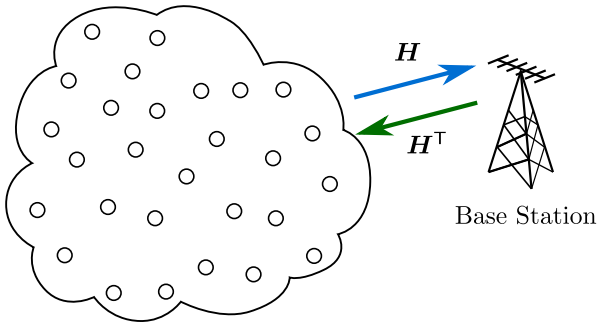

Figure 2.1: Illustration of a large-scale network. Devices deliver (MAC, blue) or receive (BC, green) independent signals simultaneously on the same time-frequency resource.

Note that due to the very nature of spatial diversity, up to M users using the same resource can be independently served in downlink or uplink. Although methods such as successive interference cancellation (SIC) could help in servicing more users at a time, they are constrained by operation conditions (such as a significant power gap between signals), back-and-forth coordination and overhead (such as power control) and transceiver complexity (which is limited in IoT devices), and hence will not be considered in this dissertation.

In the following, we shall denote the uplink wireless MIMO channel as a complex matrix $\boldsymbol{H}$ of appropriate size, whose elements correspond to the transmitter-receiver antenna pairs formed by active devices and the BS. We assume a flat-fading channel that has no inter-symbol interference (ISI) during the link. As a single-carrier system, channel reciprocity ensures that the corresponding downlink MIMO channel matrix is $\boldsymbol{H}^{\mathsf{T}}$. The transmitted signal corresponding to user u will be denoted by $s_u[k]$, where k indicates the k-th symbol. $x_m[k]$ denotes the k-th symbol of the received signal (at the m-th BS antenna in the case of uplink), corresponding to the mixture of all transmitted signals through the MIMO channel. Finally, we use y for the processed received signal, whose subindex will denote either the user (in downlink) or the recovered signal stream (in uplink).

2.2 Blind Grant-Free Access

In uplink grant-free access, multiple signals could collide at the BS. In IoT applications, the energy and bandwidth consumption due to significant pilot overhead is undesirable, and we opt instead for blind signal recovery techniques.

Blind equalization has been a staple idea in terms of achieving this goal by diminishing the impact of pilots or preambles, aiming to reduce their impact in the overall bandwidth efficiency. Among blind equalization algorithms, the Constant Modulus Algorithm (CMA) presented by Godard [24] in the 1980s is often considered the most widespread technique due to its computational simplicity and practical effectiveness [25, 26]. We shall introduce the signal model for CMA-based signal recovery, and the current state of the art in solving the CMA formulation.

2.2.1 CMA-based Blind Signal Recovery

We consider the signal recovery of multiple users in one access group in a grant-free access system, as depicted in Figure 2.2. In particular, all potential uplink users in each access group have acquired network timing such that their uplink transmission bursts would span one given set of receiver time slots. Users in each designated access group may randomly transmit within their shared channel in terms of allocated resources. Appropriate coding and rate-matching is utilized by all source nodes to have equal number of data symbols K within each access group and burst. Furthermore, we design systems such that with very high probability or certainty the number of single-antenna active nodes L shall fall below the number of diversity antennas M at the receiver node. In particular, the receiver node does not necessarily know L. Since the BS recovers multiple user signals during blind demixing without prior knowledge of their identities, the receiver can utilize user-ID scrambled CRC to check which recovered user signal belongs to which user, similar to the blind detection of PDCCH by users using RNTI-scrambled CRC in LTE or 5G [27, 28].

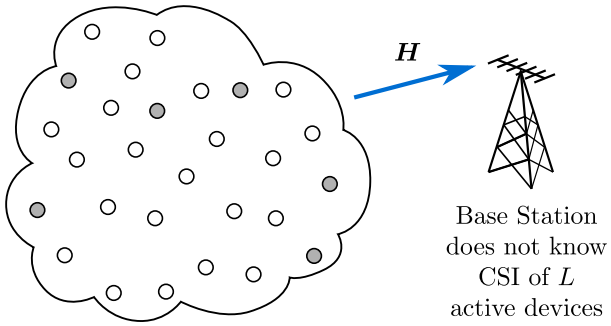

Figure 2.2: L active sources (shaded gray) share a common resource block and transmit independent signals to the base station with M antennas through an *unknown* physical channel.

To summarize, we define the received signal vector $\boldsymbol{x}_k$, the transmitted signal vector $\boldsymbol{s_k}$, and the flat fading channel $\boldsymbol{H}$, respectively, as

$$\boldsymbol{x}_k = \begin{bmatrix} x_1[k] \\ \vdots \\ x_M[k] \end{bmatrix}, \; \boldsymbol{s}_k = \begin{bmatrix} s_1[k] \\ \vdots \\ s_L[k] \end{bmatrix}, \; \boldsymbol{H} = \begin{bmatrix} h_{11} & \cdots & h_{1L} \\ \vdots & \ddots & \vdots \\ h_{M1} & \cdots & h_{ML} \end{bmatrix}. \tag{2.1}$$

Then the received signal vector at the BS can be written as

$$\boldsymbol{x}_k = \boldsymbol{H}\boldsymbol{s}_k + \boldsymbol{n}_k, \tag{2.2}$$

where the (uplink) MIMO channel matrix $\boldsymbol{H} \in \mathbb{C}^{M \times L}$ is assumed to have full column rank L (with $L \leq M$) and $\boldsymbol{n}_k \in \mathbb{C}^M$ is the vector of additive white Gaussian noises (AWGN) in that resource block, of the same size as $\boldsymbol{x}_k$ in Eq.(2.1). Furthermore, and without loss of generality, we assume that all sources transmit equal average symbol energy $E_s = \mathbb{E}\{|s[k]|^2\}$. This assumption can be made as the different symbol energies of the sources $E_{s,\ell}$ can be included in the channel as $\boldsymbol{H} = \boldsymbol{H}'\boldsymbol{D}^{1/2}$, with $\boldsymbol{H}'$ modeling only the channel fading across sources and receiver, and $\boldsymbol{D} = \mathrm{diag}(E_{s,1}/E_s, \ldots, E_{s,L}/E_s)$. Furthermore, note that although this signal model considers non-fading channels, the same formulation can be used for blind equalization by redefining the signal vectors and channel matrix [26].

Note that the receiver has explicit knowledge on neither the unknown channels $\boldsymbol{H}$ nor the number of active sources L, except for the statistical properties and the constellation of each source signal.

Recovering a Single Source

When attempting to blindly recover one signal, the goal is to adaptively find a demixer such that its output corresponds to one of the transmitted signals with minimal interference, i.e.

$$y[k] = \boldsymbol{w}^{\mathsf{H}}\boldsymbol{x}_k \approx \hat{s}_\ell[k], \quad \ell \in \{1, \ldots, L\}. \tag{2.3}$$

The problem of blind signal recovery has been extensively studied before. In particular, Godard [24] proposed what was later known [25] as the constant modulus algorithm (CMA) to find an optimum $\boldsymbol{w} \in \mathbb{C}^M$ by minimizing the mean CM cost for equalization:

$$E\Big\{\big(|y_k|^2 - R_2\big)^2\Big\}, \quad R_2 = \frac{\mathbb{E}\{|s_\ell[k]|^4\}}{\mathbb{E}\{|s_\ell[k]|^2\}}, \tag{2.4}$$

where the constant R_2 is computed from the high-order statistics of the source symbols $s[k]$ to match the input-output constellation scale [24]. It is known that CMA can be applied to i.i.d. signals using QAM constellations of arbitrary size and magnitude [26]. Moreover, R_2 can be replaced by an arbitrary scalar, e.g. 1, scaling $\boldsymbol{w}$ accordingly, and CMA will still converge such that its output recovers QAM source signals, without affecting signal integrity. In batch implementation, the single-source CM cost can be rewritten as

$$f(\boldsymbol{w}) = \frac{1}{2K}\sum_{k=1}^{K}\Big(|\boldsymbol{x}_k^{\mathsf{H}}\boldsymbol{w}|^2 - R_2\Big)^2, \tag{2.5}$$

which is a smooth real-valued nonconvex function of $\boldsymbol{w}$. Note that f presents phase invariance, i.e., if $\widehat{\boldsymbol{w}}$ is a solution that minimizes $f(\widehat{\boldsymbol{w}})$, then the entire set $\mathcal{W}(\widehat{\boldsymbol{w}}) = \{\mathrm{e}^{j\theta}\widehat{\boldsymbol{w}} : \theta \in [0, 2\pi]\}$ contains equivalent solutions that achieve the same minimum $f(\widehat{\boldsymbol{w}})$.

Simultaneous Multiple Signal Recovery

In a more general setting, we are interested in deriving J simultaneous demixers $\boldsymbol{w}_\ell \in \mathbb{C}^M$, $\ell \in \{1, \ldots, J\}$ that allow the recovery of J sources with minimal interference, each tuned to a distinct signal. Without loss of generality, we consider $J \leq L$. We can also collect all demixers as columns of the receiver blind demixing matrix $\boldsymbol{W} = \big[\boldsymbol{w}_1 \; \boldsymbol{w}_2 \; \cdots \boldsymbol{w}_\ell\big]$, such that

$$\boldsymbol{y}_k = \begin{bmatrix} \boldsymbol{w}_1^{\mathsf{H}} \\ \vdots \\ \boldsymbol{w}_\ell^{\mathsf{H}} \end{bmatrix} \boldsymbol{x}_k = \boldsymbol{W}^{\mathsf{H}} \boldsymbol{x}_k = \begin{bmatrix} \hat{s}_{\nu(1)}[k] \\ \vdots \\ \hat{s}_{\nu(\ell)}[k] \end{bmatrix}, \quad \ell \in \{1, \ldots, J\}, \; \nu(\ell) \in \{1, \ldots, L\}, \tag{2.6}$$

where the permutation $\nu(\cdot)$ highlights that the BS has no prior knowledge of the identities of the transmitters.

CMA has been adapted in the past for simultaneous recovery of multiple independent source signals. In these applications, the first step is to define a cumulative demixing cost consisting of J copies of CM costs, each one using a different demixer:

$$f(\boldsymbol{W}) = \frac{1}{2K} \sum_{\ell=1}^{J} \sum_{k=1}^{K} \Big(|\boldsymbol{x}_k^{\mathsf{H}} \boldsymbol{w}_\ell|^2 - R_2 \Big)^2. \tag{2.7}$$

The joint blind demixing problem is to optimize multiple solution vectors $\widehat{\boldsymbol{W}} = \big[\widehat{\boldsymbol{w}}_1 \; \cdots \; \widehat{\boldsymbol{w}}_\ell\big]$ that jointly minimize the cumulative CM cost of (2.7). Note that this cumulative CM cost by itself cannot guarantee that the recovered signals are indeed from different sources. In fact, even if every one column vector of $\widehat{\boldsymbol{W}}$ captures the same signal source, the cumulative CM cost of (2.7) is still minimized and cannot prevent such solutions. For this reason, it is clear that the cumulative CM cost of (2.7) is non-convex and is in fact multi-modal. Therefore, when considering simultaneous multiple signal recovery, additional constraints must be enforced for demixers $\boldsymbol{w}_\ell$, $\ell \in \{1, \ldots, J\}$ to recover different source signals.

2.2.2 Constant Modulus Algorithm

Among blind equalization algorithms, CMA [24] is often considered the most widespread blind technique due to its computational simplicity and practical effectiveness, as its independence of carrier recovery [26]. It is also well-known that it enjoys global convergence properties in noiseless scenarios under full rank channel conditions [29].

Traditionally, CMA is implemented using stochastic gradient descent and variations. However, one of its major issues in its practical applications is the presence of local minima in the constant modulus (CM) cost function as a result of additive channel noise [30, 31]. The convergence properties of such stochastic gradient descent algorithms have not been fully understood under limited samples and additive channel noise [26, 32, 33]. Moreover, the stochastic gradient descent approach has fundamental tradeoffs and requires finely tuning of e.g., initialization, normalization and stepsize, for satisfactory convergence and decent speed.

Several works have proposed different approaches that try to overcome these inherent shortcomings. One interesting approach is the transformation of CMA-based equalization to a convex problem, via Semidefinite relaxation [34–36], which provides global convergent solutions in a lifted higher dimensional parameter space that are further projected to the original solution space. As with any relaxation approach, CMA based on convex relaxation relies on the expectation that the convex problem yields solutions that can be projected to near optimum CMA solutions. However, projecting back to the original parameter space via rank 1 decomposition remains difficult and elusive [37]. Additionally, the problem size grows polynomially with increasing parameter size of the linear system and multiple users, and poses severe practical challenges in many scenarios.

Other line of works tries to solve CMA problems analytically [38, 39]. These solutions and its variants [40, 41], have no convergence issues as the solutions are found algebraically. However, they are more complex in general, and usually require stricter assumptions, such as constant modulus constellations, and cannot work with general QAM source signals such as 16-QAM. There are also multistage schemes [42], that depend heavily on the estimation

error being close to the MMSE estimate in earlier stages, or the error accumulates through different stages [43].

Moreover, several CMA-based approaches have been proposed to enforce the recovery of multiple signals at a time. One family of solutions is to consider regularization terms in the cost function [44–46], which enforce the recovered signals to be uncorrelated. Other schemes propose to modify the iterate after the gradient descent update, such as performing an iterative orthogonality enforcement on the combiners [47]. In general, these approaches are slow, as they require a rather large amount of samples and/or iterations to attain sufficient interference rejection of all recovered sources.

A new line of research is delivering algorithms to directly solve nonconvex optimization problems, and have been successfully applied in different domains, such as phase retrieval [48, 49], matrix completion [50, 51], blind deconvolution [52], among others. These are attractive solutions, as they do not require a prohibitive problem size or approximate relaxations, and provide good results with reasonable complexity and sample efficiency. Thus, these techniques can be better suited for grant-free access in resource limited networks. In Chapter 3, we adapt these results to the CMA-based signal recovery problem. By applying the Wirtinger Flow [48], we provide theoretical convergence guarantees in the finite-sample regime for both single and multiple source recovery, and demonstrate the efficiency of this methods via numerical simulations.

In a separate line of work, Riemannian manifold optimization [53] has rapidly attracted interest due to its ability to tackle non-convex problems with reasonable computational cost, and has been successfully applied to several domains, such as low-rank matrix decomposition [51], singular value decomposition [54], phase retrieval [55], blind signal demixing [56], dictionary learning [57, 58], among many others. In this framework, a constrained optimization problem in Euclidean space is transformed into an unconstrained problem over a Riemannian manifold, a subset of Euclidean space with nice properties. As the manifold contains only the interesting search directions for the problem, this approach potentially reduces

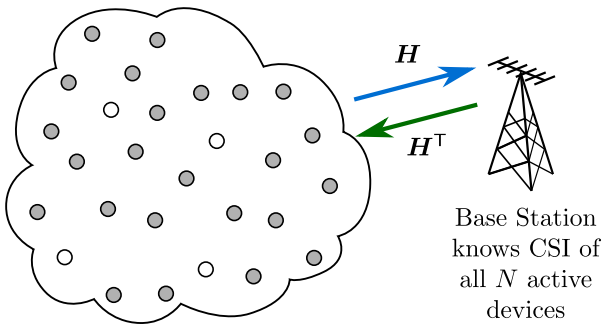

Figure 2.3: N active users (shaded gray) share a common resource block and transmit (MAC, blue) or receive (BC, green) independent signals simultaneously through a *known* physical channel.

computation. Moreover, it can avoid directions of invariance of the cost function, significantly facilitating theoretical analysis and direct application of optimization techniques. We show in Chapter 3 our application of the Riemannian manifold optimization framework to CMA-based signal recovery. By defining an adequate Riemannian manifold, we provide a non-regularized approach for multiple signal recovery that enjoys convergence guarantees with second order methods. Our experiments show excellent signal recovery capabilities with low sample complexity and computational complexity, and presents the Riemannian framework as a promising direction to the improvement of grant-free communications.

2.3 User Scheduling

We now consider a user scheduling scenario as depicted in Figure 2.3. We assume that the BS knows the CSI of all N active devices (also denoted users), and therefore the BS shall manage user scheduling, in both uplink (MAC) and downlink (BC). We further assume that the users only know their own CSI.

Without loss of generality, we consider MIMO systems that leverage spatial diversity to accommodate spectrum-sharing user groups allocated into distinct resources in multiple access strategies such as OFDMA and TDMA, among others. As stated before, we impose that resource-sharing groups (RSGs) shall have at most M users, to ensure linear independence

of user CSIs within each group.

In agreement with the general model of Section 2.1, $\boldsymbol{h}_u \in \mathbb{C}^M$ and $\boldsymbol{h}_u^{\mathsf{T}}$ denote the uplink and downlink CSI vector of the u-th user, respectively, with $u \in \{1, \ldots, N\}$. We assume the CSIs are random and independent from each other. We let s_u denote the $u-$th user data symbol of zero mean and unit average power, i.e. $\mathbb{E}\left[|s_u|^2\right] = 1$. Let G the total number of groups to be assigned, and let $\pi_{g,u} \in \{0, 1\}$ indicate whether the u-th user is scheduled in group $g \in \{1, \ldots, G\}$ exclusively, i.e.

$$\pi_{g,u} = \begin{cases} 1 & \text{the } u\text{-th user belongs to group } g \text{ only,} \\ 0 & \text{otherwise,} \end{cases} \tag{2.8}$$

and the set $\mathcal{S}_g = \{u | \pi_{g,u} = 1, u \in \{1, \ldots, N\}\}$ denotes the scheduled user set of the g-th group with cardinality $|\mathcal{S}_g|$. As the BS manages user scheduling, it also manages the transmit power allocated to each user, denoted p_u.

2.3.1 Uplink (MAC) Model

At the BS, the $|\mathcal{S}_g|$ user signals from the scheduled MAC user group g arrive at the BS receiver through their respective channel responses $\{\boldsymbol{h}_u\}_{u \in \mathcal{S}_g}$, which are then decoded using a linear receiver $\boldsymbol{W}_g$ such as the MRC, ZF and MMSE receivers [59], to generate the decoded signal vector

$$\boldsymbol{y}_g^{\text{MAC}} = \boldsymbol{W}_g^{\mathsf{H}} \left(\sum\nolimits_{u \in \mathcal{S}_g} \boldsymbol{h}_u \sqrt{p_u} s_u + \boldsymbol{n}_g \right) = \boldsymbol{W}_g^{\mathsf{H}} \left(\sum\nolimits_{n=1}^{N} \boldsymbol{h}_u \sqrt{p_u} s_u \pi_{g,u} + \boldsymbol{n}_g \right) \tag{2.9}$$

where $\boldsymbol{n}_g \sim \mathcal{CN}(\boldsymbol{0}_M, \sigma^2 \boldsymbol{I}_M)$ represents the AWGN vector corresponding to the resource block assigned to group g.

2.3.2 Downlink (BC) Model

In the case of BC, we operate under equal assumptions. However, the signal model changes as the single-antenna receivers will experience CCI but will not be aware of the CSI of other users in the RSG. Furthermore, the received signal and noise are scalars, and the BS uses a linear, unitary beamforming precoder $\boldsymbol{z}_u$ for each user u, which can be selected as the weighted MMSE [60], MRT [61] or ZF precoder [62] among others. For notational simplicity, we abuse notation and we use g to also denote the group index of the group that contains user u. Therefore, the signal model for the signal that user u receives in BC mode with AWGN $n_u \sim \mathcal{CN}(0, \sigma^2)$ corresponds to:

$$y_n^{\mathrm{BC}} = \boldsymbol{h}_u^{\mathsf{T}} \sum\nolimits_{i \in \mathcal{S}_g} \boldsymbol{z}_i \sqrt{p_i} s_i + n_u = \boldsymbol{h}_u^{\mathsf{T}} \sum\nolimits_{i=1}^{N} \boldsymbol{z}_i \sqrt{p_i} s_i \pi_{g,i} + n_u. \tag{2.10}$$

2.3.3 State of the Art

Given a large number of serviced devices N and increasing large number of base-station antennas M, the number of user scheduling options is of order $\mathcal{O}(N^M)$. Thus, to optimally schedule users in resource-sharing groups, one needs to examine the CSIs of each possible user grouping among potentially very large number of users in e.g., the thousands. However, since MIMO user scheduling is a combinatorial, NP-hard problem, even for a moderate number of users (e.g. hundreds), it is difficult to exhaustively evaluate all possible user combinations as MIMO user groups against one or more objectives.

Therefore, algorithms typically rely on heuristics when the user number becomes very large as in the case of IoT. For example, some recent methods take advantage of proportional fairness (PF) and the determinant pairing algorithm (DPS) [63–65]. However, these schemes rely on exhaustive computation of spatial cross-correlations for various possible user groups, and as such still require heavy computational workload.

Other approaches exploit localized characteristics shared among small subsets of users. One proposal examines $N(N-1)/2$ pairwise CSI correlations among all N users and proposes

to form user groups by setting a maximum correlation threshold [66,67]. Other schemes such as [68,69] directly group users of similar CSI covariance matrices. Nevertheless, information on pairwise or small user subsets fail to capture broad comprehensive characteristics on the entire user set. In the case of pairwise correlation, e.g., multiple users with low pairwise correlation in an MIMO user group may still suffer from significant interference accumulation. Localized approaches are also very sensitive to choices of manual parameter tuning and are harder to scale, as different choices might lead to drastically different performance as the user number changes or as the CSI models vary.

Recently, (machine) learning based approaches have been applied to a diverse array of difficult networking problems, including MAC user scheduling [70–73]. In fact, both supervised and unsupervised learning algorithms have found applications in wireless CSI characterization [70] that could be utilized in MIMO user scheduling. Machine learning is particularly attractive for large, NP-hard problems such as user scheduling that would require very high complexity to solve directly. In the context of wireless networking, supervised learning requires a rich labeled training set of diverse CSIs and correspondingly optimized scheduled user groups that attain strong performance. Such labeled training set must account for different system conditions such as number of antennas, number of users, wireless channel characteristics, noise levels, different power constraints, among others. However, it is not practically feasible to build such a huge set of optimum solutions. Ironically, supervised learning itself cannot be trained to find such optimum solutions for training.

In contrast, unsupervised learning explores underlying data features and characteristics without relying on labeled training set. Importantly in the context of large-scale user scheduling, unsupervised learning can effectively identify users with highly similar CSIs, as proposed for direct user grouping in downlink multi-cast [72, 73]. However, for the more general multi-user MIMO systems operating in either uplink MAC or downlink BC (also known as MU-MIMO), scheduling users with similar CSI leads to poor joint spatial diversity. Such outcome deviates from the original goal of diversity-based user scheduling, aimed

at scheduling users with highly dissimilar CSIs into MIMO co-channel groups to promote spatial diversity and to mitigate mutual interference. Clearly, a direct application of traditional learning algorithms over CSI vectors is incompatible with the MIMO user scheduling task. Additionally, unsupervised learning is often based in Euclidean space, but Euclidean distance of CSI does not correspond to spatial diversity as the latter is related to subspace span.

In the second part of this dissertation (Chapter 5), we propose a novel approach that leverages unsupervised learning to indirectly allocate users into RSGs. We will show that this strategy provides significant performance gains with modest computational cost, and can be generalized to consider a variety of performance metrics and different algorithms to further improve its results.

Chapter 3

Grant-Free Access via Blind Signal Recovery using Wirtinger Flow

In the first part of this dissertation, we focus on blind signal recovery methods to enable grant-free access in large scale networks. We adopt recent results in non-convex optimization and leverage a geometric analysis of the blind signal recovery problem with limited data samples. This approach demonstrates that these non-convex problems enjoy a rather benign geometry and can be solved with relative ease. Moreover, it also allows us to formulate theoretical guarantees, ensuring convergence with high probability.

In this chapter, we consider a prominent non-convex algorithm known as Wirtinger Flow (WF), which has shown strong results in related nonconvex problems in the literature. Due to the strong similarity between CMA-based signal recovery and the phase retrieval problem [48], we adopt the WF algorithm directly in CMA-based blind signal recovery, which we denote WF-CMA. In light of the convergence properties of WF under limited data samples, we leverage and generalize the original convergence analysis of WF in phase retrieval and obtain theoretical convergence guarantees for CMA in a finite-sample regime, both for single

Part of this chapter is reprinted, with permission, from [C. Feres and Z. Ding, "Wirtinger Flow Meets Constant Modulus Algorithm: Revisiting Signal Recovery for Grant-Free Access" in *IEEE Transactions on Signal Processing (Early Access)*, Aug. 2021] and followup modifications for final publication. Notations may have changed for consistency throughout this dissertation.

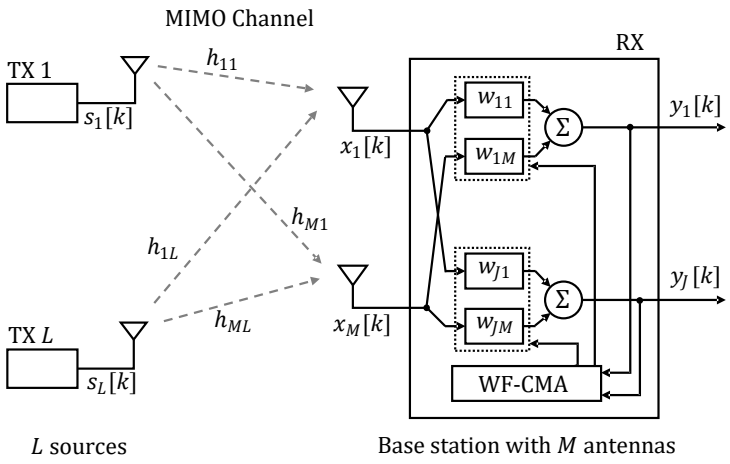

Figure 3.1: L sources share a common resource block and transmit independent signals to a host station with M antennas through an unknown physical channel. The host receiver aims to find multiple adaptive linear demixers $\boldsymbol{w}_1, \ldots, \boldsymbol{w}_J$ to recover $J \leq L$ sources with little mutual interference.

and multiple source recovery [74].

3.1 CMA-based Blind Signal Recovery

Figure 3.1 depicts a blind signal recovery system at the base station. As presented in Section 2.2.1, such a system attempts to find a demixer $\boldsymbol{w}$ that recovers one of the transmitted signals with minimal interference, or more generally, to find J demixers $\boldsymbol{w}_\ell$, $\ell \in \{1, \cdots, J\}$ that recover J distinct source signals with minimal mutual interference.

3.1.1 Single Source Recovery

Recall from Section 2.2.1 the constant-modulus cost function proposed by Godard [24]:

$$f(\boldsymbol{w}) = \frac{1}{2K} \sum_{k=1}^{K} \left(|\boldsymbol{x}_k^{\mathsf{H}} \boldsymbol{w}|^2 - R_2 \right)^2, \tag{3.1}$$

where R_2 is defined as in Eq.(2.4), but can be set to any value (e.g. $R_2 = 1$) and will scale the magnitude of the demixer $\boldsymbol{w}$ accordingly. As stated in Section 2.2.1, we assume that all

sources have equal average energy, as different signal energies can be considered as a channel effect. Additionally, recall that the base station does not know the active number of sources L, and we only assume that $L \leq M$ to ensure a full-column rank channel.

The CM cost function 3.1 has been proven to converge in expectation under noiseless scenarios and full-column rank channel [26, 29]. Nevertheless, to the best of our knowledge there were no convergence guarantees under limited data samples in the literature previous to this work. This is one of the main results we present later in this chapter, and we further make use of this result to prove convergence in the multiple source recovery setting.

3.1.2 Regularization for Multiple Signal Recovery

As we assume that multiple devices may access the channel in a grant-free scenario, it is desirable to recover multiple source signals at a time as described in Section 2.2.1. If we attempt to simultaneously recover multiple sources by solving for multiple demixer vectors $\boldsymbol{w}_\ell \in \{1 \dots, J\}$, we need to ensure that they do not restore the same source signal, possibly with different phases or delays [26].

Therefore, additional adjustments must be considered. Now, given that the different sources are independent, this is equivalent to force statistical uncorrelatedness of the signals in the cost function. For the case of complex outputs y_ℓ, y_i, their covariance is given by:

$$\mathrm{Cov}\{y_i, y_\ell\} = \mathbb{E}\{y_i y_\ell^*\} = \mathbb{E}\{\boldsymbol{w}_i^{\mathsf{H}} \boldsymbol{x}_{\boldsymbol{k}} (\boldsymbol{w}_\ell^{\mathsf{H}} \boldsymbol{x}_{\boldsymbol{k}})^*\} = \boldsymbol{w}_i^{\mathsf{H}} \mathbb{E}\{\boldsymbol{x}_k \boldsymbol{x}_k^{\mathsf{H}}\} \boldsymbol{w}_\ell. \tag{3.2}$$

Thus, we propose to regularize the CMA cost function with the squared magnitude of the pairwise covariances of the outputs, to obtain a smooth real-valued cost function. The modified CMA cost function for multiple sources considers J copies of the CM cost function (3.1), each one depending on a different demixer, and our proposed regularization:

$$g(\boldsymbol{w}_1, \dots, \boldsymbol{w}_J) = \sum_{\ell=1}^{J} f(\boldsymbol{w}_\ell) + \gamma_0 \sum_{\ell=1}^{J} \sum_{i \neq \ell}^{J} \left| \boldsymbol{w}_i^{\mathsf{H}} \boldsymbol{R}_{\boldsymbol{x}} \boldsymbol{w}_\ell \right|^2, \tag{3.3}$$

where $\gamma_0 > 0$ is a constant and the sample covariance matrix

$$\boldsymbol{R}_{\boldsymbol{x}} = \frac{1}{K}\sum_{k=1}^{K} \boldsymbol{x}_k \boldsymbol{x}_k^{\mathsf{H}}. \tag{3.4}$$

This is related to the regularization proposed in [75] which uses joint cumulants for source separation. The joint cumulants also consider the potential correlatedness of delayed versions of the demixer outputs, but in the presented case of source recovery the channels have no ISI, and the information from different delays of the outputs is not necessary. Other similar regularized approaches have been proposed in [44, 45].

3.2 WF-Based Constant Modulus Solutions

3.2.1 CMA meets Wirtinger Flow

A recent stream of nonconvex optimization procedures have been developed for solving quadratic equations, in particular for the phase retrieval problem. The phase retrieval problem can be stated as the recovery of an unknown signal $\boldsymbol{z}$ using known sampling vectors $\boldsymbol{a}_k$ from magnitudes $r_k = |\boldsymbol{a}_k^{\mathsf{H}}\boldsymbol{z}|^2$ only for which the smooth cost function is

$$\min_{\boldsymbol{z}\in\mathbb{C}^M} \quad \frac{1}{2K}\sum_{k=1}^{K} \left(|\boldsymbol{a}_k^{\mathsf{H}}\boldsymbol{z}|^2 - r_k\right)^2. \tag{3.5}$$

Note that in terms of the cost functions, phase retrieval is equivalent to the single-source CMA problem in Eq.(3.1), by setting $r_k = R_2$ and $\boldsymbol{a_k} = \boldsymbol{x}_k$, $k \in \{1, \ldots, K\}$, and using $\boldsymbol{z}$ as the unknown variable. If the source signal has constant modulus, e.g., $|s_\ell[k]|^2 = R_2$ for PSK signals, then the CM cost is the same as in the phase retrieval. One the other hand, for non-constant modulus source signals, e.g. 16-QAM, the CM cost is akin to phase retrieval based on an "average magnitude".

This similarity stimulates this study on the link between optimization methods for phase

retrieval and the CMA problem. However, there are some fundamental differences: (A) In phase retrieval, there is a known reference signal r_k as ground truth which is fully exploited in its convergence analysis. However, in CM-based demixing we only have a desired "average magnitude" R_2. (B) Phase retrieval has only one solution (up to common rotations), where in blind demixing, there may be many ideal demixer vectors to recover multiple source signals in different order (up to common rotations). (C) The sampling vectors $\boldsymbol{a}_k$ are chosen typically as Gaussian by users in phase retrieval. In CMA, $\boldsymbol{x}_k$ is (noisy) channel output that is not under user control and has a more complex distribution. (D) In phase retrieval, the signal $\boldsymbol{z}$ typically does not have additional constraints, whereas in CMA, the parameter vector $\boldsymbol{w}$ does not have other constraints but the source signals often do.

3.2.2 Wirtinger Flow in Phase Retrieval

For such a problem formulation, the *Wirtinger Flow* (WF) presented in [48] has received considerable attention as it guarantees convergence to a solution via gradient-descent with only $\mathcal{O}(M \log M)$ measurements with Gaussian sampling vectors, obtaining ε-accuracy within $\mathcal{O}(KM^2 \log 1/\varepsilon)$ iterations. This algorithm has received significant research attention and several works have improved WF for the phase retrieval problem [76–78] or adapted WF for seemingly different and unrelated optimization problems [52, 79].

In more depth, WF is a two stage approach consisting in spectral initialization and gradient descent updates. The latter is characterized by the notion of Wirtinger calculus (also known as $\mathbb{CR}$-calculus [80]). The gradient of a real value function $p(\boldsymbol{z})$ with respect to a complex variable vector $\boldsymbol{z} = \mathbf{z}_r + i\boldsymbol{z}_i$ can be simply viewed as a complex vector

$$\nabla_{\boldsymbol{z}} p(\boldsymbol{z}) = \frac{\partial p(\boldsymbol{z})}{\partial \boldsymbol{z}_r} + i\frac{\partial p(\boldsymbol{z})}{\partial \boldsymbol{z}_i}. \tag{3.6}$$

The same principle applies when deriving Hessians.

Spectral initialization yields (with high probability) an initial iterate for gradient descent

that is located within the basin of attraction of the ground truth, that is, a neighborhood of the ground truth with defined convexity and smoothness. Defining

$$\boldsymbol{R}_a = \frac{1}{K}\sum_{k=1}^{K} r_k \boldsymbol{a}_k \boldsymbol{a}_k^{\mathsf{H}}, \tag{3.7}$$

the initial iterate is a properly scaled eigenvector of $\boldsymbol{R}_a$ corresponding to its leading eigenvalue. This initial iterate is then highly correlated with ground truth, and has been proven to be close to the ground truth with high probability [48].

3.2.3 Wirtinger Flow for Single Source Recovery (SSR)

We now reformulate WF for our CM-based source recovery problem. Using $\mathbb{CR}$-calculus, the gradient of the CMA objective function f can be defined as

$$\nabla_{\boldsymbol{w}} f(\boldsymbol{w}) = \frac{1}{K}\sum_{k=1}^{K} \Big(|\boldsymbol{x}_k^{\mathsf{H}}\boldsymbol{w}|^2 - R_2\Big)\boldsymbol{x}_k\boldsymbol{x}_k^{\mathsf{H}}\boldsymbol{w}, \tag{3.8}$$

and the gradient descent rule is

$$\boldsymbol{w}^{t+1} = \boldsymbol{w}^t - \frac{\mu}{K\|\boldsymbol{w}^t\|^2}\sum_{k=1}^{K} \Big(|\boldsymbol{x}_k^{\mathsf{H}}\boldsymbol{w}^t|^2 - R_2\Big)\boldsymbol{x}_k\boldsymbol{x}_k^{\mathsf{H}}\boldsymbol{w}^t, \tag{3.9}$$

where the stepsize $\mu > 0$ could be constant or vary, either as a predefined function of the iteration t [48] or using an adaptive approach such as backtracking [81], among others.

This gradient rule, which notably shows a normalization factor, has in fact been previously introduced for the CM problem as Normalized CMA [82–84]. The idea is similar to normalized LMS by adjusting the stepsize in to avoid parameter divergence. Nevertheless, existing works have not thoroughly analyzed how to select the stepsize μ in NCMA, often resorting to trial-and-error. By connecting CMA to WF, we aim to define the stepsize selection according to the local geometry of CMA, thereby simplifying implementation and improving the algorithm convergence rate. We call this new approach WF-based Constant

Modulus Algorithm or WF-CMA.

Applying the spectral initialization of [48] for blind source recovery yields the covariance matrix of the received signal vectors $\boldsymbol{x}_k$ (corresponding to the known observations) scaled by the constant R_2 (corresponding to desired outcomes):

$$\frac{1}{K}\sum_{k=1}^{K} R_2 \boldsymbol{x}_k \boldsymbol{x}_k^{\mathsf{H}} = R_2 \boldsymbol{R}_{\boldsymbol{x}}. \tag{3.10}$$

The initial iterate for gradient descent is then chosen as $\boldsymbol{w}^0 = \eta \hat{\boldsymbol{v}}_1$, where $\hat{\boldsymbol{v}}_1$ is the normalized eigenvector corresponding to the largest eigenvalue of $R_2 \boldsymbol{R}_{\boldsymbol{x}}$, and the magnitude η is equal to

$$\eta = \sqrt{\frac{M \sum_k R_2}{\sum_k \|\boldsymbol{x}_k\|^2}} = \sqrt{\frac{MKR_2}{\sum_k \boldsymbol{x}_k^{\mathsf{H}} \boldsymbol{x}_k}}. \tag{3.11}$$

Algorithm 3.1 summarizes the steps for WF-CMA single source recovery.

Algorithm 3.1 WF-CMA for Single Source Recovery

Given: $\boldsymbol{x}_k \in \mathbb{C}^M$, $k \in \{1, \ldots, K\}$, number of iterations T and stepsize μ

A) Spectral Initialization:

Compute $\eta = \sqrt{\frac{MKR_2}{\sum_k \|\boldsymbol{x}_k\|^2}}$

Let $\hat{\boldsymbol{v}}_1$ be the normalized eigenvector corresponding to the largest eigenvalue of $\frac{R_2}{K}\sum_{k=1}^{K} \boldsymbol{x}_k \boldsymbol{x}_k^{\mathsf{H}}$

Set $\boldsymbol{w}^0 = \eta \hat{\boldsymbol{v}}_1$

B) Gradient Descent:

for $t = 0, \ldots, T-1$ **do**

$$\boldsymbol{w}^{t+1} = \boldsymbol{w}^t - \frac{\mu}{K\|\boldsymbol{w}^t\|^2} \sum_{k=1}^{K} \Big(|\boldsymbol{x}_k^{\mathsf{H}} \boldsymbol{w}^t|^2 - R_2 \Big) \boldsymbol{x}_k \boldsymbol{x}_k^{\mathsf{H}} \boldsymbol{w}^t$$

end for

3.2.4 Wirtinger Flow for Multiple Signal Recovery (MSR)

In the case of multiple signal recovery, we can apply the same principles. Using the sample covariance matrix in the cost function of (3.3), gradients with respect to each demixer vector $\boldsymbol{w}_\ell$ are

$$\nabla_\ell g = \frac{1}{K}\sum_{k=1}^{K}\Big(|\boldsymbol{x}_k^{\mathsf{H}}\boldsymbol{w}_\ell|^2 - R_2\Big)\boldsymbol{x}_k\boldsymbol{x}_k^{\mathsf{H}}\boldsymbol{w}_\ell + \gamma_0\sum_{\ell=1}^{J}\sum_{i\neq\ell}^{J}\boldsymbol{R}_{\boldsymbol{x}}\boldsymbol{w}_i\boldsymbol{w}_i^{\mathsf{H}}\boldsymbol{R}_{\boldsymbol{x}}\boldsymbol{w}_\ell, \tag{3.12}$$

where ∇_ℓ denotes the gradient with respect to demixer $\boldsymbol{w}_\ell$, and the new update rule is

$$\boldsymbol{w}_\ell^{t+1} = \boldsymbol{w}_\ell^t - \frac{\mu}{\|\boldsymbol{w}_\ell^t\|^2}\nabla_\ell g(\boldsymbol{w}_1^t,\ldots,\boldsymbol{w}_J^t). \tag{3.13}$$

Analogously, spectral initialization in this case is an extension of the single source case, and considers the J unit eigenvectors corresponding to the J largest eigenvalues of $\boldsymbol{R}_{\boldsymbol{x}}$:

$$\boldsymbol{w}_\ell^0 = \sqrt{\lambda_\ell^{-1}}\hat{\boldsymbol{v}}_\ell, \quad j\in\{1,\ldots,J\}, \tag{3.14}$$

where λ_ℓ is the ℓ-th leading eigenvalue of $\boldsymbol{R}_{\boldsymbol{x}}$ and $\hat{\boldsymbol{v}}_\ell$ is its corresponding eigenvector, normalized to unit magnitude.

Algorithm 3.2 WF-CMA Multiple Source Recovery

Given: $\boldsymbol{x}_k \in \mathbb{C}^M$, $k \in \{1, \ldots, K\}$, number of sources to recover J, number of iterations T and stepsize μ

A) Spectral Initialization:

1: Compute the J leading eigenvalues λ_ℓ and corresponding normalized eigenvectors $\hat{\boldsymbol{v}}_\ell$ of $\frac{R_2}{K}\sum_{k=1}^{K}\boldsymbol{x}_k\boldsymbol{x}_k^{\mathsf{H}}$

2: Set $\boldsymbol{w}_\ell^0 = \sqrt{\lambda_\ell^{-1}}\hat{\boldsymbol{v}}_\ell \; \forall j = \{1, \ldots, J\}$

B) Gradient Descent:

3: **for** $t = 0, \ldots, T-1$ **do**

4: **for** $j = 1, \ldots, J$ **do**

5: $\boldsymbol{w}_\ell^{t+1} = \boldsymbol{w}_\ell^t - \dfrac{\mu}{\|\boldsymbol{w}_\ell^t\|^2}\nabla_\ell g(\boldsymbol{w}_1^t, \ldots, \boldsymbol{w}_J^t)$

6: **end for**

7: **end for**

It is important to note that, depending on the data and channel, the initialization scheme for MSR might be ill-defined as the data samples might lead to a degenerate case that it is not possible to separate some sources [85]. Nevertheless, when considering the noiseless scenario (i.e., removing AWGN noise from the received signal vectors), the received signals are linear combinations of independent transmitted signals under independent Rayleigh channels. Thus, when $K \to \infty$, $\boldsymbol{R}_{\boldsymbol{x}}$ converges to the scaled expected value of $\boldsymbol{x}\boldsymbol{x}^{\mathsf{H}}$ thanks to the Central Limit Theorem. This implies that, when K is large enough, the leading eigenvectors of $\boldsymbol{R}_{\boldsymbol{x}}$ will align with the leading eigenvectors of $\mathbb{E}\{\boldsymbol{x}\boldsymbol{x}^{\mathsf{H}}\}$, up to a scaling factor.

3.3 Theoretical Convergence Analysis

3.3.1 Convergence Guarantee of CMA

The global convergence properties of CMA for PAM and QAM input signals in noiseless scenarios are well known [26, Chapters 4, 7]. The presented CMA-based single source recovery corresponds to a particular case of the MIMO-CMA blind equalizer, where the MIMO channel has zero ISI and only multi-user interference is to be suppressed. Thus, the mean CM cost of Eq.(2.4) has been shown to only possess global minima, each of which corresponds to the successful recovery (demixing) of one source signal with a phase rotation in the noiseless case if the channel matrix $\boldsymbol{H}$ has full column rank. In other words, if $\boldsymbol{H}$ has full column rank, then the minimization of the mean CM cost leads to guaranteed global convergence in noiseless scenarios, regardless of initial conditions [45]. Moreover, if $\boldsymbol{H}$ rank deficient a solution of the mean CM cost is close to optimal Wiener solutions [86], which further highlights the applicability of CMA-based blind signal recovery in the presence of multiple sources. The resulting combiner will exhibit some bounded interference, which is tolerable in most practical implementations. Nevertheless, we shall consider only the case when $\boldsymbol{H}$ has full-column rank that guarantees global convergence for blind signal recovery.

We do not require the number of sources L to be known at any point. In the case that the receiver tries to recover more sources than the existing ones, i.e. $J \geq L$, the receiver would obtain L demixers that recover signals and $J - L$ demixers that only recover noise. In any case, the receiver can perform a rank estimation procedure if it needs to estimate L [87, 88].

When considering noisy channels, it is well known that channel noise introduces additional local minima to the mean CM cost function [26]. Thus, even carefully selected stepsize (based on trial and error) cannot guarantee convergence to global minima. Thus, new results that can reveal better convergence properties in stepsize selection are of special interest.

Given the known properties of the mean CM cost, what remains unclear is the convergence

of CMA under finite data samples and additive noise. In this scenario, we aim to determine convergence properties for CM-based demixing by leveraging the convergence analysis of WF.

3.3.2 Adapting Wirtinger Flow to CMA

The convergence properties of the Wirtinger Flow phase retrieval have been proven in [48] for Eq.(3.5). However, the new WF-CMA exhibits two special characteristics different from the original WF in phase retrieval:

- The spectral initialization proposed for WF in phase retrieval [48] yields an eigendecomposition of the sample covariance matrix that is highly correlated with the ground truth in expectation, and the initial iterate is provably close to the ground truth to guarantee convergence. However, the same initialization in CMA-based SSR does not readily provide an initial estimate that is highly correlated with the problem solutions.

- The sampling vectors $\boldsymbol{a}_k$ are assumed to either have a standard complex normal distribution, i.e. $\boldsymbol{a}_k \sim \mathcal{CN}(\boldsymbol{0}, \boldsymbol{I})$, or be admissible distributions for coded diffraction patterns (CDPs) [48]. However, the received signal vectors $\boldsymbol{x}_k$ in CMA given by Eq.(2.2), are linear mixtures of independent source signals by the channel matrix $\boldsymbol{H}$, plus additive white Gaussian channel noise. They do not correspond in general with these sampling vector models, or even with those from recent work using subgaussian variables [89]. Moreover, the elements of $\boldsymbol{x}_k$ are linear mixtures of independent QAM signals which are non-Gaussian, and are not mutually independent, a distinct issue that makes convergence analysis difficult.

We first examine spectral initialization. Consider the noiseless case and assume all source signals have equal symbol energy E_s without loss of generality. Taking expectation on the

scaled sample covariance matrix in Eq.(3.10) for initialization:

$$\mathbb{E}\{R_2 \boldsymbol{R}_{\boldsymbol{x}}\} = \frac{R_2}{K} \sum_{k=1}^{K} \boldsymbol{H} \mathbb{E}\{\boldsymbol{s}_k \boldsymbol{s}_k^{\mathsf{H}}\} \boldsymbol{H}^{\mathsf{H}} = R_2 E_s \boldsymbol{H} \boldsymbol{H}^{\mathsf{H}}, \tag{3.15}$$

which depends on the channel but is not explicitly dependent on the solutions. From (2.6), the global CMA solutions satisfy

$$\hat{\boldsymbol{w}}^{\mathsf{H}} \boldsymbol{H} \boldsymbol{s}_{\boldsymbol{k}} = \mathrm{e}^{j\varphi} s_\ell[k], \ \ell \in \{1, \ldots, L\}, \ \theta \in [0, 2\pi]. \tag{3.16}$$

Thus, the optimal demixers are not directly extractable from the sample covariance matrix. Therefore, our work shall not analyze this initialization effect on WF-CMA. Nevertheless, we will show later in experiments that such initialization appears to benefit WF-CMA convergence. Thus, we still include this spectral initialization for CMA in Algorithm 3.1.

With respect to the dependent elements of $\boldsymbol{x}_k$, recall that the fading channel matrix has full column rank. Under this assumption, we can rewrite

$$y[k] = \boldsymbol{w}^{\mathsf{H}} \boldsymbol{x}_k = \boldsymbol{w}^{\mathsf{H}} \boldsymbol{H} \boldsymbol{s}_k + \boldsymbol{w}^{\mathsf{H}} \boldsymbol{n}_k = \boldsymbol{q}^{\mathsf{H}} \boldsymbol{s}_k + \breve{n}[k], \tag{3.17}$$

where $\boldsymbol{q} = \boldsymbol{H}^{\mathsf{H}} \boldsymbol{w}$ is the combined (channel plus demixer) parameter vector, and $\breve{n}_k$ is demixer output noise. Given full column rank $\boldsymbol{H}$, we can study the WF-CMA in the combined parameter space $\boldsymbol{q}$, which directly interacts with independent source signals. This parameter transformation mitigates the challenge posed by dependent signals in the WF algorithm. We now study the convergence of WF in the $\boldsymbol{q}$ domain since the $\boldsymbol{q}$ space can be fully spanned by adjusting $\boldsymbol{w}$.

Onwards, our approach to specifying the local convergence properties of WF is to characterize the local behavior of the CM cost function in the $\boldsymbol{q}$ domain, in which we describe the gradient and Hessian of the CM-cost in the neighborhood of a ground truth. We show that the local geometry near each ground truth admits convergence to a global minimum

using gradient-descent based WF algorithm.

3.3.3 Convergence of WF-CMA for single source recovery

In the following, and without loss of generality, we assume that all sources use the same square QAM constellation of size Q with equally likely symbols. These correspond to discrete finite sets, and as such, signals of each source at each time k are bounded random variables, and by definition, subgaussian random variables [90, Definition 5.7]. In other words, the signal vectors $\boldsymbol{s}_k$ are supported on an exponentially large set of size Q^L, and thus are subgaussian random vectors for the purposes of concentration of measure and non-asymptotic approaches [91, Section 3.4.2]. We will use this fact to support our theoretical analysis.

We also denote the second moment, fourth moment, and kurtosis of the transmitted signals as

$$m_2 = \mathbb{E}\{|s[k]|^2\},\ m_4 = \mathbb{E}\{|s[k]|^4\},\ \kappa = m_4 - 2m_2^2 < 0. \tag{3.18}$$

Additionally, as QAM constellations are discrete and bounded, with probability 1 we have $\forall\, k \in \{1, \ldots, K\}$

$$\big|s_\ell[k]\big| \leq \sqrt{\frac{3m_2}{Q-1}}(\sqrt{Q}-1) = B \ \Rightarrow\ \|\boldsymbol{s}_k\| \leq B\sqrt{L}. \tag{3.19}$$

We need some definitions. Let $\boldsymbol{z}$ be a solution to the CM cost in the $\boldsymbol{q}$-domain, i.e. $\boldsymbol{z}$ minimizes $f(\cdot)$. Also, note that as $\boldsymbol{z}$ is related only to the channel $\boldsymbol{H}$ as implied in Eqs.(3.16) and (3.17), is independent of the signals $\boldsymbol{s}_k$. For any vector $\boldsymbol{q} \in \mathbb{C}^L$ we define

$$\operatorname{dist}(\boldsymbol{q}, \boldsymbol{z}) = \min_{\phi\in[0,2\pi]} \|\boldsymbol{q} - \mathrm{e}^{j\phi}\boldsymbol{z}\|. \tag{3.20}$$

We define a set of solutions due to a rotation factor ϕ as

$$P := \{\mathrm{e}^{j\phi}\boldsymbol{z} : \phi \in [0, 2\pi]\} \tag{3.21}$$

and the set of vectors within ϵ distance from P is

$$E(\epsilon) := \{\boldsymbol{q} \in \mathbb{C}^L : \mathrm{dist}(\boldsymbol{q}, P) \leq \epsilon\}. \tag{3.22}$$

For any $\boldsymbol{q} \in \mathbb{C}^L$, we define the alignment phase $\phi(\boldsymbol{q})$ as

$$\phi(\boldsymbol{q}) := \underset{\phi\in[0,2\pi]}{\arg\min} \|\boldsymbol{q} - \mathrm{e}^{j\phi}\boldsymbol{z}\| = \angle(\boldsymbol{z}^{\mathsf{H}}\boldsymbol{q}), \tag{3.23}$$

such that

$$\mathrm{dist}(\boldsymbol{q}, \boldsymbol{z}) = \|\boldsymbol{q} - \mathrm{e}^{j\phi(\boldsymbol{q})}\boldsymbol{z}\|. \tag{3.24}$$

By defining

$$\boldsymbol{A}(\boldsymbol{q}) = \frac{1}{K}\sum_{k=1}^{K} |\boldsymbol{s}_k^{\mathsf{H}}\boldsymbol{q}|^2 \boldsymbol{s}_k\boldsymbol{s}_k^{\mathsf{H}}, \quad \boldsymbol{B}(\boldsymbol{q}) = \frac{1}{K}\sum_{k=1}^{K} (\boldsymbol{s}_k^{\mathsf{H}}\boldsymbol{q})^2 \boldsymbol{s}_k\boldsymbol{s}_k^{\mathsf{T}}, \quad \boldsymbol{S} = \frac{1}{K}\sum_{k=1}^{K} \boldsymbol{s}_k\boldsymbol{s}_k^{\mathsf{H}}, \tag{3.25}$$

the Wirtinger Hessian of the cost function f is simply

$$\nabla^2 f(\boldsymbol{q}) = \begin{bmatrix} 2\boldsymbol{A}(\boldsymbol{q}) - R_2\boldsymbol{S} & \boldsymbol{B}(\boldsymbol{q}) \\ \overline{\boldsymbol{B}(\boldsymbol{q})} & 2\overline{\boldsymbol{A}(\boldsymbol{q})} - R_2\overline{\boldsymbol{S}} \end{bmatrix}. \tag{3.26}$$

We now present our main convergence result for single source recovery.

Theorem 1. *Consider the signal vectors $\boldsymbol{s}_k \in \mathbb{C}^L$ with i.i.d. elements from a square QAM constellation of size Q. Let $\boldsymbol{z}$ be a solution of the CMA problem with cost function (3.1). Additionally, let $\alpha \geq 3+80\cdot\mathbf{1}[Q \neq 4]$, $\beta \geq 235+724\cdot\mathbf{1}[Q \neq 4]$, $\epsilon = (10B\sqrt{L})^{-1}$ and $\delta = 0.01$. There exist $C_1 > 0$ and $c_1 > 0$ such that, if the number of measurements $K \geq C_1 L$, then for*

all $\boldsymbol{q} \in E(\epsilon)$*, the cost function* $f(\cdot)$ *satisfies the generalized regularity condition*

$$\mathrm{Re}\Big(\big\langle \nabla f(\boldsymbol{q}) - \nabla f(\mathrm{e}^{j\phi(\boldsymbol{q})}\boldsymbol{z}), \boldsymbol{q} - \mathrm{e}^{j\phi(\boldsymbol{q})}\boldsymbol{z}\big\rangle\Big) \geq \frac{1}{\alpha}\mathrm{dist}^2(\boldsymbol{q}, \boldsymbol{z}) + \frac{1}{\beta}\big\|\nabla f(\boldsymbol{q}) - \nabla f(\mathrm{e}^{j\phi(\boldsymbol{q})}\boldsymbol{z})\big\|^2 \tag{3.27}$$

with probability of at least $1 - 6\mathrm{e}^{-c_1 K}$*. Furthermore, by selecting a stepsize* $0 < \mu \leq 2/\beta$*, if* $\boldsymbol{q}^t \in E(\epsilon)$*, then the update of Algorithm 3.1*

$$\boldsymbol{q}^{t+1} = \boldsymbol{q}^t - \mu \nabla f(\boldsymbol{q}^t) \tag{3.28}$$

leads to $\boldsymbol{q}^{t+1} \in E(\epsilon)$ *and contraction*

$$\mathrm{dist}^2(\boldsymbol{q}^{t+1}, \boldsymbol{z}) \leq \Big(1 - \frac{2\mu}{\alpha}\Big)\mathrm{dist}^2(\boldsymbol{q}^t, \boldsymbol{z}). \tag{3.29}$$

The proof of Theorem 1 is an extension and modification of the original Wirtinger Flow proof [48], but considering subgaussian signal vectors (QAM constellations) and an average modulus, as the actual magnitude samples are unknown. The steps of the proof are summarized below:

(1) **Establishing concentration of measure of the Hessian and deriving related scalar inequalities.** In Lemma 1, we show that with high probability, the WF-CMA Hessian is close to its expectation given sufficient samples.

(2) **Characterizing the local geometry of the CMA objective function.** We show that the cost function has strong convexity and smoothness in the ϵ-vicinity of the ground truth, which are respectively proven in Lemmas 2 and 3 based on the concentration of Hessian and the resulting inequalities. These results describe the geometry of the cost function in the neighborhood of any local minimum, which are known to correspond to global minima in noiseless CMA-based equalization.

(3) **Proving that the WF-CMA update rule is a contraction.** In Lemma 4, we finally show that the update rule is a contraction with geometric rate within the basin of attraction $E(\epsilon)$.

We first tackle the concentration of measure of the Hessian of $f(\cdot)$ in the following lemma.

Lemma 1 (Concentration of the Hessian). *Let $\boldsymbol{z}$ be a solution of (3.1) and independent of the signal vectors $\boldsymbol{s}_k$ under the setup of Theorem 1, and $\delta > 0$. There exist $C_1(\delta) > 0$ and $c_1(\delta) > 0$ such that, if $K \geq C_1(\delta)L$, then*

$$\left\|\nabla^2 f(\boldsymbol{z}) - \mathbb{E}\{\nabla^2 f(\boldsymbol{z})\}\right\| \leq \delta \tag{3.30}$$

holds with probability of at least $1 - 6\mathrm{e}^{-c_1(\delta)K}$.

Proof. Refer to Appendix A.2 for details. ■

The local geometry of the cost function can be characterized using both lemmas below. Combined, they yield inequality (3.27). In particular, Lemma 2 describes the strong convexity of the cost function, and Lemma 3 proves the cost function is well behaved near local optimizers.

Lemma 2 (Local Curvature Condition). *Under the conditions of Lemma 1, let $\alpha \geq 3 + 80 \cdot \mathbf{1}[Q \neq 4]$, $\epsilon = (10B\sqrt{L})^{-1}$ and $\delta = 0.01$. Then, for all vectors $\boldsymbol{q} \in E(\epsilon)$, the cost function $f(\cdot)$ satisfies*

$$\begin{aligned}\mathrm{Re}\Big(\big\langle \nabla f(\boldsymbol{q}) - \nabla f(\mathrm{e}^{j\phi(\boldsymbol{q})}\boldsymbol{z}), \boldsymbol{q} - \mathrm{e}^{j\phi(\boldsymbol{q})}\boldsymbol{z}\big\rangle\Big) \geq \Big(\frac{1}{\alpha} + \frac{2m_2^2 - R_2 m_2 - \delta}{19}\Big)\mathrm{dist}^2(\boldsymbol{q}, \boldsymbol{z}) \\ + \frac{1}{20K}\sum_{k=1}^{K}\Big|\boldsymbol{s}_k^{\mathsf{H}}(\boldsymbol{q} - \mathrm{e}^{j\phi(\boldsymbol{q})}\boldsymbol{z})\Big|^4.\end{aligned} \tag{3.31}$$

Proof. See Appendix A.3. ■

Lemma 3 (Local Smoothness Condition). *Under the conditions of Lemma 1, let $\beta \geq 235 + 724 \cdot \mathbf{1}[Q \neq 4]$, $\epsilon = (10B\sqrt{L})^{-1}$ and $\delta = 0.01$. Then, for all vectors $\boldsymbol{q} \in E(\epsilon)$, the cost*

function $f(\cdot)$ satisfies

$$\frac{1}{\beta}\left\|\nabla f(\boldsymbol{q})-\nabla f(\mathrm{e}^{j\phi(\boldsymbol{q})}\boldsymbol{z})\right\|^2 \leq \frac{2m_2^2-R_2m_2-\delta}{19}\mathrm{dist}^2(\boldsymbol{q},\boldsymbol{z})+\frac{1}{20K}\sum_{k=1}^{K}\left|\boldsymbol{s}_k^{\mathsf{H}}(\boldsymbol{q}-\mathrm{e}^{j\phi(\boldsymbol{q})}\boldsymbol{z})\right|^4. \tag{3.32}$$

Proof. See Appendix A.4. ■

Finally, based on the local behavior of the cost function, we establish the contraction of the iterative rule of Algorithm 3.1.

Lemma 4 (Contraction of Update Rule). *Under the conditions of Theorem 1, consider $0<\mu\leq 2/\beta$ and $\boldsymbol{q}^t\in E(\epsilon)$. Using the update rule of Algorithm 1,*

$$\boldsymbol{q}^{t+1}=\boldsymbol{q}^t-\mu\nabla f(\boldsymbol{q}^t), \tag{3.33}$$

we have that $\boldsymbol{q}^{t+1}\in E(\epsilon)$ and contraction

$$\mathrm{dist}^2(\boldsymbol{q}^{t+1},\boldsymbol{z})\leq\Big(1-\frac{2\mu}{\alpha}\Big)\mathrm{dist}^2(\boldsymbol{q}^t,\boldsymbol{z}). \tag{3.34}$$

Proof. This proof follows [48, Lemma 7.10], as our problem also has non-unique global solutions. ■

3.3.4 Convergence for Multiple Source Recovery

Recall that our cost function for MSR is a simpler version of the one in [45], which has been shown to exhibit global convergence properties under noiseless full rank channel conditions. Thus, in a way similar to the SSR case, we will describe the local geometry of the CM cost for MSR and show how the WF algorithm recovers source signals with high probability. For full column rank channel matrix, we can use the overall system parameter space as in Eq.(3.17)

by introducing $\boldsymbol{q} = [\boldsymbol{q}_1^{\mathsf{T}} \dots \boldsymbol{q}_J^{\mathsf{T}}]^{\mathsf{T}}$ as the aggregation of the J demixers:

$$y_\ell[k] = \boldsymbol{w}_\ell^{\mathsf{H}} \boldsymbol{x}_k = \boldsymbol{q}_\ell^{\mathsf{H}} \boldsymbol{s}_k + \breve{n}_\ell[k]. \tag{3.35}$$

Thus, the cost function is

$$g(\boldsymbol{q}) = \sum_{\ell=1}^{J} f(\boldsymbol{q}_\ell) + \gamma_0 \sum_{\ell=1}^{J} \sum_{i \neq \ell}^{J} \left| \boldsymbol{q}_i^{\mathsf{H}} \boldsymbol{S} \boldsymbol{q}_\ell \right|^2 \tag{3.36}$$

where $\boldsymbol{S}$ is the sample covariance matrix defined in Eq.(3.25).

For the MSR proofs, we need to generalize the previous definitions. Let $\boldsymbol{z} = [\boldsymbol{z}_1^{\mathsf{T}} \dots \boldsymbol{z}_J^{\mathsf{T}}]^{\mathsf{T}} \in \mathbb{C}^{JL}$ be a solution that minimizes $g(\cdot)$ and is independent of the signals $\boldsymbol{s}_k$. For any vector $\boldsymbol{q} \in \mathbb{C}^{JL}$,

$$\operatorname{dist}(\boldsymbol{q}, \boldsymbol{z}) = \left(\sum_{\ell=1}^{J} \min_{\phi \in [0, 2\pi]} \|\boldsymbol{q}_\ell - \mathrm{e}^{j\phi} \boldsymbol{z}_\ell\|^2 \right)^{\frac{1}{2}}. \tag{3.37}$$

We define the set of all vectors that differ from the solution by a rotation factor in each demixer as

$$P := \left\{ [\mathrm{e}^{j\phi_1} \boldsymbol{z}_1^{\mathsf{T}} \dots \mathrm{e}^{j\phi_J} \boldsymbol{z}_J^{\mathsf{T}}]^{\mathsf{T}} : \phi_\ell \in [0, 2\pi] \quad \forall \ell \in \{1, \dots, J\} \right\}. \tag{3.38}$$

The sets of vectors close to P are

$$E(\epsilon) := \{\boldsymbol{q} \in \mathbb{C}^{JL} : \operatorname{dist}(\boldsymbol{q}, P) \leq \epsilon\}, \tag{3.39}$$

and, for any vector $\boldsymbol{q} \in \mathbb{C}^{JL}$ we define the phases $\phi_\ell(\boldsymbol{q})$ as

$$\phi_\ell(\boldsymbol{q}) := \phi(\boldsymbol{q}_\ell) = \operatorname*{arg\,min}_{\phi \in [0, 2\pi]} \|\boldsymbol{q}_\ell - \mathrm{e}^{j\phi} \boldsymbol{z}_\ell\| = \angle(\boldsymbol{z}_\ell^{\mathsf{H}} \boldsymbol{q}_\ell) \tag{3.40}$$

such that

$$\operatorname{dist}(\boldsymbol{q}, \boldsymbol{z}) = \left(\sum_{\ell=1}^{J} \|\boldsymbol{q}_\ell - \mathrm{e}^{j\phi(\boldsymbol{q}_\ell)} \boldsymbol{z}_\ell\|^2 \right)^{\frac{1}{2}}. \tag{3.41}$$

The Wirtinger Hessian of the cost function g is

$$\nabla^2 g(\boldsymbol{q}) = \mathrm{Bdiag}\Big(\big\{\nabla^2 f(\boldsymbol{q}_\ell)\big\}_{\ell=1}^{J}\Big) + \gamma_0 \begin{bmatrix} \boldsymbol{G}_1(\boldsymbol{q}) & \cdots & \boldsymbol{H}_{1J}(\boldsymbol{q}) \\ \vdots & \ddots & \vdots \\ \boldsymbol{H}_{J1}(\boldsymbol{q}) & \cdots & \boldsymbol{G}_J(\boldsymbol{q}) \end{bmatrix} \tag{3.42}$$

where Bdiag() constructs a block diagonal matrix out of the matrices

$$\nabla^2 f(\boldsymbol{q}_\ell) = \begin{bmatrix} 2\boldsymbol{A}(\boldsymbol{q}_\ell) - R_2\boldsymbol{S} & \boldsymbol{B}(\boldsymbol{q}_\ell) \\ \overline{\boldsymbol{B}(\boldsymbol{q}_\ell)} & 2\overline{\boldsymbol{A}(\boldsymbol{q}_\ell)} - R_2\overline{\boldsymbol{S}} \end{bmatrix}. \tag{3.43}$$

$\boldsymbol{A}(\boldsymbol{q}_\ell)$, $\boldsymbol{B}(\boldsymbol{q}_\ell)$, and $\boldsymbol{S}$ have been defined in Eq.(3.25) and

$$\boldsymbol{G}_\ell(\boldsymbol{q}) = \begin{bmatrix} \boldsymbol{C}_\ell(\boldsymbol{q}) & \boldsymbol{0} \\ \boldsymbol{0} & \overline{\boldsymbol{C}_\ell(\boldsymbol{q})} \end{bmatrix}, \quad \boldsymbol{C}_\ell(\boldsymbol{q}) = \sum_{i\neq\ell}^{J} \boldsymbol{S}\boldsymbol{q}_i\boldsymbol{q}_i^{\mathsf{H}}\boldsymbol{S}. \tag{3.44}$$

Furthermore, we have

$$\boldsymbol{H}_{\ell i}(\boldsymbol{q}) = \begin{bmatrix} \boldsymbol{E}_{\ell i}(\boldsymbol{q}) & \boldsymbol{F}_{\ell i}(\boldsymbol{q}) \\ \overline{\boldsymbol{F}_{\ell i}(\boldsymbol{q})} & \overline{\boldsymbol{E}_{\ell i}(\boldsymbol{q})} \end{bmatrix}, \quad \boldsymbol{E}_{\ell i}(\boldsymbol{q}) = \boldsymbol{q}_i^{\mathsf{H}}\boldsymbol{S}\boldsymbol{q}_\ell\boldsymbol{S}, \quad \boldsymbol{F}_{\ell i}(\boldsymbol{q}) = \boldsymbol{S}\boldsymbol{q}_i\boldsymbol{q}_\ell^{\mathsf{T}}\boldsymbol{S}^{\mathsf{T}}. \tag{3.45}$$

We now introduce the convergence analysis of Algorithm 3.2.

Theorem 2. *Consider signal vectors $\boldsymbol{s}_k \in \mathbb{C}^L$ with i.i.d elements from a square QAM constellation of size Q. Let $J \geq 2$ and $\boldsymbol{z}$ be a solution to the MSR CMA problem with cost function (3.3). Additionally, let $\alpha \geq 4{+}223{\cdot}\mathbf{1}[Q \neq 4]$, $\beta \geq 730{+}267(J{-}1){+}\big(1234{+}127(J{-}1)\big){\cdot}\mathbf{1}[Q \neq 4]$, $\epsilon = (10JB\sqrt{L})^{-1}$, $\gamma_0 = 1$ and $\delta = 0.001$. There exist $C_2 > 0$ and $c_2 > 0$ such that, if the number of samples $K \geq C_2 L$, then for all $\boldsymbol{q} \in E(\epsilon)$, the cost function $g(\cdot)$ satisfies the*

generalized regularity condition

$$\sum_{\ell=1}^{J} \mathrm{Re}\Big(\big\langle \nabla_\ell g(\boldsymbol{q}) - \nabla_\ell g(\mathrm{e}^{j\phi(\boldsymbol{q}_\ell)}\boldsymbol{z}), \boldsymbol{q}_\ell - \mathrm{e}^{j\phi(\boldsymbol{q}_\ell)}\boldsymbol{z}_\ell \big\rangle\Big)$$
$$\geq \frac{1}{\alpha}\mathrm{dist}^2(\boldsymbol{q},\boldsymbol{z}) + \frac{1}{\beta}\sum_{\ell=1}^{J} \big\|\nabla_\ell g(\boldsymbol{q}) - \nabla_\ell g(\mathrm{e}^{j\phi(\boldsymbol{q}_\ell)}\boldsymbol{z})\big\|^2 \tag{3.46}$$

with probability of at least $1 - 12\mathrm{e}^{-c_2 K}$. *Furthermore, by selecting a stepsize* $0 < \mu \leq 2/\beta$ *and* $\boldsymbol{q}^t \in E(\epsilon)$, *the MSR WF-CMA updates from Algorithm 3.2*

$$\boldsymbol{q}_\ell^{t+1} = \boldsymbol{q}_\ell^t - \mu \nabla_\ell g(\boldsymbol{q}^t) \tag{3.47}$$

will lead to $\boldsymbol{q}^{t+1} \in E(\epsilon)$ *and contraction*

$$\mathrm{dist}^2(\boldsymbol{q}^{t+1},\boldsymbol{z}) \leq \Big(1 - \frac{2\mu}{\alpha}\Big)\mathrm{dist}^2(\boldsymbol{q}^t,\boldsymbol{z}). \tag{3.48}$$

The proof of Theorem 2 follows a similar approach as proof of Theorem 1, with requisite modifications to account for the additional terms in the cost function $g(\cdot)$, i.e. the multiple CM costs for each demixer and the pairwise covariances of demixers in Eq.(3.36). To summarize:

(1) **Establish concentration of measure for the MSR Hessian.** Lemma 5 proves that the MSR Hessian is also close to its expected value with high probability.

(2) **Describe local geometry of the MSR cost function.** We show that the MSR cost function exhibits strong convexity and smoothness in the ϵ-vicinity of the ground truth. These properties are proven in Lemmas 6 and 7 by way of Lemmas 1, 2, 3 and 5.

(3) **Prove that the MSR update is a contraction.** This is shown in Lemma 8 for iteration within the basin of attraction $E(\epsilon)$.

Lemma 5 (Concentration of the MSR Hessian). *Let $\boldsymbol{z}$ be a solution to (3.3) independent of the signal vectors $\boldsymbol{s}_k$, under the setup of Theorem 2. Then, there exists $C_2 > 0$ and $c_2 > 0$ such that, if $K \geq C_2 L$, then*

$$\left\|\nabla^2 g(\boldsymbol{z}) - \mathbb{E}\{\nabla^2 g(\boldsymbol{z})\}\right\| \leq \delta \tag{3.49}$$

holds with probability of at least $1 - 12\mathrm{e}^{-c_2 K}$.

Proof. Refer to Appendix A.6 for details. ■

Lemma 6 (MSR Local Curvature Condition). *Under the conditions of Lemma 5, let $\alpha \geq 4 + 223 \cdot \mathbf{1}[Q \neq 4]$, $\epsilon = (10JB\sqrt{L})^{-1}$, $\gamma_0 = 1$ and $\delta = 0.001$. Then for all vectors $\boldsymbol{q} \in E(\epsilon)$, the cost function $g(\cdot)$ satisfies*

$$\begin{aligned}
&\sum_{\ell=1}^{J} \mathrm{Re}\Big(\big\langle \nabla_\ell g(\boldsymbol{q}) - \nabla_\ell g(\mathrm{e}^{j\phi(\boldsymbol{q}_\ell)}\boldsymbol{z}), \boldsymbol{q}_\ell - \mathrm{e}^{j\phi(\boldsymbol{q}_\ell)}\boldsymbol{z}_\ell \big\rangle\Big) \\
&\quad \geq \frac{1}{\alpha}\mathrm{dist}^2(\boldsymbol{q}, \boldsymbol{z}) + \frac{2m_2^2 - R_2 m_2 - \delta}{19}\mathrm{dist}^2(\boldsymbol{q}, \boldsymbol{z}) + \frac{1}{20K}\sum_{k=1}^{K}\sum_{\ell=1}^{J}\left|\boldsymbol{s}_k^{\mathsf{H}}(\boldsymbol{q}_\ell - \mathrm{e}^{j\phi(\boldsymbol{q}_\ell)}\boldsymbol{z}_\ell)\right|^4 \\
&\qquad + \gamma_0^2 \sum_{\ell=1}^{J}\sum_{i\neq\ell}^{J}\left|(\boldsymbol{q}_i - \mathrm{e}^{j\phi(\boldsymbol{q}_i)}\boldsymbol{z}_i)^{\mathsf{H}}\boldsymbol{S}(\boldsymbol{q}_\ell - \mathrm{e}^{j\phi(\boldsymbol{q}_\ell)}\boldsymbol{z}_\ell)\right|^2.
\end{aligned} \tag{3.50}$$

Proof. See Appendix A.7. ■

Lemma 7 (MSR Local Smoothness Condition). *Under the conditions of Lemma 5, let $\beta \geq 730 + 267(J-1) + \big(1234 + 127(J-1)\big) \cdot \mathbf{1}[Q \neq 4]$, $\epsilon = (10JB\sqrt{L})^{-1}$, $\gamma_0 = 1$ and $\delta = 0.001$. Then for all vectors $\boldsymbol{q} \in E(\epsilon)$, the cost function $g(\cdot)$ satisfies*

$$\begin{aligned}
&\frac{1}{\beta}\sum_{\ell=1}^{J}\left\|\nabla_\ell g(\boldsymbol{q}) - \nabla_\ell g(\mathrm{e}^{j\phi(\boldsymbol{q}_\ell)}\boldsymbol{z})\right\|^2 \\
&\quad \leq \frac{2m_2^2 - R_2 m_2 - \delta}{19}\mathrm{dist}^2(\boldsymbol{q}, \boldsymbol{z}) + \frac{1}{20K}\sum_{k=1}^{K}\sum_{\ell=1}^{J}\left|\boldsymbol{s}_k^{\mathsf{H}}(\boldsymbol{q}_\ell - \mathrm{e}^{j\phi(\boldsymbol{q}_\ell)}\boldsymbol{z}_\ell)\right|^4 \\
&\qquad + \gamma_0^2 \sum_{\ell=1}^{J}\sum_{i\neq\ell}^{J}\left|(\boldsymbol{q}_i - \mathrm{e}^{j\phi(\boldsymbol{q}_i)}\boldsymbol{z}_i)^{\mathsf{H}}\boldsymbol{S}(\boldsymbol{q}_\ell - \mathrm{e}^{j\phi(\boldsymbol{q}_\ell)}\boldsymbol{z}_\ell)\right|^2.
\end{aligned} \tag{3.51}$$

Proof. See Appendix A.8. ■

Lemma 8 (Contraction of MSR Update Rule). *Under the conditions of Theorem 2, consider* $\boldsymbol{q}^t \in E(\epsilon)$ *and* $0 < \mu \leq 2/\beta$. *Using the update rules of Algorithm 3.2,*

$$\boldsymbol{q}_\ell^{t+1} = \boldsymbol{q}_\ell^t - \mu \nabla_\ell g(\boldsymbol{q}^t), \tag{3.52}$$

we have that $\boldsymbol{q}^{t+1} \in E(\epsilon)$ *and contraction*

$$\mathrm{dist}^2(\boldsymbol{q}^{t+1}, \boldsymbol{z}) \leq \Big(1 - \frac{2\mu}{\alpha}\Big)\mathrm{dist}^2(\boldsymbol{q}^t, \boldsymbol{z}). \tag{3.53}$$

Proof. Thanks to Lemmas 4, 6 and 7, this proof is an straightforward adaptation of [48, Lemma 7.10]. ■

3.3.5 Computational Complexity

The complexity of our algorithm lies in its initialization, its iteration, and number of iterations.

(1) The initialization step is dominated by the computation of sample covariance matrix $\boldsymbol{R}_{\boldsymbol{x}}$, whose complexity is of $\mathcal{O}(M^2K)$. Computing the largest eigenvector of $\boldsymbol{R}_{\boldsymbol{x}}$ typically has a cost of $\mathcal{O}(M^2)$ [48].

(2) The iteration cost is dominated by the products $\boldsymbol{x}_k \boldsymbol{x}_k^{\mathsf{H}} \boldsymbol{w}$, whose complexity is of $\mathcal{O}(M^2K)$. Other operations including scalar multiplications and divisions are of $\mathcal{O}(M)$ or $\mathcal{O}(MK)$ over sample-related quantities. Therefore, the iteration cost becomes dominant over the initialization cost after a few iterations.

The same analysis applies to multiple signal recovery with J sources. Succinctly, each operation repeats J times, as now there are J gradients. Therefore, the dominant cost of the multiple signal recovery variations for both algorithms are increased by a factor of J, and

the resulting total cost is J times than the single source recovery case. Table 3.1 summarizes the complexity of both proposed algorithms, where T is the number of iterations in each case.

Table 3.1: Computational complexity of proposed algorithms.

	Iteration cost	Total cost
WF-SSR	$\mathcal{O}(M^2K)$	$\mathcal{O}(M^2KT)$
WF-MSR	$\mathcal{O}(JM^2K)$	$\mathcal{O}(JM^2KT)$

3.4 Simulation Results

In our simulation tests, we consider a grant-free access scenario as described in Section 2.2.1, in which there are L sources each sequentially transmitting K independent QAM symbols with normalized average energy. The receiver has M antennas and aims to recover J distinct sources. A stationary Rayleigh channel $\boldsymbol{H}$ has i.i.d. elements $H_{ml} \sim \mathcal{N}(0, 0.5) + i\mathcal{N}(0, 0.5)$. The channel noise vector $\boldsymbol{n}_k$ has i.i.d. and circularly symmetric complex normal elements $n_m[k] \sim \mathcal{CN}(0, \sigma_w^2)$. To evaluate the recovery efficacy, we measure the total interference to signal (power) ratio TISR for each recovered source [26], defined as

$$\mathrm{TISR}_\ell = \frac{\sum_i |q_{j,i}|^2 - \max_i |q_{j,i}|^2}{\max_i |q_{j,i}|^2}, \tag{3.54}$$

where $\boldsymbol{q}_\ell = \boldsymbol{H}^{\mathsf{H}}\boldsymbol{w}_\ell$ is the equalized channel at demixer j. In SSR tests, $J = 1$ and we can drop the j index.

Our simulation uses MATLAB on a PC with an Intel Core i7-7700HQ CPU, 16GB of RAM and 64-bit OS to implement the algorithms and run the simulations. We use $T = 1000$ iterations per run of the WF algorithm, and average 100 runs to obtain our results.

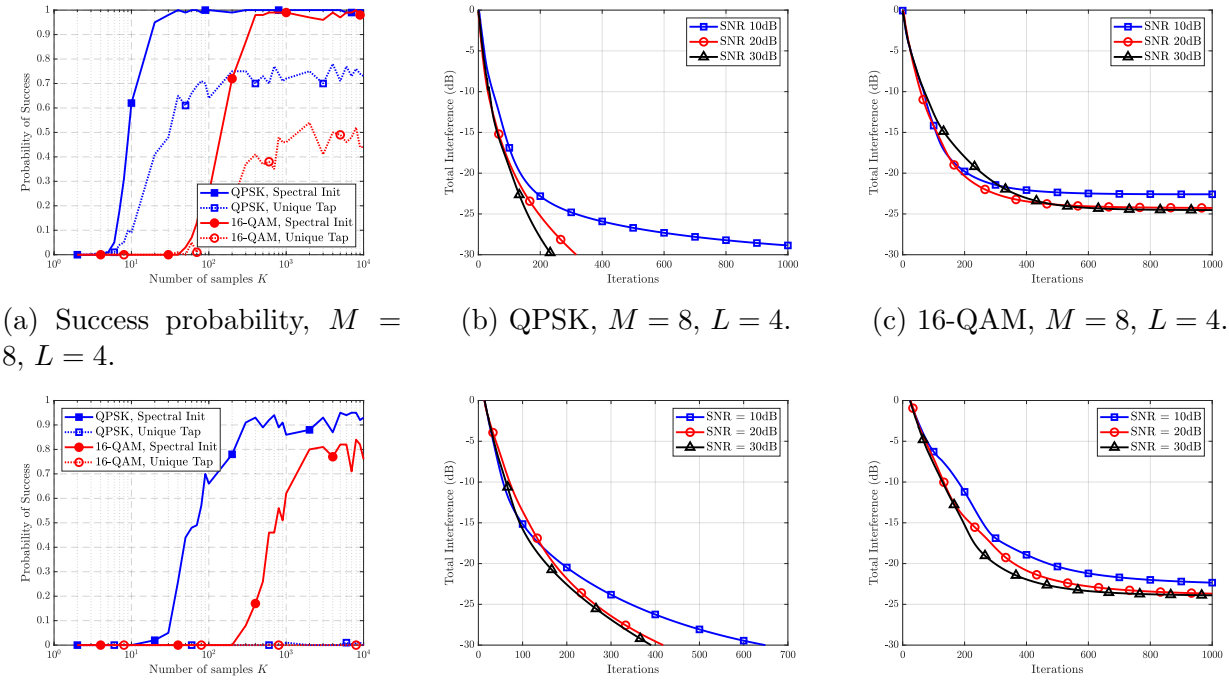

(a) Success probability, $M = 8$, $L = 4$.

(b) QPSK, $M = 8$, $L = 4$.

(c) 16-QAM, $M = 8$, $L = 4$.

(d) Success probability, $M = 16$, $L = 9$.

(e) QPSK, $M = 16$, $L = 9$.

(f) 16-QAM, $M = 16$, $L = 9$.

Figure 3.2: Numerical results of WF-CMA for single source recovery.

3.4.1 Single source recovery

To test the convergence of WF-CMA in SSR, we first consider an adaptive demixer to recover one source. We define a step-size $\mu = 5 \cdot 10^{-4} < 2/\beta$ as determined according to Theorem 1.

Figure 3.2a presents the probability of successful recovery of a single source in a noiseless system with $L = 4$ sources and $M = 8$ receiving antennas. We define "success" as the event of TISR reaching below $-20\,\mathrm{dB}$ after $T = 1000$ iterations. Two modulations (QPSK and 16-QAM) are tested. The results show that for QPSK, WF-CMA can actually converge to a solution even with a very small number of samples. For the higher-order modulation of 16-QAM, successful convergence requires about 10 times more data samples. More important, our test results show that spectral initialization of WF achieves better convergence than the traditional initialization that sets a random, unique tap of the demixer to 1 and others as 0. The higher probability of success achieved by spectral initialization empirically justifies its additional computational cost.

Figure 3.2b illustrates the average TISR under QPSK modulation under different SNR values. In this test, we used $K = 400$ samples, $L = 4$ sources and $M = 8$ receiver antennas. The results demonstrate desirable convergence with increasing number of iterations. On the other hand, Figure 3.2c shows the average TISR for 16-QAM modulation under the same test settings. For QPSK, the total interference to signal ratio can drop below $-27\,\mathrm{dB}$ even for $10\,\mathrm{dB}$ of SNR. For 16-QAM, the interference power remains several dB higher. Such results are expected for a more complex modulation without constant modulus. Nevertheless, as shown in our analytical results, the WF-CMA converges with the stepsize chosen according to Theorem 1 and successfully suppresses multi-user interference.

We repeat the experiments for a larger problem size of $L = 9$ sources and $M = 16$ receiver antennas. Under similar conditions, the success probability of the WF-CMA under different sample sizes K are also clearly shown in Figure 3.2d. These results further demonstrate the superior performance achieved using spectral initialization. Correspondingly, the average TISR is shown in Figure 3.2e and Figure 3.2f for QPSK and 16-QAM, respectively. According to our analysis, we lowered the stepsize to $\mu = 10^{-4}$ since the basin of attraction for size ϵ (depending on B) decreases with the number of sources L. The resulting WF-CMA also shows successful recovery of a single source with sufficiently high interference suppression in for both QPSK and 16-QAM at different levels of SNR.

3.4.2 Multiple source recovery

We now replicate the experiments above, attempting to simultaneously recover $J = 2$ sources at a time. We also set $\gamma_0 = 1$ and $\mu = 1 \cdot 10^{-3} < 2/\beta$ according to Theorem 2.

Figure 3.3a shows the probability of successful recovery of both sources given different numbers of samples in a noiseless system. We considered $L = 4$ sources, $M = 8$ receiving antennas for two different modulations of QPSK and 16-QAM. In the MSR case, success is defined as achieving less than $-20\,\mathrm{dB}$ TISR after $T = 1000$ iterations in each demixer, both recovering distinct sources. Once again, the required number of samples for successful

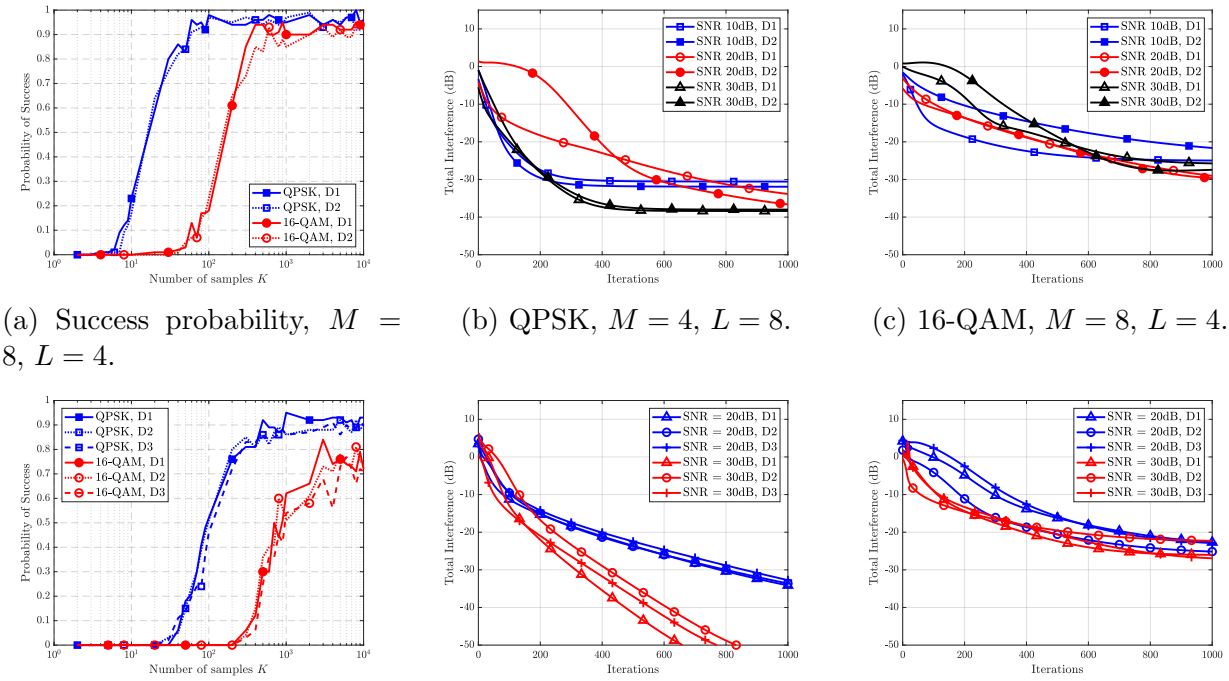

(a) Success probability, $M = 8$, $L = 4$.

(b) QPSK, $M = 4$, $L = 8$.

(c) 16-QAM, $M = 8$, $L = 4$.

(d) Success probability, $M = 16$, $L = 9$.

(e) QPSK, $M = 16$, $L = 9$.

(f) 16-QAM, $M = 16$, $L = 9$.

Figure 3.3: Numerical results of WF-CMA for multiple source recovery. We recover either $J = 2$ or $J = 3$ signals in each setting.

QPSK recovery appears quite small, whereas the number of samples required for successful 16-QAM recovery is approximately 10 times higher.

In Figure 3.3b we show the average TISR of both demixers for QPSK signals under different levels of SNR. We let $K = 400$ samples, $L = 4$ sources and $M = 8$ receiver antennas. Figure 3.3c shows the achieved TISR for 16-QAM signals under the same setup. For QPSK source signals, the average TISR drops below -30 dB for SNR of 20dB and 30dB within 400 iterations. For 16-QAM source signals, the convergence rate is noticeably slower as 16-QAM constellation exhibits variable moduli.

Next, we also consider the larger problem size with $L = 9$ sources and $M = 16$ receiver antennas. We use a stepsize of $\mu = 10^{-4}$ for the same reasons explained in the single source recovery case. Figure 3.3d shows the probability of successful recovery of both sources with under -20 dB TISR after 1000 iterations. The number of samples required for recovery

increases with a larger system size, but not significantly. Figure 3.3e and Figure 3.3f show the achieved average TISR for QPSK and 16-QAM sources, respectively. Both figures show that WF-CMA is able to recover two signals reliably at the same time.

3.5 Summary

In this chapter, we established a connection between Wirtinger Flow used in phase retrieval and CMA-based blind signal recovery in grant-free access. We generalized the convergence analysis of WF for our proposed algorithm by incorporating new conditions of subgaussian signal sources and average modulus, demonstrating its global convergence for blind signal recovery with high probability under limited data samples. We characterized the local geometry of the CM cost function in terms of local smoothness and convexity, which enables parameter updates to remain within the basin of attraction for a defined stepsize. Furthermore, we presented theoretical convergence guarantees for both single and multiple source recovery. Our numerical tests demonstrated that our proposed algorithm can solve CMA-based blind signal recovery with a fast convergence rate and reasonable computational cost.

Chapter 4

Grant-Free Access via Riemannian Blind Signal Recovery

In the previous chapter, we proposed a CMA-based source recovery method that uses regularization to recover multiple distinct source signals. Even when theoretical analysis and numerical simulations show satisfactory performance of WF-CMA, there are still aspects to be addressed. First, there is still no theoretical guarantee that spectral initialization (or any other initialization method) would yield an initial iterate within the basin of attraction of the CMA cost function. In practical scenarios, the initialization could be inadequate in different channel conditions or settings. Second, we assumed that the number of active sources was known at the BS, which might not be true in practice and the BS would need to estimate the number of sources. Finally and more importantly, regularization usually requires parameter tuning for different realizations, and often increases computational complexity.

In this chapter, we explore a Riemannian optimization framework for blind multiple signal recovery. We leverage Riemannian geometry and encode the orthogonality requirement of recovered signals into a Riemannian manifold. This new search space transforms the original signal recovery problem into an unconstrained, regularization-free optimization problem over

Part of this chapter has been previously submitted to *IEEE Transactions on Signal Processing* and is currently under review.

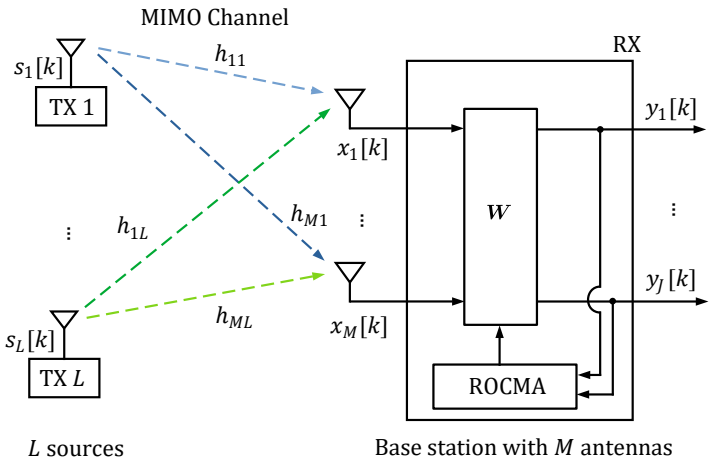

Figure 4.1: L sources share a common resource block and transmit independent signals to a host station with M antennas through an unknown physical channel. The host receiver aims to find an adaptive linear matrix demixer $\boldsymbol{W}$ to recover $J \leq L$ sources with little mutual interference.

this Riemannian manifold. By exploiting efficient, low complexity solvers, this approach demonstrates full recovery of distinct source signals without special initialization or tuning, with high probability of success and modest sample complexity compared to traditional gradient descent approaches.

4.1 Constrained Multiple Signal Recovery

Figure 4.1 depicts a blind signal recovery system, whose goal is to find multiple demixers that recover distinct source signals with minimal interference. As stated in Section 2.2.1, CMA-based multiple source recovery requires additional constraints to ensure that the process actually accomplishes this task. Several works have proposed to add regularization term(s) to the cost function (2.7) to penalize against the recovery of identical signals by more than one solution vectors in $\widehat{\boldsymbol{W}}$. For example, in [44, 45] the authors proposed adding a norm of joint cumulants for such source separation objective. Other proposals such as [47] enforce orthogonality of the combiners at each gradient descent iteration, either via orthogonal projection or Gram-Schmidt orthogonalization.

Despite their demonstrated successes, regularization approaches exhibit some drawbacks. First, the regularizing term typically requires to tune a scalar weight, e.g. γ_0 in Eq.(3.3), often by trial and error, and there is no performance guarantee under various possible scenarios. Second, different regularization approaches might lead to different solutions and performance, while no solution is consistently better than others. Additionally, regularizing terms often increase the computation complexity as regularized cost functions would either require additional computations or delicate non-convex optimization steps. Finally, regularizing terms proposed in the literature generally are limited to promote pairwise signal orthogonality instead of multi-lateral signal orthogonality, and also require more data samples to successfully suppress mutual interference.

Therefore, we now reformulate the multiple signal recovery problem and enforce signal orthogonality among demixer outputs by directly restricting the solution space. Recall the definition of $\boldsymbol{W}$ as joint demixer matrix in Section 2.2.1. Owing to the phase invariance of the CM cost function, the optimum solution satisfies $\hat{\boldsymbol{W}}^{\mathsf{H}}\boldsymbol{H} = \boldsymbol{P}$ where $\boldsymbol{P} \in \mathbb{C}^{J\times L}$ a generalized permutation matrix whose non-zero entries are all of the form $e^{j\phi}$ instead of being restricted to 1. As a result, at the optimum solution we have $\boldsymbol{P}\boldsymbol{P}^{\mathsf{H}} = \boldsymbol{I}$, with $\boldsymbol{I}$ the identity matrix of appropriate size. We therefore write the joint signal recovery constraint as

$$\hat{\boldsymbol{W}}^{\mathsf{H}}\boldsymbol{H}\boldsymbol{H}^{\mathsf{H}}\hat{\boldsymbol{W}} = \boldsymbol{I}. \tag{4.1}$$

However, the BS has no knowledge of the channel $\boldsymbol{H}$. Therefore, we can leverage source signal orthogonality and white noise property to estimate $\boldsymbol{H}\boldsymbol{H}^{\mathsf{H}}$ from the sample covariance matrix of the received data vectors $\boldsymbol{x}_k$ (2.2):

$$\boldsymbol{R}_{\boldsymbol{X}} = \frac{1}{K}\sum_{k=1}^{K}\boldsymbol{x}_k\boldsymbol{x}_k^{\mathsf{H}} \xrightarrow{K\to\infty} \mathbb{E}\{\boldsymbol{R}_{\boldsymbol{X}}\} = \boldsymbol{H}\boldsymbol{H}^{\mathsf{H}} + \sigma^2\boldsymbol{I}. \tag{4.2}$$

Note that, in the absence of noise, the rank of matrix $\boldsymbol{H}\boldsymbol{H}^{\mathsf{H}} \in \mathbb{C}^{M\times M}$ is L ($L \leq M$), i.e.,

the rank of $\boldsymbol{H}$. Thus, we formulate the optimization problem for multiple signal recovery as orthogonal constant modulus algorithm (**OCMA**):

$$\min \quad f(\boldsymbol{W}) = \frac{1}{2K} \sum_{k=1}^{K} \left\| (\boldsymbol{W}^{\mathsf{H}} \boldsymbol{X}_k \boldsymbol{W}) \circ \boldsymbol{I} - R_2 \boldsymbol{I} \right\|_F^2 \tag{4.3a}$$

$$\text{s.t.} \quad \boldsymbol{W}^{\mathsf{H}} \boldsymbol{R}_{\boldsymbol{X}} \boldsymbol{W} = \boldsymbol{I}, \tag{4.3b}$$

where $\boldsymbol{X}_k = \boldsymbol{x}_k \boldsymbol{x}_k^{\mathsf{H}}$. Hence, the Euclidean gradient of $f(\boldsymbol{W})$ is

$$\nabla_{\boldsymbol{W}} f(\boldsymbol{W}) = \frac{1}{K} \sum_{k=1}^{K} \boldsymbol{X}_k \boldsymbol{W} \big((\boldsymbol{W}^{\mathsf{H}} \boldsymbol{X}_k \boldsymbol{W}) \circ \boldsymbol{I} - R_2 \boldsymbol{I} \big), \tag{4.4a}$$

and for a matrix $\boldsymbol{G}$ of the same size as $\boldsymbol{W}$, the directional derivative of $\nabla_{\boldsymbol{W}} f(\boldsymbol{W})$ in direction $\boldsymbol{G}$ is

$$\begin{aligned} &\mathrm{D}\big(\nabla_{\boldsymbol{W}} f(\boldsymbol{W})\big)[\boldsymbol{G}] \\ &\quad = \frac{1}{K} \sum_{k=1}^{K} \Big(\boldsymbol{X}_k \boldsymbol{W} \big(\boldsymbol{I} \circ (\boldsymbol{W}^{\mathsf{H}} \boldsymbol{X}_k \boldsymbol{G} + \boldsymbol{G}^{\mathsf{H}} \boldsymbol{X}_k \boldsymbol{W}) \big) + \boldsymbol{X}_k \boldsymbol{G} \big((\boldsymbol{W}^{\mathsf{H}} \boldsymbol{X}_k \boldsymbol{W}) \circ \boldsymbol{I} - R_2 \boldsymbol{I} \big) \Big). \end{aligned} \tag{4.4b}$$

4.1.1 Estimating the Number of Active Sources for Demixing

Because of the number of active sources L may vary in practice, the literature has often assumed that L is known. However, in grant-free access, such assumption would not be practical, since, at best, we would only be able to limit the maximum number of simultaneous users according to synchronization and slotted scheduling. Thus we shall first present an approach to estimate the number of active sources.

Given that $\boldsymbol{H}$ has rank $L \leq M$, the sample covariance matrix $\boldsymbol{R}_{\boldsymbol{X}}$ in restriction (4.3b) is not strictly positive definite in the absence of noise. Thus, (4.3b) cannot be directly defined

as a Riemannian manifold. In noisy scenarios and with several data samples, the sample covariance matrix will likely be positive definite, but could be numerically ill-conditioned with large condition number. However, in both cases we can extract a strictly positive definite matrix from the sample covariance matrix from its rank-L approximation.

We first estimate the number of transmitted signals embedded in the received data via Minka's Laplace method [92], and let the result be L. Let the SVD of the channel matrix $\boldsymbol{H} = \boldsymbol{U}\boldsymbol{\Sigma}\boldsymbol{V}^{\mathsf{H}}$, with $\boldsymbol{U} \in \mathcal{U}(M)$, and $\boldsymbol{V} \in \mathcal{U}(L)$, i.e.,

$$\begin{aligned} \boldsymbol{H} &= [\boldsymbol{U}_L \; \boldsymbol{U}_L^{\perp}] \begin{bmatrix} \boldsymbol{\Sigma}_L \\ \boldsymbol{0}_{(M-L)\times L} \end{bmatrix} \boldsymbol{V}^{\mathsf{H}} = \boldsymbol{U}_L \boldsymbol{\Sigma}_L \boldsymbol{V}^{\mathsf{H}}, \\ & \boldsymbol{U}_L \in \mathrm{ST}(M \times L), \boldsymbol{U}_L^{\perp} \in \mathrm{ST}(M \times M - L), \\ & \boldsymbol{\Sigma}_L = \mathrm{diag}(\sigma_1, \ldots, \sigma_L), \end{aligned} \tag{4.5}$$

where $\mathrm{ST}(M \times L) = \{\boldsymbol{A} \in \mathbb{C}^{M \times L} : \boldsymbol{A}^{\mathsf{H}}\boldsymbol{A} = \boldsymbol{I}_L\}$ is the complex Stiefel manifold of orthonormal L-frames in $\mathbb{C}^M$ [54, 93].

First, consider the noiseless scenario, i.e. $\boldsymbol{R}_{\boldsymbol{X}} = \mathbb{E}\{\boldsymbol{R}_{\boldsymbol{X}}\}$ which equals to

$$\boldsymbol{H}\boldsymbol{H}^{\mathsf{H}} = \boldsymbol{U}\boldsymbol{\Sigma}\boldsymbol{\Sigma}^{\mathsf{H}}\boldsymbol{U}^{\mathsf{H}} = \boldsymbol{U}_L\boldsymbol{\Sigma}_L\boldsymbol{\Sigma}_L^{\mathsf{H}}\boldsymbol{U}_L^{\mathsf{H}} = \boldsymbol{U}_L\boldsymbol{\Lambda}^{\mathsf{H}}\boldsymbol{U}_L^{\mathsf{H}}. \tag{4.6}$$

From the above decomposition, we can obtain $\boldsymbol{U}$ and $\boldsymbol{\Sigma}$, but not $\boldsymbol{V}$. Also, note that $\boldsymbol{\Lambda} = \boldsymbol{\Sigma}_L\boldsymbol{\Sigma}_L^{\mathsf{H}}$ is diagonal with strictly positive entries because $\boldsymbol{H}$ has full-column rank. Both $\boldsymbol{U}_L, \boldsymbol{U}_L^{\perp}$ are full-column rank.

In the noisy case with infinite samples, we have

$$\boldsymbol{H}\boldsymbol{H}^{\mathsf{H}} + \sigma^2\boldsymbol{I} = \boldsymbol{U}\boldsymbol{\Sigma}\boldsymbol{\Sigma}^{\mathsf{H}}\boldsymbol{U}^{\mathsf{H}} + \sigma^2\boldsymbol{I} = \boldsymbol{U}\big(\boldsymbol{\Sigma}\boldsymbol{\Sigma}^{\mathsf{H}} + \sigma^2\boldsymbol{I}\big)^{\mathsf{H}}\boldsymbol{U}^{\mathsf{H}} = \boldsymbol{U}\boldsymbol{\Lambda}_1\boldsymbol{U}^{\mathsf{H}}, \tag{4.7}$$

and we form a diagonal matrix $\boldsymbol{\Lambda}$ using the L largest diagonal components of $\boldsymbol{\Lambda}_1 - \sigma^2\boldsymbol{I}$, corresponding to eigenvector matrix $\boldsymbol{U}_L$. We further define $\boldsymbol{\Sigma}_L = \boldsymbol{\Lambda}^{1/2}$. Note that σ^2 can be

estimated by, e.g., averaging the $M - L$ smallest diagonal elements of $\mathbf{\Lambda}_1$. This approach is very similar to the so-called probabilistic PCA [94], which obtains the principal components of data and a generative model. However, even though Minka's Laplace method is known for satisfactory performance in the limited sample regime, it relies on the assumption of Gaussian signals and could introduce bias when estimating the number of discrete sources.

Nevertheless, all independent sources contribute with a significant component of the sample covariance matrix, related to its significant eigenvalues, whereas noise will only have minor contributions in other directions as their related eigenvalues are much smaller in high SNR regimes. For an under-estimated L, the L-rank approximation of the sample covariance matrix would likely fail to capture all relevant directions of the channel, leading to mutual signal interference in signal recovery. Therefore, we compute the normalized L-rank approximation error

$$\frac{\left\|\boldsymbol{R}_{\boldsymbol{X}} - \boldsymbol{U}_L \mathbf{\Lambda} \boldsymbol{U}_L^{\mathsf{H}}\right\|}{\|\boldsymbol{R}_{\boldsymbol{X}}\|} \tag{4.8}$$

for comparison against a preset threshold ϵ_r to decide whether L needs to be increased in a update. We also update the L-rank approximation of the sample covariance matrix. Our test results to be shown later demonstrate the general reliability of this rank estimation method for demixing.

4.2 A Riemannian Manifold Optimization Framework for CMA

The Riemannian framework for optimization on manifolds [53] has gained a lot of attention owing to its capability to handle problems with a real-valued objective function defined on a constrained space,

$$\underset{\boldsymbol{M} \in \mathbb{C}^{m \times n}}{\text{minimize}} \quad f(\boldsymbol{M}) \quad \text{s.t.} \quad \boldsymbol{M} \in \mathcal{M}. \tag{4.9}$$

Note that the (nonlinear) space $\mathcal{M}$ may not be well-defined in terms of addition, continuity, and/or other properties that are typically exploited by regular optimization approaches in Euclidean spaces. The main idea is to redefine a constrained optimization in Euclidean space into an unconstrained optimization problem over a manifold. Manifolds are topological spaces that, equipped with a metric, locally resemble Euclidean spaces of equal dimension size, but may be quite different globally. Some manifold examples include spheres, the set of rotations, the set of positive semidefinite matrices, the set of fixed-rank matrices, and Stiefel manifolds, among many others.

In this section, we first obtain a suitable Riemannian manifold representation of the CMA problem with orthogonality constraints (4.3), which we denote Riemannian Orthogonal CMA, or ROCMA. Next, we further exploit the obtained Riemannian manifold to define a quotient Riemannian manifold, with which we can tackle the phase invariance of the demixers directly in the optimization process.

4.2.1 Redefining the Geometry of Signal Recovery

Our goal here is to find a suitable geometry that encodes the orthogonality condition of demixers in the search space of Problem (4.3). Even with a method to estimate the number of sources L, we derive a general version of the geometry where the receiver attempts to recover $J \leq L$ sources. Considering Eq.(4.6) in restriction (4.3b), we have

$$\boldsymbol{I}_J = \hat{\boldsymbol{W}}^{\mathsf{H}} \boldsymbol{H} \boldsymbol{H}^{\mathsf{H}} \hat{\boldsymbol{W}} = \hat{\boldsymbol{W}}^{\mathsf{H}} \boldsymbol{U}_L \boldsymbol{\Sigma}_L \boldsymbol{\Sigma}_L^{\mathsf{H}} \boldsymbol{U}_L^{\mathsf{H}} \hat{\boldsymbol{W}}. \tag{4.10}$$

By introducing a new variable $\boldsymbol{Y}$ such that

$$\boldsymbol{W} = \boldsymbol{U}_L \boldsymbol{\Sigma}_L^{-1} \boldsymbol{Y}, \tag{4.11}$$

Eq.(4.10) yields $\boldsymbol{Y}^{\mathsf{H}} \boldsymbol{Y} = \boldsymbol{I}_\ell$, which defines the complex Stiefel manifold $\mathrm{ST}(L \times J)$. Hence, by means of the transformation (4.11), we obtain a Riemannian manifold representation of

restriction (4.3b) as $\overline{\mathcal{M}} = \mathrm{ST}(L \times J)$ that we can use for optimization purposes. From the solution in terms of $\boldsymbol{Y}$, we obtain the demixer matrix directly by a one-to-one scaling by $\boldsymbol{U}_L \boldsymbol{\Sigma}_L^{-1}$. The variable transformation (4.11) implies the need to rewrite the cost function, Euclidean gradient, and directional derivatives of the gradient. Defining $\boldsymbol{z}_k = \boldsymbol{\Sigma}_L^{-1} \boldsymbol{U}_L^{\mathsf{H}} \boldsymbol{x}_k$ and $\boldsymbol{Z}_k = \boldsymbol{z}_k \boldsymbol{z}_k^{\mathsf{H}} = \boldsymbol{\Sigma}_L^{-1} \boldsymbol{U}_L^{\mathsf{H}} \boldsymbol{X}_k \boldsymbol{U}_L \boldsymbol{\Sigma}_L^{-1}$, we have a new cost function

$$\overline{\overline{g}}(\boldsymbol{Y}) = \frac{1}{2K} \sum_{k=1}^{K} \left\| (\boldsymbol{Y}^{\mathsf{H}} \boldsymbol{Z}_k \boldsymbol{Y}) \circ \boldsymbol{I} - R_2 \boldsymbol{I} \right\|_F^2, \tag{4.12}$$

whose Euclidean gradient is

$$\nabla_{\boldsymbol{Y}} \overline{\overline{g}}(\boldsymbol{Y}) = \frac{1}{K} \sum_{k=1}^{K} \boldsymbol{Z}_k \boldsymbol{Y} \big((\boldsymbol{Y}^{\mathsf{H}} \boldsymbol{Z}_k \boldsymbol{Y}) \circ \boldsymbol{I} - R_2 \boldsymbol{I} \big), \tag{4.13}$$

and the directional derivative of (4.13) in direction $\boldsymbol{G}$ is

$$\mathrm{D}\big(\nabla_{\boldsymbol{Y}} \overline{\overline{g}}(\boldsymbol{Y})\big)[\boldsymbol{G}] = \frac{1}{K} \sum_{k=1}^{K} \boldsymbol{Z}_k \boldsymbol{Y} \big((\boldsymbol{Y}^{\mathsf{H}} \boldsymbol{Z}_k \boldsymbol{G} + \boldsymbol{G}^{\mathsf{H}} \boldsymbol{Z}_k \boldsymbol{Y}) \circ \boldsymbol{I} \big) + \boldsymbol{Z}_k \boldsymbol{G} \big((\boldsymbol{Y}^{\mathsf{H}} \boldsymbol{Z}_k \boldsymbol{Y}) \circ \boldsymbol{I} - R_2 \boldsymbol{I} \big). \tag{4.14}$$

To optimize $\boldsymbol{Y}$ over $\overline{\mathcal{M}}$, we need to first define the linear space that approximates the manifold around a point $\boldsymbol{Y}$, which is called the tangent space at $\boldsymbol{Y}$ and is denoted as $\mathrm{T}_{\boldsymbol{Y}} \overline{\mathcal{M}}$. For $\overline{\mathcal{M}} = \mathrm{ST}(L \times J)$, the tangent space is

$$\mathrm{T}_{\boldsymbol{Y}} \overline{\mathcal{M}} = \{ \boldsymbol{E} \in \mathbb{C}^{L \times J} : \boldsymbol{E} = \boldsymbol{Y} \boldsymbol{\Omega} + \boldsymbol{Y}_{\perp} \boldsymbol{A},\, \boldsymbol{\Omega} = -\boldsymbol{\Omega}^{\mathsf{H}} \in \mathbb{C}^{J \times J}, \boldsymbol{A} \in \mathbb{C}^{(L-J) \times J} \}. \tag{4.15}$$

In other words, $\boldsymbol{Y}^{\mathsf{H}} \boldsymbol{E} = \boldsymbol{\Omega}$ is skew-Hermitian $\forall \boldsymbol{E} \in \mathrm{T}_{\boldsymbol{Y}} \overline{\mathcal{M}}$. Its orthogonal complement is known as *normal* space $\mathrm{N}_{\boldsymbol{Y}} \overline{\mathcal{M}}$ and it is given by

$$\mathrm{N}_{\boldsymbol{Y}} \overline{\mathcal{M}} = \{ \boldsymbol{Y} \boldsymbol{A},\ \boldsymbol{A} = \boldsymbol{A}^{\mathsf{H}} \in \mathbb{C}^{J \times J} \}. \tag{4.16}$$

We can now define length in the tangent space with a Riemannian metric $d_{\boldsymbol{Y}}$, which is a smooth inner product defined at each element $\boldsymbol{Y}$ for elements of the tangent space $\mathrm{T}_{\boldsymbol{Y}}\overline{\mathcal{M}}$. Here, we use the real-trace inner product, given by

$$d_{\boldsymbol{Y}}(\boldsymbol{E},\boldsymbol{C}) = \mathrm{Re}\big(\mathrm{Tr}(\boldsymbol{E}^{\mathsf{H}}\boldsymbol{C})\big)\,, \quad \boldsymbol{E},\boldsymbol{C} \in \mathrm{T}_{\boldsymbol{Y}}\overline{\mathcal{M}}. \tag{4.17}$$

We also define a projection to the tangent space, which allows us to restrict optimization only in the directions of interest, which indeed belong to the tangent space. For $\boldsymbol{G} \in \mathbb{C}^{L\times J}$, the projection operator is

$$\mathrm{Proj}^{\mathrm{T}}_{\boldsymbol{Y}}(\boldsymbol{G}) = \boldsymbol{G} - \boldsymbol{Y}\mathrm{herm}\big(\boldsymbol{Y}^{\mathsf{H}}\boldsymbol{G}\big) \in \mathrm{T}_{\boldsymbol{Y}}\overline{\mathcal{M}}\,, \tag{4.18}$$

which enables us to define the Riemannian gradient and Riemannian Hessian from the Euclidean gradient and its directional derivative, respectively.

For optimization purposes, the motion along the manifold from point $\boldsymbol{Y}$ in a given direction $\boldsymbol{E}$ is given by a retraction $\mathrm{R}^{\mathrm{St}}_{\boldsymbol{Y}}(\boldsymbol{E})$, which in our case we select as the polar retraction for the complex Stiefel manifold [93]

$$\mathrm{R}^{\mathrm{St}}_{\boldsymbol{Y}}(\boldsymbol{E}) = (\boldsymbol{Y}+\boldsymbol{E})\big((\boldsymbol{Y}+\boldsymbol{E})^{\mathsf{H}}(\boldsymbol{Y}+\boldsymbol{E})\big)^{-0.5} = (\boldsymbol{Y}+\boldsymbol{E})\big(\boldsymbol{I}+\boldsymbol{E}^{\mathsf{H}}\boldsymbol{E}\big)^{-0.5}. \tag{4.19}$$

4.2.2 Riemannian Quotient Geometry

In the context of Riemannian manifold optimization, quotient Riemannian manifolds are used to define a manifold that presents invariance of the cost function or the representation of the manifold itself [95]. It can be defined by equipping the original or ambient manifold with an equivalence relation between its points to describe the aforementioned invariance.

Let $\sim$ be such an equivalence relation, i.e., $\boldsymbol{Y} \sim \boldsymbol{Y}_0$ denotes that $\boldsymbol{Y}$ and $\boldsymbol{Y}_0$ are equivalent in terms of the invariance of interest. Thus, we can identify equivalent points to $\boldsymbol{Y}$ as one

single set known as equivalence class, denoted as

$$[\boldsymbol{Y}] = \{\boldsymbol{Y}_0 \in \mathcal{M} : \boldsymbol{Y}_0 \sim \boldsymbol{Y}\}. \tag{4.20}$$

When the quotient space of the ambient manifold $\overline{\mathcal{M}}$ under the equivalence relation $\sim$ satisfies certain conditions [53, Chapter 3], it is a Riemannian quotient manifold, which is the set of equivalence classes:

$$\mathcal{M} = \overline{\mathcal{M}}/\sim = \big\{[\boldsymbol{Y}] : \boldsymbol{Y} \in \overline{\mathcal{M}}\big\}. \tag{4.21}$$

A quotient manifold is an abstract space whose elements are subsets of the ambient manifold. However, the use of quotient manifolds in Riemannian optimization has additional advantages, such as the ability of obtaining a strictly positive definite Hessian by neglecting directions related to the cost function invariance, and potential reduction of problem dimensionality by applying a simple representation of the elements in the space. Even in a case when there is no such representation and the ambient manifold is used for computational purposes, the quotient geometry is theoretically important to establish convergence properties of second-order methods that rely on the positive definiteness of the Hessian on the manifold.

Now, recall that the cost function (4.3a) presents permutation invariance in the demixers, and unimodular phase invariance in each demixer such that for each demixer $\boldsymbol{w}_\ell$, a rotated demixer $\mathrm{e}^{j\theta}\boldsymbol{w}_\ell, \theta \in [0, 2\pi]$ yields the same cost value. However, the permutation group is discrete, and thus is a Lie group of dimension 0. This means that in terms of local behavior, the equivalence classes of permutations behaves exactly the same as the ambient manifold, and thus we dismiss the permutations in our analysis and focus exclusively in the phase invariance.

When considering multiple demixers in $\boldsymbol{W}$, we want to describe unimodular phase invariance on each of the J demixers simultaneously. Let $\mathcal{U}(1)^{\times J}$ be the group of diagonal

unitary matrices of size J, i.e.

$$\mathcal{U}(1)^{\times J} = \Big\{ \boldsymbol{D} \in \mathcal{U}(J) : \boldsymbol{D} = \operatorname{diag}\big(\mathrm{e}^{j\theta_1} \ \cdots \ \mathrm{e}^{j\theta_J}\big) \,,\, \theta_\ell \in [0, 2\pi) \,\forall \ell \in \{1, \cdots, J\} \Big\}.$$

Thus, the group action of $\mathcal{U}(1)^{\times J}$ defines an equivalence relation between demixer matrices. The corresponding equivalence class is then

$$[\boldsymbol{W}] = \big\{ \boldsymbol{W}\boldsymbol{D} : \boldsymbol{D} \in \mathcal{U}(1)^{\times J} \big\},$$

and by means of (4.11), we have that $\boldsymbol{W}\boldsymbol{D} = \boldsymbol{U}_L \boldsymbol{\Sigma}_L^{-1} \boldsymbol{Y}\boldsymbol{D}$, i.e. the equivalence class in terms of $\boldsymbol{Y}$ is

$$[\boldsymbol{Y}] = \big\{ \boldsymbol{Y}\boldsymbol{D} : \boldsymbol{D} \in \mathcal{U}(1)^{\times J} \big\}, \tag{4.22}$$

and we obtain a quotient space that considers the cost function invariance as

$$\mathcal{M} = \overline{\mathcal{M}} / \mathcal{U}(1)^{\times J} \tag{4.23}$$

with a canonical projection $\pi : \overline{\mathcal{M}} \to \mathcal{M} : \boldsymbol{Y} \mapsto [\boldsymbol{Y}]$.

Furthermore, $\mathcal{M}$ is indeed a Riemannian quotient manifold (which ensures π is smooth). This follows from the fact that the group action of diagonal unitary matrices is smooth, free and proper [95, Section 9.2]: (a) it is smooth because it is a matrix multiplication; (b) it is free because $\boldsymbol{Y}\boldsymbol{D} = \boldsymbol{Y}$ implies $\boldsymbol{D} = \boldsymbol{I}$ by left multiplication of $\boldsymbol{Y}^{\mathsf{H}}$; and (c) it is proper because $\mathcal{U}(1)^{\times J}$ is the maximal torus of the unitary group (a compact group), and thus is compact. Hence, the equivalence classes all have dimension J and are closed embedded submanifolds of $\mathcal{M}$. This quotient manifold has been introduced before in the context of subspace estimation [96], but to the best of our knowledge it has not been developed or used in Riemannian optimization.

The quotient manifold $\mathcal{M}$ is an abstract space, and requires matrix representations in the computational space $\overline{\mathcal{M}}$. Fortunately, an (abstract) element $\boldsymbol{Y}_q$ on the quotient manifold can be represented by an element $\boldsymbol{Y}$ in the computational space. Thus, every geometry-related operation over the quotient manifold can be defined in terms of elements and operations in the computational space.

In particular, we look for a representation of the tangent space of the quotient manifold $\mathrm{T}_{\boldsymbol{Y}}\mathcal{M}$ using tangent vectors of the ambient manifold $\overline{\mathcal{M}}$. We accomplish this by characterizing the tangent space $\mathrm{T}_{\boldsymbol{Y}}\overline{\mathcal{M}}$ as the direct sum of two orthogonal spaces: the *vertical* space $\mathrm{V}_{\boldsymbol{Y}}$, which contains the directions tangent to the equivalence classes, and the *horizontal* space $\mathrm{H}_{\boldsymbol{Y}}$, which contains the tangent directions orthogonal to the vertical space. That is, the horizontal space contains the directions of interest in terms of optimization. Hence, an (abstract) tangent vector of the quotient manifold $\boldsymbol{\eta}_{[\boldsymbol{Y}]}$ can be represented as an horizontal vector $\boldsymbol{\eta}_{\mathrm{H}_{\boldsymbol{Y}}}$ of the ambient manifold, which is called the *horizontal lift*, defined as $\boldsymbol{\eta}_{\mathrm{H}_{\boldsymbol{Y}}} = \mathrm{lift}_{\boldsymbol{Y}}(\boldsymbol{\eta}_{[\boldsymbol{Y}]})$. When $\mathcal{M}$ is endowed with the Riemannian metric inherited from $\overline{\mathcal{M}}$,

$$d_{[\boldsymbol{Y}]}(\boldsymbol{\eta}, \boldsymbol{\xi}) = d_{\boldsymbol{Y}}\left(\mathrm{lift}_{\boldsymbol{Y}}(\boldsymbol{\eta}), \mathrm{lift}_{\boldsymbol{Y}}(\boldsymbol{\xi})\right), \ \boldsymbol{\eta}, \boldsymbol{\xi} \in \mathrm{T}_{[\boldsymbol{Y}]}\mathcal{M},$$

the canonical projection π forms a Riemannian submersion from the quotient manifold to the computational space, thereby defining a correspondence between elements of $\mathcal{M}$ and elements of $\overline{\mathcal{M}}$ [53]. Figure 4.2 shows a depiction of the quotient manifold geometry and its relation to the ambient manifold.

We now define the vertical and horizontal spaces. Let $\boldsymbol{D} : \mathbb{R} \to \mathcal{U}(1)^{\times J}$ be a path in the equivalence class such that $\boldsymbol{D}(0) = \boldsymbol{I}$. The vertical space is given by vectors of the form $\boldsymbol{Y}\boldsymbol{D}'(0)$ where vectors $\boldsymbol{D}'(t)$ are tangent to $\mathcal{U}(1)^{\times J}$, whose tangent set corresponds to the Lie algebra of unitary diagonal matrices $\mathfrak{t}(J)$, consisting of diagonal imaginary matrices of

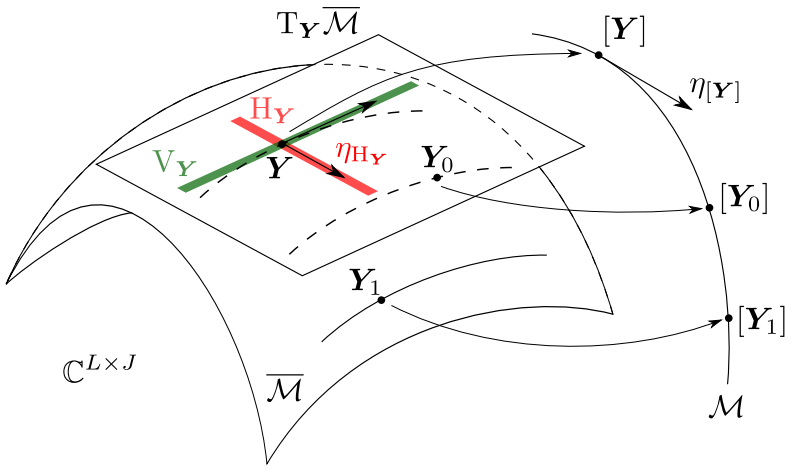

Figure 4.2: Representation of the ambient manifold $\overline{\mathcal{M}}$ and quotient manifold $\mathcal{M}$. The tangent space $\mathrm{T}_{\boldsymbol{Y}}\overline{\mathcal{M}}$ is divided into a vertical space $\mathrm{V}_{\boldsymbol{Y}}$ (in green) and a horizontal space $\mathrm{H}_{\boldsymbol{Y}}$ (in red), which contains the relevant search directions $\eta_{\mathrm{H}_{\boldsymbol{Y}}}$. These directions correspond to tangent directions $\eta_{[\boldsymbol{Y}]}$ at the point $[\boldsymbol{Y}]$ in the quotient manifold.

size $J \times J$. Therefore,

$$\mathrm{V}_{\boldsymbol{Y}} = \big\{\boldsymbol{Y}\boldsymbol{T} : \boldsymbol{T} \in \mathfrak{t}(J)\big\} = \{\boldsymbol{Y}\boldsymbol{T} : \boldsymbol{T} \in \mathbb{C}^{J\times J} \text{ diagonal imaginary}\}, \tag{4.24}$$

and the horizontal space is then given by

$$\begin{aligned}
\mathrm{H}_{\boldsymbol{Y}} = \big(\mathrm{V}_{\boldsymbol{Y}}\big)^{\perp} &= \{\boldsymbol{E} \in \mathrm{T}_{\boldsymbol{Y}}\mathcal{M} : \langle \boldsymbol{E}, \boldsymbol{F}\rangle = 0 \quad \forall \boldsymbol{F} \in \mathrm{V}_{\boldsymbol{Y}}\} \\
&= \{\boldsymbol{E} \in \mathrm{T}_{\boldsymbol{Y}}\mathcal{M} : \langle \boldsymbol{E}, \boldsymbol{Y}\boldsymbol{T}\rangle = 0 \quad \forall \boldsymbol{T} \in \mathfrak{t}(J)\} \\
&= \{\boldsymbol{E} \in \mathrm{T}_{\boldsymbol{Y}}\mathcal{M} : \mathrm{Re}\big(\mathrm{Tr}(\boldsymbol{E}^{\mathsf{H}}\boldsymbol{Y}\boldsymbol{T})\big) = 0 \quad \forall \boldsymbol{T} \in \mathfrak{t}(J)\}
\end{aligned} \tag{4.25}$$

and thus $\boldsymbol{Y}^{\mathsf{H}}\boldsymbol{E}$ is skew-Hermitian with zero diagonal, to be orthogonal to any $\boldsymbol{T} \in \mathfrak{t}(J)$. This is equivalent to state that the projection to horizontal space is given by

$$\begin{aligned}
\mathrm{Proj}^{\mathrm{H}}_{\boldsymbol{Y}}(\boldsymbol{G}) &= \mathrm{Proj}^{\mathrm{T}}_{\boldsymbol{Y}}(\boldsymbol{G}) - \boldsymbol{Y}\Big(\boldsymbol{I} \circ \big(\boldsymbol{Y}^{\mathsf{H}}\mathrm{Proj}^{\mathrm{T}}_{\boldsymbol{Y}}(\boldsymbol{G})\big)\Big) \\
&= \boldsymbol{G} - \boldsymbol{Y}\mathrm{herm}\big(\boldsymbol{Y}^{\mathsf{H}}\boldsymbol{G}\big) - \boldsymbol{Y}\big(\boldsymbol{I} \circ \mathrm{skew}(\boldsymbol{Y}^{\mathsf{H}}\boldsymbol{G})\big).
\end{aligned} \tag{4.26}$$

Finally, we can inherit the retraction from the ambient manifold via lifting and enforcing the equivalence class. Indeed, for $\boldsymbol{E} = \mathrm{lift}_{\boldsymbol{Y}}(\boldsymbol{\eta})$, we can see that the polar retraction depends only on the equivalence class:

$$\mathrm{R}_{[\boldsymbol{Y}]}(\boldsymbol{\eta}) = \mathrm{R}^{\mathrm{St}}_{\boldsymbol{YD}}(\boldsymbol{E}) = (\boldsymbol{YD} + \boldsymbol{ED})\big(\boldsymbol{I} + (\boldsymbol{ED})^{\mathsf{H}}\boldsymbol{ED}\big)^{-0.5} = \mathrm{R}^{\mathrm{St}}_{\boldsymbol{Y}}(\boldsymbol{E})\boldsymbol{D} = \big[\mathrm{R}^{\mathrm{St}}_{\boldsymbol{Y}}(\boldsymbol{E})\big]. \quad (4.27)$$

Consequently, we can effectively optimize over the quotient manifold $\mathcal{M}$ using representatives from the ambient manifold $\overline{\mathcal{M}}$. Moreover, as $\overline{\mathcal{M}}$ is an embedded submanifold of Euclidean space, we can obtain the Riemannian gradient and Hessian in terms of objects in Euclidean space, which is convenient as we already know the cost function $\overline{\overline{g}}$ in Euclidean space given by (4.12) with corresponding derivatives (4.13) and (4.14). We denote $\overline{g} = \overline{\overline{g}}\big|_{\overline{\mathcal{M}}}$ the restriction of the Euclidean cost function to the ambient manifold. As $\overline{g}$ is invariant under $\sim$, the cost function g defined in $\mathcal{M}$ is smooth and $g([\boldsymbol{Y}]) = \overline{g}(\boldsymbol{Y})$. Hence, by definition, the Riemannian gradient of g is zero for vertical vectors (as they are invariance directions), and we have

$$\mathrm{lift}_{\boldsymbol{Y}}\big(\mathrm{grad}_{[\boldsymbol{Y}]}g([\boldsymbol{Y}])\big) = \mathrm{grad}_{\boldsymbol{Y}}\overline{g}(\boldsymbol{Y}) = \mathrm{Proj}^{\mathrm{H}}_{\boldsymbol{Y}}\big(\nabla_{\boldsymbol{Y}}\overline{\overline{g}}(\boldsymbol{Y})\big) = \mathrm{Proj}^{\mathrm{T}}_{\boldsymbol{Y}}\big(\nabla_{\boldsymbol{Y}}\overline{\overline{g}}(\boldsymbol{Y})\big), \quad (4.28)$$

where we can choose the most convenient projection to obtain the lifted gradient, thus we use the projection to tangent space:

$$\begin{aligned}\mathrm{lift}_{\boldsymbol{Y}}\big(\mathrm{grad}_{[\boldsymbol{Y}]}g([\boldsymbol{Y}]\big) &= \mathrm{Proj}^{\mathrm{T}}_{\boldsymbol{Y}}\big(\nabla_{\boldsymbol{Y}}\overline{\overline{g}}(\boldsymbol{Y})\big) = \nabla_{\boldsymbol{Y}}\overline{\overline{g}}(\boldsymbol{Y}) - \boldsymbol{Y}\mathrm{herm}\big(\boldsymbol{Y}^{\mathsf{H}}\nabla_{\boldsymbol{Y}}\overline{\overline{g}}(\boldsymbol{Y})\big) \\ &= \frac{1}{K}\sum_{k=1}^{K}\boldsymbol{Z}_k\boldsymbol{Y}\big((\boldsymbol{Y}^{\mathsf{H}}\boldsymbol{Z}_k\boldsymbol{Y}) \circ \boldsymbol{I} - R_2\boldsymbol{I}\big) - \boldsymbol{Y}\mathrm{herm}\big(\boldsymbol{Y}^{\mathsf{H}}\boldsymbol{Z}_k\boldsymbol{Y}\big((\boldsymbol{Y}^{\mathsf{H}}\boldsymbol{Z}_k\boldsymbol{Y}) \circ \boldsymbol{I} - R_2\boldsymbol{I}\big)\big).\end{aligned} \quad (4.29)$$

The horizontal lift of the Riemannian Hessian of g in terms of $\overline{\overline{g}}$ is given by

$$\mathrm{lift}_{\boldsymbol{Y}}\big(\mathrm{Hess}_{[\boldsymbol{Y}]}g([\boldsymbol{Y}])[\boldsymbol{\eta}]\big) = \mathrm{Proj}^{\mathrm{H}}_{\boldsymbol{Y}}\big(\mathrm{Hess}_{\boldsymbol{Y}}\overline{g}(\boldsymbol{Y})[\boldsymbol{E}]\big)\mathrm{Proj}^{\mathrm{H}}_{\boldsymbol{Y}}\big(\mathrm{D}\overline{\overline{r}}(\boldsymbol{Y})[\boldsymbol{E}]\big), \quad (4.30)$$

with $\boldsymbol{E} = \mathrm{lift}_{\boldsymbol{Y}}(\boldsymbol{\eta})$ and $\overline{\overline{r}}$ a smooth extension of $\mathrm{grad}_{\boldsymbol{Y}}\overline{g}$ to a neighborhood of $\overline{\mathcal{M}}$ in Euclidean space $\mathbb{C}^{L\times J}$. An obvious choice is

$$\begin{aligned}\overline{\overline{r}}(\boldsymbol{Y}) &= \nabla_{\boldsymbol{Y}}\overline{\overline{g}}(\boldsymbol{Y}) - \boldsymbol{Y}\mathrm{herm}\big(\boldsymbol{Y}^{\mathsf{H}}\nabla_{\boldsymbol{Y}}\overline{\overline{g}}(\boldsymbol{Y})\big)\\ &= \frac{1}{K}\sum_{k=1}^{K}\boldsymbol{Z}_k\boldsymbol{Y}\big((\boldsymbol{Y}^{\mathsf{H}}\boldsymbol{Z}_k\boldsymbol{Y})\circ\boldsymbol{I} - R_2\boldsymbol{I}\big) - \boldsymbol{Y}\mathrm{herm}\big(\boldsymbol{Y}^{\mathsf{H}}\boldsymbol{Z}_k\boldsymbol{Y}\big((\boldsymbol{Y}^{\mathsf{H}}\boldsymbol{Z}_k\boldsymbol{Y})\circ\boldsymbol{I} - R_2\boldsymbol{I}\big)\big),\end{aligned}$$

with directional derivatives

$$\mathrm{D}\overline{\overline{r}}(\boldsymbol{Y})[\boldsymbol{G}] = \mathrm{D}\big(\nabla_{\boldsymbol{Y}}\overline{\overline{g}}(\boldsymbol{Y})\big)[\boldsymbol{G}] - \boldsymbol{G}\mathrm{herm}\big(\boldsymbol{Y}^{\mathsf{H}}\nabla_{\boldsymbol{Y}}\overline{\overline{g}}(\boldsymbol{Y})\big) - \boldsymbol{Y}\mathrm{herm}\big(\mathrm{D}\big(\boldsymbol{Y}^{\mathsf{H}}\nabla_{\boldsymbol{Y}}\overline{\overline{g}}(\boldsymbol{Y})\big)[\boldsymbol{G}]\big),$$

and the lifted Riemannian Hessian is

$$\begin{aligned}&\mathrm{lift}_{\boldsymbol{Y}}\big(\mathrm{Hess}_{[\boldsymbol{Y}]}g\big([\boldsymbol{Y}]\big)[\boldsymbol{\eta}]\big)\\ &\quad= \mathrm{Proj}^{\mathrm{H}}_{\boldsymbol{Y}}\Big(\mathrm{D}\big(\nabla_{\boldsymbol{Y}}\overline{\overline{g}}(\boldsymbol{Y})\big)[\boldsymbol{E}] - \boldsymbol{E}\mathrm{herm}\big(\boldsymbol{Y}^{\mathsf{H}}\nabla_{\boldsymbol{Y}}\overline{\overline{g}}(\boldsymbol{Y})\big) - \boldsymbol{Y}\mathrm{herm}\big(\mathrm{D}\big(\boldsymbol{Y}^{\mathsf{H}}\nabla_{\boldsymbol{Y}}\overline{\overline{g}}(\boldsymbol{Y})\big)[\boldsymbol{E}]\big)\Big)\\ &\quad= \mathrm{Proj}^{\mathrm{H}}_{\boldsymbol{Y}}\Big(\mathrm{D}\big(\nabla_{\boldsymbol{Y}}\overline{\overline{g}}(\boldsymbol{Y})\big)[\boldsymbol{E}] - \boldsymbol{E}\mathrm{herm}\big(\boldsymbol{Y}^{\mathsf{H}}\nabla_{\boldsymbol{Y}}\overline{\overline{g}}(\boldsymbol{Y})\big)\Big),\end{aligned} \tag{4.31}$$

where the last term of the first equality vanishes through the horizontal projection, because the term belongs to the normal space and $\mathrm{H}_{\boldsymbol{Y}} \subset \mathrm{T}_{\boldsymbol{Y}}\overline{\mathcal{M}} \perp \mathrm{N}_{\boldsymbol{Y}}\overline{\mathcal{M}}$.

Table 4.1 summarizes the geometric definitions of the quotient manifold $\mathcal{M}$ (using representatives in $\overline{\mathcal{M}}$) for ROCMA. Readers interested in additional details of the quotient manifold discussions may refer to [95, Chapter 9].

4.2.3 Riemannian Optimization for Blind Signal Recovery

We use a Riemannian Trust-Region (RTR) algorithm, which is a second-order optimization approach with superlinear convergence rate [97]. At each iteration, to search a direction $\boldsymbol{E}$

in the horizontal space $\mathrm{H}_{\boldsymbol{Y}}$ of iterate $\boldsymbol{Y} \in \overline{\mathcal{M}}$, RTR solves the trust-region subproblem

$$\begin{aligned} \mathcal{T}: \ \underset{\boldsymbol{E}\in \mathrm{H}_{\boldsymbol{Y}}}{\text{minimize}} \quad & q_{\boldsymbol{Y}}(\boldsymbol{E}) \\ \text{s.t.} \quad & d_{\boldsymbol{Y}}(\boldsymbol{E},\boldsymbol{E}) \leq \varepsilon^2 \end{aligned} \tag{4.32}$$

in the ambient manifold, where $q_{\boldsymbol{Y}}$ is a quadratic model of the cost function at $\boldsymbol{Y} \in \overline{\mathcal{M}}$, and ε denotes the trust region radius. The model is given by

$$q_{\boldsymbol{Y}}(\boldsymbol{E}) = \overline{g}(\boldsymbol{Y}) + d_{\boldsymbol{Y}}\Big(\boldsymbol{E}, \mathrm{grad}_{\boldsymbol{Y}}\overline{g}(\boldsymbol{Y})\Big) + \frac{1}{2} d_{\boldsymbol{Y}}\Big(\boldsymbol{E}, \mathrm{Proj}^{\mathrm{H}}_{\boldsymbol{Y}}\big(\mathrm{Hess}_{\boldsymbol{Y}}\overline{g}(\boldsymbol{Y})[\boldsymbol{E}]\big)\Big),$$

using the horizontal lifts of both Riemannian gradient and Hessian derived in Eqs.(4.28)-(4.31). In its general formulation, RTR uses a self-adjoint linear operator instead of the Riemannian Hessian for ease of computation, but can obtain a better performance match using the Hessian.

Table 4.1: Riemannian geometry definitions required for manifold optimization of ROCMA.

Name	Definition
Computational space $\overline{\mathcal{M}}$	$\mathrm{ST}(L \times J)$
Quotient space $\mathcal{M} = \overline{\mathcal{M}}/\sim$	$\mathrm{ST}(L \times J)/\mathcal{U}(1)^{\times J}$
Horizontal space $\mathrm{H}_{\boldsymbol{Y}}$	$\mathrm{H}_{\boldsymbol{Y}} = \{\boldsymbol{E} \in \mathrm{T}_{\boldsymbol{Y}}\overline{\mathcal{M}} : \mathrm{Re}\big(\mathrm{Tr}(\boldsymbol{E}^{\mathsf{H}}\boldsymbol{Y}\boldsymbol{T})\big) = 0 \quad \forall \boldsymbol{T} \in \mathfrak{t}(J)\}$
Horizontal space projection $\mathrm{Proj}^{\mathrm{H}}_{\boldsymbol{Y}}$	$\mathrm{Proj}^{\mathrm{H}}_{\boldsymbol{Y}}(\boldsymbol{G}) = \boldsymbol{G} - \boldsymbol{Y}\mathrm{herm}\big(\boldsymbol{Y}^{\mathsf{H}}\boldsymbol{G}\big) - \boldsymbol{Y}\big(\boldsymbol{I} \circ \mathrm{skew}(\boldsymbol{Y}^{\mathsf{H}}\boldsymbol{G})\big)$
Riemannian metric $d_{\boldsymbol{Y}}$	$d_{\boldsymbol{Y}}(\boldsymbol{E},\boldsymbol{C}) = \mathrm{Re}\big(\mathrm{Tr}(\boldsymbol{E}^{\mathsf{H}}\boldsymbol{C})\big)$, $\boldsymbol{E},\boldsymbol{C} \in \mathrm{H}_{\boldsymbol{Y}}$
Retraction $\mathrm{R}^{\mathrm{St}}_{\boldsymbol{Y}}$	$\mathrm{R}^{\mathrm{St}}_{\boldsymbol{Y}}(\boldsymbol{E}) = (\boldsymbol{Y}+\boldsymbol{E})\big(\boldsymbol{I} + \boldsymbol{E}^{\mathsf{H}}\boldsymbol{E}\big)^{-0.5}$
Riemannian gradient $\mathrm{grad}_{[\boldsymbol{Y}]}g$	$\mathrm{lift}_{\boldsymbol{Y}}\big(\mathrm{grad}_{[\boldsymbol{Y}]}g([\boldsymbol{Y}]\big) = \mathrm{Proj}^{\mathrm{T}}_{\boldsymbol{Y}}\big(\nabla_{\boldsymbol{Y}}\overline{\overline{g}}(\boldsymbol{Y})\big)$
Riemannian Hessian $\mathrm{Hess}_{[\boldsymbol{Y}]}g$	$\mathrm{lift}_{\boldsymbol{Y}}\big(\mathrm{Hess}_{[\boldsymbol{Y}]}g(\boldsymbol{Y})[\boldsymbol{E}]\big)$ $= \mathrm{Proj}^{\mathrm{H}}_{\boldsymbol{Y}}\Big(\mathrm{D}\big(\nabla_{\boldsymbol{Y}}\overline{\overline{g}}(\boldsymbol{Y})\big)[\boldsymbol{E}] - \boldsymbol{E}\mathrm{herm}\big(\boldsymbol{Y}^{\mathsf{H}}\nabla_{\boldsymbol{Y}}\overline{\overline{g}}(\boldsymbol{Y})\big)\Big)$

We can now define the ROCMA algorithm as summarized in Algorithm 4.1. Succinctly, we first initialize by estimating the number of sources L, perform an L-rank eigendecomposition that removes noise contribution in eigenvalues, and by corroborating that the L-rank approximation is close to the sample covariance matrix to adjust L if needed. After scaling the data vectors, we define cost function, quotient Riemannian manifold, and geometry operations. Thereafter, we determine Riemannian Trust Regions: in each iteration we solve

the trust-regions subproblem $\mathcal{T}$ in the horizontal space of the current iterate, obtaining a descent direction $\boldsymbol{E}$ in the horizontal space $\mathrm{H}_{\boldsymbol{Y}}$, whose magnitude is given by the size of the accepted trust region [53]. The subsequent solution iterate is computed using the retraction of $\boldsymbol{E}$, which brings the result back to the manifold. Once the algorithm converges, we compute the demixer matrix by scaling the obtained solution with $\boldsymbol{U}_L\boldsymbol{\Sigma}_L^{-1}$.

Algorithm 4.1 Riemannian Orthogonal CMA (ROCMA)

Given: $\boldsymbol{x}_k \in \mathbb{C}^M$, $k \in \{1, \ldots, K\}$, trust region radius ε, low-rank approximation tolerance ϵ_r

A) Source estimation:

Estimate number of independent sources L with Minka's Laplace method
Obtain L largest eigenvalues and corresponding eigenvectors of sample covariance matrix $\boldsymbol{R}_{\boldsymbol{X}}$ to construct L-rank approximation $\boldsymbol{R}_{\boldsymbol{X}} = \sum_k \boldsymbol{x}_k\boldsymbol{x}_k^{\mathsf{H}} \approx \boldsymbol{U}_L\boldsymbol{\Sigma}_L^2\boldsymbol{U}_L^{\mathsf{H}}$
while $\|\boldsymbol{R}_{\boldsymbol{X}} - \boldsymbol{U}_L\boldsymbol{\Sigma}_L^2\boldsymbol{U}_L^{\mathsf{H}}\| > \epsilon_r\|\boldsymbol{R}_{\boldsymbol{X}}\|$ **do**
    $L = L + 1$
    Update $\boldsymbol{\Sigma}_L$, $\boldsymbol{\Sigma}_L$ and $\boldsymbol{U}_L$ with new components
end while

B) Initialization:

Define $\boldsymbol{z}_k = \boldsymbol{\Sigma}_L^{-1}\boldsymbol{U}_L^{\mathsf{H}}\boldsymbol{x}_k$ and objective function g
Define geometry ingredients of $\mathcal{M}$ with representatives in $\overline{\mathcal{M}}$ according to Table 4.1

C) Riemannian Trust Regions:

while not converged **do**
    Obtain descent direction $\boldsymbol{E}_t$ by solving $\mathcal{T}$ in $\mathrm{H}_{\boldsymbol{Y}_t}$
    $\boldsymbol{Y}_{t+1} = \mathrm{R}^{\mathrm{St}}_{\boldsymbol{Y}_t}(\boldsymbol{E}_t)$
end while
$\boldsymbol{W}_{\text{final}} = \boldsymbol{U}_L\boldsymbol{\Sigma}_L^{-1}\boldsymbol{Y}_{\text{final}}$

A known algorithm to solve the trust-region subproblem $\mathcal{Q}$ based in a truncated Conjugate Gradient approach is available as Algorithm 11 in [53, Section 7.3]. The manifold optimization toolbox Manopt [98] implements a variation of this algorithm. We use this open-source toolbox Manopt in our implementation of Algorithm 4.1 by leveraging its flexibility for selectable choices of stopping criteria, tolerances, and other parameters.

4.3 Convergence and Analysis

4.3.1 Convergence Conditions and Properties of CMA

The global convergence properties of CMA for a single PAM or QAM source recovery in noiseless scenarios are well known [26, Chapters 4-7]. The case of SIMO-CMA blind equalizers, also known as fractionally-spaced CMA or CMA-FSE (when applied to blind equalization scenarios), correspond to the case of recovering one transmitted signal in a grant-free scenario. The CMA-FSE equalizer has guaranteed global convergence so long as the channel matrix H has full column rank [29]. Additionally, in [99] the authors show that in the asymptotic regime and under the aforementioned assumptions, for all stable critical points (desirable or not) the only direction of invariance of the CMA cost function corresponds to the 1-dimensional manifold of rotations of the combiner, or $\mathcal{U}(1)$ using our notation in this chapter. This invariance result is exploited in [100] to further establish conditions for convergence of CMA and adapt a Newton method, discarding search directions in the equivalence class of rotations.

Multi-channel CMA equalizers are an extension of CMA-FSE, where multiple transmitters simultaneously send independent source signals on a set of shared channels. Targeting one source signal, we can apply CMA to update a receiver equalizer that recovers the signal with minimal co-channel multi-user interference and minimum inter-symbol interference (ISI) [45, 101]. Global convergence of MIMO-CMA equalizers have similar requirements as the case of CMA-FSE equalizers, which in turn is equivalent to have the channel convolution matrix $\boldsymbol{H}$ with full column rank. Thus, channel matrix $\boldsymbol{H}$ of full-column rank provides guaranteed global convergence in noiseless scenarios. Multiple source recovery as presented here is a special case of the multiple source recovery scheme presented in [45] with zero-ISI subchannels. Thus, global convergence is also guaranteed under similar conditions. The effect of moderate channel noises on CMA has been shown to be mild by introducing additional local minima in the vicinity of the global solution [102, 103]. Hence, in the following

we will always assume that the channel matrix $\boldsymbol{H}$ has full-column rank.

However, most of these works focus in the asymptotic behavior of the CMA cost function and its geometry. Under finite data sample, our recent work [104] provides the first analysis for CMA-based source recovery. Our findings in [104] show that despite being non-convex, the CMA cost function is geometrically well-behaved in terms of strong convexity and bounded curvature in a neighborhood of the optimal solutions. The CMA convergence is therefore tractable in the non-asymptotic case. In the remainder of this section, we shall utilize some of the recent results to bound the minimum eigenvalue of the Euclidean Hessian, in order to provide convergence guarantee for RTR.

4.3.2 Known Results in Relation to ROCMA

Riemannian manifold optimization with different solvers, such as Riemannian Trust-Regions, has well-known convergence guarantees [97] over several classical manifolds, such as the Stiefel manifold and the generalized Stiefel manifold, [93], the Grassmannian manifold [53], and many others. These properties also apply to the quotient Riemannian manifolds, as the computational space is still the ambient manifold [53]. In particular, Riemannian Trust regions will converge superlinearly [97].

Previous works have analyzed some particular cases of cost functions that are mathematically similar to Eq.(4.12). These works present scenarios closely related to the constant modulus portion of the OCMA problem, but did not exploit the (scaled) orthogonality of several solutions in the problem geometry. In [105] the authors optimize over the Stiefel manifold to maximize the diagonal terms of a matrix quadratic form for joint diagonalization, which is similar to the CMA cost function by setting $R_2 = 0$. Another work [106] tackles the phase retrieval problem by defining a manifold geometry with the so-called fixed-norms manifold.

We now adopt and extend existing analysis to investigate the convergence properties of ROCMA.

4.3.3 Convergence of ROCMA

We first make slight modifications to simplify analysis. Recall the SVD of the full rank channel matrix H from Section 4.1.1. we can rewrite

$$\boldsymbol{W}^{\mathsf{H}}\boldsymbol{x}_k = \boldsymbol{Y}^{\mathsf{H}}\boldsymbol{z}_k = \boldsymbol{Y}^{\mathsf{H}}\boldsymbol{V}^{\mathsf{H}}\boldsymbol{s}_k + \boldsymbol{Y}^{\mathsf{H}}\boldsymbol{n}_k = \boldsymbol{Q}^{\mathsf{H}}\boldsymbol{s}_k + \breve{\boldsymbol{n}}_k,$$

where we use $\breve{\boldsymbol{n}}_k = \boldsymbol{Y}^{\mathsf{H}}\boldsymbol{n}_k$ to denote the demixer output noise vector. Note that here we use $\boldsymbol{Q} = \boldsymbol{V}\boldsymbol{Y} = \boldsymbol{H}^{\mathsf{H}}\boldsymbol{W} \in \mathbb{C}^{L\times J}$ to denote the matrix of combined (channel plus demixer) parameter vectors. This linear variable transformation between $\boldsymbol{Q}$ and $\boldsymbol{Y}$ is bijective since $\boldsymbol{H}$ is full-column rank and $\boldsymbol{V}$ is orthonormal. Hence, our analysis will equivalently be performed in $\boldsymbol{Q}$-space and $\boldsymbol{Y}$-space. Without loss of generality, we consider noiseless scenario for ease of exposition.

As $\boldsymbol{Q}$ interacts with independent source signals directly, it is straightforward to check whether CMA converges to a joint demixer of the form $\widehat{\boldsymbol{Q}} = \boldsymbol{P}\boldsymbol{D}$, in which $\boldsymbol{P} \in \mathbb{C}^{L\times J}$ is a tall permutation matrix, and $\boldsymbol{D}$ a diagonal unitary matrix. Hence, any optimum solution of ROCMA in the quotient manifold $\mathcal{M} = \mathrm{ST}(L \times J)/\mathcal{U}(1)^{\times J}$ has to be of the form $[\widehat{\boldsymbol{Y}}] = [\boldsymbol{V}^{\mathsf{H}}\boldsymbol{P}]$. Equivalently, in the ambient manifold, the horizontal lift of the optimum is $\widehat{\boldsymbol{Y}} = \mathrm{lift}_{[\widehat{\boldsymbol{Y}}]}([\widehat{\boldsymbol{Y}}])$. In the following, we adopt all these representations equivalently.

Recall that the second order moment, fourth order moment, and kurtosis of QAM source signals are defined [26] by

$$m_2 = \mathbb{E}\{|s[k]|^2\},\ m_4 = \mathbb{E}\{|s[k]|^4\},\ \kappa = m_4 - 2m_2^2 < 0.$$

We note here that for QAM signals, $4m_2^2 + 3\kappa \geq m_2^2$ holds. We now present the two main theorems that ensure convergence guarantees for ROCMA using RTR.

Theorem 9 (Positive Definiteness of Riemannian Hessian). *Consider signal vector $\boldsymbol{s}_k \in \mathbb{C}^L$ with i.i.d. elements from a square QAM constellation of size Q. Additionally, let the channel*

matrix $\boldsymbol{H}$ *be full-column rank. Let* $[\widehat{\boldsymbol{Y}}]$ *be a solution of the ROCMA problem on the quotient manifold* $\mathcal{M} = \mathrm{ST}(L \times J)/\mathcal{U}(1)^{\times J}$. *There exist* $C_1 > 0$ *and* $c_1 > 0$ *such that, if the number of measurements* $K \geq C_1 L$, *the Riemannian Hessian of the cost function* $g(\cdot)$ *in* $\mathcal{M}$ *is positive definite in the neighborhood of* $[\widehat{\boldsymbol{Y}}]$ *with probability of at least* $1 - 6\mathrm{e}^{-c_1 K}$.

Proof. We begin our proof from the case of single-source recovery ($J = 1$) before generalizing to multiple sources $J > 1$.

As the cost function is a sample average, we study the expectation of its Hessian and invoke concentration of measure to approximate the behavior of the Hessian with that of its mean with high probability. Let $\widehat{\boldsymbol{Q}} \in \mathbb{C}^L$ be an ROCMA minimum in combined parameter space. Specifically, $\widehat{\boldsymbol{Q}} = \mathrm{e}^{\jmath\theta}\boldsymbol{e}_i$ which denotes arbitrary θ rotation of a canonical vector $\boldsymbol{e}_i$. Invoking [104, Lemma 1], for $\delta > 0$ there exist $C_1(\delta) > 0$ and $c_1(\delta) > 0$ such that for $K \geq C_1(\delta)L$, the single-source sample Euclidean Hessian is concentrated around its mean, i.e., $\left\|\nabla^2\overline{\overline{g}}(\widehat{\boldsymbol{Q}}) - \mathbb{E}\{\nabla^2\overline{\overline{g}}(\widehat{\boldsymbol{Q}})\}\right\| \leq \delta$ with probability at least $1 - 6\mathrm{e}^{-c_1(\delta)K}$.

Let $\boldsymbol{U} \in \mathbb{C}^L$ a nonzero vector , and let $\tilde{\boldsymbol{U}} = [\boldsymbol{U}^{\mathsf{T}}\ \boldsymbol{U}^{\mathsf{H}}]^{\mathsf{T}}$. From [74], the quadratic form of the mean single-source Euclidean Hessian at $\widehat{\boldsymbol{Q}}$ (using Wirtinger derivatives as in [100]) is

$$\begin{aligned}
&\frac{1}{2}\tilde{\boldsymbol{U}}^{\mathsf{H}}\mathbb{E}\{\nabla^2\overline{\overline{g}}(\widehat{\boldsymbol{Q}})\}\tilde{\boldsymbol{U}} \\
&\quad = (2m_2^2 - R_2 m_2)\|\boldsymbol{U}\|^2 + (3m_2^2 + 2\kappa)\mathrm{Re}(\boldsymbol{U}^{\mathsf{H}}\widehat{\boldsymbol{Q}})^2 - m_2^2\mathrm{Im}(\boldsymbol{U}^{\mathsf{H}}\widehat{\boldsymbol{Q}})^2 + (m_2^2 + \kappa)|\boldsymbol{U}^{\mathsf{H}}\widehat{\boldsymbol{Q}}|^2 \\
&\quad = |\kappa| \cdot \|\boldsymbol{U}\|^2 + (4m_2^2 + 3\kappa)\mathrm{Re}(\boldsymbol{U}^{\mathsf{H}}\widehat{\boldsymbol{Q}})^2 + \kappa\mathrm{Im}(\boldsymbol{U}^{\mathsf{H}}\widehat{\boldsymbol{Q}})^2. \qquad (4.33)
\end{aligned}$$

Additionally, knowing that $4m_2^2 + 3\kappa \geq m_2^2$ and

$$\mathrm{Im}(\boldsymbol{U}^{\mathsf{H}}\widehat{\boldsymbol{Q}})^2 \leq \max|U_i|^2 \leq \sum_{i=1}^{L}|U_i|^2 = \|\boldsymbol{U}\|^2, \qquad (4.34)$$

we see that $\boldsymbol{U}$ is a zero solution of Eq.(4.33) if and only if $\boldsymbol{U}$ has one nonzero element corresponding to the nonzero element of $\widehat{\boldsymbol{Q}}$, and $\boldsymbol{U}^{\mathsf{H}}\boldsymbol{Q}$ is purely imaginary, i.e. $\|\boldsymbol{U}\|^2 = \mathrm{Im}(\boldsymbol{U}^{\mathsf{H}}\widehat{\boldsymbol{Q}})^2$. Let $\widehat{\boldsymbol{Y}} \in \overline{\mathcal{M}} = \mathrm{ST}(L \times 1)$ be the horizontal lift of the optimum $[\widehat{\boldsymbol{Y}}]$. Recall that

$\widehat{\boldsymbol{Y}}^H\widehat{\boldsymbol{Y}} = 1$. From the relationship between $\overline{\mathcal{M}}$ and combined parameter space, i.e. $\boldsymbol{Q} = \boldsymbol{V}\boldsymbol{Y}$ with the matrix $\boldsymbol{V}$ formed by right singular vectors of $\boldsymbol{H}$, we have that the optimum in combined parameter space is $\widehat{\boldsymbol{Q}} = \boldsymbol{V}\widehat{\boldsymbol{Y}}$. Now let $\boldsymbol{G} = \boldsymbol{V}^{\mathsf{H}}\boldsymbol{U}$, which we decompose in three orthogonal components: a vertical direction $\boldsymbol{E} = \widehat{\boldsymbol{Y}}\boldsymbol{T} \in \mathrm{V}_{\widehat{\boldsymbol{Y}}}$ with $\boldsymbol{T}$ imaginary diagonal (i.e., a scalar), a horizontal direction $\boldsymbol{F} \in \mathrm{H}_{\widehat{\boldsymbol{Y}}}$ and a normal direction $\boldsymbol{C} = \widehat{\boldsymbol{Y}}\boldsymbol{A} \in \mathrm{N}_{\widehat{\boldsymbol{Y}}}\overline{\mathcal{M}}$, where $\boldsymbol{A}$ is Hermitian (i.e., a real scalar). Hence,

$$\boldsymbol{U}^{\mathsf{H}}\widehat{\boldsymbol{Q}} = \boldsymbol{G}^{\mathsf{H}}\widehat{\boldsymbol{Y}} = \boldsymbol{E}^{\mathsf{H}}\widehat{\boldsymbol{Y}} + \boldsymbol{F}^{\mathsf{H}}\widehat{\boldsymbol{Y}} + \boldsymbol{C}^{\mathsf{H}}\widehat{\boldsymbol{Y}} = \boldsymbol{T}^{\mathsf{H}} + \boldsymbol{A}, \tag{4.35}$$

where we use that $\boldsymbol{F}^{\mathsf{H}}\widehat{\boldsymbol{Y}} = 0$ because it is skew-Hermitian with zero diagonal and a scalar. Now, given $\boldsymbol{U}$ for which $\boldsymbol{U}^{\mathsf{H}}\widehat{\boldsymbol{Q}}$ is purely imaginary, the Hermitian $\boldsymbol{A}$ must be 0. In conclusion, the *only* directions in the nullspace of the Euclidean Hessian at $\widehat{\boldsymbol{Q}}$ in combined parameter space correspond only to vertical directions at $\widehat{\boldsymbol{Y}}$ in $\boldsymbol{Y}$-space, i.e., $\mathrm{V}_{\widehat{\boldsymbol{Y}}}$ corresponds to the nullspace of the Hessian. Therefore, in the quotient manifold $\mathcal{M}$, where the vertical directions are eliminated, the mean Hessian must be positive definite on the manifold.

Now, according to [104, Lemma 1], $K > C_1(\delta)L$ implies that $\nabla^2\overline{\overline{g}}(\widehat{\boldsymbol{Q}}) \succeq \mathbb{E}\{\nabla^2\overline{\overline{g}}(\widehat{\boldsymbol{Q}})\} - \delta\boldsymbol{I}$ with probability of at least $1 - 6\mathrm{e}^{-c_1 K}$. From Eq.(4.33) we have

$$\begin{aligned}\frac{1}{2}\tilde{\boldsymbol{U}}^{\mathsf{H}}\nabla^2\overline{\overline{g}}(\widehat{\boldsymbol{Q}})\tilde{\boldsymbol{U}} &\geq \frac{1}{2}\tilde{\boldsymbol{U}}^{\mathsf{H}}\mathbb{E}\big\{\nabla^2\overline{\overline{g}}(\widehat{\boldsymbol{Q}})\big\}\tilde{\boldsymbol{U}} - \frac{\delta}{2}\tilde{\boldsymbol{U}}^{\mathsf{H}}\tilde{\boldsymbol{U}} \\ &\geq (|\kappa| - \delta)\|\boldsymbol{U}\|^2 + (4m_2^2 + 3\kappa)\mathrm{Re}(\boldsymbol{U}^{\mathsf{H}}\widehat{\boldsymbol{Q}})^2 + \kappa\mathrm{Im}(\boldsymbol{U}^{\mathsf{H}}\widehat{\boldsymbol{Q}})^2,\end{aligned}$$

which is strictly positive for $\delta < |\kappa|\big(\|\boldsymbol{U}\|^2 - \mathrm{Im}(\boldsymbol{U}^{\mathsf{H}}\widehat{\boldsymbol{Q}})^2\big)$, where $\mathrm{Im}(\boldsymbol{U}^{\mathsf{H}}\widehat{\boldsymbol{Q}})^2 < \|\boldsymbol{U}\|^2$ because $\boldsymbol{G} = \boldsymbol{V}^{\mathsf{H}}\boldsymbol{U}$ does not belong to the vertical space $\mathrm{V}_{\widehat{\boldsymbol{Y}}}$.

We now generalize to the multiple source recovery case ($J > 1$). Let $\widehat{\boldsymbol{Q}}$ be an optimum, that is, $\widehat{\boldsymbol{Q}} = \boldsymbol{P}\boldsymbol{D}$, with $\widehat{\boldsymbol{Q}}_\ell = \mathrm{e}^{j\theta_\ell}\boldsymbol{e}_{i_\ell}$ its ℓ-th column corresponding to the ℓ-th optimum demixer. The Euclidean cost function $\overline{\overline{g}}$, written in terms of each demixer similar to Eq.(2.7) contains no cross-product between demixing combiners. Through vectorization of $\widehat{\boldsymbol{Q}}$ and permutations of columns and rows, we obtain a Wirtinger Hessian matrix such that its

elements are ordered for each combiner as in [100, 104]. Thus, the Hessian matrix is block diagonal, with each block being the single-source Euclidean Hessian evaluated at the ℓ-th combiner, i.e. $\nabla^2\overline{\overline{g}}(\boldsymbol{Q}_\ell)$, $\ell \in \{1, \cdots, J\}$.

Let $\boldsymbol{U} \in \mathbb{C}^{L\times J}$ a nonzero matrix, and $\boldsymbol{U}_\ell$ its ℓ-th column , and let $\tilde{\boldsymbol{U}}_\ell = [\boldsymbol{U}_\ell^{\mathsf{T}}\ \boldsymbol{U}_\ell^{\mathsf{H}}]^{\mathsf{T}}$. In quadratic form, the mean Euclidean Hessian at $\widehat{\boldsymbol{Q}}$ can be rewritten as

$$\sum_{\ell=1}^{J} \frac{1}{2}\tilde{\boldsymbol{U}}_\ell^{\mathsf{H}}\mathbb{E}\{\nabla^2\overline{\overline{g}}(\widehat{\boldsymbol{Q}}_\ell)\}\tilde{\boldsymbol{U}}_\ell, \tag{4.36}$$

where each summand is derived from Eq.(4.33). Following the same reasoning as in the single-source case, $\boldsymbol{U}_\ell$ is a zero solution of the ℓ-th summand of Eq.(4.36) if and only if $\|\boldsymbol{U}_\ell\|^2 = \mathrm{Im}(\boldsymbol{U}_\ell^{\mathsf{H}}\widehat{\boldsymbol{Q}}_\ell)^2$. Furthermore, $\boldsymbol{U}_\ell$ has to correspond to the ℓ-th column of a vertical direction at $\widehat{\boldsymbol{Y}}$ in $\boldsymbol{Y}$-space.

Hence, $\boldsymbol{U} = \boldsymbol{V}\widehat{\boldsymbol{Y}}\boldsymbol{T}$ with $\boldsymbol{T}$ imaginary diagonal. Noting that $\widehat{\boldsymbol{Y}}$ has orthogonal columns by definition, and that $\boldsymbol{T}$ has J free parameters, the nullspace of the Hessian has dimension J. Again we conclude that the only directions in the nullspace of the Hessian at $\widehat{\boldsymbol{Q}}$ correspond to vertical directions at $\widehat{\boldsymbol{Y}}$. As we ignore vertical directions when g is restricted to the quotient manifold $\mathcal{M}$, the mean Hessian must be positive definite.

Now, due to the block diagonal structure of the Hessian, it is straightforward to bound the quadratic form of the sample Hessian as follows:

$$\sum_{\ell=1}^{J} \frac{1}{2}\tilde{\boldsymbol{U}}_\ell^{\mathsf{H}}\nabla^2\overline{\overline{g}}(\widehat{\boldsymbol{q}}_\ell)\tilde{\boldsymbol{U}}_\ell \geq \sum_{\ell=1}^{J}(|\kappa| - \delta)\|\boldsymbol{U}_\ell\|^2 + \kappa\mathrm{Im}(\boldsymbol{Y}_\ell^{\mathsf{H}}\widehat{\boldsymbol{Q}}_\ell)^2 + (4m_2^2 + 3\kappa)\mathrm{Re}(\boldsymbol{U}_\ell^{\mathsf{H}}\widehat{\boldsymbol{Q}}_\ell)^2,$$

which again is strictly positive for δ small enough with high probability, following the same procedure as above. ■

Theorem 10 (Convergence of RTR). *Under the conditions of Theorem 9, ROCMA is globally and locally convergent in $\mathcal{M}$ with high probability using Riemannian Trust Regions as defined in Algorithm 4.1.*

Proof. First, we prove global convergence. The Riemannian quotient manifold $\mathcal{M}$ is smooth and it is compact since it is a quotient space of $\mathrm{ST}(L \times J)$, which itself is compact. The cost function g is smooth because its lifted version is a (smooth) matrix polynomial. Invoking [97, Corollary 4.6], ROCMA satisfies all conditions for global convergence.

For local convergence, we prove that [97, Theorem 4.12] holds for ROCMA. In particular, ROCMA needs to meet the following requirements:

- All conditions of [97, Theorem 4.2], which are satisfied owing to global convergence.
- The retraction needs to satisfy the bound [97, Eq.(18)], which holds because: (a) $\mathcal{M}$ is compact, and (b) the retraction from lifting is smooth.
- The norm of the inverse Hessian operator needs to be bounded in a neighborhood of an optimum. Invoking Theorem 9, the Riemannian Hessian in $\mathcal{M}$ is strictly positive definite in $\mathcal{M}$ with minimum eigenvalue $\lambda_{\min} > 0$. Since the Hessian is also continuous, its inverse is bounded by $\lambda_{\min}^{-1}$ in a neighborhood of any optimum.

Hence, with high probability, ROCMA enjoys global and local convergence guarantees using RTR. ■

4.3.4 Computational Complexity

We can estimate the computational complexity of the ROCMA algorithm by analyzing each step of Algorithm 4.1. In particular, the Riemannian Trust-Region step includes iterations needed for convergence and also iterations of each call to the trust-region subproblem algorithm. Henceforth, we refer to the former as outer iterations, and the latter as inner iterations.

(1) The source estimation step is dominated by the computation of Minka's Laplace method, with complexity of $\mathcal{O}(ML)$, and a number of eigendecompositions, to be obtained iteratively with a cost of $\mathcal{O}(M^3)$.

(2) The initialization is dominated by obtaining $\boldsymbol{z}_k$ via scaling, with a complexity level of $\mathcal{O}(MLK)$. Other computations have relatively insignificant, mainly for defining geometry operations.

(3) Each inner iteration is dominated by the computation of Riemannian Hessian, at complexity $\mathcal{O}(L^2K)$. Other operations are linear over the samples with a cost of $\mathcal{O}(LK)$.

(4) Each outer iteration is dominated by the total inner iterations required in the particular outer iteration I_t. Thus, this amounts to complexity of $\mathcal{O}(L^2KI_t)$. The Riemannian retraction $\mathrm{R}_{\boldsymbol{Y}}$ requires $\mathcal{O}(L^3)$, whereas other operations are linear over scalars and of $\mathcal{O}(1)$. The final scaling by $\boldsymbol{U}_L\boldsymbol{\Sigma}_L^{-1}$ has a cost of $\mathcal{O}(ML^2)$.

Based on the aforementioned steps, Table 4.2 summarizes the complexity of ROCMA in each step.

Table 4.2: Computational complexity of ROCMA.

ROCMA Steps	Total cost
Estimate L	$\mathcal{O}(ML)$
Iterative eigendecomposition $\boldsymbol{R}_{\boldsymbol{Y}}$	$\mathcal{O}(M^3)$
Define $\boldsymbol{z}_k$	$\mathcal{O}(MLK)$
RTR outer iteration	$\mathcal{O}(L^3 + L^2KI_t)$
Final scaling	$\mathcal{O}(ML^2)$

In comparison, the computational complexity of a typical gradient-descent scheme in Euclidean space is of $\mathcal{O}(M^2LK)$ per iteration [104], which is lower than the cost of RTR iterations for a moderate number of inner iterations. The iteration complexity of RTR can be found in [95, Theorem 6.10]. In our numerical results, we shall consider some benchmark applications and provide a computation comparison of RTR with other Riemannian and traditional CMA algorithms.

4.4 Simulation Results

4.4.1 Definitions

For performance illustration and comparison. We consider a multi-user signal recovery scenario consisting of L source nodes, each transmitting K independent symbols from a typical QAM (QPSK or 16-QAM) constellation with normalized average power. The serving node has M receive antennas whereas each low cost source node has a single antenna. We model wireless channels $\boldsymbol{H}$ as stationary Rayleigh with i.i.d. entries $H_{ml} \sim \mathcal{N}(0, \frac{1}{2}) + i\mathcal{N}(0, \frac{1}{2})$, in addition to additive white Gaussian noise vector $\boldsymbol{n}_k$ with i.i.d. entries and variance (power) σ^2 consistent with receiver SNR of 20dB. To measure signal recovery performance, we evaluate normalized total interference (NTI) for each recovered source, defined by

$$\mathrm{NTI}_\ell = \frac{\sum_i |C_{\ell i}|^2 - \max_i |C_{\ell i}|^2}{\max_i |C_{\ell i}|^2} \tag{4.37}$$

where $C_{\ell i}$ are the entries of the final mixing matrix $\boldsymbol{C} = \boldsymbol{W}^{\mathsf{H}}\boldsymbol{H}$ after demixing, with its rows corresponding to each equalized channel-demixer pair. Unless otherwise stated, we average 100 runs per setting.

4.4.2 Signal Recovery Efficacy

We test and compare the power of source recovery capabilities under different system sizes, different number of samples, and different QAM constellations.

Figure 4.3 presents the probability of successful recovery of multiple sources based on different numbers of received data samples, under 20dB SNR. We test both QPSK and 16-QAM modulations for system sizes of $M \times L = 8 \times 4$ and 16×8. We define *success* as the event that *all* source signals are recovered with NTI below -20dB.

Figure 4.3a shows a 8×4 system using QPSK source modulation. Our proposed RTR and RGD exhibit nearly the same probability of success for various sample size K, both

successfully achieving 100% success for $K \geq 300$ samples. In comparison, the existing WF algorithm exhibits similar or slightly higher recovery success rate at first, but stagnates and fails to achieve 100% of success with increasing data size. Unlike RTR and RGD, the WF receiver requires at least 900 data samples to achieve a probability of success above 98%. Applying sequential Gram-Schmidt orthogonalization, GS-CMA requires even more samples to achieve higher probability of success. In fact, our test fails to reach above 96% success probability despite utilizing thousands of data samples.

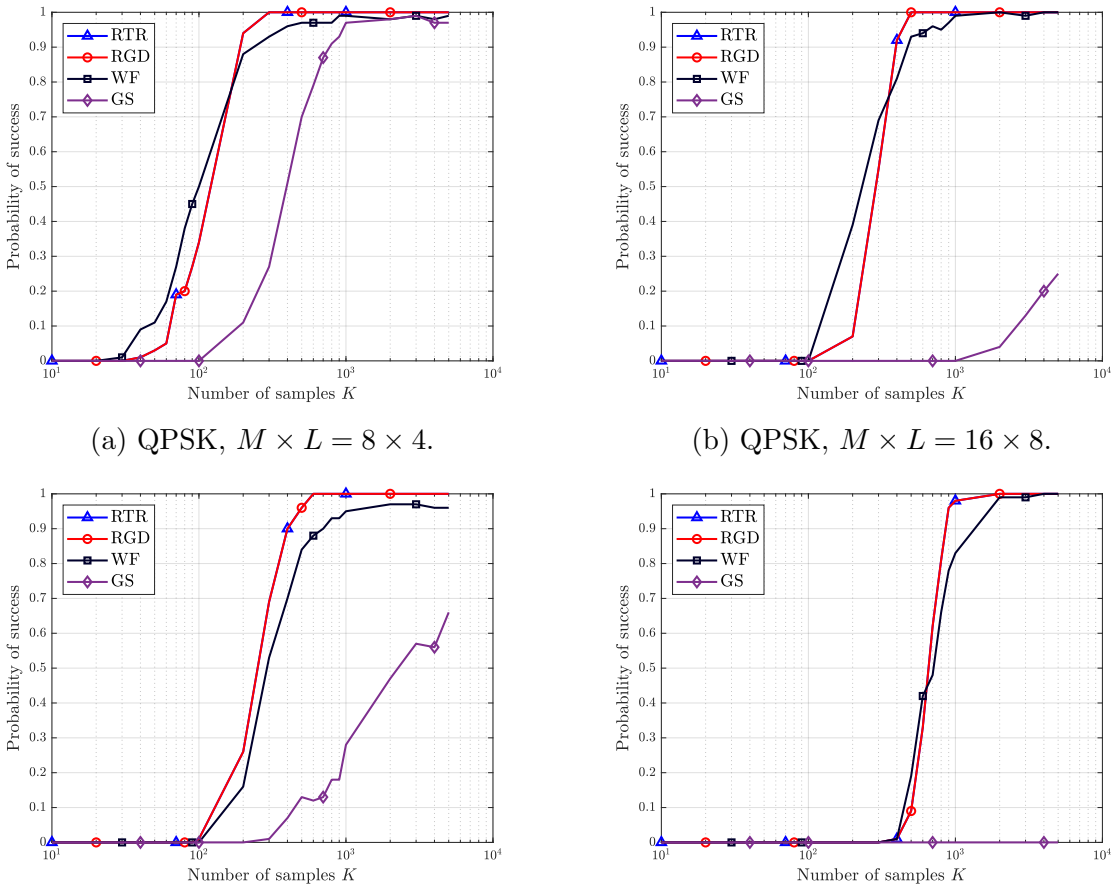

(a) QPSK, $M \times L = 8 \times 4$.

(b) QPSK, $M \times L = 16 \times 8$.

(c) 16-QAM, $M \times L = 8 \times 4$.

(d) 16-QAM, $M \times L = 16 \times 8$.

Figure 4.3: Probability of successful recovery of all detected demixers vs. number of samples.

Testing a larger system using QPSK, results from Figure 4.3b demonstrate similar relative performance by RTR, RGD and WF, requiring 500 and 1000 samples to achieve over 99% probability of success. The GS-CMA demixer, however, is much more sensitive to problem

size, and struggles to jointly recover all signals even with 5000 received data samples.

We now consider the more challenging case of 16-QAM source signals. Figures 4.3c and 4.3d respectively provide the results for problem size of 8×4 and 16×8. The test results show that the two Riemann methods (RTR and RGD) again achieve high probability of successful signal recovery, now requiring only 600 and 2000 samples, respectively for near 100% success rate. The WF algorithm is less successful in comparison, requiring at least 2000 samples to achieve more than 95% of success probability. On other other hand, GS-CMA only achieves 60% probability of success for 16-QAM for the smaller 8×4 system size. For the more complex system of size 16×8, GS-CMA in fact is unable to recover all 8 detected sources under the stated simulation settings. Indeed, this phenomenon was anticipated by [47]. Since GS-CMA relies on sequential Gram-Schmidt orthogonalization for signal separation, error propagation can lead to weaker interference suppression. As the ℓ-th demixer relies on all previous demixers in order to isolate a different signal, GS-CMA becomes increasingly more vulnerable to error propagation with increasing number of signals.

Overall, both proposed Riemann algorithms (RTR and RGD) demonstrate strong performance across different modulations and system sizes under test than their Euclidean counterparts. WF-CMA still shows high probability of successful recovery, albeit at the cost of more samples than RTR or RGD. GS-CMA, on the other hand, struggles against moderately large system sizes or higher-order modulations.

4.4.3 Computation and Interference Rejection

For the purposes of signal recovery, computation complexity must be jointly analyzed with respect to the achieved level of interference rejection in recovered signals. For this reason, in the following presentation we show how well our proposed methods (RTR and RGD) work in terms of both interference rejection and computational load. We also provide benchmark comparison with the two algorithms (WF and GS).

We first investigate algorithm runtime ("wall-clock" time). Runtime depends on com-

puter, platform and code implementation. Thus, runtime comparison alone may not fully capture true algorithm runtime. To mitigate this possible bias, we let all source codes for RTR, RGD and WF utilize the same Manopt structure and libraries. GS-CMA, on the other hand, uses a direct implementation using the fastest routines available (matrix products, etc.) for each iteration.

Figure 4.4 depicts the average interference rejection over all runs of the algorithms with respect to their runtime, for a fixed number of samples $K = 2000$. From the results of all tested modulation schemes and system sizes, both RGD and RTR, by exploiting the proposed geometry, are faster than GS by at least 4 times, and are faster than WF by an order of magnitude. Such advantage is consistent across nearly all tested modulation schemes and system sizes. Moreover, RTR and RGD exhibit similar runtime across modulations, and require about double the time to converge in the larger system of 16×8, which contains 2 times more sources and antennas (Figures 4.4b and 4.4d). There are some modest differences between the two Riemann solvers. In particular, RGD converges slightly faster initially to achieve moderate interference mitigation of approximately -15dB. For higher interference rejection, both RGD and RTR show similar runtime complexity.

WF-CMA exhibits a similar efficacy in terms of interference rejection, but it does require longer runtime to achieve a particular level of interference rejection. On the other hand, GS-CMA requires more runtime to converge than the Riemannian methods across all tested scenarios. Moreover, GS-CMA is less effective in interference mitigation, particularly for more complex source signals of 16-QAM, as shown in Figure 4.4c and Figure 4.4d. From the test results, it is evident that GS-CMA stalls in terms of interference rejection and additional iterations do not improve the performance of interference rejection. This phenomenon is consistent with the discussion of error propagation in sequential orthogonalization of the GS-CMA approach. The performance loss of GS-CMA becomes more severe with increasing modulation and system size, e.g. is about -30dB of interference for QPSK signals and a 8×4 system (Figure 4.4a), but is less than -10dB for 16QAM and 16×8 system (Figure 4.4d).

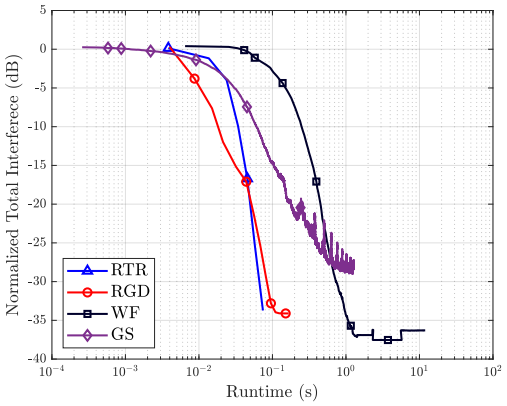

(a) QPSK, $M \times L = 8 \times 4$.

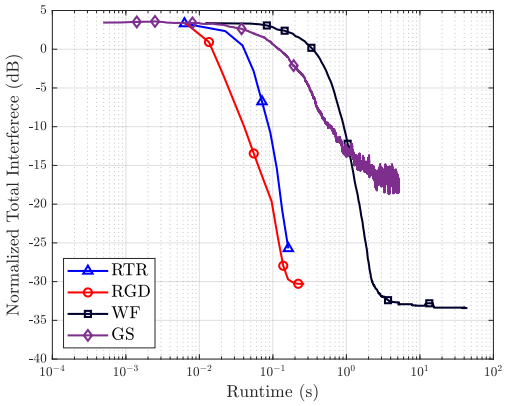

(b) QPSK, $M \times L = 16 \times 8$.

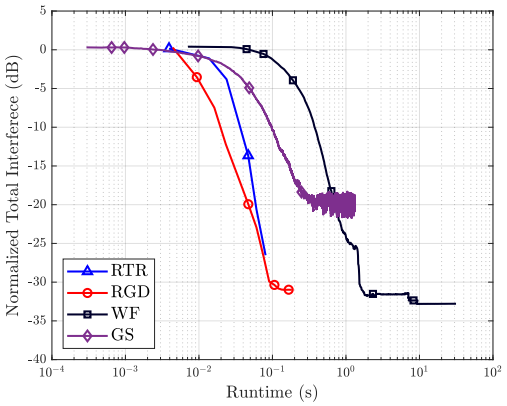

(c) 16-QAM, $M \times L = 8 \times 4$.

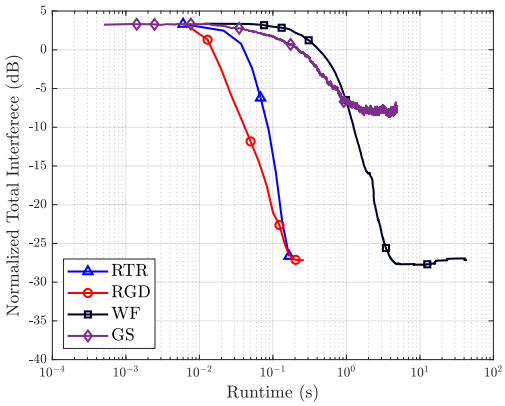

(d) 16-QAM, $M \times L = 16 \times 8$.

Figure 4.4: Average total interference for all detected demixers vs. runtime.

To address the potential bias of over-reliance on runtime when analyzing computation complexity, we also compare the algorithm behavior respect to *oracle calls*, that is, the total number of cost function, gradient, Hessian and GS orthogonalization calls/evaluations of each algorithm. These operations are dominant contributors to total computational complexity, they act as a proxy for platform-independent computational load assessment. Recall that GS-CMA uses only one sample per gradient update and its orthogonalization does not increase with the number of samples, we normalize the number of oracles calls by K in order to provide a fair comparison with the other methods, that use sample averages in all its oracle calls.

Figure 4.5 shows the average achieved NTI of each algorithm with respect to their oracle

calls, for a fixed number of samples $K = 2000$. As seen in previous comparisons, RTR and RGD have similar computational cost. Across the tested modulations and system sizes, both RGD and RTR require at least an order of magnitude fewer function computations than WF-CMA to achieve 20dB of interference mitigation. Even if we account for their larger computational complexity per iteration than WF or GS, the total cost of every algorithm is dominated by the number of iterations, and RTR and RGD incur significantly lower total computational load than WF-CMA. WF-CMA shows good interference rejection power, but requires about 10-20 times more oracle computations than the Riemannian methods to achieve equal levels of interference mitigation.

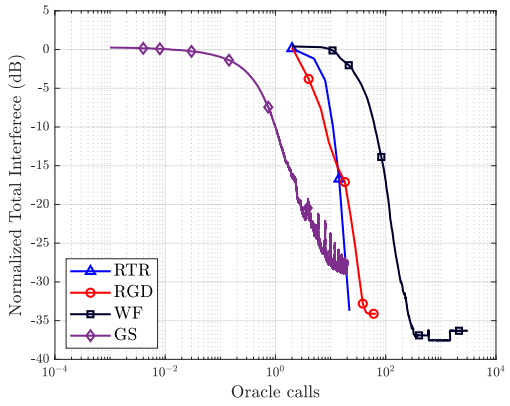

(a) QPSK, $M \times L = 8 \times 4$.

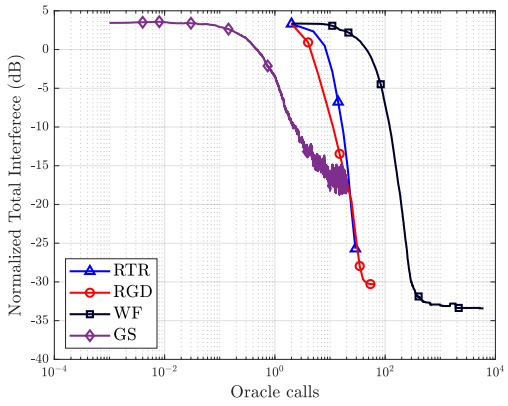

(b) QPSK, $M \times L = 16 \times 8$.

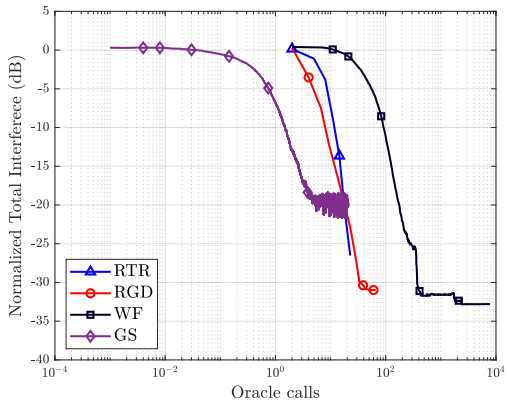

(c) 16-QAM, $M \times L = 8 \times 4$.

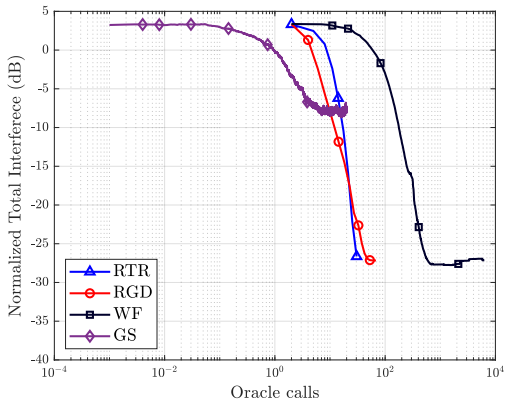

(d) 16-QAM, $M \times L = 16 \times 8$.

Figure 4.5: Average total interference for all detected demixers vs. oracle calls.

As expected, GS is the least complex algorithm owing to its simply stochastic gradient

update using only one sample in each iteration. At an average interference suppression of 20dB, the computational cost of GS is about 5-8 times lower than the Riemannian methods, as seen in Figs 4.5a-4.5c. However, the sequential nature of the GS-CMA leads to poorer interference rejection, particularly for higher-dimensional QAM constellation and/or larger system sizes. In comparison, the proposed Riemann algorithms can achieve substantially better performance of signal recovery with only a modest increase of computation complexity. Exploiting Riemannian geometry provides a good complexity-efficacy tradeoff.

4.5 Summary

In this chapter, we investigated an alternative formulation for CMA-based signal recovery based on Riemannian manifolds. We avoided regularization by imposing constraints in the original optimization problem. Then, we developed a Riemannian geometry that encodes the orthogonality requirement of distinct source signals, and thus we rewrite the CMA problem as an unconstrained optimization problem over our proposed manifold geometry. We leveraged Riemannian optimization techniques to solve this problem without the need for parameter tuning or special initialization, and furthermore, provided theoretical convergence guarantees with high probability under mild conditions. Our numerical test corroborated these claims when compared with traditional CMA solutions, showing lower requirement of sample size, computations and runtime.

Chapter 5

An Unsupervised Learning Paradigm for MIMO User Scheduling

In this chapter, we propose an effective and scalable user scheduling based on unsupervised learning. Given channel state information (CSI) of users, we first apply unsupervised learning to identify mobile users with highly similar CSI. We develop a new scheduling principle to enhance spatial diversity by dispersing users of high CSI similarity into different MIMO access groups. We formulate a user clustering problem over Grassmannian manifold to identify users that can pose strong co-channel interference. We consider downlink MIMO and uplink MIMO, with or without power control for simple implementation. Our new scheduling approach is generalizable to a variety of different simple and scalable unsupervised learning tools and different diversity optimization criteria. Numerical tests demonstrate the substantial gain in terms of spectrum efficiency and interference suppression at modest computation complexity.

Part of this chapter has been previously submitted to *IEEE Transactions on Wireless Communications* and is currently under review.

5.1 The Scheduling Problem

Previous works on resource-sharing MIMO systems have studied optimal decoder (MAC) and precoder (BC) designs that achieve channel capacity for a given resource-sharing group, such as the MMSE-SIC receiver [59] for MAC or dirty-paper precoding [107] with MMSE filters for BC. However, these designs were proposed with the premise that users have already been scheduled in MIMO user groups. To benefit from these exciting works in the literature, we investigate the scheduling problem that is a foundation step to MIMO precoding and rate maximization.

In the following, we adopt the system model developed in Section 2.3. We assume similar data rate requirements for all users, and thus we use spectrum efficiency as performance metric. Hence, we first obtain the spectrum efficiency in terms of co-channel interference and user rates. Note that because the system model assumes single-carrier systems, we use normalized bandwidth.

5.1.1 Co-Channel Interference and Sum-Rate

The interference that user $u \in \mathcal{S}_g$ experiences is measured by their signal-to-interference-and-noise ratio or SINR. In the case of MAC, the SINR of user u is

$$\mathrm{SINR}_u^{\mathrm{MAC}} = \frac{p_u |\boldsymbol{W}_g^{\mathsf{H}} \boldsymbol{h}_u|^2}{\sigma^2 + \sum_{i \in \mathcal{S}_g, i \neq u} p_i |\boldsymbol{W}_g^{\mathsf{H}} \boldsymbol{h}_i|^2}. \tag{5.1}$$

Among several receiver designs, without loss of generality we adopt the MMSE receivers [59] for their straightforward implementation and to fully leverage spatial diversity. In the g-th group, the MMSE design defines the column of the g-th decoder matrix $\boldsymbol{W}_g$ corresponding to user $u \in \mathcal{S}_g$ as

$$\boldsymbol{W}_g = \left(\sigma^2 \boldsymbol{I}_M + \sum_{i \in \mathcal{S}_g, i \neq u} p_i \boldsymbol{h}_i \boldsymbol{h}_i^{\mathsf{H}} \right)^{-1} \boldsymbol{h}_u, \tag{5.2}$$

with a resulting SINR of

$$\mathrm{SINR}_u^{\mathrm{MAC}} = p_u \boldsymbol{h}_u^{\mathsf{H}} \left(\sigma^2 \boldsymbol{I}_M + \sum_{i \in \mathcal{S}_g, i \neq u} p_i \boldsymbol{h}_i \boldsymbol{h}_i^{\mathsf{H}} \right)^{-1} \boldsymbol{h}_u. \tag{5.3}$$

For BC, the SINR of user u corresponds to

$$\mathrm{SINR}_u^{\mathrm{BC}} = \frac{p_u |\boldsymbol{h}_u^{\mathsf{T}} \boldsymbol{z}_u|^2}{\sigma^2 + \sum_{i \in \mathcal{S}_g, i \neq u} p_i |\boldsymbol{h}_u^{\mathsf{T}} \boldsymbol{z}_i|^2}, \tag{5.4}$$

and, without loss of generality and for the sake of simplicity, we use the MRT precoders [61]

$$\boldsymbol{z}_u = \frac{\overline{\boldsymbol{h}_u}}{\|\boldsymbol{h}_u\|}, \ \forall u \in \{1, \ldots, N\}, \tag{5.5}$$

which yield a resulting SINR for user u of

$$\mathrm{SINR}_u^{\mathrm{BC}} = \frac{p_u \|\boldsymbol{h}_u\|^2}{\sigma^2 + \sum_{i \in \mathcal{S}_g, i \neq u} p_i |\boldsymbol{h}_u^{\mathsf{T}} \overline{\boldsymbol{h}_i}|^2 / \|\boldsymbol{h}_i\|^2}. \tag{5.6}$$

The normalized sum-rate of the g-th group is given by

$$R_g = \sum_{u \in \mathcal{S}_g} \log_2 \left(1 + \mathrm{SINR}_u\right), \tag{5.7}$$

with R_g^{MAC} and R_g^{BC} denoting the sum-rates for uplink and downlink, respectively, using the corresponding expressions for SINR.

5.1.2 Problem Formulation

Ideally, we aim to optimize the design of the indicator variables $\pi_{g,u}$ and user power allocation p_u to maximize the efficiency of resource usage in terms of sum rate, that is, maximizing the sum-rate of each RSG and minimizing the number of groups simultaneously. A mathematical

formulation of this approach, valid for either MAC or BC scheduling, is

$$\mathcal{P}: \max_{G,\, \pi_{g,u},\, p_u} \quad \frac{1}{G} \sum\nolimits_{g=1}^{G} R_g \tag{5.8a}$$

$$\text{s.t.} \quad \sum\nolimits_{u=1}^{N} \pi_{g,u} \leq M,\ \forall g\,, \tag{5.8b}$$

$$\pi_{g,u} \in \{0,1\},\ \forall g\,, \forall u\,, \tag{5.8c}$$

$$\sum\nolimits_{n=1}^{N} p_u \pi_{g,u} \leq p_{\text{BS}}^{\max},\ \forall g\ \text{(BC)}, \tag{5.8d}$$

$$0 \leq p_u \leq p_{\text{UE}}^{\max},\ \forall n\ \text{(MAC)}. \tag{5.8e}$$

In Problem $\mathcal{P}$, constraint (5.8b) limits the number of MAC/BC users up to the number of BS antennas M without requiring further non-orthogonal multiple access. By design, each user belongs to one group only (5.8c). Additionally, in practical BC systems the BS transmission power is limited by $p_{\text{BS}}^{\max}$ in every time slot and needs to be properly allocated (5.8d), whereas in MAC each user has a maximum transmission power $p_{\text{UE}}^{\max}$ (5.8e). In order to further mitigate CCI, additional constraints can be considered when more design parameters are available, such as resource availability, cooperation in BC, individual rate requirements, among other criteria. Note that our formulation of problem $\mathcal{P}$ for maximizing spectrum efficiency can be modified as required to attain different objectives, and as such is without loss of generality. Other tractable performance metrics for MAC/BC user scheduling include the minimization of MSE [108, 109], weighted MSE [110], maximization of SINR [111], or minimization of BER [112], among others.

Regardless of the selected objective, $\mathcal{P}$ is NP-hard and shares similar complexity as general nonlinear mixed integer programming. To find the optimum MAC/BC user grouping $\pi_{g,u}^{\star}$, a direct exhaustive search method would need to evaluate all possible $\pi_{g,u}$ in terms of mean sum-rate (5.8a) to determine the optimum MAC/BC user grouping solution that achieves the best spectrum efficiency. However, the resulting search space is combinatorial even with a modest number of users and fixed G and p_u, and as such requires very high computational load.

Therefore, the challenge in MIMO user scheduling for massive wireless systems is to develop a low complexity and effective algorithm that can achieve high spectrum efficiency and low CCI with relative independence of system parameters such as the total number of users, number of users within a group, BS antennas, channel realizations, etc.

5.1.3 Proposed Novel Solution Paradigm

Any solution to the scheduling challenge will essentially try to find MAC or BC groups such that all users in each group enjoy low CCI, or in other words, their CSIs are distinct enough in the spatial sense, while still incurring in reasonable computational cost. To attain this goal, such solution has to study the whole dataset, instead of looking at portions of it (such as pairwise relationships). Even then, the solution needs to measure dissimilarity, which is not well-defined in a general form and instead is variable, highly dependant on the particular realization of CSIs and the system itself. This leads to either trial-and-error approaches to define dissimilarity in particular scenarios, or the need to design a dynamic metric of dissimilarity that accounts for system parameters and CSI variability in several different scenarios, which is both hard and impractical.

Nevertheless, the fast development of scalable solutions of challenging problems in the field of machine learning techniques offer hope in tackling the scheduling problem. These techniques analyze all data points and are able to adapt to several changes in the dataset, known or not. Moreover, machine learning techniques have been thoroughly used across a large variety of computationally difficult problems with the goal of reducing complexity and/or runtime, and has offered novel perspectives and approaches in different aspects of wireless systems [70–73, 113].

Regrettably, both supervised and unsupervised learning cannot be directly applied to the scheduling problem. On one hand, supervised learning (which usually enjoys better performance) requires a rich labeled dataset or near-optimum solutions for training, which in the context of CSI scheduling is nearly unfeasible to obtain. First, the large number

of system parameters and possible channel characteristics demands for an incredibly large dataset to avoid sampling biases. Moreover, such ground-truth labels are not known even in simulations, as the optimum scheduling solution of a particular system is unknown due to the very nature of the scheduling problem.

On the other hand, unsupervised learning cannot be directly applied in user scheduling: a proper scheduling scheme will avoid grouping users with similar CSI, which diminishes performance and channel capacity, and conversely assigns users with dissimilar CSIs in RSGs to reduce CCI.

However, unsupervised learning techniques excel at finding common features in a dataset in an efficient manner among data points, such as user CSI, without having to know beforehand which features to study and without the need of labeled datasets. This realization leads to the main contribution of this chapter: a general and scalable two-step strategy that uses unsupervised learning techniques to *first* identify in a global manner which users share similar CSI, to *then* exploit that information and define MAC/BC RSGs such that their users do not share spatial similarities.

In the following section, we present the details of our scheduling approach, valid for both MAC and BC systems, that tackles the inherent complexity of the scheduling problem without sacrificing performance.

5.2 Principled User Scheduling Through Unsupervised Learning

To accomplish our goal, we first examine CSI similarity and introduce a corresponding transformation to a geometric manifold that contains CSI vectors. Using this similarity measure, we directly apply unsupervised learning on active users to identify similar CSIs in terms of subspace span and form clusters of similar CSIs. Thus, users within each similarity cluster tend to exhibit strong CCI due to low CSI diversity (high similarity) such that no

two users from a particular cluster should be jointly scheduled in an RSG. Based on the outcomes of unsupervised learning, we define a scheduling algorithm to group users from different CSI clusters into RSGs, thereby achieving high CSI diversity within a group to generate lower mutual interference and higher spectrum efficiency. Figure 5.1 illustrates our two-step strategy, and we further summarize our scheduling approach in Algorithm 5.1.

Algorithm 5.1 Scalable User Scheduling Strategy

Input: $\boldsymbol{h}_u \in \mathbb{C}^M$, $u \in \{1, \ldots, N\}$

Learning-based CSI Clustering:

1: Identify user CSI with high similarity (subspace span) through unsupervised learning;

Similarity-Assisted User Grouping:

2: Assign users from different clusters in RSGs for MAC/BC operation, such that no two users from the same CSI cluster are in any scheduled group, and further exploit clustering results in user selection.

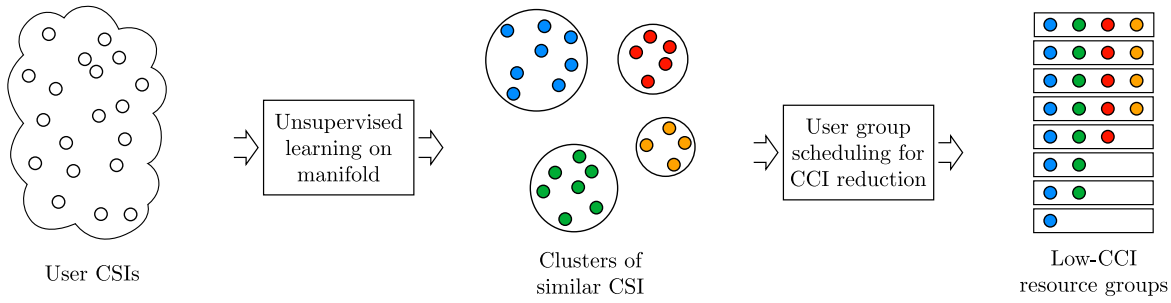

Figure 5.1: Illustration of the proposed user scheduling strategy based on unsupervised learning. In the *first step*, we employ unsupervised learning to classify user CSIs into clusters with strong similarity in the sense of subspace span. In the *second step*, we allocate users into resource-sharing groups that exploit the CSI similarity such that not 2 users of the same cluster share resources.

5.2.1 Geometric Perspective of CSI Similarity

In our setting, channel similarity is directly related to the colinearity of user CSIs in spatial domain, or equivalent in subspace span. Hence, we start by examining the pairwise CSI correlation coefficient

$$\rho\left(\boldsymbol{h}_u, \boldsymbol{h}_i\right) = \frac{\left|\boldsymbol{h}_u^{\mathsf{H}} \boldsymbol{h}_i\right|}{\left\|\boldsymbol{h}_u\right\| \left\|\boldsymbol{h}_i\right\|}, \tag{5.9}$$

which determines the amount of CCI between two co-channel users. In particular, if two user CCIs are orthogonal, then there is zero CCI when scheduled in the same RSG. In practice, full CSI orthogonality is rare. One practical solution is to set an upper threshold to limit the norm of the pairwise CSI correlation coefficient within each RSG. The challenge is that setting such a threshold cannot guarantee the level of co-channel interference (CCI) among users in an RSG. First, the CCI among users in an RSG would vary depending on the magnitude of user CSIs, and on multi-lateral geometric relationship among CSIs. Second, direct user scheduling also depend on the user selection order considered for scheduling, whose optimization involves a combinatorial and computationally intensive process. To ensure overall system efficiency (5.8a), consistency, and fairness for both MAC and BC, we need to develop a consistent, simple, and scalable scheduling method to effectively limit CCI among users in a RSG for both BC and MAC scenarios.

Note that traditional unsupervised learning in Euclidean space is incompatible with identifying similar/dissimilar CSI vectors, as the Euclidean distance does not measure spatial correlation/diversity. Instead of using Euclidean distance, Eq.(5.9) shows that the spatial similarity or dissimilarity of CSI vectors is insensitive to phase rotations and/or magnitude variation of the individual CSI vectors, as

$$\rho\left(\boldsymbol{h}_u, \alpha \mathrm{e}^{i\theta}\boldsymbol{h}_i\right) = \rho\left(\boldsymbol{h}_u, \boldsymbol{h}_i\right) \; \forall \alpha \in \mathbb{R}/0, \; \theta \in [0, 2\pi).$$

To account for CCI invariance in a global manner, we can redefine the geometry of the space when analyzing CSIs, transforming from Euclidean space to a manifold geometry. Such transformation in unsupervised learning has been used to characterize the underlying low-dimension space of data [114]. However, by analyzing and clustering CSIs on a manifold that naturally measures the desired notion of diversity, the resulting clusters will effectively identify users that have highly similar CSIs and consequently strong CCI.

As explained, CSI correlation disregards the common phase and magnitude of each vector.

Therefore, we need a manifold geometry invariant to magnitude and/or phase variations. Formally, we define an equivalence relation

$$\boldsymbol{h}_u \sim \boldsymbol{h}_i \quad \text{if} \quad \boldsymbol{h}_i = a\mathrm{e}^{i\theta}\boldsymbol{h}_u,\, a \in \mathbb{R}/\{0\},\, \theta \in [0, 2\pi), \tag{5.10}$$

which states that any two vectors that differ in magnitude and/or phase are considered the same. With Eq. (5.10) we can define an equivalence class for each CSI vector

$$[\boldsymbol{h}_u] = \big\{a\mathrm{e}^{j\theta}\boldsymbol{h}_u : \theta \in [0, 2\pi], a \in \mathbb{R}/\{0\}\big\} = \big\{\alpha\boldsymbol{h}_u : \alpha \in \mathbb{C}/\{0\}\big\}. \tag{5.11}$$

In other words, the equivalence class $[\boldsymbol{h}_u]$ is the complex line that passes through $\boldsymbol{h}_i$ and the origin. The set of all such lines is known as the complex Grassmannian manifold of complex lines in $\mathbb{C}^M$, or Grassmannian, which we denote by $\mathrm{GR}(M, 1)$. This is a well-known geometry that has been extensively studied for both clustering and optimization [93,115,116]. For computation purposes, every equivalence class $[\boldsymbol{h}_u] \in \mathrm{GR}(M, 1)$ is represented by its unit vector $\boldsymbol{h}_u\|\boldsymbol{h}_u\|^{-1}$ on behalf of all the points contained in the class.

To cluster data points in a manifold, we need to define: (1) a Riemannian distance that measures the space; (2) the tangent spaces, which are linear spaces that approximate the manifold in a neighborhood of a particular point; and (3) geodesics, which are the minimal smooth curves in the manifold that connect two of its points. The complex Grassmannian $\mathrm{GR}(M, 1)$ can be endowed with the following distance function:

$$\mathrm{dist}\big([\boldsymbol{h}_u], [\boldsymbol{h}_i]\big) = \arccos\Big(\frac{|\boldsymbol{h}_u^{\mathsf{H}}\boldsymbol{h}_i|}{\|\boldsymbol{h}_u\|\|\boldsymbol{h}_i\|}\Big) = \arccos\big(\rho(\boldsymbol{h}_u, \boldsymbol{h}_i)\big).$$

Note that this distance is a function of the CSI correlation, and as such, is invariant to scale and phase variations as intended.

The tangent space $\mathrm{T}_{[\boldsymbol{h}_u]}\mathrm{GR}(M, 1)$ is a linear space that contains the tangent directions of all 1-dimensional curves on the manifold passing through $[\boldsymbol{h}_u]$. In the case of $\mathrm{GR}(M, 1)$,

we have

$$\mathrm{T}_{[\boldsymbol{h}_u]}\mathrm{GR}(M,1) = \{\boldsymbol{v} \in \mathbb{C}^M : \boldsymbol{h}_u^{\mathsf{H}}\boldsymbol{v} = 0\}. \tag{5.12}$$

We define a Riemannian metric for the linear $\mathrm{T}_{[\boldsymbol{h}_u]}\mathrm{GR}(M,1)$:

$$\langle \boldsymbol{u}, \boldsymbol{v} \rangle_{[\boldsymbol{h}_u]} = \mathrm{Re}\big(\boldsymbol{u}^{\mathsf{H}}\boldsymbol{v}\big),\ \boldsymbol{u}, \boldsymbol{v} \in \mathrm{T}_{[\boldsymbol{h}_u]}\mathrm{GR}(M,1) \tag{5.13}$$

that induces a norm $\|\boldsymbol{v}\|_{[\boldsymbol{h}_u]} = \sqrt{\langle \boldsymbol{v}, \boldsymbol{v} \rangle_{[\boldsymbol{h}_u]}}$ for tangent vectors $\boldsymbol{v} \in \mathrm{T}_{[\boldsymbol{h}_u]}\mathrm{GR}(M,1)$.

Finally, we characterize geodesics connecting two points in $\mathrm{GR}(M,1)$. Formally, we define $\gamma(t)$ as the geodesic from the starting point $[\boldsymbol{h}_u] = \gamma(0)$ reaching the point $[\boldsymbol{h}_i]$ at $\gamma(1)$ at $t = 1$. This scaling implies that the geodesic has a defined initial velocity $\boldsymbol{v} = \gamma'(0)$. By construction, $\boldsymbol{v} \in \mathrm{T}_{[\boldsymbol{h}_u]}\mathrm{GR}(M,1)$, which can be computed with the *logarithm map*:

$$\mathrm{Log}_{[\boldsymbol{h}_u]}\big([\boldsymbol{h}_i]\big) = \frac{\boldsymbol{u}}{\|\boldsymbol{u}\|} \arctan\big(\|\boldsymbol{u}\|\big),\ \boldsymbol{u} = \frac{\|\boldsymbol{h}_u\|\boldsymbol{h}_i}{\boldsymbol{h}_u^{\mathsf{H}}\boldsymbol{h}_i} - \frac{\boldsymbol{h}_u}{\|\boldsymbol{h}_u\|}.$$

Conversely, for a geodesic $\gamma_{\boldsymbol{v}}(t)$ starting at $[\boldsymbol{h}_u]$ and with initial velocity $\boldsymbol{v} \in \mathrm{T}_{[\boldsymbol{h}_u]}\mathrm{GR}(M,1)$, the *exponential map* yields the point $\gamma_{\boldsymbol{v}}(1)$, and is given by

$$\mathrm{Exp}_{[\boldsymbol{h}_u]}\big(\boldsymbol{v}\big) = \frac{\boldsymbol{h}_u}{\|\boldsymbol{h}_u\|} \cos\big(\|\boldsymbol{v}\|_{[\boldsymbol{h}_u]}\big) + \frac{\boldsymbol{v}}{\|\boldsymbol{v}\|_{[\boldsymbol{h}_u]}} \sin\big(\|\boldsymbol{v}\|_{[\boldsymbol{h}_u]}\big).$$

We therefore have $[\boldsymbol{h}_i] = \mathrm{Exp}_{[\boldsymbol{h}_u]}\big(\mathrm{Log}_{[\boldsymbol{h}_u]}\big([\boldsymbol{h}_i]\big)\big)$. We can use both maps above to move on the manifold. Note that these expressions are equivalent to the general expressions of logarithm and exponential maps for general Grassmannians $\mathrm{GR}(M,p)$ based on singular value decompositions, but simplified for the particular case of $\mathrm{GR}(M,1)$ [53]. Figure 5.2 visually depicts the Grassmannian manifold discussed above and the relationship among tangent space, geodesic, logarithm and exponential map.

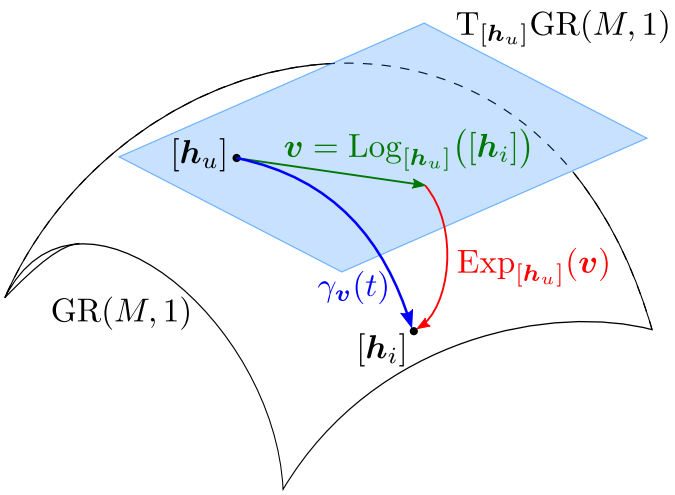

Figure 5.2: Depiction of Grassmannian manifold: we show the tangent space at $[\boldsymbol{h}_u]$, the geodesic connecting $[\boldsymbol{h}_u]$ and $[\boldsymbol{h}_i]$, the corresponding exponential and logarithm maps, and their relationships.

5.2.2 Unsupervised CSI Clustering

Among the plethora of unsupervised learning algorithms, e.g., [117], that are generally all useful in our user scheduling paradigm, we consider two simple and well-known data clustering methods: K-means clustering and agglomerative hierarchical clustering [118]. We adapt both unsupervised learning algorithms in the first step of manifold CSI clustering. Our goal is to classify N users into K clusters $\{\mathcal{C}_1, \cdots, \mathcal{C}_K\}$ based on the available CSI $\{\boldsymbol{h}_u\}_{u=1}^N$ at the scheduling server such that users in each cluster exhibit high CSI similarity in the Grassmannian $\mathrm{GR}(M,1)$.

Grassmannian K-means (GKM) Clustering

The basic K-means algorithm applies a greedy iterative approach to find a data partition that minimizes the distance between cluster members and their respective cluster centers. At the t-th iteration, the center of the k-th cluster $\mathcal{C}_k^t$ is defined by $\boldsymbol{u}_k^t \in \mathbb{C}^M$, which in Euclidean space is given by

$$\boldsymbol{\mu}_k^t = \frac{1}{|\mathcal{C}_k^t|} \sum_{n \in \mathcal{C}_k^t} \boldsymbol{h}_u. \tag{5.14}$$

In case of manifolds, the cluster centers are given by the intrinsic mean of cluster members,

$$\boldsymbol{\mu}_k^t = \underset{[\boldsymbol{u}]\in \mathrm{GR}(M,1)}{\arg\min} \sum_{n\in\mathcal{C}_k^t} \mathrm{dist}\big([\boldsymbol{h}_u], [\boldsymbol{u}]\big), \tag{5.15}$$

which has no closed-form solution as it depends on reference points, which are not fixed. The computation of the intrinsic mean is shown in Algorithm 5.2, where we use the unit-vector representatives of the equivalence classes for computation.

Algorithm 5.2 Intrinsic Mean for Cluster k in $\mathrm{GR}(M, 1)$

Input: $[\boldsymbol{h}_u] \in \mathcal{C}_k^t$, threshold ϵ, maximum number of iterations T_{im}
Initialize $t = 1$, $[\boldsymbol{u}] = [\boldsymbol{h}_i]$ for a random i in the cluster
while $t \leq T_{\mathrm{im}}$ or $\|\boldsymbol{v}\|_{\boldsymbol{u}} \geq \epsilon$ **do**
    Compute tangent vector $\boldsymbol{v} = |\mathcal{C}_k^t|^{-1} \sum_u \mathrm{Log}_{[\boldsymbol{u}]}\big([\boldsymbol{h}_u]\big)$
    Update $[\boldsymbol{u}] = \mathrm{Exp}_{[\boldsymbol{u}]}(\boldsymbol{v})$
    Set $t = t + 1$
end while
Return $[\boldsymbol{\mu}_k^t] = [\boldsymbol{u}]$

For the initial centers for K-means clustering, namely $\boldsymbol{\mu}_k^0, k \in \{1, \ldots, K\}$, we can randomly select K users out of the M users. However, performance of K-means could suffer due to poor initialization, and instead we initialize using K-means++ to mitigate this effect [119].

At the t-th iteration, each user is assigned to a cluster $\mathcal{C}_{k^\star}$ based on the center that is closest to the user, that is,

$$k^\star = \arg\min_k \mathrm{dist}\big([\boldsymbol{h}_u], [\boldsymbol{\mu}_k^t]\big). \tag{5.16}$$

The K cluster centers are updated. The clustering and center update steps continue until all clusters stay the same (or any other stopping criteria). Our implementation of Grassmannian K-means is summarized in Algorithm 5.3.

Algorithm 5.3 Grassmannian K-means

Input: $\boldsymbol{h}_u \in \mathbb{C}^M$, $n \in \{1, \ldots, N\}$, intrinsic mean parameters ϵ and T_{im}

Normalize CSIs to obtain Grassmannian representatives.
Set $t = 0$ and $\mathcal{C}_k^0 = \emptyset \ \forall k$
Select initial cluster centers according to K-means++ using the Grassmannian distance.
while $\mathcal{C}_k^t \neq \mathcal{C}_k^{t-1}$ for any k **do**
    Set $t = t + 1$ and $\mathcal{C}_k^t = \emptyset \ \forall k$
    for each user u **do**
        Find the center $[\boldsymbol{\mu}_k]$ closest to $[\boldsymbol{h}_u]$
        Assign user u to $\mathcal{C}_k^t$
    end for
    for each cluster k **do**
        Update cluster center $[\boldsymbol{\mu}_k]$ using Algorithm 5.2.
    end for
end while

Agglomerative Hierarchical Clustering (AHP)

This bottom-up hierarchical clustering approach begins by treating each data point as a single point cluster. It proceeds to successively merge the most similar cluster pairs until reaching the target number of clusters using a "linkage" rule to define the distances among merged pairs. Here, we use the complete linkage rule [72], i.e., at the t-th agglomeration, the similarity measure between clusters $\mathcal{C}_k^t$ and $\mathcal{C}_j^t$ is

$$d\left(\mathcal{C}_k^t, \mathcal{C}_j^t\right) = \max_{\boldsymbol{h}_m \in \mathcal{C}_k^t, \boldsymbol{h}_u \in \mathcal{C}_j^t} \operatorname{dist}\big([\boldsymbol{h}_m], [\boldsymbol{h}_u]\big). \tag{5.17}$$

In particular, the linkage between two single-user clusters is $d\left(\mathcal{C}_m^t, \mathcal{C}_u^t\right) = \operatorname{dist}\big([\boldsymbol{h}_m], [\boldsymbol{h}_u]\big)$. Given a set of clusters $\{\mathcal{C}_1^t, \cdots, \mathcal{C}_{K'}^t\}$, where $K' \geq K$, at each iteration, we determine the most similar pairs of clusters according to the linkage rule (5.17). After merging the two closest clusters, the process is repeated on the new set of clusters until the target number of clusters K is reached.

Note that in the context of Grassmannian manifold framework, any effective clustering approach is a valid option. We only focus on the two simpler approaches for their low complexity and ease of exposition.

5.2.3 CSI-Based User Scheduling

Direct Greedy Scheduling

One way to control CCI among users scheduled in the same group is to apply a simple greedy algorithm to form RSGs. This direct greedy method can be used a basic benchmark. Starting from a user group of one random user, we can consider each new user by examining its pairwise CSI correlation with all users in the group against a set threshold β, and only add the new user if each pairwise correlation is below β until the group size reaches M. We can then continue to schedule additional groups. This **direct greedy scheduling**, which we denote DS, does not rely on any supervised learning. Its scheduling results would vary significantly according to the order of the users being considered during scheduling.

User Scheduling with Unsupervised Learning

MIMO user scheduling optimization can consider different performance criteria. However, co-channel interference (CCI) among users scheduled for the same RSG should always reduced for any sensible performance metric. Based on the outcomes of CSI clustering, users within the same cluster have highly similar CSIs in terms of strong pairwise correlation coefficient, which can lead to strong CCI and challenge the receiving accuracy. From this perspective, users from different clusters are dissimilar and should induce low CCI, and thus are good candidates to be scheduled for MIMO resource sharing.

Our proposed GKM and AHP algorithms exploit the outcomes from CSI learning in the form of CSI clusters. Since there are multiple CSI clusters, our proposed GKM scheduling would compute the inter-cluster distances and sort clusters in descending order of minimum inter-cluster distance. We can then start GKM scheduling by forming user scheduling groups by considering clusters that are as far apart as possible to contain CCI. In the case of AHP, we apply cluster merging from the smallest cluster sizes.

5.2.4 Power Control in MAC Scheduling

CSI gains and power control must be considered differently in MAC and BC scheduling systems. In MAC, different receiver designs will benefit from different strategies: joint MMSE receiver benefits from CSIs with similar gains, whereas interference cancellation (e.g. SIC) receiver thrives when CSIs have large gain differences. In practice, power control in MAC plays an important role to mitigate the near-far problem. It is well known that optimal power control is achieved by waterfilling with respect to a target interference and noise level [59]. However, it can be hard to accurately apply power control at the scheduling stage for a large number of distinct groups. Thus, we can consider two scenarios: (a) equal power transmission, where maximum user transmit power $p_u = p_{\mathrm{UE}}^{\max}$ is used for all u without power control, despite having different channel gains $\|\boldsymbol{h}_u\|$ (MAC-U); (b) effective power control such that $p_u\|\boldsymbol{h}_u\|^2$ is nearly constant at the receiver (MAC-P).

Consider each user signal quality in MAC. Note that using an MMSE receiver with σ^2 being the noise power, the resulting user SINR is

$$\mathrm{SINR}_u^{\mathrm{MAC}} = \frac{\boldsymbol{h}_u^{\mathsf{H}}}{\|\boldsymbol{h}_u\|^2}\left(\frac{\sigma^2\boldsymbol{I}}{p_u\|\boldsymbol{h}_u\|^2} + \sum_{i\in\mathcal{S}_g, i\neq n}\frac{p_i\boldsymbol{h}_i\boldsymbol{h}_i^{\mathsf{H}}}{p_u\|\boldsymbol{h}_u\|^2}\right)^{-1}\boldsymbol{h}_u,$$

which means that SINR depends on all pairwise correlations of users within a group and the ratio of their received powers. Hence, the MMSE receiver benefits when the users within a group have similar received power $p_u\|\boldsymbol{h}_u\|^2$, and thus the received power ratios are close to 1. Such power ratios have minimum near-far effect and more consistent performance. These power ratios are often achieved under power control. Hence, we define the following grouping rule for MAC-P:

$$\varphi_{\mathrm{P}}^{\mathrm{MAC}}(\boldsymbol{h}_u, \mathcal{S}_g) = \begin{cases} 1 & \rho(\boldsymbol{h}_u, \boldsymbol{h}_\ell) \leq \beta \ \ \forall \ell \in \mathcal{S}_g \ \ \wedge \ \ |\mathcal{S}_g| < M, \\ 0 & \text{otherwise.} \end{cases} \tag{5.18}$$

5.2.5 MAC Scheduling without Power Control

In large scale systems such as IoT deployment, power control may not be practical. Without power control (MAC-U), our proposed scheduling algorithm shall attempt to reduce CCI by forming RSGs of similar channel gain and low similarity.

Specifically, we partition CSI gains of all N users into B levels. Users scheduled in group $\mathcal{S}_g$ must have CSI belonging to the same partition. Hence, we modify the grouping rule $\varphi_{\mathrm{P}}^{\mathrm{MAC}}$ to include this additional criteria:

$$\varphi_{\mathrm{U}}^{\mathrm{MAC}}(\boldsymbol{h}_u, \mathcal{S}_g) = \begin{cases} 1 & \rho(\boldsymbol{h}_u, \boldsymbol{h}_\ell) \leq \beta \ \ \forall \ell \in \mathcal{S}_g \ \ \wedge \ \ |\mathcal{S}_g| < M \ \ \wedge \ \ \|\boldsymbol{h}_u\| \in b(\mathcal{S}_g), \\ 0 & \text{otherwise.} \end{cases} \tag{5.19}$$

5.2.6 BC Scheduling for Low Complexity Transceivers

Practical individual receivers in BC systems do not share CSI information. For massive deployment, dirty paper coding (DPC) [120] is also challenging to implement practically. Our user scheduling will target low complexity transceivers that only utilize local CSI. Therefore, power control for scheduled user groups could prove useful. We consider a simple power control by allocating uniform transmit power among BC group members, i.e. $p_u = p_{\mathrm{BS}}^{\max}|\mathcal{S}_g|^{-1}$. Other simple schemes could be applied, e.g. allocating power such that users within a group exhibit close to identical received signal power $p_u\|\boldsymbol{h}_i\|^2$.

Furthermore, users with weaker CSI gain experience lower SNR. To compensate, our BC scheduling algorithm considers the CSI gain and allocate fewer users of similarly low CSI gain into an RSG to maintain sufficiently high SINR. As a simple two-tier implementation example, we shall partition downlink CSI gains into two levels with a threshold δ. We assign users with weaker CSI gains below δ into weaker CSI groups, up to a maximum of E users in such groups. Conversely, we assign users with stronger CSI gains above δ into stronger CSI groups, up to a maximum of D users in such groups where $D \geq E$.

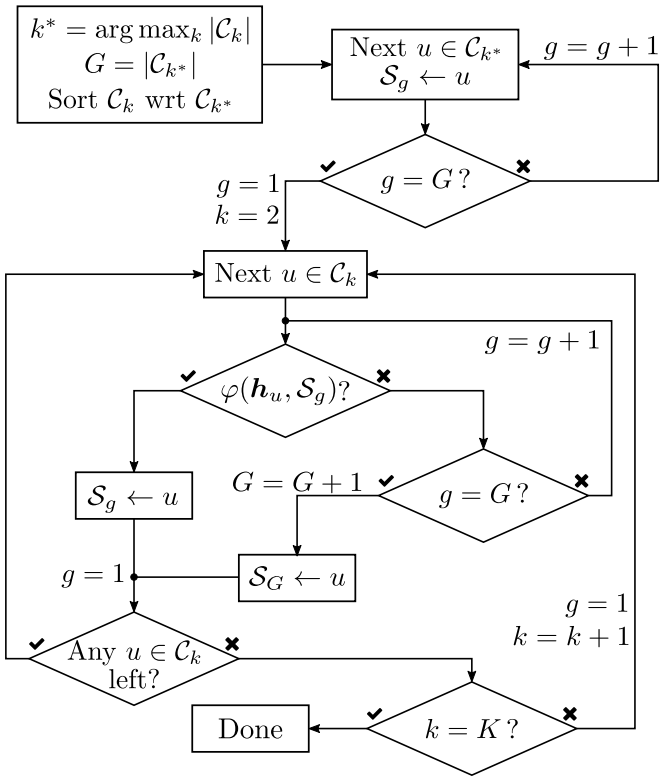

Figure 5.3: Flowchart of a greedy algorithm under the proposed scheduling principle, using rule (5.18) for MAC-P, (5.19) for MAC-U and (5.20) for BC.

The corresponding grouping rule is:

$$\varphi^{\mathrm{BC}}(\boldsymbol{h}_u, \mathcal{S}_g) = \begin{cases} 1 & \rho(\boldsymbol{h}_u, \boldsymbol{h}_\ell) \leq \beta \ \wedge \ |\mathcal{S}_g| < E \ \wedge \ \|\boldsymbol{h}_u\|, \|\boldsymbol{h}_\ell\| \leq \delta, \quad \forall \ell \in \mathcal{S}_g, \\ 1 & \rho(\boldsymbol{h}_u, \boldsymbol{h}_\ell) \leq \beta \ \wedge \ |\mathcal{S}_g| < D \ \wedge \ \|\boldsymbol{h}_u\|, \|\boldsymbol{h}_\ell\| > \delta, \quad \forall \ell \in \mathcal{S}_g \\ 0 & \text{otherwise.} \end{cases} \tag{5.20}$$

To summarize, Figure 5.3 depicts a flowchart of a greedy algorithm under our proposed user scheduling principle based on unsupervised learning outcomes. The application for uplink MAC-P, MAC-U or downlink BC depends on the choice of the selection rule $\varphi(\boldsymbol{h}_u, \mathcal{S}_g)$ according to (5.18), (5.19) or (5.20), respectively. Moreover, DS uses the same grouping rules for benchmarking purposes.

More generally, variants of the proposed scheduling algorithm can exploit both the knowledge of CSI similarity and CSI gains in different ways without changing significantly the

underlying methodology supporting our proposed strategy. Even more broadly, the unsupervised learning paradigm can also accommodate CSI features based on system performance and design choices.

5.2.7 Complexity Analysis

Clustering

First, we determine the complexity of Grassmannian K-means as follows:

- The CSI normalization step has a cost of $\mathcal{O}(MN)$.
- The Grassmannian distance has a cost of $\mathcal{O}(M)$, and thus the k-means++ initialization has a cost of $\mathcal{O}(KMN)$.
- Each iteration of the algorithm consists on two steps. First, assigning N users to K clusters, with a total cost of $\mathcal{O}(KMN)$. Then, the cluster center update for K clusters, which requires the computation of N logarithm maps and K exponential maps, both operations with a cost of $\mathcal{O}(M)$. This process is iterative, but in practice takes only a few intrinsic mean iterations and the cost of center updates is $\mathcal{O}(KMN)$.

Accordingly, the total cost for t iterations of Grassmannian K-means is $\mathcal{O}(tKMN)$.

In the case of Agglomerative Hierarchical Clustering, optimal implementations depend on the linkage criteria [121]. When considering complete linkage, it is known that the optimal algorithm has complexity $\mathcal{O}(N^2)$ with respect to similarity comparisons. Furthermore, the pairwise CSI correlation has a total cost of $\mathcal{O}(MN^2)$ as there are $N(N-1)$ pairwise computations, and thus the complexity of this clustering approach is $\mathcal{O}(MN^2)$.

User Grouping

All user grouping approaches (similarity-assisted and DS) exploit pairwise correlation information, which has cost $\mathcal{O}(M)$. For the similarity-assisted approaches (GKM and AHP),

the algorithm checks $K-1$ clusters with a total of $N' = N - |\mathcal{C}_k^*|$ users, which we can approximate in average with an uniform partition as $N' = N - N/K = N(K-1)/K$. In the case of DS, there is no clustering information, and hence $N-1$ users need to be tested for assignment. Hence, the computation complexity of similarity-assisted methods and DS is of order $\mathcal{O}(MN)$. Of course, in average we expect to observe some computational gains in similarity-assisted grouping, depending on system parameters and selected threshold, but cannot guarantee that they are going to be dramatically significant.

5.3 Numerical Experiments

In this section we test our proposed scheduling principle based on unsupervised learning. Considering a variety of user service needs and CSI properties, we provide a simple MIMO system model for both uplink and downlink applications.

We examined one BS equipped with $M = 8$ antennas, serving N single-antenna users. The mobile user CSI in uplink/downlink is modeled as random vectors that incorporate both shadowing and Rayleigh fading. A circularly complex normal vector of size M represents MIMO Rayleigh fading. The shadowing effect is modeled as a power gain that follows a lognormal distribution, with zero mean and standard deviation σ_L of 3dB in logarithmic scale. Additive channel noise is included in both uplink/downlink directions, corresponding to 20dB of average SNR.

We generate 100 different channels and perform 10 runs per channel realization in our Monte-Carlo simulations. All tests are performed in MATLAB using a 64-bit Windows PC with an i7-7700K processor and 32GB RAM.

5.3.1 Performance Metrics

Clustering

Though our scheduling method is compatible with any clustering algorithm, we adopt the well known and simple K-means clustering algorithms, though other clustering algorithms would have been equally applicable.

Recall that K-means clustering begins a pre-determined cluster number K. However, choosing the best K is a non-trivial problem which is problem dependent and does not have a best consensus solution [122]. Still there are several metrics that can help determine the number of clusters, such as the Silhouette value [123], the Krzanowski-Lai index [124], and the Hartigan index [125]. Regardless, we know that the nature of the MAC and BC systems imply that RSGs cannot have more than M users, since more users necessarily lead to more ill-conditioned group CSI matrix, impacting performance significantly. Hence, we set the number of clusters to be $K \leq M$ depending on the scenario, and show the pairwise correlation matrices obtained with both clustering methods.

CCI Evaluation

CCI leads a loss of signal-to-interference and noise ratio (SINR) in reference to SNR. To evaluate the efficacy of user scheduling, we compute the loss in SINR that each user experiences. In other words, we normalize the SINR of user u by its SNR if it were scheduled without co-channel users (a singleton group), such that it does not share resources and is only hampered by noise. Let p_u be the transmit power of the u-th user and σ^2 be the additive channel noise variance. This SINR loss is given by

$$10 \log_{10} \left(\frac{\mathrm{SINR}_u}{p_u \|\boldsymbol{h}_u\|^2 / \sigma^2} \right) \text{ dB}. \tag{5.21}$$

Thus, 0dB SINR loss corresponds fully orthogonal CSIs among co-channel users and zero CCI.

Resource Efficiency

To compare how well each scheduling method utilizes limited spectrum resources, we consider the overall MIMO spectrum efficiency by assuming that each scheduled MIMO user group is allocated the same bandwidth (or same amount of spectrum resource). In such case, the spectrum efficiency of the scheduling can be measured by averaging the achieved sum-rate of all groups over G total RSGs: $\frac{1}{G}\sum_{g=1}^{G} R_g$.

Runtime

As a proxy for computational complexity, in all simulations we store the "wall-clock" time for successful execution of the algorithms under test. Naturally, runtime often depends on computer, platform and code implementation. Thus, runtime by itself it may not fully capture the complexity of scheduling algorithms. Hence, we apply the same built-in functions, establish similar program structure and implementation for all algorithms under test to mitigate platform biases. Additionally, we also test scheduling for different number of users N to compare the scalability of the algorithms.

5.3.2 Uplink MAC MIMO Performance

In MAC, we set the number of clusters to $K = 8$ and we adopt linear MMSE receiver based on CSI of all received user signals in an RSG. This choice of K ensures that the scheduling process will attempt to utilize all spatial degrees of freedom for high spectrum efficiency.

Clustering Outcomes

Figure 5.4 shows the pairwise correlation matrix of $N = 800$ user CSIs after GKM and AHP clustering. Using grayscale of $[0, 1]$, larger values correspond to darker colors. An ideal clustering outcome should show 8 blocks of darker squares along the diagonal. GKM yields user clusters that show strong within-cluster similarity to be used later in scheduling. All 8 clusters contain many pairs that exhibit high spatial correlation. AHP shows less defined

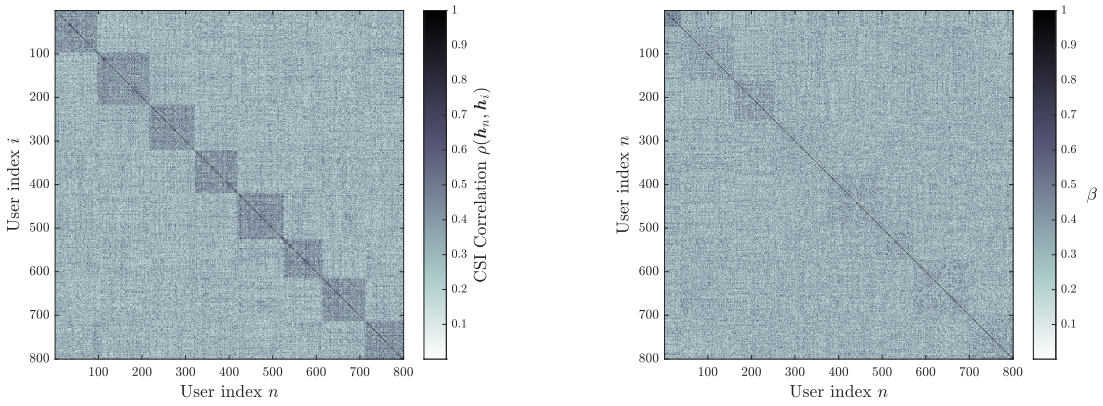

(a) GKM. (b) AHP.

Figure 5.4: Example of pairwise CSI correlation coefficient matrices after clustering $N = 800$ users with $K = 8$ clusters. Larger correlation values are darker. (a) Grassmannian K-means. (b) Hierarchical Clustering.

clusters: each cluster exhibits less highly correlated pairs, or in other words, users have weaker CSI correlation (i.e. weaker similarity) within each cluster.

Scheduling Performance

To systematically evaluate the the effect of exploiting similarity identified during clustering, we analyze our approach in MAC by considering the two scenarios described in the previous section:

(1) perfect power control, where each received user signal has unit power, i.e. $p_u\|\boldsymbol{h}_u\|^2 = 1\,\forall n \in \{1, \ldots, N\}$, denoted as MAC-P;

(2) no power control, where user CSI powers follow a log-normal distribution with parameter 3 dB, and $p_u = p_{\text{UE}}^{\max} = 1$ for all u, denoted as MAC-U.

We first test the MAC-P scenario, which helps isolate the benefits of unsupervised learning without the effect of variable receive powers. We consider three scheduling algorithms: the proposed GKM scheduling, AHP scheduling, and DS scheduling. For these three methods, Figure 5.5a shows the comparison of SINR mean and SINR distribution (10% to 90%

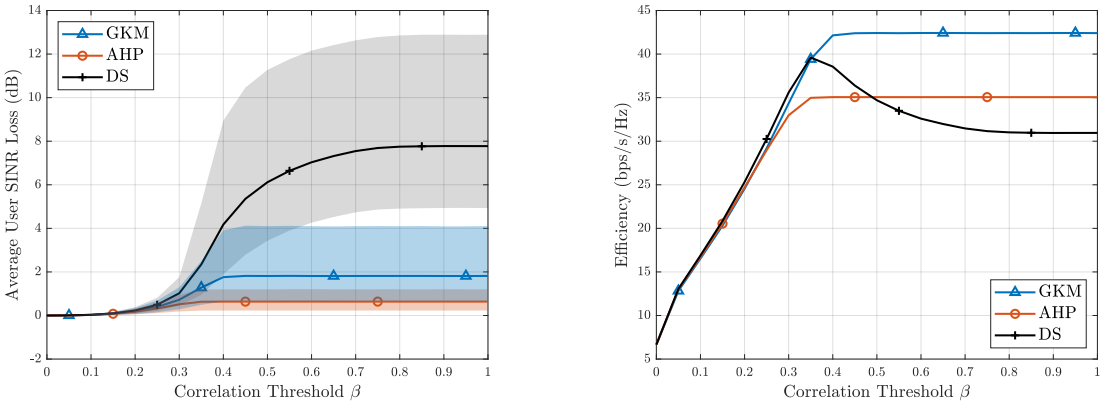

(a) Average user SINR loss.

(b) Average efficiency.

Figure 5.5: Performance of all scheduling algorithms in MAC with perfect power control (MAC-P). Here, $M = K = 8$ and $N = 800$. Solid lines represent the average over channel realizations, and shaded areas show all values within the 10th and 90th percentiles.

percentiles) of the resulting user SINR loss. The corresponding spectral efficiency is shown in Figure 5.5b.

From our test results, when β is set low, only very small amount of CCI is tolerated. In such cases, scheduling performance continues to be dominated by channel noise (i.e., SNR) and allowing little if any resource-sharing. Thus it is natural that, for $\beta < 0.25$, all three scheduling algorithms exhibit little SINR loss and relatively low spectrum efficiency. As we increase β, the spectrum efficiency starts go grow for all algorithms, as shown in Figure 5.5b. Eventually, spectrum efficiency of both GKM and AHP saturate. More specifically, GKM achieves higher spectrum efficiency but also larger SINR loss. AHP on the other hand, achieves lower spectrum efficiency but also lower SINR loss. In terms of SINR loss, both GKM and AHP exhibit very modest amount of SINR loss that saturates at 2dB and 1dB on average, respectively. These tests show that MIMO user scheduling can achieve spectrum efficiency and SINR loss tradeoff, with GKM being more efficient in spectrum utilization.

For DS, spectrum efficiency would peak at $\beta = 0.35$ before decreasing with increasing β. The spread of SINR is also large for DS, with some users experimenting more than -12dB of SINR loss. Both GKM and AHP have a tighter spread, which means most of the users will only experience 5dB of loss at most for GKM, and 2dB for AHP. This demonstrates the

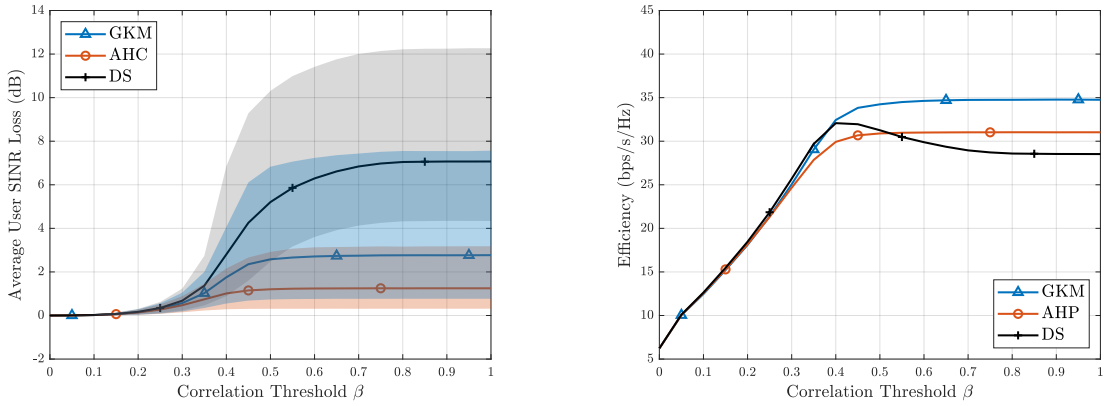

(a) Average user SINR loss.

(b) Average efficiency.

Figure 5.6: Performance of all scheduling algorithms in MAC without power control (MAC-U). Here, $M = K = 8$ and $N = 800$. Solid lines represent the average over channel realizations, and shaded areas show all values within the 10th and 90th percentiles.

failure of DS in grouping users of low mutual CCI to achieve good tradeoff between spectrum efficiency and SINR loss.

We next test the more practical case of unequal CSI gains in a network without power control, MAC-U. Against users of unequal CSI gain, for the scheduling rule $\varphi_{\mathrm{U}}^{\mathrm{MAC}}$ we partition users according to their CSI powers uniformly with power interval of 3 dB such that users are divided according to power level boundaries of $\ldots, -4.5, -1.5, 1.5, 4.5, \ldots$ in dB. Figs.5.6a and 5.6b show the SINR loss and average efficiency of all methods in MAC-U.

Again we observe that for smaller β, channel noise dominates the scheduling performance and all algorithms attain similar performance. With increasing β, users experience more SINR losses as more of them share resources, while the system enjoys the corresponding improvement in spectrum efficiency. The efficiency of GKM and AHP saturate for large β, with a modest increase of 1dB of SINR loss in average compared to MAC-U. Again, GKM achieves better performance with a small tradeoff in user SINR, compared to AHP that grants better user SINR at the expense of reduced efficiency. These tests confirm that similarity-assisted methods improve MIMO user scheduling, even when considering random channel gains and uniform power allocation.

In contrast, DS achieves peak efficiency at $\beta = 0.35$ and decreases steadily for larger β.

It also incurs greater SINR losses without any benefit in spectrum efficiency, being smaller than the efficiency of GKM and AHP in almost all cases. In average, users experience 7dB of SINR loss, and even more, the users that experience the largest losses are at least 4dB worse than with GKM or AHP. It is clear that DS offers no reasonable tradeoff between user SINR and spectral efficiency.

Additionally, note that the performance of MAC-P is naturally better than MAC-U, as the former enjoys perfect power control and can effectively deal with CSI power variability. Nevertheless, our proposed algorithms still attain good performance under the simpler setup of MAC-U, with only minor performance loss.

In both MAC-U and MAC-P tests, GKM and AHP scheduling deliver much better spectrum efficiency and lower SINR loss. Compared with DS, our tests strongly support the efficacy of the proposed MIMO user scheduling principle based on unsupervised learning on the Grassmannian manifold.

5.3.3 Performance for Downlink (BC)

In BC, we set the number of clusters to $K = 4$. Recall that the MRT precoders do not exploit the CSI of users in an RSG, and hence a smaller K better controls the SINR experienced by each user without incurring in severe degradation, due to oversharing resources.

Clustering Outcomes

We first analyze the CSI correlation matrices for GKM and AHP in Figure 5.7, where darker colors in grayscale denote larger correlation coefficient. Even for a low number of clusters, GKM is able to produce discriminative clusters that contain several user pairs with relatively high correlation compared to the members of other clusters. In this case, however, AHP produces clusters with fairly lower correlation, hinting that users within a cluster are not highly similar. This can also be explained by the bottom-up nature of hierarchical clustering of large datasets, as the last steps (merging large subclusters) are not very discriminative.

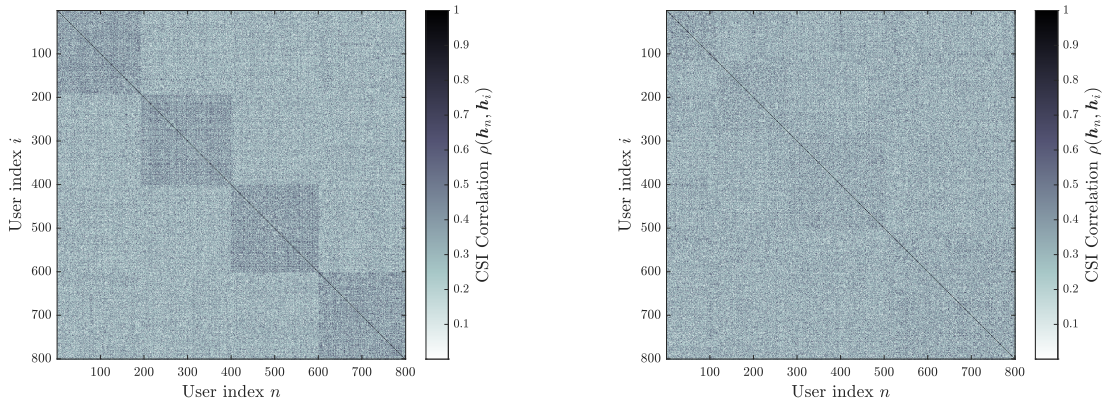

(a) GKM. (b) AHP.

Figure 5.7: Example of pairwise CSI correlation coefficient matrices after clustering $N = 800$ users with $K = 4$ clusters. Larger correlation values are darker. (a) Grassmannian K-means. (b) Hierarchical Clustering.

Scheduling Performance

For BC systems, we only consider the case where all users have random log-normal distributed CSI power, as the SINR of each user does not depend on the power of the rest of the co-channel users. Here, for the BC grouping rule φ^{BC} we consider a maximum number of users $D = K = 4$, a gain threshold for weak users $\delta = 0.5$ corresponding to -6dB of CSI power with respect to the average channel power, and a maximum number of weak users in an exclusive group $E = 2$. We also set $p_{\mathrm{BS}}^{\max} = M$ and use uniform power allocation within scheduled groups, although a different scheme can also apply.

Figs. 5.6a and 5.6b depict the SINR loss distribution and corresponding spectrum efficiency of all tested scheduling methods in BC. We first observe higher achieved SINR loss for BC than for MAC. Such outcome is expected since the selected UE receiver cannot utilize CSI of other users in its co-channel MIMO group. Correspondingly, the BC spectrum efficiency is lower. Similar to MAC systems, all three methods under comparison show comparable performance in terms of efficiency and SINR loss for $\beta \leq 0.15$. For larger β, AHP stalls and GKM offers a modest growth in efficiency, reaching 13% higher efficiency than AHP for $\beta > 0.3$. By comparison, AHP scheduling shows the best SINR losses, whereas

GKM offers a good tradeoff and outperforms AHP in spectral efficiency over all values of β.

In BC, the efficiency of DS peaks at at $\beta = 0.2$ before dropping by 58% from its peak. Both the proposed GKM and AHP out-perform DS for $\beta \geq 0.25$. DS also suffers the worst losses for all users, with an average SINR loss of up to 12dB, and 18dB SINR loss for the 10% of users that experience the worst conditions. Moreover, most users experience significantly worse SINR conditions on DS than GKM or AHP. Clearly, our test results in BC show that our proposed scheduling strategy, by exploiting similarity obtained via unsupervised learning, provides better SINR for the UE receivers and achieve higher spectrum efficiency than a direct approach.

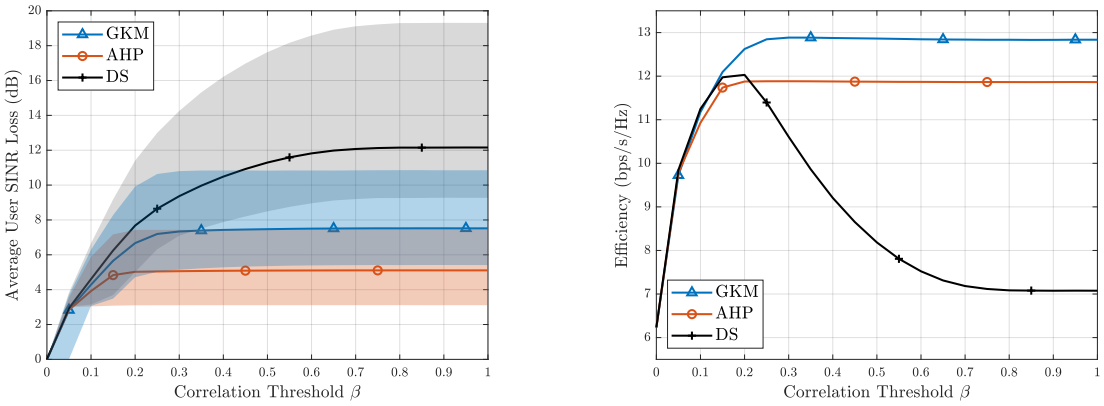

(a) Average user SINR loss.

(b) Average efficiency.

Figure 5.8: Performance of all scheduling algorithms in BC. Here, $M = 8$, $N = 800$, $K = D = 4$, $E = 2$ and $\delta = 0.5$. Solid lines represent the average over channel realizations, and shaded areas show all values within the 10th and 90th percentiles.

5.3.4 Runtime and Scalability

Table 5.1 summarizes the average runtime of all 3 algorithms under test for various number of users N under the same test settings specified earlier. In particular, we set a correlation threshold of $\beta = 0.8$, where there is significant performance difference between DS and the two proposed methods based on learning. As expected, the runtime grows with increasing N in both uplink and downlink. The runtime is not affected by different channel gains (MAC-

P vs. MAC-U). Because of its clustering complexity, AHP requires the largest runtime, whereas DS can be faster without clustering for smaller number of users. On the other hand, the proposed GKM only requires a modest level of computation, in view of the performance benefits shown in terms of SINR loss and spectrum efficiency. For example, GKM scheduling under uplink MAC only requires a modest increase of computation to provide significant performance improvement with respect to DS. For larger number of nodes N, the runtime of GKM scheduling scales mildly, as opposed to the sharper rise of runtime for AHP. In BC downlink, we observe similar results, in which the complexity gap between GKM scheduling and DS is less significant. The BC runtime comparison shows that for large N deployment smart scheduling methods based on unsupervised learning offer improved performance with little or no increase in computation complexity.

Table 5.1: Average runtime of all algorithms, in seconds, for $\beta = 0.8$.

	Mode	MAC-P			MAC-U			BC		
	Method	GKM	AHP	DS	GKM	AHP	DS	GKM	AHP	DS
	800	0.41	0.77	0.11	0.42	0.78	0.11	0.76	1.22	0.38
	1600	1.97	4.05	0.96	2.03	4.12	1.00	2.96	6.29	3.03
N	2400	5.95	11.02	2.85	6.05	10.99	2.87	8.41	13.78	8.93
	3200	11.20	25.28	8.37	11.47	25.69	8.08	19.30	32.45	22.93
	4000	20.25	42.56	14.29	20.29	41.98	14.27	36.21	54.12	40.74

5.4 Summary

In this chapter, we investigated the NP-hard problem of MIMO user scheduling in a general setting for large scale networks. We considered both uplink (MAC) and downlink (BC) operation. Recognizing the computational complexity of of traditional solutions due to network size, and the difficulties inherent to direct application of machine learning schemes, we proposed a new two-step paradigm for scalable MIMO user scheduling. In the first step, our method implemented unsupervised learning to identify users with highly similar CSI. This goal is achieved by clustering CSIs in the complex Grassmannian manifold, where distances

are directly related to spatial diversity. In the second step, a simple greedy scheduling scheme exploited the learned similarities to schedule user groups with high CSI diversity, minimizing co-channel interference. Our numerical tests demonstrated substantial performance gains and robustness of similarity-assisted scheduling when compared to direct scheduling, both in terms of user SINR and spectrum efficiency, with a modest increase in computational effort.

Chapter 6

Conclusions and Future Work

In this chapter, we summarize the contributions of this dissertation and discuss possible future research directions.

6.1 Summary

The goal of this dissertation is to explore geometrical approaches that enable efficient wireless service in large scale networks. These approaches identify key characteristics of the underlying geometry to better manage the radio resources in different network settings.

In Chapter 2, we lay the foundation for a general system model that allows the study of massive wireless networks with a multi-antenna base station (BS) and multiple single-antenna devices, in both uplink (MAC) and downlink (BC) scenarios. This model is then developed for two distinct operating regimes, depending on the activity level of the devices.

In the case of low-activity devices, with sporadic and non-timed links, an unknown number of devices transmit to the BS in uplink operation at any given time. To service the devices, the BS attempts to provide *access control*, without knowing which devices are active. Due to the limitations of traditional approaches for providing access to those users, we propose the adoption of grant-free access via use blind signal recovery methods, and in particular, using the Constant Modulus Algorithm (CMA). In the first part of this disserta-

tion (Chapters 3 and 4), we formulate two CMA-based approaches for blind signal recovery under different optimization perspectives.

In Chapter 3, we develop a regularized CMA-based cost function for multiple source recovery. The regularization term forces recovered signals to be uncorrelated, recovering distinct sources. To solve the optimization problem, we adopt the promising Wirtinger Flow (WF) algorithm. As WF provides theoretical guarantees for similar nonconvex problems under mild conditions and limited data samples, we leverage the convergence analysis of WF and generalize to consider the statistical characteristics of the signals in CMA. By characterizing the local geometry of CMA, we obtain convergence guarantees for CMA in the finite-sample scenario and general QAM modulations, both for simple and multiple source recovery. Furthermore, these results facilitate the selection of a more aggressive stepsize than commonly used in traditional gradient-descent methods, tackling slow convergence with no significant increase in computational cost.

In Chapter 4 we dismiss regularization and instead opt for a constrained optimization of CMA-based multiple source recovery, where the search space forces multi-lateral orthogonality of recovered signals. We characterize and redefine the constraint set as a Riemannian manifold, which we further develop to remove search directions corresponding to rotations of the demixers. This steps ensures that the cost function, restricted to the manifold, has a positive definite Riemannian Hessian in optimum solutions. Using this fact, we provide global convergence guarantees with high probability and limited data samples, regardless of initialization or parameter tuning. Numerical tests show successful recovery of all detected sources with a reasonable number of samples, for practical system sizes and different modulation schemes. Furthermore, the proposed Riemannian approach offers a good tradeoff between computation complexity and interference suppression.

In the second part of this dissertation, we turn to the problem of servicing a large number of very active users known to the base station, both in uplink and downlink scenarios. In this operation mode, the base station needs to attempt efficient *user scheduling* to service most

or all users with reasonable quality of service and using limited resources, i.e., it needs to allocate users in groups with low co-channel interference (CCI). In Chapter 5, we investigate the user scheduling problem by exploiting spatial diversity in MIMO systems. To mitigate CCI, instead of directly scheduling users with high channel dissimilarity, we propose a new unsupervised learning paradigm for MIMO user scheduling. This two-step strategy leverages the strengths of unsupervised learning with domain knowledge for the specific characterization of spatial diversity for low CCI. In a first step, we identify users whose channel state information (CSI) are highly similar in the sense of spatial correlation. This is possible by clustering CSI vectors in the Grassmannian manifold, which encodes subspace span in the geometry itself. After clustering, a greedy scheduling scheme exploits learning outcomes and determines user groups with low CCI. Our numerical test indicate that a combination of learning-enabled channel clustering can exploit the spatial compatibility effectively to reduce inter-group interference when compared with other benchmarks. Furthermore, this paradigm is generalizable to different learning schemes and scheduling metrics.

6.2 Extensions

- **Stronger convergence guarantees for Blind Signal Recovery:** Our convergence guarantees are formulated in noiseless scenarios. Reformulations of WF in phase retrieval have shown robustness against arbitrary corruptions [126] or random noise [127, 128] under mild assumptions, and these results could be leveraged in the context of blind signal recovery. Another interesting possibility is to consider stronger initialization methods with provable convergence improvement, and the study of our proposed methods in the more practical scenario of blind recovery under MIMO ISI fading channels

- **Exploiting additional information in Blind Signal Recovery:** Practical wireless systems consist of sophisticated protocols, and even in the case of IoT deployments,

the transceivers will commonly have access to more information than just the received (incoming) signal samples. For example, the devices will use forward error correction codes and channel coding, and the algorithm could verify if the recovered signal belongs to the set of valid codewords. Signals can also change constellation size over the duration of the data packet, e.g. WiFi, which has QPSK preambles and M-QAM payloads. Overall, our proposed signal recovery process could be enhanced if we consider and exploit these characteristics, be it by modifying the underlying geometry, leverage other non-convex optimization techniques such as proximal gradients, among other options.

- **Complexity reduction for Blind Signal Recovery:** Different families of cost functions have been proposed for blind equalization and beamforming [129–131], which are either nonconvex or nonsmooth. Moreover, similar cost functions have been studied in WF-like extensions for phase retrieval [126–128], which enjoy reduced computational and iteration complexity. These recent works use different approaches for their analysis, which could be leveraged to improve our theoretical results. Nonconvex and non-smooth cost functions can also be adopted in Riemannian optimization [132, 133]. Additionally, the proposed algorithms could be reformulated to consider stochastic or mini-batch implementations, further reducing computational complexity without incurring in performance loss.

- **Generalizations of MIMO User Scheduling:** Our results of unsupervised user scheduling are promising, although the system model is rather simple and could include common practical considerations. One clear example is systems with both time- and frequency-division multiple access (TDMA/FDMA), which are now commonplace in commercial applications. New geometries can leverage the similarity of users in multiple bands within a time slot, providing further insights to be considered in the scheduling problem. Other example is to consider users with different rate requirements

that could utilize multiple resource blocks in a given frame, and how to leverage CSI similarity with unequal rates. Moreover, the design of similarity-assisted scheduling algorithms can further exploit additional information and consider other performance metrics such as user data rate and fairness.

Appendix A

Proofs for CMA Convergence under Wirtinger Flow

A.1 Technical Lemmas and Corollaries for Single Source Recovery

Here, we establish several useful results to prove Theorem 1.

Lemma 11 (Concentration of sample covariance). *Consider independent subgaussian vectors* $\boldsymbol{a}_k \in \mathbb{C}^L$. *For every* $\delta > 0$, *there exist* $C(\delta) > 0$ *and* $c(\delta) > 0$ *such that for* $K \geq C(\delta)L$,

$$\left\| \frac{1}{K} \sum_{k=1}^{K} \boldsymbol{a}_k \boldsymbol{a}_k^{\mathsf{H}} - \mathbb{E}\{\boldsymbol{a}_k \boldsymbol{a}_k^{\mathsf{H}}\} \right\| \leq \delta,$$

holds with probability of at least $1 - 2\mathrm{e}^{-c(\delta)K}$.

Proof. Subgaussian vectors $\boldsymbol{a}_k$ can be defined as the independent rows of a $K \times L$ matrix A. Hence, Lemma 11 is a direct consequence of [90, Theorem 5.39]. ■

Part of this chapter is reprinted, with permission, from [C. Feres and Z. Ding, "Wirtinger Flow Meets Constant Modulus Algorithm: Revisiting Signal Recovery for Grant-Free Access" in *IEEE Transactions on Signal Processing (Early Access)*, Aug. 2021], its supplemental material, and followup modifications for final publication. Notations may have changed for consistency throughout this dissertation.

Corollary 12. *Under the conditions of Lemma 11, for* $K \geq C(\delta)L$ *and* $\boldsymbol{h} \in \mathbb{C}^L$, *with probability at least* $1 - 2\mathrm{e}^{-c(\delta)K}$,

$$-\delta\|\boldsymbol{h}\|^2 \leq \frac{1}{K}\sum_{k=1}^{K}|\boldsymbol{a}_k^{\mathsf{H}}\boldsymbol{h}|^2 - \boldsymbol{h}^{\mathsf{H}}\mathbb{E}\{\boldsymbol{a}_k\boldsymbol{a}_k^{\mathsf{H}}\}\boldsymbol{h} \leq \delta\|\boldsymbol{h}\|^2.$$

The expectation of matrices $\boldsymbol{A}(\boldsymbol{q})$ and $\boldsymbol{B}(\boldsymbol{q})$ are:

$$\mathbb{E}\{\boldsymbol{A}(\boldsymbol{q})\} = m_2^2(\|\boldsymbol{q}\|^2\boldsymbol{I} + \boldsymbol{q}\boldsymbol{q}^{\mathsf{H}}) + \kappa\boldsymbol{I}\circ(\boldsymbol{q}\boldsymbol{q}^{\mathsf{H}}),$$
$$\mathbb{E}\{\boldsymbol{B}(\boldsymbol{q})\} = 2m_2^2\boldsymbol{q}\boldsymbol{q}^{\mathsf{T}} + \kappa\boldsymbol{I}\circ(\boldsymbol{q}\boldsymbol{q}^{\mathsf{T}}).$$

The solutions of the CMA problem of Eq.(3.1) are of the form $\boldsymbol{z} = \mathrm{e}^{j\theta}\boldsymbol{e}_{\ell_j}$, with $\ell_j \in \{1,\ldots,L\}, \theta \in [0, 2\pi]$.

Two corollaries are helpful to prove Lemmas 2 and 3:

Corollary 13. *Let* $K \geq C_1(\delta)L$. *Then, with probability of at least* $1 - 6\mathrm{e}^{-c_1(\delta)K}$, *for all* $\boldsymbol{h} \in \mathbb{C}^L$ *such that* $\|\boldsymbol{h}\| = 1$, *we have*

$$(m_2^2 - \delta)\|\boldsymbol{h}\|^2 + (m_2^2 + \kappa)|\boldsymbol{h}^{\mathsf{H}}\boldsymbol{z}|^2 \leq \frac{1}{K}\sum_{k=1}^{K}|\boldsymbol{s}_k^{\mathsf{H}}\boldsymbol{z}|^2|\boldsymbol{s}_k^{\mathsf{H}}\boldsymbol{h}|^2 \leq (m_2^2 + \delta)\|\boldsymbol{h}\|^2 + (m_2^2 + \kappa)|\boldsymbol{h}^{\mathsf{H}}\boldsymbol{z}|^2.$$

Proof. Note that $\frac{1}{K}\sum_{k=1}^{K}|\boldsymbol{s}_k^{\mathsf{H}}\boldsymbol{z}|^2|\boldsymbol{s}_k^{\mathsf{H}}\boldsymbol{h}|^2 = \boldsymbol{h}^{\mathsf{H}}\boldsymbol{A}(\boldsymbol{z})\boldsymbol{h}$ and from Lemma 1 it follows that $-\delta\boldsymbol{I} \preceq \boldsymbol{A}(\boldsymbol{z}) - \mathbb{E}\{\boldsymbol{A}(\boldsymbol{z})\} \preceq \delta\boldsymbol{I}$. For the lower bound, we obtain

$$\boldsymbol{h}^{\mathsf{H}}\boldsymbol{A}(\boldsymbol{z})\boldsymbol{h} \geq m_2^2(\|\boldsymbol{h}\|^2 + |\boldsymbol{h}^{\mathsf{H}}\boldsymbol{z}|^2) - \delta\|\boldsymbol{h}\|^2 + \kappa\boldsymbol{h}^{\mathsf{H}}\big(\boldsymbol{I}\circ(\boldsymbol{z}\boldsymbol{z}^{\mathsf{H}})\big)\boldsymbol{h},$$

and knowing that $\boldsymbol{z} = \mathrm{e}^{\theta}\boldsymbol{e}_{\ell}$, we have

$$\kappa\boldsymbol{h}^{\mathsf{H}}\big(\boldsymbol{I}\circ(\boldsymbol{z}\boldsymbol{z}^{\mathsf{H}})\big)\boldsymbol{h} = \kappa\sum_{a=1}^{L}|\overline{h_a}z_a|^2 = \kappa|\boldsymbol{h}^{\mathsf{H}}\boldsymbol{z}|^2.$$

The upper bound is obtained similarly. ■

Corollary 14. *Let $K \geq C_1(\delta)L$. Then, with probability of at least $1 - 6\mathrm{e}^{-c_1(\delta)K}$, for all $\boldsymbol{h} \in \mathbb{C}^L$ such that $\|\boldsymbol{h}\| = 1$, we have*

$$\begin{aligned}
&\frac{m_2^2 - \delta}{2}\|\boldsymbol{h}\|^2 + \frac{3m_2^2 + 2\kappa}{2}\mathrm{Re}(\boldsymbol{h}^{\mathsf{H}}\boldsymbol{z})^2 - \frac{m_2^2}{2}\mathrm{Im}(\boldsymbol{h}^{\mathsf{H}}\boldsymbol{z})^2 \\
&\quad \leq \frac{1}{K}\sum_{k=1}^{K}\mathrm{Re}\big(\boldsymbol{h}^{\mathsf{H}}\boldsymbol{s}_k\boldsymbol{s}_k^{\mathsf{H}}\boldsymbol{z}\big)^2 \\
&\quad \leq \frac{m_2^2 + \delta}{2}\|\boldsymbol{h}\|^2 + \frac{3m_2^2 + 2\kappa}{2}\mathrm{Re}(\boldsymbol{h}^{\mathsf{H}}\boldsymbol{z})^2 - \frac{m_2^2}{2}\mathrm{Im}(\boldsymbol{h}^{\mathsf{H}}\boldsymbol{z})^2.
\end{aligned}$$

Proof. Lemma 1 states that $\delta\boldsymbol{I} \preceq \boldsymbol{U}(\boldsymbol{z}) - \mathbb{E}\{\boldsymbol{U}(\boldsymbol{z})\} \preceq \delta\boldsymbol{I}$. For the lower bound, recall that $2\mathrm{Re}(c)^2 = |c|^2 + \mathrm{Re}(c^2)$ for $c \in \mathbb{C}$, and

$$\begin{aligned}
\frac{1}{K}\sum_{k=1}^{K}\mathrm{Re}\big(\boldsymbol{h}^{\mathsf{H}}\boldsymbol{s}_k\boldsymbol{s}_k^{\mathsf{H}}\boldsymbol{z}\big)^2 &= \frac{1}{4}\begin{bmatrix}\boldsymbol{h}\\ \overline{\boldsymbol{h}}\end{bmatrix}^{\mathsf{H}}\begin{bmatrix}\boldsymbol{A}(\boldsymbol{z}) & \boldsymbol{B}(\boldsymbol{z})\\ \overline{\boldsymbol{B}(\boldsymbol{z})} & \overline{\boldsymbol{A}(\boldsymbol{z})}\end{bmatrix}\begin{bmatrix}\boldsymbol{h}\\ \overline{\boldsymbol{h}}\end{bmatrix} \\
&\geq \frac{m_2^2 - \delta}{2}\|\boldsymbol{h}\|^2 + \frac{3m_2^2}{2}\mathrm{Re}(\boldsymbol{h}^{\mathsf{H}}\boldsymbol{z})^2 - \frac{m_2^2}{2}\mathrm{Im}(\boldsymbol{h}^{\mathsf{H}}\boldsymbol{z})^2 \\
&\qquad + \frac{\kappa}{2}\mathrm{Re}\Big(\boldsymbol{h}^{\mathsf{H}}\big(\boldsymbol{I}\circ(\boldsymbol{z}\boldsymbol{z}^{\mathsf{H}})\big)\boldsymbol{h} + \boldsymbol{h}^{\mathsf{H}}\big(\boldsymbol{I}\circ(\boldsymbol{z}\boldsymbol{z}^{\mathsf{T}})\big)\overline{\boldsymbol{h}}\Big).
\end{aligned}$$

Knowing that $\boldsymbol{z} = \mathrm{e}^{\theta}\boldsymbol{e}_\ell$, the last term is equal to

$$\frac{\kappa}{2}\mathrm{Re}\Big(\boldsymbol{h}^{\mathsf{H}}\big(\boldsymbol{I}\circ(\boldsymbol{z}\boldsymbol{z}^{\mathsf{H}})\big)\boldsymbol{h} + \boldsymbol{h}^{\mathsf{H}}\big(\boldsymbol{I}\circ(\boldsymbol{z}\boldsymbol{z}^{\mathsf{T}})\big)\overline{\boldsymbol{h}}\Big) = \kappa\sum_{a=1}^{L}\mathrm{Re}(\overline{h_a}z_a)^2 = \kappa\mathrm{Re}(\boldsymbol{h}^{\mathsf{H}}\boldsymbol{z})^2.$$

The upper bound is obtained similarly. ■

A.2 Proof of Lemma 1

Rewrite the Hessian

$$\begin{aligned}\nabla^2 f(\boldsymbol{z}) &= \begin{bmatrix} \boldsymbol{A}(\boldsymbol{z}) & \boldsymbol{B}(\boldsymbol{z}) \\ \overline{\boldsymbol{B}(\boldsymbol{z})} & \overline{\boldsymbol{A}(\boldsymbol{z})} \end{bmatrix} + \begin{bmatrix} \boldsymbol{A}(\boldsymbol{z}) & \boldsymbol{0} \\ \boldsymbol{0} & \overline{\boldsymbol{A}(\boldsymbol{z})} \end{bmatrix} - R_2 \begin{bmatrix} \boldsymbol{S} & \boldsymbol{0} \\ \boldsymbol{0} & \overline{\boldsymbol{S}} \end{bmatrix} \\ &= \boldsymbol{U}(\boldsymbol{z}) + \boldsymbol{A}'(\boldsymbol{z}) - R_2 \boldsymbol{S}'.\end{aligned}$$

Observe that $\boldsymbol{U}(\boldsymbol{z})$ corresponds to the Hessian of the Phase Retrieval problem, which differs from the CMA Hessian due to the use of a desired average magnitude instead of known sampled amplitudes. Using the triangle inequality, to prove the lemma we show that

$$\left\| \boldsymbol{S} - \mathbb{E}\{\boldsymbol{S}\} \right\| \leq \delta_S = \delta/(8R_2), \tag{A.1}$$

$$\left\| \boldsymbol{A}(\boldsymbol{z}) - \mathbb{E}\{\boldsymbol{A}(\boldsymbol{z})\} \right\| \leq \delta_A = \delta/8, \tag{A.2}$$

$$\left\| \boldsymbol{U}(\boldsymbol{z}) - \mathbb{E}\{\boldsymbol{U}(\boldsymbol{z})\} \right\| \leq \delta_U = \delta/2. \tag{A.3}$$

Recall that the signal vectors are independent for $k \in \{1, \ldots, K\}$. Moreover, QAM constellations are bounded. Thus, the signal vectors are subgaussian. Hence, via Lemma 11, Eq.(A.1) holds with probability of at least $1 - 2\mathrm{e}^{-c_3(\delta_S)K}$ by choosing $K \geq C_3(\delta_S)L$.

Let $\boldsymbol{a}_k = \left(\boldsymbol{s}_k^{\mathsf{H}} \boldsymbol{z}\right) \boldsymbol{s}_k$, which are independent for $k \in \{1, \ldots, K\}$. Note that $\boldsymbol{s}_k^{\mathsf{H}} \boldsymbol{z} = \sqrt{m_2}\, \mathrm{e}^{j\varphi} \overline{s_{\ell_j}[k]}$. Therefore, vectors $\boldsymbol{a}_k$ have bounded, discrete elements over an exponentially large set, and as such they are subgaussian [91]. Additionally, we have

$$\boldsymbol{A}(\boldsymbol{z}) = \frac{1}{K} \sum_{k=1}^{K} \boldsymbol{a}_k \boldsymbol{a}_k^{\mathsf{H}}.$$

Therefore, by invoking Lemma 11, Eq.(A.2) holds with probability of at least $1 - 2\mathrm{e}^{-c_4(\delta_A)K}$ for $K \geq C_4(\delta_A)L$.

Now define $\boldsymbol{u}_k^{\mathsf{H}} = [\boldsymbol{a}_k^{\mathsf{H}} \ \boldsymbol{a}_k^{\mathsf{T}}]$. Using a similar reasoning as above, $\boldsymbol{u}_k$ are also subgaussian

and independent for $k \in \{1, \ldots, K\}$, and

$$\boldsymbol{U}(\boldsymbol{z}) = \frac{1}{K} \sum_{k=1}^{K} \boldsymbol{u}_k \boldsymbol{u}_k^{\mathsf{H}}.$$

Lemma 11 then states that Eq.(A.3) holds with probability of at least $1 - 2\mathrm{e}^{-c_5(\delta/2)K}$ by choosing $K \geq C_5(\delta_U)L$.

Finally, set $C_1(\delta) \geq \max\{C_3(\delta_S), C_4(\delta_A), C_5(\delta_U)\}$. By selecting $K \geq C_1(\delta)L$, Lemma 1 holds with probability of at least $1 - 6\mathrm{e}^{-c_1(\delta)K}$, where $c_1(\delta) = \min\{c_3(\delta_S), c_4(\delta_A), c_5(\delta_U)\}$.

A.3 Proof of Lemma 2

Let $\boldsymbol{q} \in E(\epsilon)$ and $\boldsymbol{h} = \mathrm{e}^{-i\phi(\boldsymbol{q})}\boldsymbol{q} - \boldsymbol{z}$. Hence $\|\boldsymbol{h}\| \leq \epsilon$ and $\mathrm{Im}(\boldsymbol{h}^{\mathsf{H}}\boldsymbol{z}) = 0$, as $\boldsymbol{h}$ and $\boldsymbol{z}$ are geometrically aligned:

$$\boldsymbol{h}^{\mathsf{H}}\boldsymbol{z} = \mathrm{e}^{-i\angle(\boldsymbol{q}^{\mathsf{H}}\boldsymbol{z})}\boldsymbol{q}^{\mathsf{H}}\boldsymbol{z} - \boldsymbol{z}^{\mathsf{H}}\boldsymbol{z} = |\boldsymbol{q}^{\mathsf{H}}\boldsymbol{z}| - \|\boldsymbol{z}\|^2 \in \mathbb{R}. \tag{A.4}$$

The proof is equivalent to proving

$$\begin{aligned}
&\mathrm{Re}\Big(\big\langle \nabla f(\boldsymbol{q}) - \nabla f(\mathrm{e}^{j\phi(\boldsymbol{q})}\boldsymbol{z}), \boldsymbol{q} - \mathrm{e}^{j\phi(\boldsymbol{q})}\boldsymbol{z} \big\rangle\Big) \\
&\quad = \frac{1}{K}\sum_{k=1}^{K} \Big(2\mathrm{Re}(\boldsymbol{h}^{\mathsf{H}}\boldsymbol{s}_k\boldsymbol{s}_k^{\mathsf{H}}\boldsymbol{z})^2 + 3\mathrm{Re}(\boldsymbol{h}^{\mathsf{H}}\boldsymbol{s}_k\boldsymbol{s}_k^{\mathsf{H}}\boldsymbol{z})|\boldsymbol{s}_k^{\mathsf{H}}\boldsymbol{h}|^2 + \frac{19}{20}|\boldsymbol{s}_k^{\mathsf{H}}\boldsymbol{h}|^4 + \big(|\boldsymbol{s}_k^{\mathsf{H}}\boldsymbol{z}|^2 - R_2\big)|\boldsymbol{s}_k^{\mathsf{H}}\boldsymbol{h}|^2\Big) \\
&\quad \geq \Big(\frac{1}{\alpha} + \frac{2m_2^2 - R_2 m_2 - \delta}{19}\Big)\|\boldsymbol{h}\|^2
\end{aligned}$$

for all $\boldsymbol{h}$ satisfying $\mathrm{Im}(\boldsymbol{h}^{\mathsf{H}}\boldsymbol{z}) = 0$ and $\|\boldsymbol{h}\| \leq \epsilon$. It suffices to show that for all $\boldsymbol{h}$ such that $\mathrm{Im}(\boldsymbol{h}^{\mathsf{H}}\boldsymbol{z}) = 0$ and $\|\boldsymbol{h}\| = 1$, and for all ξ with $0 \leq \xi \leq \epsilon$, the following inequality holds

$$\begin{aligned}
&\frac{1}{K}\sum_{k=1}^{K} \Big(2\mathrm{Re}(\boldsymbol{h}^{\mathsf{H}}\boldsymbol{s}_k\boldsymbol{s}_k^{\mathsf{H}}\boldsymbol{z})^2 + 3\xi\mathrm{Re}(\boldsymbol{h}^{\mathsf{H}}\boldsymbol{s}_k\boldsymbol{s}_k^{\mathsf{H}}\boldsymbol{z})|\boldsymbol{s}_k^{\mathsf{H}}\boldsymbol{h}|^2 + \frac{19}{20}\xi^2|\boldsymbol{s}_k^{\mathsf{H}}\boldsymbol{h}|^4 + \big(|\boldsymbol{s}_k^{\mathsf{H}}\boldsymbol{z}|^2 - R_2\big)|\boldsymbol{s}_k^{\mathsf{H}}\boldsymbol{h}|^2\Big) \\
&\quad \geq \frac{1}{\alpha} + \frac{2m_2^2 - R_2 m_2 - \delta}{19}.
\end{aligned}$$

Invoking Corollary 14, we show that for all $\boldsymbol{h}$ such that $\mathrm{Im}(\boldsymbol{h}^{\mathsf{H}}\boldsymbol{z}) = 0$ and $\|\boldsymbol{h}\| = 1$, and for all ξ with $0 \leq \xi \leq \epsilon$,

$$\frac{1}{K}\sum_{k=1}^{K}\Big(\frac{45}{19}\mathrm{Re}(\boldsymbol{h}^{\mathsf{H}}\boldsymbol{s}_k\boldsymbol{s}_k^{\mathsf{H}}\boldsymbol{z})^2 + 3\xi\mathrm{Re}(\boldsymbol{h}^{\mathsf{H}}\boldsymbol{s}_k\boldsymbol{s}_k^{\mathsf{H}}\boldsymbol{z})|\boldsymbol{s}_k^{\mathsf{H}}\boldsymbol{h}|^2 + \frac{19}{20}\xi^2|\boldsymbol{s}_k^{\mathsf{H}}\boldsymbol{h}|^4 + \big(|\boldsymbol{s}_k^{\mathsf{H}}\boldsymbol{z}|^2 - R_2\big)|\boldsymbol{s}_k^{\mathsf{H}}\boldsymbol{h}|^2\Big)$$
$$\geq \frac{1}{\alpha} + \frac{11m_2^2 - 2R_2m_2 + 5\delta}{38} + \frac{21m_2^2 + 14\kappa}{38}\mathrm{Re}(\boldsymbol{h}^{\mathsf{H}}\boldsymbol{z})^2. \tag{A.5}$$

For constant modulus signals, the last averaging term of the LHS of Eq.(A.5) is zero. For non-constant modulus QAM signals, the term is bounded by Corollaries 12 and 13:

$$\frac{1}{K}\sum_{k=1}^{K}\Big(|\boldsymbol{s}_k^{\mathsf{H}}\boldsymbol{h}|^2|\boldsymbol{s}_k^{\mathsf{H}}\boldsymbol{z}|^2 - R_2|\boldsymbol{s}_k^{\mathsf{H}}\boldsymbol{h}|^2\Big) \geq \big(m_2^2 - R_2m_2 - (1+R_2)\delta + (m_2^2+\kappa)|\boldsymbol{h}^{\mathsf{H}}\boldsymbol{z}|^2\big).$$

Let

$$\boldsymbol{Y}(\boldsymbol{h},\xi) = \frac{1}{K}\sum_{k=1}^{K}\Big(\frac{45}{19}\mathrm{Re}(\boldsymbol{h}^{\mathsf{H}}\boldsymbol{s}_k\boldsymbol{s}_k^{\mathsf{H}}\boldsymbol{z})^2 + 3\xi\mathrm{Re}(\boldsymbol{h}^{\mathsf{H}}\boldsymbol{s}_k\boldsymbol{s}_k^{\mathsf{H}}\boldsymbol{z})|\boldsymbol{s}_k^{\mathsf{H}}\boldsymbol{h}|^2 + \frac{19\xi^2}{20}|\boldsymbol{s}_k^{\mathsf{H}}\boldsymbol{h}|^4\Big).$$

Since $(a-b)^2 \geq \frac{a^2}{2} - b^2$, we have that

$$\begin{aligned}\boldsymbol{Y}(\boldsymbol{h},\xi) &\geq \left(\sqrt{\frac{45}{19K}\sum_{k=1}^{K}\mathrm{Re}(\boldsymbol{h}^{\mathsf{H}}\boldsymbol{s}_k\boldsymbol{s}_k^{\mathsf{H}}\boldsymbol{z})^2} - \sqrt{\frac{19\xi^2}{20K}\sum_{k=1}^{K}|\boldsymbol{s}_k^{\mathsf{H}}\boldsymbol{h}|^4}\right)^2 \\ &\geq \frac{45}{38K}\sum_{k=1}^{K}\mathrm{Re}(\boldsymbol{h}^{\mathsf{H}}\boldsymbol{s}_k\boldsymbol{s}_k^{\mathsf{H}}\boldsymbol{z})^2 - \frac{19\xi^2}{20K}\sum_{k=1}^{K}|\boldsymbol{s}_k^{\mathsf{H}}\boldsymbol{h}|^4.\end{aligned}$$

By means of Corollary 12, with high probability we have

$$\frac{1}{K}\sum_{k=1}^{K}|\boldsymbol{s}_k^{\mathsf{H}}\boldsymbol{h}|^4 \leq \max_k\|\boldsymbol{s}_k\|^2\Big(\frac{1}{K}\sum_{k=1}^{K}|\boldsymbol{s}_k^{\mathsf{H}}\boldsymbol{h}|^2\Big) \leq B^2L(m_2+\delta).$$

Using this result and the first inequality of Corollary 14, for $\|\boldsymbol{h}\| = 1$, it holds with high

probability that

$$\boldsymbol{Y}(\boldsymbol{h},\xi) \geq \frac{135m_2^2+90\kappa}{76}\mathrm{Re}(\boldsymbol{h}^{\mathsf{H}}\boldsymbol{z})^2 + \frac{45}{76}(m_2^2-\delta) - \frac{19B^2L}{20}\xi^2(m_2+\delta).$$

Hence, Lemma 2 holds under the following condition:

$$\begin{aligned}
&\frac{135m_2^2+90\kappa}{76}\mathrm{Re}(\boldsymbol{h}^{\mathsf{H}}\boldsymbol{z})^2 + \frac{45}{76}(m_2^2-\delta) - \frac{19B^2L}{20}\xi^2(m_2+\delta) \\
&\quad + \left(m_2^2 - R_2m_2 - (1+R_2)\delta + (m_2^2+\kappa)|\boldsymbol{h}^{\mathsf{H}}\boldsymbol{z}|^2\right)\cdot \mathbf{1}[Q\neq 4] \\
&\quad \geq \frac{1}{\alpha} + \frac{11m_2^2 - 2R_2m_2 + 5\delta}{38} + \frac{21m_2^2+14\kappa}{38}\mathrm{Re}(\boldsymbol{h}^{\mathsf{H}}\boldsymbol{z})^2. \qquad \text{(A.6)}
\end{aligned}$$

With $\xi \leq \epsilon = (10B\sqrt{L})^{-1}$ and $\delta \leq 0.01$, Eq.(A.6) holds for

$$\begin{aligned}
\alpha &\geq 3 \quad \text{for} \quad Q = 4, \\
\alpha &\geq 83 \quad \text{for} \quad Q \neq 4.
\end{aligned}$$

A.4 Proof of Lemma 3

Let $\boldsymbol{q} \in E(\epsilon)$ and $\boldsymbol{h} = \mathrm{e}^{-i\phi(\boldsymbol{q})}\boldsymbol{q} - \boldsymbol{z}$. For any $\boldsymbol{u} \in \mathbb{C}^L$ such that $\|\boldsymbol{u}\| = 1$, let $\boldsymbol{v} = \mathrm{e}^{-i\phi(\boldsymbol{q})}\boldsymbol{u}$. Therefore, it suffices to show that

$$
\begin{aligned}
&\Big|\boldsymbol{u}^{\mathsf{H}}\big(\nabla f(\boldsymbol{q}) - \nabla f(\mathrm{e}^{j\phi(\boldsymbol{q})}\boldsymbol{z})\big)\Big|^2 \\
&= \bigg|\frac{1}{K}\sum_{k=1}^{K} \boldsymbol{v}^{\mathsf{H}}\boldsymbol{s}_k\boldsymbol{s}_k^{\mathsf{H}}\boldsymbol{z}\Big(|\boldsymbol{s}_k^{\mathsf{H}}\boldsymbol{h}|^2 + 2\mathrm{Re}(\boldsymbol{h}^{\mathsf{H}}\boldsymbol{s}_k\boldsymbol{s}_k^{\mathsf{H}}\boldsymbol{z})\Big) \\
&\qquad + \Big(|\boldsymbol{s}_k^{\mathsf{H}}\boldsymbol{h}|^2 + 2\mathrm{Re}(\boldsymbol{h}^{\mathsf{H}}\boldsymbol{s}_k\boldsymbol{s}_k^{\mathsf{H}}\boldsymbol{z}) + |\boldsymbol{s}_k^{\mathsf{H}}\boldsymbol{z}|^2 - R_2\Big)\boldsymbol{v}^{\mathsf{H}}\boldsymbol{s}_k\boldsymbol{s}_k^{\mathsf{H}}\boldsymbol{h}\bigg|^2 \\
&\le \bigg(\frac{1}{K}\sum_{k=1}^{K} 2|\boldsymbol{s}_k^{\mathsf{H}}\boldsymbol{z}|^2|\boldsymbol{s}_k^{\mathsf{H}}\boldsymbol{v}||\boldsymbol{s}_k^{\mathsf{H}}\boldsymbol{h}| + 3|\boldsymbol{s}_k^{\mathsf{H}}\boldsymbol{z}||\boldsymbol{s}_k^{\mathsf{H}}\boldsymbol{v}||\boldsymbol{s}_k^{\mathsf{H}}\boldsymbol{h}|^2 + |\boldsymbol{s}_k^{\mathsf{H}}\boldsymbol{h}|^3|\boldsymbol{s}_k^{\mathsf{H}}\boldsymbol{v}| \\
&\qquad + \big(|\boldsymbol{s}_k^{\mathsf{H}}\boldsymbol{z}|^2 - R_2\big)\boldsymbol{v}^{\mathsf{H}}\boldsymbol{s}_k\boldsymbol{s}_k^{\mathsf{H}}\boldsymbol{h}\bigg)^2 \\
&\le \beta\Big(\frac{2m_2^2 - R_2m_2 - \delta}{19}\|\boldsymbol{h}\|^2 + \frac{1}{20K}\sum_{k=1}^{K}|\boldsymbol{s}_k^{\mathsf{H}}\boldsymbol{h}|^4\Big)
\end{aligned}
$$

holds for all $\boldsymbol{h}$ and $\boldsymbol{v}$ such that $\mathrm{Im}(\boldsymbol{h}^{\mathsf{H}}\boldsymbol{z}) = 0$, $\|\boldsymbol{h}\| \le \epsilon$, and $\|\boldsymbol{v}\| = 1$. Equivalently, we prove that for all $\boldsymbol{h}$ and $\boldsymbol{v}$ such that $\mathrm{Im}(\boldsymbol{h}^{\mathsf{H}}\boldsymbol{z}) = 0$, $\|\boldsymbol{h}\| = \|\boldsymbol{v}\| = 1$ and for all ξ with $0 \le \xi \le \epsilon$, the following inequality holds

$$
\begin{aligned}
&\bigg(\frac{1}{K}\sum_{k=1}^{K} 2|\boldsymbol{s}_k^{\mathsf{H}}\boldsymbol{z}|^2|\boldsymbol{s}_k^{\mathsf{H}}\boldsymbol{v}||\boldsymbol{s}_k^{\mathsf{H}}\boldsymbol{h}| + 3\xi|\boldsymbol{s}_k^{\mathsf{H}}\boldsymbol{z}||\boldsymbol{s}_k^{\mathsf{H}}\boldsymbol{v}||\boldsymbol{s}_k^{\mathsf{H}}\boldsymbol{h}|^2 + \xi^2|\boldsymbol{s}_k^{\mathsf{H}}\boldsymbol{h}|^3|\boldsymbol{s}_k^{\mathsf{H}}\boldsymbol{v}| \\
&\qquad + \big(|\boldsymbol{s}_k^{\mathsf{H}}\boldsymbol{z}|^2 - R_2\big)\boldsymbol{v}^{\mathsf{H}}\boldsymbol{s}_k\boldsymbol{s}_k^{\mathsf{H}}\boldsymbol{h}\bigg)^2 \\
&\le \beta\Big(\frac{2m_2^2 - R_2m_2 + \delta}{19} + \frac{\xi^2}{20K}\sum_{k=1}^{K}|\boldsymbol{s}_k^{\mathsf{H}}\boldsymbol{h}|^4\Big).
\end{aligned}
$$

Note that $|\boldsymbol{s}_k^{\mathsf{H}}\boldsymbol{z}|^2 = m_2 = R_2$ for constant-modulus signals, and thus the last term in the LHS is zero if $Q = 4$, and non-zero otherwise. Let $D = 3 + \mathbf{1}[Q \ne 4]$, and knowing that

$\big(\sum_{i=1}^n a_i\big)^2 \le n\sum_{i=1}^n a_i^2$, we have

$$\begin{aligned}
&\Big|\boldsymbol{u}^{\mathsf{H}}\big(\nabla f(\boldsymbol{q}) - \nabla f(\mathrm{e}^{j\phi(\boldsymbol{q})}\boldsymbol{z})\big)\Big|^2 \\
&\quad\le 4D\Big(\frac{1}{K}\sum_{k=1}^K |\boldsymbol{s}_k^{\mathsf{H}}\boldsymbol{z}|^2|\boldsymbol{s}_k^{\mathsf{H}}\boldsymbol{v}||\boldsymbol{s}_k^{\mathsf{H}}\boldsymbol{h}|\Big)^2 + 9D\xi^2\Big(\frac{1}{K}\sum_{k=1}^K |\boldsymbol{s}_k^{\mathsf{H}}\boldsymbol{z}||\boldsymbol{s}_k^{\mathsf{H}}\boldsymbol{v}||\boldsymbol{s}_k^{\mathsf{H}}\boldsymbol{h}|^2\Big)^2 \\
&\qquad + D\xi^4\Big(\frac{1}{K}\sum_{k=1}^K |\boldsymbol{s}_k^{\mathsf{H}}\boldsymbol{h}|^3|\boldsymbol{s}_k^{\mathsf{H}}\boldsymbol{v}|\Big)^2 + \Big|\frac{1}{K}\sum_{k=1}^K \big(|\boldsymbol{s}_k^{\mathsf{H}}\boldsymbol{z}|^2 - R_2\big)\boldsymbol{v}^{\mathsf{H}}\boldsymbol{s}_k\boldsymbol{s}_k^{\mathsf{H}}\boldsymbol{h}\Big|^2 \cdot \mathbf{1}[Q\neq 4] \\
&\quad\le 4DI_1 + 9D\xi^2 I_2 + D\xi^4 I_3 + I_4\cdot\mathbf{1}[Q\neq 4].
\end{aligned}$$

We now bound these terms on the right-hand side. By means of the Cauchy-Schwarz inequality and Corollary 13,

$$I_1 \le \Big(\frac{1}{K}\sum_{k=1}^K |\boldsymbol{s}_k^{\mathsf{H}}\boldsymbol{z}|^2|\boldsymbol{s}_k^{\mathsf{H}}\boldsymbol{v}|^2\Big)\Big(\frac{1}{K}\sum_{k=1}^K |\boldsymbol{s}_k^{\mathsf{H}}\boldsymbol{z}|^2|\boldsymbol{s}_k^{\mathsf{H}}\boldsymbol{h}|^2\Big) \le (2m_2^2+\kappa+\delta)^2,$$

and

$$I_2 \le \Big(\frac{1}{K}\sum_{k=1}^K |\boldsymbol{s}_k^{\mathsf{H}}\boldsymbol{h}|^4\Big)\Big(\frac{1}{K}\sum_{k=1}^K |\boldsymbol{s}_k^{\mathsf{H}}\boldsymbol{v}|^2|\boldsymbol{s}_k^{\mathsf{H}}\boldsymbol{z}|^2\Big) \le \frac{2m_2^2+\kappa+\delta}{K}\sum_{k=1}^K |\boldsymbol{s}_k^{\mathsf{H}}\boldsymbol{h}|^4.$$

Invoking Corollary 12, the bounded norm $\|\boldsymbol{s}_k\| \le B\sqrt{L}$, and the Cauchy-Schwarz inequality, we obtain

$$I_3 \le \Big(\frac{1}{K}\sum_{k=1}^K |\boldsymbol{s}_k^{\mathsf{H}}\boldsymbol{h}|^3 \max_k \|\boldsymbol{s}_k\|\Big)^2 \le \frac{B^2L(m_2+\delta)}{K}\sum_{k=1}^K |\boldsymbol{s}_k^{\mathsf{H}}\boldsymbol{h}|^4.$$

For non-constant modulus QAM signals, we can bound I_4 by invoking Corollaries 12 and 13:

$$I_4 = \Big|\boldsymbol{h}^{\mathsf{H}}\big(\boldsymbol{A}(\boldsymbol{z}) - R_2\boldsymbol{S}\big)\boldsymbol{h}\Big|^2 \le \Big|m_2^2 - R_2m_2 - (1+R_2)\delta\Big|^2 = \big(m_2^2+\kappa+(1+R_2)\delta\big)^2.$$

Therefore, we obtain

$$\begin{aligned}\left\|\nabla f(\boldsymbol{q})\right\|^2 &= \max_{\|\boldsymbol{u}\|=1} \left|\boldsymbol{u}^{\mathsf{H}}\big(\nabla f(\boldsymbol{q}) - \nabla f(\mathrm{e}^{j\phi(\boldsymbol{q})}\boldsymbol{z})\big)\right|^2 \\ &\le 4D(2m_2^2+\kappa+\delta)^2 + \frac{9D\xi^2(2m_2^2+\kappa+\delta)}{K}\sum_{k=1}^{K}|\boldsymbol{s}_k^{\mathsf{H}}\boldsymbol{h}|^4 \\ &\quad + \frac{DB^2L\xi^4(m_2+\delta)}{K}\sum_{k=1}^{K}|\boldsymbol{s}_k^{\mathsf{H}}\boldsymbol{h}|^4 + \big(m_2^2+\kappa+(1+R_2)\delta\big)^2\cdot\mathbf{1}[Q\neq 4] \\ &\le \beta\Big(\frac{2m_2^2-R_2m_2-\delta}{19} + \frac{\xi^2}{20K}\sum_{k=1}^{K}|\boldsymbol{s}_k^{\mathsf{H}}\boldsymbol{h}|^4\Big).\end{aligned}$$

Hence, Lemma 3 holds under the following condition:

$$\begin{aligned}\beta \ge \max\Big\{&\frac{76D(2m_2^2+\kappa+\delta)^2}{2m_2^2-R_2m_2-\delta} + \frac{19(m_2^2+\kappa+(1+R_2)\delta\big)^2}{2m_2^2-R_2m_2-\delta}\cdot\mathbf{1}[Q\neq 4], \\ &180D(2m_2^2+\kappa+\delta) + 20DB^2L\epsilon^2(m_2+\delta)\Big\}. \qquad \text{(A.7)}\end{aligned}$$

With $\epsilon = (10B\sqrt{L})^{-1}$ and $\delta \le 0.01$, Eq.(A.7) holds for

$$\begin{aligned}\beta &\ge 235 \quad \text{for} \quad Q = 4, \\ \beta &\ge 959 \quad \text{for} \quad Q \neq 4.\end{aligned}$$

A.5 Technical Lemmas and Corollaries for Multiple Source Recovery

We first introduce additional notations to aid exposition. Using the overall system parameter space $\boldsymbol{q}$, we rewrite the cost function for MSR as

$$g(\boldsymbol{q}) = \sum_{\ell=1}^{J} f(\boldsymbol{q}_\ell) + \gamma_0 \sum_{\ell=1}^{J}\sum_{i\neq\ell}^{J} \left|\boldsymbol{q}_i\boldsymbol{S}\boldsymbol{q}_\ell\right|^2 = \sum_{\ell=1}^{J} f(\boldsymbol{q}_\ell) + \gamma_0 r(\boldsymbol{q}), \qquad \text{(A.8)}$$

where $\boldsymbol{q} = \big[\boldsymbol{q}_1^{\mathsf{T}} \ \dots \ \boldsymbol{q}_J^{\mathsf{T}}\big]^{\mathsf{T}}$ is the aggregation of the J demixers, f is the CMA cost function for single source recovery, and $\boldsymbol{S}$ is the sample covariance matrix of source signals. The gradient of g, using Wirtinger calculus, is given by

$$\nabla_\ell g = \frac{1}{K}\sum_{k=1}^{K}\Big(|\boldsymbol{s}_k^{\mathsf{H}}\boldsymbol{q}_\ell|^2 - R_2\Big)\boldsymbol{s}_k\boldsymbol{s}_k^{\mathsf{H}}\boldsymbol{q}_\ell + \gamma_0\sum_{i\neq\ell}^{J}\boldsymbol{S}\boldsymbol{q}_i\boldsymbol{q}_i^{\mathsf{H}}\boldsymbol{S}\boldsymbol{q}_\ell = \nabla f(\boldsymbol{q}_\ell) + \gamma_0\nabla_\ell r(\boldsymbol{q}), \tag{A.9}$$

and the Wirtinger Hessian of the cost function g is

$$\begin{aligned}\nabla^2 g(\boldsymbol{q}) &= \mathrm{Bdiag}\Big(\big\{\nabla^2 f(\boldsymbol{q}_\ell)\big\}_{\ell=1}^{J}\Big) + \gamma_0\begin{bmatrix}\boldsymbol{G}_1(\boldsymbol{q}) & \cdots & \boldsymbol{H}_{1J}(\boldsymbol{q})\\ \vdots & \ddots & \vdots\\ \boldsymbol{H}_{J1}(\boldsymbol{q}) & \cdots & \boldsymbol{G}_J(\boldsymbol{q})\end{bmatrix}\\ &= \mathrm{Bdiag}\Big(\big\{\nabla^2 f(\boldsymbol{q}_\ell)\big\}_{\ell=1}^{J}\Big) + \gamma_0\nabla^2 r(\boldsymbol{q}).\end{aligned} \tag{A.10}$$

The expectation of matrices $\boldsymbol{A}(\boldsymbol{q})$ and $\boldsymbol{B}(\boldsymbol{q})$ are defined in Section A.1, and the matrices $\boldsymbol{C}_\ell(\boldsymbol{q})$, $\boldsymbol{E}_{\ell i}(\boldsymbol{q})$ and $\boldsymbol{F}_{\ell i}(\boldsymbol{q})$ of the MSR Hessian satisfy

$$\begin{aligned}\mathbb{E}\{\boldsymbol{C}_\ell(\boldsymbol{q})\} &= \sum_{i\neq\ell}^{J}\Big(m_2^2\boldsymbol{q}_i\boldsymbol{q}_i^{\mathsf{H}} + \frac{m_2^2}{K}\|\boldsymbol{q}_i\|^2\boldsymbol{I} + \frac{\kappa}{K}\big(\boldsymbol{I}\circ(\boldsymbol{q}_i\boldsymbol{q}_i^{\mathsf{H}})\big)\Big),\\ \mathbb{E}\{\boldsymbol{E}_{\ell i}(\boldsymbol{q})\} &= m_2^2(\boldsymbol{q}_i^{\mathsf{H}}\boldsymbol{q}_\ell)\boldsymbol{I} + \frac{m_2^2}{K}\boldsymbol{q}_\ell\boldsymbol{q}_i^{\mathsf{H}} + \frac{\kappa}{K}\big(\boldsymbol{I}\circ(\boldsymbol{q}_\ell\boldsymbol{q}_i^{\mathsf{H}})\big),\\ \mathbb{E}\{\boldsymbol{F}_{\ell i}(\boldsymbol{q})\} &= m_2^2\boldsymbol{q}_i\boldsymbol{q}_\ell^{\mathsf{T}} + \frac{m_2^2}{K}\boldsymbol{q}_\ell\boldsymbol{q}_i^{\mathsf{T}} + \frac{\kappa}{K}\big(\boldsymbol{I}\circ(\boldsymbol{q}_\ell\boldsymbol{q}_i^{\mathsf{T}})\big),\end{aligned}$$

and thus, the expectation of the ℓ-th gradient of the regularizing term is

$$\mathbb{E}\{\nabla_\ell r(\boldsymbol{q})\} = \mathbb{E}\big\{\boldsymbol{C}_\ell(\boldsymbol{q})\big\}\boldsymbol{q}_\ell = \sum_{i\neq\ell}^{J}\big(m_2^2\boldsymbol{q}_i\boldsymbol{q}_i^{\mathsf{H}}\boldsymbol{q}_\ell + \frac{m_2^2}{K}\|\boldsymbol{q}_i\|^2\boldsymbol{q}_\ell + \frac{\kappa}{K}\big(\boldsymbol{I}\circ(\boldsymbol{q}_i\boldsymbol{q}_i^{\mathsf{H}})\big)\boldsymbol{q}_\ell. \tag{A.11}$$

Note that at a MSR CMA solution $\boldsymbol{z} = \big[\mathrm{e}^{j\theta_{\ell_1}}\boldsymbol{e}_{\ell_1}^{\mathsf{T}} \ \dots \mathrm{e}^{j\theta_{\ell_J}}\boldsymbol{e}_{\ell_J}^{\mathsf{T}}\big]^{\mathsf{T}}$, we have $\boldsymbol{z}_i^{\mathsf{H}}\boldsymbol{z}_\ell = 0$ for all

$i \neq \ell$. Hence,

$$\begin{aligned}\mathbb{E}\{\nabla_\ell r(\boldsymbol{z})\} &= \sum_{i\neq\ell}^{J}\Big(m_2^2\boldsymbol{z}_i\boldsymbol{z}_i^{\mathsf{H}}\boldsymbol{z}_\ell + \frac{m_2^2}{K}\|\boldsymbol{z}_i\|^2\boldsymbol{z}_\ell + \frac{\kappa}{K}\boldsymbol{I}\circ(\boldsymbol{z}_i\boldsymbol{z}_i^{\mathsf{H}})\boldsymbol{z}_\ell\Big)\\ &= \sum_{i\neq\ell}^{J}\Big(\frac{m_2^2}{K}\boldsymbol{z}_\ell + \frac{\kappa}{K}\boldsymbol{e}_i\boldsymbol{e}_i^{\mathsf{T}}\boldsymbol{z}_\ell\Big) = \frac{(J-1)m_2^2}{K}\boldsymbol{z}_\ell,\end{aligned}$$

which is non-zero, but decreases with the number of samples K and is aligned with the ℓ-th component of the solution. Therefore, for large K, the CMA solution corresponds to an approximate stationary point in gradient-descent schemes, which often yields satisfactory numerical solutions. In particular, we have the following result that defines the CMA solution in multiple source recovery as a approximate stationary point.

Corollary 15. *Let $K \geq C_2(\delta)L$. Then, with probability at least $1 - 12\mathrm{e}^{-c_2(\delta)K}$,*

$$\Big\|\nabla_\ell g(\boldsymbol{z}) - \mathbb{E}\big\{\nabla_\ell g(\boldsymbol{z})\big\}\Big\| \leq (1 + R_2 + \gamma_0)\delta.$$

Proof. By definition and the triangular inequality,

$$\begin{aligned}\Big\|\nabla_\ell g(\boldsymbol{z}) - \mathbb{E}\big\{\nabla_\ell g(\boldsymbol{z})\big\}\Big\| &= \max_{\boldsymbol{v}\in\mathbb{C}^L,\,\|\boldsymbol{v}\|=1}\Big|\boldsymbol{v}^{\mathsf{H}}\Big(\nabla_\ell g(\boldsymbol{z}) - \mathbb{E}\big\{\nabla_\ell g(\boldsymbol{z})\big\}\Big)\Big|\\ &\leq \max_{\boldsymbol{v}\in\mathbb{C}^L,\,\|\boldsymbol{v}\|=1}\Big|\boldsymbol{v}^{\mathsf{H}}\Big(\nabla f(\boldsymbol{z}_\ell) - \mathbb{E}\big\{\nabla f(\boldsymbol{z}_\ell)\big\}\Big)\Big|\\ &\quad + \gamma_0\max_{\boldsymbol{v}\in\mathbb{C}^L,\,\|\boldsymbol{v}\|=1}\Big|\boldsymbol{v}^{\mathsf{H}}\Big(\nabla_\ell r(\boldsymbol{z}) - \mathbb{E}\big\{\nabla_\ell r(\boldsymbol{z})\big\}\Big)\Big|.\end{aligned}$$

Note that $\nabla f(\boldsymbol{z}_\ell) = \boldsymbol{A}(\boldsymbol{z}_\ell)\boldsymbol{z}_\ell - R_2\boldsymbol{S}\boldsymbol{z}_\ell$ and $\nabla_\ell r(\boldsymbol{z}) = \boldsymbol{C}_\ell(\boldsymbol{z})\boldsymbol{z}_\ell$. Invoking Lemma 5 and the triangular inequality, we have that for all $\boldsymbol{v} \in \mathbb{C}^L$ such that $\|\boldsymbol{v}\| = 1$,

$$\begin{aligned}\Big|\boldsymbol{v}^{\mathsf{H}}\Big(\nabla f(\boldsymbol{z}_\ell) - \mathbb{E}\big\{\nabla f(\boldsymbol{z}_\ell)\big\}\Big)\Big| &\leq \Big(\big\|\boldsymbol{A}(\boldsymbol{z}_\ell) - \mathbb{E}\big\{\boldsymbol{A}(\boldsymbol{z}_\ell)\big\}\big\| + R_2\big\|\boldsymbol{S} - \mathbb{E}\big\{\boldsymbol{S}\big\}\big\|\Big)\|\boldsymbol{z}_\ell\|\|\boldsymbol{v}\|\\ &\leq (1 + R_2)\delta,\\ \Big|\boldsymbol{v}^{\mathsf{H}}\Big(\nabla_\ell r(\boldsymbol{z}) - \mathbb{E}\big\{\nabla_\ell r(\boldsymbol{z})\big\}\Big)\Big| &\leq \Big\|\boldsymbol{C}_\ell(\boldsymbol{z}) - \mathbb{E}\big\{\boldsymbol{C}_\ell(\boldsymbol{z})\big\}\Big\|\|\boldsymbol{z}_\ell\|\|\boldsymbol{v}\| \leq \delta.\end{aligned}$$

■

We now define corollaries that will be useful to prove Lemmas 6 and 7:

Corollary 16. *Let $K \geq C_2(\delta)L$. Then, with probability at least $1-12\mathrm{e}^{-c_2(\delta)K}$, for all $\boldsymbol{v} \in \mathbb{C}^L$ such that $\|\boldsymbol{v}\| = 1$, we have*

$$\Big(\frac{J-1}{K}m_2^2 - \delta\Big)\|\boldsymbol{v}\|^2 \leq \boldsymbol{v}^{\mathsf{H}}\boldsymbol{C}_\ell(\boldsymbol{z})\boldsymbol{v} \leq \Big(\frac{K+J-1}{K}m_2^2 + \frac{\kappa}{K} + \delta\Big)\|\boldsymbol{v}\|^2.$$

Proof. From Lemma 5, we have that $-\delta\boldsymbol{I} \preceq \boldsymbol{C}_\ell(\boldsymbol{z}) - \mathbb{E}\{\boldsymbol{C}_\ell(\boldsymbol{z})\} \preceq \delta\boldsymbol{I}$. Hence, the lower bound is

$$\begin{aligned}\boldsymbol{v}^{\mathsf{H}}\boldsymbol{C}_\ell(\boldsymbol{z})\boldsymbol{v} &\geq \sum_{i\neq\ell}^{J}\Big(m_2^2|\boldsymbol{v}^{\mathsf{H}}\boldsymbol{z}_i|^2 + \frac{m_2^2}{K}\|\boldsymbol{z}_i\|^2\|\boldsymbol{v}\|^2 + \frac{\kappa}{K}\boldsymbol{v}^{\mathsf{H}}\big(\boldsymbol{I}\circ(\boldsymbol{z}_i\boldsymbol{z}_i^{\mathsf{H}})\boldsymbol{v}\big)\Big) - \delta\|\boldsymbol{v}\|^2 \\ &\geq (J-1)\frac{m_2^2}{K}\|\boldsymbol{v}\|^2 + \sum_{i\neq\ell}^{J}\Big(m_2^2|\boldsymbol{v}^{\mathsf{H}}\boldsymbol{z}_i|^2 + \frac{\kappa}{K}\boldsymbol{v}^{\mathsf{H}}\big(\boldsymbol{I}\circ(\boldsymbol{z}_i\boldsymbol{z}_i^{\mathsf{H}})\boldsymbol{v}\big)\Big) - \delta\|\boldsymbol{v}\|^2.\end{aligned}$$

Note that $Km_2^2 + \kappa > 0$ for all $K > 1$ and all QAM modulations. Additionally, knowing that $\boldsymbol{z}_\ell = \mathrm{e}^{\theta_{\ell_j}}\boldsymbol{e}_{\ell_j}$ for all $\ell_j \in \{1,\ldots,J\}$, we have that

$$0 \leq \sum_{i\neq\ell}^{J}|\boldsymbol{v}^{\mathsf{H}}\boldsymbol{z}_i|^2 = \sum_{i\neq\ell}^{J}\boldsymbol{v}^{\mathsf{H}}\big(\boldsymbol{I}\circ(\boldsymbol{z}_i\boldsymbol{z}_i^{\mathsf{H}})\big)\boldsymbol{v} = \sum_{i\neq\ell}^{J}|v_{\ell,i}|^2 \leq \|\boldsymbol{v}\|^2.$$

The upper bound is obtained similarly. ■

Corollary 17. *Let $K \geq C_2(\delta)L$. Then, with probability at least $1-12\mathrm{e}^{-c_2(\delta)K}$, we have*

$$\big|\boldsymbol{z}_\ell\boldsymbol{S}\boldsymbol{z}_i\big|^2 \leq \delta.$$

Proof. From Lemma 1, we have that $-\delta\boldsymbol{I} \preceq \boldsymbol{S} - m_2\boldsymbol{I} \preceq \delta\boldsymbol{I}$. Then, we have that for all $\boldsymbol{u}$ and $\boldsymbol{v}$ such that $\|\boldsymbol{u}\| = \|\boldsymbol{v}\| = 1$,

$$\begin{aligned}\big|\boldsymbol{u}^{\mathsf{H}}\boldsymbol{S}\boldsymbol{v}\big|^2 &\leq m_2\big|\boldsymbol{u}^{\mathsf{H}}\boldsymbol{v}\big| + \Big|\boldsymbol{u}^{\mathsf{H}}\big(\boldsymbol{S}-m_2\boldsymbol{I}\big)\boldsymbol{v}\Big|^2 \leq m_2\big|\boldsymbol{u}^{\mathsf{H}}\boldsymbol{v}\big| + \big\|\boldsymbol{S}-m_2\boldsymbol{I}\big\|\|\boldsymbol{u}\|\|\boldsymbol{v}\| \\ &\leq m_2\big|\boldsymbol{u}^{\mathsf{H}}\boldsymbol{v}\big| + \delta\|\boldsymbol{u}\|\|\boldsymbol{v}\|.\end{aligned}$$

Knowing that $\boldsymbol{z}_\ell = \mathrm{e}^{\theta_{\ell_j}} \boldsymbol{e}_{\ell_j}$ for all $\ell_j \in \{1, \ldots, J\}$, we have that $|\boldsymbol{z}_\ell^{\mathsf{H}} \boldsymbol{z}_i| = 0$ for all $i \neq \ell$, and we obtain the bound. ■

Corollary 18. *Let $K \geq C_2(\delta)L$. Then, with probability at least $1 - 12\mathrm{e}^{-c_2(\delta)K}$, we have*

$$\big\|\boldsymbol{F}_{\ell i}(\boldsymbol{z})\big\| \leq m_2^2 + \delta.$$

Proof. From Lemma 5, we have that $-\delta \boldsymbol{I} \preceq \boldsymbol{F}_{\ell i}(\boldsymbol{z}) - \mathbb{E}\big\{\boldsymbol{F}_{\ell i}(\boldsymbol{z})\big\} \preceq \delta \boldsymbol{I}$, or equivalently,

$$\big\|\boldsymbol{F}_{\ell i}(\boldsymbol{z}) - \mathbb{E}\big\{\boldsymbol{F}_{\ell i}(\boldsymbol{z})\big\}\big\| \leq \delta.$$

Furthermore, using [134, Corollary 8.6.2] for the largest singular value (i.e. the operator norm), we have

$$\big\|\boldsymbol{F}_{\ell i}(\boldsymbol{z})\big\| \leq \big\|\mathbb{E}\big\{\boldsymbol{F}_{\ell i}(\boldsymbol{z})\big\}\big\| + \delta.$$

Knowing that $\boldsymbol{z}_\ell = \mathrm{e}^{\theta_{\ell_j}} \boldsymbol{e}_{\ell_j}$ for all $\ell_j \in \{1, \ldots, J\}$, we also have that

$$\mathbb{E}\big\{\boldsymbol{F}_{\ell i}(\boldsymbol{z})\big\} = m_2^2 \boldsymbol{z}_i \boldsymbol{z}_\ell^{\mathsf{T}} + \frac{m_2^2}{K} \boldsymbol{z}_\ell \boldsymbol{z}_i^{\mathsf{T}} + \frac{\kappa}{K} \boldsymbol{I} \circ \big(\boldsymbol{z}_\ell \boldsymbol{z}_i^{\mathsf{T}}\big) = m_2^2 \mathrm{e}^{j(\theta_{\ell_\ell} + \theta_{\ell_i})} \boldsymbol{e}_i \boldsymbol{e}_\ell^{\mathsf{T}} + \frac{m_2^2}{K} \mathrm{e}^{j(\theta_{\ell_j} + \theta_{\ell_i})} \boldsymbol{e}_\ell \boldsymbol{e}_i^{\mathsf{T}},$$

which means that $\mathbb{E}\big\{\boldsymbol{F}_{\ell i}(\boldsymbol{z})\big\}$ has only two non-zero elements in positions (ℓ, i) and (i, ℓ) with $i \neq \ell$. Hence, its non-zero columns are independent, and its norm is the largest absolute value of the non-zero elements, i.e.

$$\big\|\mathbb{E}\big\{\boldsymbol{F}_{\ell i}(\boldsymbol{z})\big\}\big\| = \max\left\{\left|\mathrm{e}^{j(\theta_{\ell_j} + \theta_{\ell_i})} m_2^2\right|, \left|\mathrm{e}^{j(\theta_{\ell_j} + \theta_{\ell_i})} \frac{m_2^2}{K}\right|\right\} = m_2^2.$$ ■

Corollary 19. *Let $K \geq C_2(\delta)L$. Then, with probability at least $1 - 12\mathrm{e}^{-c_2(\delta)K}$, for all*

$\boldsymbol{h} \in \mathbb{C}^{JL}$ *such that its* J *components have unit norm, i.e.,* $\|\boldsymbol{h}_\ell\| = 1$*, we have*

$$\sum_{\ell=1}^{J}\sum_{i\neq\ell}^{J} \left|\boldsymbol{h}_\ell^{\mathsf{H}}\boldsymbol{S}\boldsymbol{z}_i\right|^2 + \mathrm{Re}\big(\boldsymbol{h}_\ell^{\mathsf{H}}\boldsymbol{S}\boldsymbol{h}_i\boldsymbol{z}_i^{\mathsf{H}}\boldsymbol{S}\boldsymbol{z}_\ell\big) + \mathrm{Re}\big(\boldsymbol{h}_\ell^{\mathsf{H}}\boldsymbol{S}\boldsymbol{z}_i\boldsymbol{h}_i^{\mathsf{H}}\boldsymbol{S}\boldsymbol{z}_\ell\big) \geq -\Big(\frac{m_2^2}{K}+\delta\Big)\big\|\boldsymbol{h}\big\|^2. \quad \text{(A.12)}$$

Proof. Recall $\nabla^2 r(\boldsymbol{z})$ as defined in Eq.(A.10). Now, notice that

$$\begin{aligned}
&\sum_{\ell=1}^{J}\sum_{i\neq\ell}^{J} \left|\boldsymbol{h}_\ell^{\mathsf{H}}\boldsymbol{S}\boldsymbol{z}_i\right|^2 + \mathrm{Re}\big(\boldsymbol{h}_\ell^{\mathsf{H}}\boldsymbol{S}\boldsymbol{h}_i\boldsymbol{z}_i^{\mathsf{H}}\boldsymbol{S}\boldsymbol{z}_\ell\big) + \mathrm{Re}\big(\boldsymbol{h}_\ell^{\mathsf{H}}\boldsymbol{S}\boldsymbol{z}_i\boldsymbol{h}_i^{\mathsf{H}}\boldsymbol{S}\boldsymbol{z}_\ell\big)\\
&\quad= \sum_{\ell=1}^{J}\sum_{i<\ell}^{J} \left|\boldsymbol{h}_\ell^{\mathsf{H}}\boldsymbol{S}\boldsymbol{z}_i\right|^2 + \left|\boldsymbol{h}_i^{\mathsf{H}}\boldsymbol{S}\boldsymbol{z}_\ell\right|^2 + 2\mathrm{Re}\big(\boldsymbol{h}_\ell^{\mathsf{H}}\boldsymbol{S}\boldsymbol{h}_i\boldsymbol{z}_i^{\mathsf{H}}\boldsymbol{S}\boldsymbol{z}_\ell\big) + 2\mathrm{Re}\big(\boldsymbol{h}_\ell^{\mathsf{H}}\boldsymbol{S}\boldsymbol{z}_i\boldsymbol{h}_i^{\mathsf{H}}\boldsymbol{S}\boldsymbol{z}_\ell\big)\\
&\quad= \frac{1}{2}\tilde{\boldsymbol{h}}^{\mathsf{H}}\nabla^2 r(\boldsymbol{z})\tilde{\boldsymbol{h}},
\end{aligned}$$

where in the second equality we collect pairs (i,ℓ) and (ℓ,i) in one summation, and $\tilde{\boldsymbol{h}}$ is the stacked version of all $\boldsymbol{h}_\ell$ and their complex conjugates, i.e. $\tilde{\boldsymbol{h}} = \big[\boldsymbol{h}_1^{\mathsf{T}}\ \boldsymbol{h}_1^{\mathsf{H}}\ \cdots\ \boldsymbol{h}_J^{\mathsf{T}}\ \boldsymbol{h}_J^{\mathsf{H}}\ \big]^{\mathsf{T}}$. From Lemma 5, we have that $-\delta\boldsymbol{I} \preceq \nabla^2 r(\boldsymbol{z}) - \mathbb{E}\{\nabla^2 r(\boldsymbol{z})\} \preceq \delta\boldsymbol{I}$. Hence, we have that

$$\begin{aligned}
\frac{1}{2}\tilde{\boldsymbol{h}}^{\mathsf{H}}\nabla^2 r(\boldsymbol{z})\tilde{\boldsymbol{h}} &\geq \frac{1}{2}\tilde{\boldsymbol{h}}^{\mathsf{H}}\mathbb{E}\big\{\nabla^2 r(\boldsymbol{z})\big\}\tilde{\boldsymbol{h}} - \frac{\delta}{2}\|\tilde{\boldsymbol{h}}\|^2\\
&= \sum_{\ell=1}^{J}\Bigg(\mathrm{Re}\big(\boldsymbol{h}_\ell^{\mathsf{H}}\mathbb{E}\big\{\boldsymbol{C}_\ell(\boldsymbol{z})\big\}\boldsymbol{h}_\ell\big) + \sum_{i\neq\ell}^{J}\mathrm{Re}\big(\boldsymbol{h}_\ell^{\mathsf{H}}\mathbb{E}\big\{\boldsymbol{E}_{\ell i}(\boldsymbol{z})\big\}\boldsymbol{h}_i\big)\\
&\qquad + \sum_{i\neq\ell}^{J}\mathrm{Re}\big(\boldsymbol{h}_\ell^{\mathsf{H}}\mathbb{E}\big\{\boldsymbol{F}_{\ell i}(\boldsymbol{z})\big\}\overline{\boldsymbol{h}_i}\big)\Bigg) - \delta\|\boldsymbol{h}\|^2\\
&= \sum_{\ell=1}^{J}\sum_{i\neq\ell}^{J}\Bigg(\mathrm{Re}\Big(\boldsymbol{h}_\ell^{\mathsf{H}}\big(m_2^2\boldsymbol{z}_i\boldsymbol{z}_i^{\mathsf{H}} + \frac{m_2^2}{K}\|\boldsymbol{z}_i\|^2\boldsymbol{I} + \frac{\kappa}{K}\boldsymbol{I}\circ(\boldsymbol{z}_i\boldsymbol{z}_i^{\mathsf{H}})\big)\boldsymbol{h}_\ell\Big)\\
&\qquad + \mathrm{Re}\Big(\boldsymbol{h}_\ell^{\mathsf{H}}\big(m_2^2(\boldsymbol{z}_i^{\mathsf{H}}\boldsymbol{z}_\ell)\boldsymbol{I} + \frac{m_2^2}{K}\boldsymbol{z}_\ell\boldsymbol{z}_i^{\mathsf{H}} + \frac{\kappa}{K}\boldsymbol{I}\circ(\boldsymbol{z}_\ell\boldsymbol{z}_i^{\mathsf{H}})\big)\boldsymbol{h}_i\Big)\\
&\qquad + \mathrm{Re}\Big(\boldsymbol{h}_\ell^{\mathsf{H}}\big(m_2^2\boldsymbol{z}_i\boldsymbol{z}_\ell^{\mathsf{T}} + \frac{m_2^2}{K}\boldsymbol{z}_\ell\boldsymbol{z}_i^{\mathsf{T}} + \frac{\kappa}{K}\boldsymbol{I}\circ(\boldsymbol{z}_\ell\boldsymbol{z}_i^{\mathsf{T}})\big)\overline{\boldsymbol{h}_i}\Big)\Bigg) - \delta\|\boldsymbol{h}\|^2.
\end{aligned}$$

Knowing that $\boldsymbol{z}_\ell = \mathrm{e}^{\theta_{\ell_j}}\boldsymbol{e}_{\ell_j}$ for all $\ell_j \in \{1,\ldots,J\}$, we have that $|h_{\ell,i}| = |\boldsymbol{h}_\ell^{\mathsf{H}}\boldsymbol{z}_i|$, and

$\boldsymbol{I} \circ (\boldsymbol{z}_\ell \boldsymbol{z}_i^{\mathsf{H}}) = \boldsymbol{I} \circ (\boldsymbol{z}_i \boldsymbol{z}_\ell^{\mathsf{H}}) = \boldsymbol{0}$ and $(\boldsymbol{z}_\ell^{\mathsf{H}} \boldsymbol{z}_i) = 0$ for all $i \neq \ell$. Hence,

$$\begin{aligned}
\frac{1}{2}\tilde{\boldsymbol{h}}^{\mathsf{H}} \nabla^2 r(\boldsymbol{z}) \tilde{\boldsymbol{h}} \geq \sum_{\ell=1}^{J} \sum_{i \neq \ell}^{J} \Bigg(& m_2^2 \big|\boldsymbol{h}_\ell^{\mathsf{H}} \boldsymbol{z}_i\big|^2 + \frac{m_2^2}{K} \|\boldsymbol{z}_i\|^2 \big\|\boldsymbol{h}_\ell\big\|^2 + \frac{\kappa}{K} + \frac{m_2^2}{K} \mathrm{Re}\big(\boldsymbol{h}_\ell^{\mathsf{H}} \boldsymbol{z}_\ell \boldsymbol{z}_i^{\mathsf{H}} \boldsymbol{h}_i\big) \\
& + m_2^2 \mathrm{Re}\big(\boldsymbol{h}_\ell^{\mathsf{H}} \boldsymbol{z}_i \boldsymbol{z}_\ell^{\mathsf{T}} \overline{\boldsymbol{h}_i}\big) + \frac{m_2^2}{K} \mathrm{Re}\big(\boldsymbol{h}_\ell^{\mathsf{H}} \boldsymbol{z}_\ell \boldsymbol{z}_i^{\mathsf{T}} \overline{\boldsymbol{h}_i}\big) \Bigg) - \delta \|\boldsymbol{h}\|^2 \\
= \sum_{\ell=1}^{J} \sum_{i \neq \ell}^{J} \Bigg(& \Big(m_2^2 + \frac{\kappa}{K}\Big) \big|\boldsymbol{h}_\ell^{\mathsf{H}} \boldsymbol{z}_i\big|^2 + \frac{m_2^2}{K} \big\|\boldsymbol{h}_\ell\big\|^2 \\
& + \frac{2m_2^2}{K} \mathrm{Re}\big(\boldsymbol{h}_\ell^{\mathsf{H}} \boldsymbol{z}_\ell\big) \mathrm{Re}\big(\boldsymbol{h}_i^{\mathsf{H}} \boldsymbol{z}_i\big) + m_2^2 \mathrm{Re}\big(\boldsymbol{h}_\ell^{\mathsf{H}} \boldsymbol{z}_i \boldsymbol{h}_i^{\mathsf{H}} \boldsymbol{z}_\ell\big) \Bigg) - \delta \|\boldsymbol{h}\|^2 \\
= m_2^2 \sum_{\ell=1}^{J} \sum_{i<\ell}^{J} \Big(& \big|\boldsymbol{h}_\ell^{\mathsf{H}} \boldsymbol{z}_i\big|^2 + \big|\boldsymbol{h}_i^{\mathsf{H}} \boldsymbol{z}_\ell\big|^2 + 2\mathrm{Re}\big(\boldsymbol{h}_\ell^{\mathsf{H}} \boldsymbol{z}_i \boldsymbol{h}_i^{\mathsf{H}} \boldsymbol{z}_\ell\big) \Big) \\
& + \frac{1}{K} \sum_{\ell=1}^{J} \sum_{i \neq \ell}^{J} \Big(\kappa \big|\boldsymbol{h}_\ell^{\mathsf{H}} \boldsymbol{z}_i\big|^2 + m_2^2 \big\|\boldsymbol{h}_\ell\big\|^2 + 2m_2^2 \mathrm{Re}\big(\boldsymbol{h}_\ell^{\mathsf{H}} \boldsymbol{z}_\ell\big) \mathrm{Re}\big(\boldsymbol{h}_i^{\mathsf{H}} \boldsymbol{z}_i\big) \Big) - \delta \|\boldsymbol{h}\|^2.
\end{aligned} \tag{A.13}$$

The first term in the RHS of Eq.(A.13) is a perfect square, and is bounded below by 0. Rewriting $\|\boldsymbol{h}_\ell\| = \sum_{a=1}^{L} |h_{\ell,a}|^2$ in the second term in the RHS, we have

$$\begin{aligned}
\frac{1}{2}\tilde{\boldsymbol{h}}^{\mathsf{H}} \nabla^2 r(\boldsymbol{z}) \tilde{\boldsymbol{h}} \geq \frac{1}{K} \sum_{\ell=1}^{J} \sum_{i \neq \ell}^{J} \Bigg(& (m_2^2 + \kappa) \big|\boldsymbol{h}_\ell^{\mathsf{H}} \boldsymbol{z}_i\big|^2 + m_2^2 \sum_{a \neq i}^{L} |h_{\ell,a}|^2 \\
& + 2m_2^2 \mathrm{Re}\big(\boldsymbol{h}_\ell^{\mathsf{H}} \boldsymbol{z}_\ell\big) \mathrm{Re}\big(\boldsymbol{h}_i^{\mathsf{H}} \boldsymbol{z}_i\big) \Bigg) - \delta \|\boldsymbol{h}\|^2 \\
= \frac{m_2^2 + \kappa}{K} \sum_{\ell=1}^{J} \sum_{i \neq \ell}^{J} & \big|\boldsymbol{h}_\ell^{\mathsf{H}} \boldsymbol{z}_i\big|^2 + \frac{m_2^2}{K} \sum_{\ell=1}^{J} \sum_{i \neq \ell}^{J} \sum_{a \neq i,\ell}^{L} |h_{\ell,a}|^2 \\
& + \frac{m_2^2}{K} \sum_{\ell=1}^{J} \sum_{i<\ell}^{J} \Big(|\boldsymbol{h}_\ell^{\mathsf{H}} \boldsymbol{z}_\ell|^2 + |\boldsymbol{h}_i^{\mathsf{H}} \boldsymbol{z}_i|^2 + 2\mathrm{Re}\big(\boldsymbol{h}_\ell^{\mathsf{H}} \boldsymbol{z}_\ell\big) \mathrm{Re}\big(\boldsymbol{h}_i^{\mathsf{H}} \boldsymbol{z}_i\big) \Big) \\
& + \frac{2m_2^2}{K} \sum_{\ell=1}^{J} \sum_{i<\ell}^{J} \mathrm{Re}\big(\boldsymbol{h}_\ell^{\mathsf{H}} \boldsymbol{z}_\ell\big) \mathrm{Re}\big(\boldsymbol{h}_i^{\mathsf{H}} \boldsymbol{z}_i\big) - \delta \|\boldsymbol{h}\|^2.
\end{aligned} \tag{A.14}$$

Knowing that in square QAM modulations $|\kappa| \leq m_2^2$, we have that the first term of the RHS is bounded below by zero. Furthermore, the second and third terms in the RHS of Eq.(A.14) are perfect squares, and are also bounded below by zero. We now focus on

bounding the remaining term

$$\frac{2m_2^2}{K}\sum_{\ell=1}^{J}\sum_{i<\ell}^{J}\mathrm{Re}\big(\boldsymbol{h}_\ell^{\mathsf{H}}\boldsymbol{z}_\ell\big)\mathrm{Re}\big(\boldsymbol{h}_i^{\mathsf{H}}\boldsymbol{z}_i\big). \tag{A.15}$$

For each (ℓ, i) pair, the summands can be negative. However, note that for $J > 2$, it is not possible that all summands are negative, i.e., for all pairs (ℓ, i) with $i < \ell$: some summands *will* be positive, as they are composed of pairwise products. Moreover, every $\boldsymbol{h}_a^{\mathsf{H}}\boldsymbol{z}_a$ can have at most magnitude equal to 1 by construction, and we also have that $\|\boldsymbol{h}\| = J$. We then count the number of negative summands to obtain the worst-case scenario. There is a total of $J(J-1)/2$ summands, and the maximum number of negative summands is equal to all combinations of half of summands with one sign and the other with the opposite sign:

$$\binom{\lfloor J/2\rfloor}{1}\binom{\lceil J/2\rceil}{1} = \left\lfloor\frac{J}{2}\right\rfloor\left\lceil\frac{J}{2}\right\rceil = \begin{cases} J^2/4 & J \text{ even}, \\ (J^2-1)/4 & J \text{ odd}. \end{cases} \tag{A.16}$$

Thus, the worst sum (with each term of the form $\boldsymbol{h}_\ell^{\mathsf{H}}\boldsymbol{z}_\ell$ having a magnitude of 1) corresponds to the maximum amount of negative summands with a negative sign, plus the remaining positive summands, i.e.,

$$-\left\lfloor\frac{J}{2}\right\rfloor\left\lceil\frac{J}{2}\right\rceil + \left(\frac{J(J-1)}{2} - \left\lfloor\frac{J}{2}\right\rfloor\left\lceil\frac{J}{2}\right\rceil\right) \geq -2\max\left\{\frac{J^2}{4}, \frac{J^2-1}{4}\right\} + \frac{J^2}{2} - \frac{J}{2} = -\frac{J}{2}. \tag{A.17}$$

Replacing in (A.15), we have

$$\frac{2m_2^2}{K}\sum_{\ell=1}^{J}\sum_{i<\ell}^{J}\mathrm{Re}\big(\boldsymbol{h}_\ell^{\mathsf{H}}\boldsymbol{z}_\ell\big)\mathrm{Re}\big(\boldsymbol{h}_i^{\mathsf{H}}\boldsymbol{z}_i\big) \geq -\frac{m_2^2}{K}J = -\frac{m_2^2}{K}\|\boldsymbol{h}\|^2, \tag{A.18}$$

which completes the proof. ■

Finally, we describe the generalized regularity condition of WFCMA-based multiple source recovery as stated throughout Section 3.3.4. Let $\nabla G(\boldsymbol{q}) = \big[\nabla_1 g(\boldsymbol{q})^{\mathsf{T}} \ \cdots \ \nabla_J g(\boldsymbol{q})^{\mathsf{T}}\big]^{\mathsf{T}}$ be the total gradient of the MSR function, stacking the gradients with respect to each CMA solution. Let $\boldsymbol{D}(\boldsymbol{q}) = \mathrm{diag}(\mathrm{e}^{j\phi_1(\boldsymbol{q})}, \ldots, \mathrm{e}^{j\phi_J(\boldsymbol{q})}) \otimes \boldsymbol{I}_L$ be the diagonal matrix that aligns the demixers $\boldsymbol{q}_\ell$ with their respective ground truths $\boldsymbol{z}_\ell$ using their optimal rotations with phases $\phi_\ell(\boldsymbol{q})$. Thus, $\boldsymbol{D}(\boldsymbol{q})\boldsymbol{z} = \big[\mathrm{e}^{j\phi(\boldsymbol{q}_1)}\boldsymbol{z}_1^{\mathsf{T}} \ \cdots \ \mathrm{e}^{j\phi(\boldsymbol{q}_J)}\boldsymbol{z}_J^{\mathsf{T}}\big]^{\mathsf{T}}$. Moreover, for all $\ell \in \{1, \ldots, J\}$, simple algebra reveals that

$$\begin{aligned}
\nabla_\ell g\big(\boldsymbol{D}(\boldsymbol{q})\boldsymbol{z}\big) &= \nabla f(\mathrm{e}^{j\phi(\boldsymbol{q}_\ell)}\boldsymbol{z}_\ell) + \gamma_0 \sum_{i\neq\ell}^{J} \boldsymbol{S}\big(\mathrm{e}^{j\phi(\boldsymbol{q}_i)}\boldsymbol{z}_i\big)\big(\mathrm{e}^{j\phi(\boldsymbol{q}_i)}\boldsymbol{z}_i\big)^{\mathsf{H}}\boldsymbol{S}\mathrm{e}^{j\phi(\boldsymbol{q}_\ell)}\boldsymbol{z}_\ell \\
&= \mathrm{e}^{j\phi(\boldsymbol{q}_\ell)}\nabla f(\boldsymbol{z}_\ell) + \gamma_0 \mathrm{e}^{j\phi(\boldsymbol{q}_\ell)} \sum_{i\neq\ell}^{J} \boldsymbol{S}\boldsymbol{z}_i\boldsymbol{z}_i^{\mathsf{H}}\boldsymbol{S}\boldsymbol{z}_\ell \\
&= \mathrm{e}^{j\phi(\boldsymbol{q}_\ell)}\nabla_\ell g(\boldsymbol{z}) = \nabla_\ell g(\mathrm{e}^{j\phi(\boldsymbol{q}_\ell)}\boldsymbol{z}),
\end{aligned}$$

and therefore we can obtain the generalized regularity condition (3.46) of Theorem 2 as follows:

$$\begin{aligned}
&\sum_{\ell=1}^{J} \mathrm{Re}\big(\langle \nabla_\ell g(\boldsymbol{q}) - \nabla_\ell g(\mathrm{e}^{j\phi(\boldsymbol{q}_\ell)}\boldsymbol{z}), \boldsymbol{q}_\ell - \mathrm{e}^{j\phi(\boldsymbol{q}_\ell)}\boldsymbol{z}_\ell\rangle\big) \\
&\quad= \sum_{\ell=1}^{J} \mathrm{Re}\big(\langle \nabla_\ell g(\boldsymbol{q}) - \nabla_\ell g\big(\boldsymbol{D}(\boldsymbol{q})\boldsymbol{z}\big), \boldsymbol{q}_\ell - \mathrm{e}^{j\phi(\boldsymbol{q}_\ell)}\boldsymbol{z}_\ell\rangle\big) \\
&\quad= \mathrm{Re}\big(\langle \nabla G(\boldsymbol{q}) - \nabla G(\boldsymbol{D}(\boldsymbol{q})\boldsymbol{z}), \boldsymbol{q} - \boldsymbol{D}(\boldsymbol{q})\boldsymbol{z}\rangle\big) \\
&\quad\geq \frac{1}{\alpha}\mathrm{dist}^2(\boldsymbol{q}, \boldsymbol{z}) + \frac{1}{\beta}\big\|\nabla G(\boldsymbol{q}) - \nabla G(\boldsymbol{D}(\boldsymbol{q})\boldsymbol{z})\big\|^2 \\
&\quad= \frac{1}{\alpha}\mathrm{dist}^2(\boldsymbol{q}, \boldsymbol{z}) + \frac{1}{\beta}\sum_{\ell=1}^{J}\big\|\nabla_\ell g(\boldsymbol{q}) - \nabla_\ell g\big(\boldsymbol{D}(\boldsymbol{q})\boldsymbol{z}\big)\big\|^2. \\
&\quad= \frac{1}{\alpha}\mathrm{dist}^2(\boldsymbol{q}, \boldsymbol{z}) + \frac{1}{\beta}\sum_{\ell=1}^{J}\big\|\nabla_\ell g(\boldsymbol{q}) - \nabla_\ell g(\mathrm{e}^{j\phi(\boldsymbol{q}_\ell)}\boldsymbol{z})\big\|^2.
\end{aligned}$$

A.6 Proof of Lemma 5

Using the triangle inequality and Eq.(A.10), to prove the lemma we show that $\forall \ell \in \{1, \ldots, J\}$ and $\forall i \neq \ell$,

$$\left\| \nabla^2 f(\boldsymbol{z}_\ell) - \mathbb{E}\{\nabla^2 f(\boldsymbol{z}_\ell)\} \right\| \leq \delta_f = \frac{\delta}{2J}, \tag{A.19}$$

$$\|\boldsymbol{C}_\ell(\boldsymbol{z}) - \mathbb{E}\{\boldsymbol{C}_\ell(\boldsymbol{z})\}\| \leq \delta_C = \frac{\delta}{8\gamma_0 J}. \tag{A.20}$$

$$\|\boldsymbol{E}_{\ell i}(\boldsymbol{z}) - \mathbb{E}\{\boldsymbol{E}_{\ell i}(\boldsymbol{z})\}\| \leq \delta_E = \frac{\delta}{8\gamma_0 J(J-1)}, \tag{A.21}$$

$$\|\boldsymbol{F}_{\ell i}(\boldsymbol{z}) - \mathbb{E}\{\boldsymbol{F}_{\ell i}(\boldsymbol{z})\}\| \leq \delta_F = \frac{\delta}{8\gamma_0 J(J-1)}. \tag{A.22}$$

Eq.(A.19) corresponds to the concentration inequality of J Hessians of the single source recovery cost function. Thus, Lemma 1 states that Eq.(A.19) holds with probability at least $1 - 6\mathrm{e}^{-c_1(\delta_f)K}$ by choosing $K \geq C_1(\delta_f)L$.

Let $\boldsymbol{c}_{i,k} = \boldsymbol{s}_k(\boldsymbol{s}_k^{\mathsf{H}} \boldsymbol{z}_i)$, which are independent for $k \in \{1, \ldots, K\}$, and in particular, $\boldsymbol{c}_{i,k}$ is independent of $\boldsymbol{c}_{i,m}$ for $m \neq k$. Note that $\boldsymbol{s}_k^{\mathsf{H}} \boldsymbol{z}_i = \sqrt{m_2}\, \mathrm{e}^{j\varphi} \overline{s_{\ell_i}[k]}$, and therefore the vectors $\boldsymbol{c}_{i,k}$ have bounded, discrete elements over an exponentially large set, and as such they are subgaussian [91]. Moreover, the sum of these vectors over index i is also subgaussian. Thus, we have

$$\boldsymbol{C}_\ell(\boldsymbol{z}) = \frac{1}{K^2} \sum_{i \neq \ell}^{J} \sum_{k=1}^{K} \sum_{m=1}^{K} \boldsymbol{c}_{i,k} \boldsymbol{c}_{i,m}^{\mathsf{H}} = \frac{1}{K^2} \sum_{i \neq \ell}^{J} \sum_{k=1}^{K} \boldsymbol{c}_{i,k} \boldsymbol{c}_{i,k}^{\mathsf{H}} + \frac{1}{K^2} \sum_{i \neq \ell}^{J} \sum_{k=1}^{K} \sum_{m \neq k}^{K} \boldsymbol{c}_{i,k} \boldsymbol{c}_{i,m}^{\mathsf{H}}, \tag{A.23}$$

and invoking Lemma 9 for each $i \neq \ell$ and results of concentration of quadratic forms [91, Chapter 6], Eq.(A.20) holds with probability at least $1 - 2\mathrm{e}^{-c_6(\delta_C)K}$ by choosing $K \geq C_6(\delta_C)L$.

In a similar fashion, note that

$$\boldsymbol{F}_{\ell i}(\boldsymbol{z}) = \frac{1}{K^2} \sum_{k=1}^{K} \sum_{m=1}^{K} \boldsymbol{c}_{i,k} \boldsymbol{c}_{\ell,m}^{\mathsf{T}} = \frac{1}{K^2} \sum_{k=1}^{K} \boldsymbol{c}_{i,k} \boldsymbol{c}_{\ell,k}^{\mathsf{T}} + \frac{1}{K^2} \sum_{k=1}^{K} \sum_{m \neq k}^{K} \boldsymbol{c}_{i,k} \boldsymbol{c}_{\ell,m}^{\mathsf{T}}, \tag{A.24}$$

where we leverage the reasoning of the previous result, the fact that $\boldsymbol{c}_{i,k}$ is independent of

$\boldsymbol{c}_{\ell,m}$ for $m \neq k$ and $i \neq \ell$, and the concentration of measure of $\boldsymbol{U}(\boldsymbol{z})$ in Lemma 1 of the main text (for the transposition instead of conjugate transpose). Hence, Eq.(A.22) holds with probability $1 - 2\mathrm{e}^{-c_7(\delta_F)K}$ by choosing $K \geq C_7(\delta_F)L$.

Now define $\boldsymbol{e}_{\ell,k,m} = (\boldsymbol{s}_k^{\mathsf{H}}\boldsymbol{z}_\ell)\boldsymbol{s}_m$. The vectors $\boldsymbol{e}_{\ell,k,k}$ are independent for $k \in \{1,\ldots,K\}$, and $\boldsymbol{e}_{\ell,k,m}$ is independent of $\boldsymbol{e}_{i,k,m}$ for $m \neq k$ and $i \neq \ell$. Following a similar reasoning as above, the $\boldsymbol{e}_{\ell,k,m}$ are subgaussian, and we obtain

$$\boldsymbol{E}_{\ell i}(\boldsymbol{z}) = \frac{1}{K^2}\sum_{k=1}^{K}\sum_{m=1}^{K}\boldsymbol{e}_{\ell,k,m}\boldsymbol{e}_{i,k,m}^{\mathsf{H}} = \frac{1}{K^2}\sum_{k=1}^{K}\boldsymbol{e}_{\ell,k,k}\boldsymbol{e}_{i,k,k}^{\mathsf{H}} + \frac{1}{K^2}\sum_{k=1}^{K}\sum_{m\neq k}^{K}\boldsymbol{e}_{\ell,k,m}\boldsymbol{e}_{i,k,m}^{\mathsf{H}}, \tag{A.25}$$

thus Eq.(A.21) holds with probability $1 - 2\mathrm{e}^{-c_8(\delta_E)K}$ by choosing $K \geq C_8(\delta_E)L$.

Finally, set $C_2(\delta) \geq \max\{C_1(\delta_f), C_6(\delta_C), C_7(\delta_F), C_8(\delta_E)\}$. By selecting $K \geq C_2(\delta)L$ and letting $c_2(\delta) = \min\{c_5(\delta_f), c_6(\delta_C), c_7(\delta_F), c_8(\delta_E)\}$, Lemma 5 holds with probability at least $1 - 12\mathrm{e}^{-c_2(\delta)K}$.

A.7 Proof of Lemma 6

Let $\boldsymbol{q} \in E(\epsilon)$, $\boldsymbol{D}(\boldsymbol{q})$ as defined in Section A.5, and $\boldsymbol{h} = \boldsymbol{D}(\boldsymbol{q})^{\mathsf{H}}\boldsymbol{q} - \boldsymbol{z}$. Hence, $\|\boldsymbol{h}\| \leq \epsilon$, $\boldsymbol{h}_\ell = \mathrm{e}^{-i\phi(\boldsymbol{q}_\ell)}\boldsymbol{q}_\ell - \boldsymbol{z}_\ell$, and $\mathrm{Im}(\boldsymbol{h}_\ell^{\mathsf{H}}\boldsymbol{z}_\ell) = 0$, as $\boldsymbol{h}_\ell$ and $\boldsymbol{z}_\ell$ are geometrically aligned for all $\ell \in \{1,\ldots,J\}$. To prove Lemma 6, we prove that

$$\begin{aligned}
&\sum_{\ell=1}^{J}\mathrm{Re}\Big(\big\langle\nabla_\ell g(\boldsymbol{q}) - \nabla_\ell g\big(\boldsymbol{D}(\boldsymbol{q})\boldsymbol{z}\big), \boldsymbol{q}_\ell - \mathrm{e}^{j\phi(\boldsymbol{q}_\ell)}\boldsymbol{z}_\ell\big\rangle\Big) \\
&\quad= \sum_{\ell=1}^{J}\mathrm{Re}\Big(\big\langle\nabla f(\boldsymbol{q}_\ell) - \nabla f(\mathrm{e}^{j\phi(\boldsymbol{q}_\ell)}\boldsymbol{z}_\ell), \boldsymbol{q}_\ell - \mathrm{e}^{j\phi(\boldsymbol{q}_\ell)}\boldsymbol{z}_\ell\big\rangle\Big) \\
&\qquad+ \gamma_0\sum_{\ell=1}^{J}\sum_{i\neq\ell}^{J}\mathrm{Re}\Big(\big\langle\boldsymbol{S}\boldsymbol{q}_i\boldsymbol{q}_i^{\mathsf{H}}\boldsymbol{S}\boldsymbol{q}_\ell - \mathrm{e}^{j\phi(\boldsymbol{q}_\ell)}\boldsymbol{S}\boldsymbol{z}_i\boldsymbol{z}_i^{\mathsf{H}}\boldsymbol{S}\boldsymbol{z}_\ell, \boldsymbol{q}_\ell - \mathrm{e}^{j\phi(\boldsymbol{q}_\ell)}\boldsymbol{z}_\ell\big\rangle\Big) \\
&\quad\geq \sum_{\ell=1}^{J}\Big(\frac{1}{\alpha} + \frac{2m_2^2 - R_2m_2 - \delta}{19}\Big)\|\boldsymbol{h}_\ell\|^2 + \frac{1}{20K}\sum_{\ell=1}^{J}\sum_{k=1}^{K}\big|\boldsymbol{s}_k^{\mathsf{H}}\boldsymbol{h}_\ell\big|^4 + \gamma_0^2\sum_{\ell=1}^{J}\sum_{i\neq\ell}^{J}\big|\boldsymbol{h}_i^{\mathsf{H}}\boldsymbol{S}\boldsymbol{h}_\ell\big|^2
\end{aligned} \tag{A.26}$$

for all $\boldsymbol{h}$ satisfying $\mathrm{Im}(\boldsymbol{h}_\ell^{\mathsf{H}}\boldsymbol{z}_\ell) = 0$ and $\|\boldsymbol{h}\| \leq \epsilon$. In the following, we set $\gamma_0 = 1$, and for simplicity, we now assume that $\|\boldsymbol{h}_\ell\| \leq \epsilon/\sqrt{J}$ for all $\ell \in \{1, \ldots, J\}$. In Lemma 2 we establish that the inner product of the CMA portion of the gradient, i.e., the terms with ∇f, are bounded below by the two first terms of the right-hand side of Eq.(A.26). Therefore, we focus on the regularizing term, which is

$$
\begin{aligned}
&\sum_{\ell=1}^{J}\sum_{i\neq\ell}^{J}\mathrm{Re}\Big(\big\langle \boldsymbol{S}\boldsymbol{q}_i\boldsymbol{q}_i^{\mathsf{H}}\boldsymbol{S}\boldsymbol{q}_\ell - \mathrm{e}^{j\phi(\boldsymbol{q}_\ell)}\boldsymbol{S}\boldsymbol{z}_i\boldsymbol{z}_i^{\mathsf{H}}\boldsymbol{S}\boldsymbol{z}_\ell, \boldsymbol{q}_\ell - \mathrm{e}^{j\phi(\boldsymbol{q}_\ell)}\boldsymbol{z}_\ell\big\rangle\Big)\\
&\quad= \sum_{\ell=1}^{J}\sum_{i\neq\ell}^{J}\Big(\big|\boldsymbol{z}_i^{\mathsf{H}}\boldsymbol{S}\boldsymbol{h}_\ell\big|^2 + \big|\boldsymbol{h}_i^{\mathsf{H}}\boldsymbol{S}\boldsymbol{h}_\ell\big|^2 + \mathrm{Re}\big(\boldsymbol{h}_\ell^{\mathsf{H}}\boldsymbol{S}\boldsymbol{h}_i\boldsymbol{h}_i^{\mathsf{H}}\boldsymbol{S}\boldsymbol{z}_\ell\big) + \mathrm{Re}\big(\boldsymbol{h}_\ell^{\mathsf{H}}\boldsymbol{S}\boldsymbol{z}_i\boldsymbol{h}_i^{\mathsf{H}}\boldsymbol{S}\boldsymbol{h}_\ell\big)\\
&\qquad\qquad + \mathrm{Re}\big(\boldsymbol{h}_\ell^{\mathsf{H}}\boldsymbol{S}\boldsymbol{h}_i\boldsymbol{z}_i^{\mathsf{H}}\boldsymbol{S}\boldsymbol{h}_\ell\big) + \mathrm{Re}\big(\boldsymbol{h}_\ell^{\mathsf{H}}\boldsymbol{S}\boldsymbol{z}_i\boldsymbol{h}_i^{\mathsf{H}}\boldsymbol{S}\boldsymbol{z}_\ell\big) + \mathrm{Re}\Big(\boldsymbol{h}_\ell^{\mathsf{H}}\boldsymbol{S}\boldsymbol{h}_i\boldsymbol{z}_i^{\mathsf{H}}\boldsymbol{S}\boldsymbol{z}_\ell\big)\Big)\\
&\quad= \sum_{\ell=1}^{J}\sum_{i<\ell}^{J}\Big(\big|\boldsymbol{z}_i^{\mathsf{H}}\boldsymbol{S}\boldsymbol{h}_\ell\big|^2 + \big|\boldsymbol{h}_i^{\mathsf{H}}\boldsymbol{S}\boldsymbol{z}_\ell\big|^2 + 2\big|\boldsymbol{h}_i^{\mathsf{H}}\boldsymbol{S}\boldsymbol{h}_\ell\big|^2 + 3\mathrm{Re}\big(\boldsymbol{h}_\ell^{\mathsf{H}}\boldsymbol{S}\boldsymbol{h}_i\boldsymbol{h}_i^{\mathsf{H}}\boldsymbol{S}\boldsymbol{z}_\ell\big)\\
&\qquad\qquad + 3\mathrm{Re}\big(\boldsymbol{h}_\ell^{\mathsf{H}}\boldsymbol{S}\boldsymbol{h}_i\boldsymbol{z}_i^{\mathsf{H}}\boldsymbol{S}\boldsymbol{h}_\ell\big) + 2\mathrm{Re}\big(\boldsymbol{h}_\ell^{\mathsf{H}}\boldsymbol{S}\boldsymbol{z}_i\boldsymbol{h}_i^{\mathsf{H}}\boldsymbol{S}\boldsymbol{z}_\ell\big) + 2\mathrm{Re}\Big(\boldsymbol{h}_\ell^{\mathsf{H}}\boldsymbol{S}\boldsymbol{h}_i\boldsymbol{z}_i^{\mathsf{H}}\boldsymbol{S}\boldsymbol{z}_\ell\big)\Big)\\
&\quad\leq \sum_{\ell=1}^{J}\sum_{i<\ell}^{J}\Big(2\big|\boldsymbol{h}_i^{\mathsf{H}}\boldsymbol{S}\boldsymbol{h}_\ell\big|^2 + 3\mathrm{Re}\big(\boldsymbol{h}_\ell^{\mathsf{H}}\boldsymbol{S}\boldsymbol{h}_i\boldsymbol{h}_i^{\mathsf{H}}\boldsymbol{S}\boldsymbol{z}_\ell\big) + 3\mathrm{Re}\big(\boldsymbol{h}_\ell^{\mathsf{H}}\boldsymbol{S}\boldsymbol{h}_i\boldsymbol{z}_i^{\mathsf{H}}\boldsymbol{S}\boldsymbol{h}_\ell\big)\Big) - \Big(\frac{m_2^2}{K} + \delta\Big)\|\boldsymbol{h}\|^2,
\end{aligned}
$$

where the second equality comes from realizing that the terms of pairs (i, ℓ) and (ℓ, i) are related through complex conjugation, and the last inequality comes from Corollary 19. Substituting in Eq.(A.26), and invoking Lemma 2, we have that

$$
\begin{aligned}
&\sum_{\ell=1}^{J}\mathrm{Re}\Big(\big\langle \nabla_\ell g(\boldsymbol{q}) - \nabla_\ell g(\boldsymbol{D}(\boldsymbol{q})\boldsymbol{z}), \boldsymbol{q}_\ell - \mathrm{e}^{j\phi(\boldsymbol{q}_\ell)}\boldsymbol{z}_\ell\big\rangle\Big)\\
&\geq \frac{1}{K}\sum_{k=1}^{K}\Big(2\mathrm{Re}(\boldsymbol{h}^{\mathsf{H}}\boldsymbol{s}_k\boldsymbol{s}_k^{\mathsf{H}}\boldsymbol{z})^2 + 3\mathrm{Re}(\boldsymbol{h}^{\mathsf{H}}\boldsymbol{s}_k\boldsymbol{s}_k^{\mathsf{H}}\boldsymbol{z})|\boldsymbol{s}_k^{\mathsf{H}}\boldsymbol{h}|^2 + |\boldsymbol{s}_k^{\mathsf{H}}\boldsymbol{h}|^4 + \big(|\boldsymbol{s}_k^{\mathsf{H}}\boldsymbol{z}|^2 - R_2\big)|\boldsymbol{s}_k^{\mathsf{H}}\boldsymbol{h}|^2\Big)\\
&\quad + \sum_{\ell=1}^{J}\sum_{i<\ell}^{J}\Big(2\big|\boldsymbol{h}_i^{\mathsf{H}}\boldsymbol{S}\boldsymbol{h}_\ell\big|^2 + 3\mathrm{Re}\big(\boldsymbol{h}_\ell^{\mathsf{H}}\boldsymbol{S}\boldsymbol{h}_i\boldsymbol{h}_i^{\mathsf{H}}\boldsymbol{S}\boldsymbol{z}_\ell\big) + 3\mathrm{Re}\big(\boldsymbol{h}_\ell^{\mathsf{H}}\boldsymbol{S}\boldsymbol{h}_i\boldsymbol{z}_i^{\mathsf{H}}\boldsymbol{S}\boldsymbol{h}_\ell\big)\Big) - \Big(\frac{m_2^2}{K} + \delta\Big)\|\boldsymbol{h}\|^2\\
&\geq \sum_{\ell=1}^{J}\Big(\frac{1}{\alpha} + \frac{2m_2^2 - R_2 m_2 - \delta}{19}\Big)\|\boldsymbol{h}_\ell\|^2 + \frac{1}{20K}\sum_{\ell=1}^{J}\sum_{k=1}^{K}\big|\boldsymbol{s}_k^{\mathsf{H}}\boldsymbol{h}_\ell\big|^4 + \sum_{\ell=1}^{J}\sum_{i\neq\ell}^{J}\big|\boldsymbol{h}_i^{\mathsf{H}}\boldsymbol{S}\boldsymbol{h}_\ell\big|^2. \qquad \text{(A.27)}
\end{aligned}
$$

Equivalently, we prove that for all $\boldsymbol{h}_\ell$ such that $\mathrm{Im}(\boldsymbol{h}_\ell^{\mathsf{H}}\boldsymbol{z}_\ell)=0$ and $\|\boldsymbol{h}_\ell\|=1$, and for all ξ with $0\le\xi\le\epsilon/\sqrt{J}$,

$$\begin{aligned}
&\frac{1}{K}\sum_{\ell=1}^{J}\sum_{k=1}^{K}\Big(2\mathrm{Re}(\boldsymbol{h}^{\mathsf{H}}\boldsymbol{s}_k\boldsymbol{s}_k^{\mathsf{H}}\boldsymbol{z})^2+3\xi\mathrm{Re}(\boldsymbol{h}^{\mathsf{H}}\boldsymbol{s}_k\boldsymbol{s}_k^{\mathsf{H}}\boldsymbol{z})|\boldsymbol{s}_k^{\mathsf{H}}\boldsymbol{h}|^2+\frac{19\xi^2}{20}|\boldsymbol{s}_k^{\mathsf{H}}\boldsymbol{h}|^4+\big(|\boldsymbol{s}_k^{\mathsf{H}}\boldsymbol{z}|^2-R_2\big)|\boldsymbol{s}_k^{\mathsf{H}}\boldsymbol{h}|^2\Big)\\
&\qquad+\sum_{\ell=1}^{J}\sum_{i<\ell}^{J}\Big(3\xi\mathrm{Re}\big(\boldsymbol{h}_\ell^{\mathsf{H}}\boldsymbol{S}\boldsymbol{h}_i\boldsymbol{h}_i^{\mathsf{H}}\boldsymbol{S}\boldsymbol{z}_\ell\big)+3\xi\mathrm{Re}\big(\boldsymbol{h}_\ell^{\mathsf{H}}\boldsymbol{S}\boldsymbol{h}_i\boldsymbol{z}_i^{\mathsf{H}}\boldsymbol{S}\boldsymbol{h}_\ell\big)\Big)-J\Big(\frac{m_2^2}{K}+\delta\Big)\\
&\ge J\Big(\frac{1}{\alpha}+\frac{2m_2^2-R_2m_2-\delta}{19}\Big).
\end{aligned}\tag{A.28}$$

Invoking Lemma 1 and Corollary 10, we have that

$$\begin{aligned}
\mathrm{Re}\big(\boldsymbol{h}_\ell^{\mathsf{H}}\boldsymbol{S}\boldsymbol{h}_i\boldsymbol{h}_i^{\mathsf{H}}\boldsymbol{S}\boldsymbol{z}_\ell\big)&\ge-\big|\boldsymbol{h}_\ell^{\mathsf{H}}\boldsymbol{S}\boldsymbol{h}_i\big|\big|\boldsymbol{h}_i^{\mathsf{H}}\boldsymbol{S}\boldsymbol{z}_\ell\big|\ge-(m_2+\delta)^2,\\
\mathrm{Re}\big(\boldsymbol{h}_\ell^{\mathsf{H}}\boldsymbol{S}\boldsymbol{h}_i\boldsymbol{z}_i^{\mathsf{H}}\boldsymbol{S}\boldsymbol{h}_\ell\big)&\ge-\big|\boldsymbol{h}_\ell^{\mathsf{H}}\boldsymbol{S}\boldsymbol{h}_i\big|\big|\boldsymbol{z}_i^{\mathsf{H}}\boldsymbol{S}\boldsymbol{h}_\ell\big|\ge-(m_2+\delta)^2,
\end{aligned}\tag{A.29}$$

and replacing in Eq.(A.28), we obtain

$$\begin{aligned}
&\frac{1}{K}\sum_{k=1}^{K}\Big(2\mathrm{Re}(\boldsymbol{h}^{\mathsf{H}}\boldsymbol{s}_k\boldsymbol{s}_k^{\mathsf{H}}\boldsymbol{z})^2+3\xi\mathrm{Re}(\boldsymbol{h}^{\mathsf{H}}\boldsymbol{s}_k\boldsymbol{s}_k^{\mathsf{H}}\boldsymbol{z})|\boldsymbol{s}_k^{\mathsf{H}}\boldsymbol{h}|^2+\frac{19\xi^2}{20}|\boldsymbol{s}_k^{\mathsf{H}}\boldsymbol{h}|^4+\big(|\boldsymbol{s}_k^{\mathsf{H}}\boldsymbol{z}|^2-R_2\big)|\boldsymbol{s}_k^{\mathsf{H}}\boldsymbol{h}|^2\Big)\\
&\qquad-3(J-1)\xi(m_2+\delta)^2-\frac{m_2^2}{K}-\delta\\
&\ge\Big(\frac{1}{\alpha}+\frac{2m_2^2-R_2m_2-\delta}{19}\Big)
\end{aligned}\tag{A.30}$$

Now, following the procedure in Lemma 2, to bound the sum in the LHS, we obtain that Lemma 6 holds under the following condition:

$$\begin{aligned}
&\frac{135m_2^2+90\kappa}{76}\mathrm{Re}(\boldsymbol{h}^{\mathsf{H}}\boldsymbol{z})^2+\frac{45}{76}(m_2^2-\delta)-\frac{19B^2L}{20}\xi^2(m_2+\delta)\\
&\qquad+\big(m_2^2-R_2m_2-(1+R_2)\delta+(m_2^2+\kappa)|\boldsymbol{h}^{\mathsf{H}}\boldsymbol{z}|^2\big)\cdot\mathbf{1}[Q\neq4]\\
&\qquad-3(J-1)\xi(m_2+\delta)^2-\frac{m_2^2}{K}-\delta\\
&\ge\frac{1}{\alpha}+\frac{11m_2^2-2R_2m_2+5\delta}{19}+\frac{21m_2^2+14\kappa}{38}\mathrm{Re}(\boldsymbol{h}^{\mathsf{H}}\boldsymbol{z})^2.
\end{aligned}\tag{A.31}$$

With $J \geq 2$, $\epsilon = (10JB\sqrt{LJ})^{-1}$ and $\delta \leq 0.001$, Eq.(A.31) holds for

$$\begin{aligned} \alpha &\geq 4 \quad \text{for} \quad Q = 4, \\ \alpha &\geq 227 \quad \text{for} \quad Q \neq 4. \end{aligned}$$

A.8 Proof of Lemma 7

Let $\boldsymbol{q} \in E(\epsilon)$ and $\boldsymbol{D}(\boldsymbol{q})$ as defined in Section A.5. Let $\boldsymbol{h} = \boldsymbol{D}(\boldsymbol{q})^{\mathsf{H}}\boldsymbol{q} - \boldsymbol{z}$. Hence, $\|\boldsymbol{h}\| \leq \epsilon$, $\boldsymbol{h}_\ell = \mathrm{e}^{-i\phi(\boldsymbol{q}_\ell)}\boldsymbol{q}_\ell - \boldsymbol{z}_\ell$ and $\mathrm{Im}(\boldsymbol{h}_\ell^{\mathsf{H}}\boldsymbol{z}_\ell) = 0$. We aim to prove that

$$\begin{aligned} &\big\|\nabla G(\boldsymbol{q}) - \nabla G(\boldsymbol{D}(\boldsymbol{q})\boldsymbol{z})\big\|^2 \\ &\qquad \leq \beta\bigg(\frac{2m_2^2 - R_2 m_2 - \delta}{19}\big\|\boldsymbol{h}\big\|^2 + \frac{1}{20K}\sum_{\ell=1}^{J}\sum_{k=1}^{K}|\boldsymbol{s}_k^{\mathsf{H}}\boldsymbol{h}_\ell|^4 + \gamma_0^2\sum_{\ell=1}^{J}\sum_{i\neq\ell}^{J}\big|\boldsymbol{h}_i^{\mathsf{H}}\boldsymbol{S}\boldsymbol{h}_\ell\big|^2\bigg), \end{aligned}$$

We first notice that

$$\big\|\nabla G(\boldsymbol{q}) - \nabla G(\boldsymbol{D}(\boldsymbol{q})\boldsymbol{z})\big\|^2 = \sum_{\ell=1}^{J}\big\|\nabla_\ell g(\boldsymbol{q}) - \nabla_\ell g\big(\boldsymbol{D}(\boldsymbol{q})\boldsymbol{z}\big)\big\|^2, \tag{A.32}$$

where

$$\Big\|\nabla_\ell g(\boldsymbol{q}) - \nabla_\ell g\big(\boldsymbol{D}(\boldsymbol{q})\boldsymbol{z}\big)\Big\|^2 = \max_{\boldsymbol{u}\in\mathbb{C}^L,\,\|\boldsymbol{u}\|=1}\Big|\boldsymbol{u}^{\mathsf{H}}\Big(\nabla_\ell g(\boldsymbol{q}) - \nabla_\ell g\big(\boldsymbol{D}(\boldsymbol{q})\boldsymbol{z}\big)\Big)\Big|^2, \tag{A.33}$$

and therefore we bound each of the J gradients. By means of the triangle inequality, we

have that

$$\begin{aligned}
&\Big|\boldsymbol{u}^{\mathsf{H}}\Big(\nabla_\ell g(\boldsymbol{q}) - \mathrm{e}^{j\phi(\boldsymbol{q}_\ell)}\nabla_\ell g\big(\boldsymbol{D}(\boldsymbol{q})\boldsymbol{z}\big)\Big)\Big|^2 \\
&= \Bigg|\boldsymbol{u}^{\mathsf{H}}\nabla f(\boldsymbol{q}_\ell) + 2\gamma_0\boldsymbol{u}^{\mathsf{H}}\Big(\sum_{i\neq\ell}^{J}\boldsymbol{S}\boldsymbol{q}_i\boldsymbol{q}_i^{\mathsf{H}}\boldsymbol{S}\boldsymbol{q}_\ell\Big) \\
&\qquad\qquad - \boldsymbol{u}^{\mathsf{H}}\nabla f(\mathrm{e}^{j\phi(\boldsymbol{q}_\ell)}\boldsymbol{z}_\ell) - \gamma_0\mathrm{e}^{j\phi(\boldsymbol{q}_\ell)}\boldsymbol{u}^{\mathsf{H}}\Big(\sum_{i\neq\ell}^{J}\boldsymbol{S}\boldsymbol{z}_i\boldsymbol{z}_i^{\mathsf{H}}\boldsymbol{S}\boldsymbol{z}_\ell\Big)\Bigg|^2 \\
&\leq 2\Big|\boldsymbol{u}^{\mathsf{H}}\nabla f(\boldsymbol{q}_\ell) - \mathrm{e}^{j\phi(\boldsymbol{q}_\ell)}\nabla f(\boldsymbol{z}_\ell)\Big|^2 + 2\gamma_0^2\Bigg|\sum_{i\neq\ell}^{J}\boldsymbol{u}^{\mathsf{H}}\Big(\boldsymbol{S}\boldsymbol{q}_i\boldsymbol{q}_i^{\mathsf{H}}\boldsymbol{S}\boldsymbol{q}_\ell - \mathrm{e}^{j\phi(\boldsymbol{q}_\ell)}\boldsymbol{S}\boldsymbol{z}_i\boldsymbol{z}_i^{\mathsf{H}}\boldsymbol{S}\boldsymbol{z}_\ell\Big)\Bigg|^2. \quad \text{(A.34)}
\end{aligned}$$

Let $D = 3 + \mathbf{1}[Q \neq 4]$. From the proof of Lemma 3, we know for all $\boldsymbol{h}_\ell$ such that $\mathrm{Im}(\boldsymbol{h}_\ell^{\mathsf{H}}\boldsymbol{z}_\ell) = 0$ and $\|\boldsymbol{h}_\ell\| = 1$, and for all ξ with $0 \leq \xi \leq \epsilon/sqrtJ$, that

$$\begin{aligned}
\Big|\boldsymbol{u}^{\mathsf{H}}\nabla f(\boldsymbol{q}_\ell) - \mathrm{e}^{j\phi(\boldsymbol{q}_\ell)}\nabla f(\boldsymbol{z}_\ell)\Big|^2 &\leq 4D\xi^2 I_1 + 9D\xi^4 I_2 + D\xi^6 I_3 + 4\xi^2 I_4 \cdot \mathbf{1}[Q \neq 4] \\
&\leq 4\xi^2 D(2m_2^2 + \kappa + \delta)^2 + \xi^2\big(m_2^2 + \kappa + (1+R_2)\delta\big)^2 \cdot \mathbf{1}[Q \neq 4] \\
&\quad + \frac{9D\xi^4(2m_2^2 + \kappa + \delta) + DB^2L\xi^6(m_2 + \delta)}{K}\sum_{k=1}^{K}|\boldsymbol{s}_k^{\mathsf{H}}\boldsymbol{h}_\ell|^4,
\end{aligned} \quad \text{(A.35)}$$

thus we only need to bound the second term in Eq.(A.34). For any $\boldsymbol{u} \in \mathbb{C}^L$ such that

$\|\boldsymbol{u}\| = 1$, let $\boldsymbol{v} = \mathrm{e}^{-i\phi(\boldsymbol{q}_\ell)}\boldsymbol{u}$. Thus,

$$
\begin{aligned}
&\left| \sum_{i\neq\ell}^{J} \boldsymbol{u}^{\mathsf{H}} \Big(\boldsymbol{S}\boldsymbol{q}_i\boldsymbol{q}_i^{\mathsf{H}}\boldsymbol{S}\boldsymbol{q}_\ell - \mathrm{e}^{j\phi(\boldsymbol{q}_\ell)}\boldsymbol{S}\boldsymbol{z}_i\boldsymbol{z}_i^{\mathsf{H}}\boldsymbol{S}\boldsymbol{z}_\ell \Big) \right|^2 \\
&\quad = \left| \sum_{i\neq\ell}^{J} \boldsymbol{v}^{\mathsf{H}}\boldsymbol{S}(\boldsymbol{h}_i+\boldsymbol{z}_i)(\boldsymbol{h}_i+\boldsymbol{z}_i)^{\mathsf{H}}\boldsymbol{S}(\boldsymbol{h}_\ell+\boldsymbol{z}_\ell) - \boldsymbol{v}^{\mathsf{H}}\boldsymbol{S}\boldsymbol{z}_i\boldsymbol{z}_i^{\mathsf{H}}\boldsymbol{S}\boldsymbol{z}_\ell \right|^2 \\
&\quad = \Bigg| \boldsymbol{v}^{\mathsf{H}}\boldsymbol{C}_\ell(\boldsymbol{z})\boldsymbol{h}_\ell + \boldsymbol{v}^{\mathsf{H}}\boldsymbol{C}_\ell(\boldsymbol{h})\boldsymbol{z}_\ell + \boldsymbol{v}^{\mathsf{H}}\boldsymbol{C}_\ell(\boldsymbol{h})\boldsymbol{h}_\ell + \sum_{i\neq\ell}^{J} \Big(\boldsymbol{v}^{\mathsf{H}}\boldsymbol{S}\boldsymbol{h}_i\boldsymbol{z}_i^{\mathsf{H}}\boldsymbol{S}\boldsymbol{h}_\ell + \boldsymbol{v}^{\mathsf{H}}\boldsymbol{S}\boldsymbol{z}_i\boldsymbol{h}_i^{\mathsf{H}}\boldsymbol{S}\boldsymbol{h}_\ell \\
&\qquad\qquad + \boldsymbol{v}^{\mathsf{H}}\boldsymbol{S}\boldsymbol{h}_i\boldsymbol{z}_i^{\mathsf{H}}\boldsymbol{S}\boldsymbol{z}_\ell + \boldsymbol{v}^{\mathsf{H}}\boldsymbol{S}\boldsymbol{z}_i\boldsymbol{h}_i^{\mathsf{H}}\boldsymbol{S}\boldsymbol{z}_\ell \Big) \Bigg|^2 \\
&\quad \leq \Bigg(\big|\boldsymbol{v}^{\mathsf{H}}\boldsymbol{C}_\ell(\boldsymbol{z})\boldsymbol{h}_\ell\big| + \big|\boldsymbol{v}^{\mathsf{H}}\boldsymbol{C}_\ell(\boldsymbol{h})\boldsymbol{z}_\ell\big| + \big|\boldsymbol{v}^{\mathsf{H}}\boldsymbol{C}_\ell(\boldsymbol{h})\boldsymbol{h}_\ell\big| + \sum_{i\neq\ell}^{J} \big|\boldsymbol{v}^{\mathsf{H}}\boldsymbol{S}\boldsymbol{h}_i\boldsymbol{z}_i^{\mathsf{H}}\boldsymbol{S}\boldsymbol{h}_\ell\big| \\
&\qquad\qquad + \sum_{i\neq\ell}^{J} \big|\boldsymbol{v}^{\mathsf{H}}\boldsymbol{S}\boldsymbol{z}_i\boldsymbol{h}_i^{\mathsf{H}}\boldsymbol{S}\boldsymbol{h}_\ell\big| + \sum_{i\neq\ell}^{J} \big|\boldsymbol{v}^{\mathsf{H}}\boldsymbol{S}\boldsymbol{h}_i\boldsymbol{z}_i^{\mathsf{H}}\boldsymbol{S}\boldsymbol{z}_\ell\big| + \sum_{i\neq\ell}^{J} \big|\boldsymbol{v}^{\mathsf{H}}\boldsymbol{S}\boldsymbol{z}_i\boldsymbol{h}_i^{\mathsf{H}}\boldsymbol{S}\boldsymbol{z}_\ell\big| \Bigg)^2 .
\end{aligned}
$$

Equivalently, for all $\boldsymbol{h}_\ell$ and $\boldsymbol{v}$ such that $\mathrm{Im}(\boldsymbol{h}_\ell^{\mathsf{H}}\boldsymbol{z}_\ell) = 0$, $\|\boldsymbol{h}_\ell\| = \|\boldsymbol{v}\| = 1$ and for all ξ with $0 \leq \xi \leq \epsilon/\sqrt{J}$,

$$
\begin{aligned}
&\left| \sum_{i\neq\ell}^{J} \boldsymbol{u}^{\mathsf{H}} \Big(\boldsymbol{S}\boldsymbol{q}_i\boldsymbol{q}_i^{\mathsf{H}}\boldsymbol{S}\boldsymbol{q}_\ell - \mathrm{e}^{j\phi(\boldsymbol{q}_\ell)}\boldsymbol{S}\boldsymbol{z}_i\boldsymbol{z}_i^{\mathsf{H}}\boldsymbol{S}\boldsymbol{z}_\ell \Big) \right|^2 \\
&\quad \leq \Bigg(\xi\big|\boldsymbol{v}^{\mathsf{H}}\boldsymbol{C}_\ell(\boldsymbol{z})\boldsymbol{h}_\ell\big| + \xi^2\big|\boldsymbol{v}^{\mathsf{H}}\boldsymbol{C}_\ell(\boldsymbol{h})\boldsymbol{z}_\ell\big| + \xi^3\big|\boldsymbol{v}^{\mathsf{H}}\boldsymbol{C}_\ell(\boldsymbol{h})\boldsymbol{h}_\ell\big| + \xi^2 \sum_{i\neq\ell}^{J} \big|\boldsymbol{v}^{\mathsf{H}}\boldsymbol{S}\boldsymbol{h}_i\boldsymbol{z}_i^{\mathsf{H}}\boldsymbol{S}\boldsymbol{h}_\ell\big| \\
&\qquad\qquad + \xi^2 \sum_{i\neq\ell}^{J} \big|\boldsymbol{v}^{\mathsf{H}}\boldsymbol{S}\boldsymbol{z}_i\boldsymbol{h}_i^{\mathsf{H}}\boldsymbol{S}\boldsymbol{h}_\ell\big| + \xi \sum_{i\neq\ell}^{J} \big|\boldsymbol{v}^{\mathsf{H}}\boldsymbol{S}\boldsymbol{h}_i\boldsymbol{z}_i^{\mathsf{H}}\boldsymbol{S}\boldsymbol{z}_\ell\big| + \xi \sum_{i\neq\ell}^{J} \big|\boldsymbol{v}^{\mathsf{H}}\boldsymbol{S}\boldsymbol{z}_i\boldsymbol{h}_i^{\mathsf{H}}\boldsymbol{S}\boldsymbol{z}_\ell\big| \Bigg)^2 .
\end{aligned}
$$

Knowing that $\big(\sum_{i=1}^{n} a_i\big)^2 \leq n \sum_{i=1}^{n} a_i^2$,

$$\begin{aligned}
&\left| \sum_{i\neq\ell}^{J} \boldsymbol{u}^{\mathsf{H}} \Big(\boldsymbol{S}\boldsymbol{q}_i \boldsymbol{q}_i^{\mathsf{H}} \boldsymbol{S}\boldsymbol{q}_\ell - \mathrm{e}^{j\phi(\boldsymbol{q}_\ell)} \boldsymbol{S}\boldsymbol{z}_i \boldsymbol{z}_i^{\mathsf{H}} \boldsymbol{S}\boldsymbol{z}_\ell \Big) \right|^2 \\
&\quad \leq 7\xi^2 \big| \boldsymbol{v}^{\mathsf{H}} \boldsymbol{C}_\ell(\boldsymbol{z}) \boldsymbol{h}_\ell \big|^2 + 7\xi^4 \big| \boldsymbol{v}^{\mathsf{H}} \boldsymbol{C}_\ell(\boldsymbol{h}) \boldsymbol{z}_\ell \big|^2 + 7\xi^6 \big| \boldsymbol{v}^{\mathsf{H}} \boldsymbol{C}_\ell(\boldsymbol{h}) \boldsymbol{h}_\ell \big|^2 + 7\xi^4 \Big(\sum_{i\neq\ell}^{J} \big| \boldsymbol{v}^{\mathsf{H}} \boldsymbol{S}\boldsymbol{h}_i \boldsymbol{z}_i^{\mathsf{H}} \boldsymbol{S}\boldsymbol{h}_\ell \big| \Big)^2 \\
&\qquad + 7\xi^4 \Big(\sum_{i\neq\ell}^{J} \big| \boldsymbol{v}^{\mathsf{H}} \boldsymbol{S}\boldsymbol{z}_i \boldsymbol{h}_i^{\mathsf{H}} \boldsymbol{S}\boldsymbol{h}_\ell \big| \Big)^2 + 7\xi^2 \Big(\sum_{i\neq\ell}^{J} \big| \boldsymbol{v}^{\mathsf{H}} \boldsymbol{S}\boldsymbol{h}_i \boldsymbol{z}_i^{\mathsf{H}} \boldsymbol{S}\boldsymbol{z}_\ell \big| \Big)^2 + 7\xi^2 \Big(\sum_{i\neq\ell}^{J} \big| \boldsymbol{v}^{\mathsf{H}} \boldsymbol{S}\boldsymbol{z}_i \boldsymbol{h}_i^{\mathsf{H}} \boldsymbol{S}\boldsymbol{z}_\ell \big| \Big)^2 \\
&\quad = 7\xi^2 I_5 + 7\xi^4 I_6 + 7\xi^6 I_7 + 7\xi^4 I_8 + 7\xi^4 I_9 + 7\xi^2 I_{10} + 7\xi^2 I_{11}.
\end{aligned}$$

We now bound the terms on the right-hand side. By means of Corollary 16 and large enough K,

$$I_5 = \big| \boldsymbol{v}_\ell^{\mathsf{H}} \boldsymbol{C}_\ell(\boldsymbol{z}) \boldsymbol{h}_\ell \big|^2 \leq \Big(\big\| \boldsymbol{C}_\ell(\boldsymbol{z}) \big\| \big\| \boldsymbol{h}_\ell \big\| \|\boldsymbol{v}\| \Big)^2 \leq \Big(\frac{K+J-1}{K} m_2^2 + \frac{\kappa}{K} + \delta \Big)^2.$$

Additionally, knowing that $\max_k \|\boldsymbol{s}_k\| = B\sqrt{L} \geq 1$ for all $k \in \{1, \ldots, K\}$, and by means of Corollaries 10 and 11 and the Cauchy-Schwarz inequality, we have

$$I_6 = \left| \sum_{i\neq\ell}^{J} \boldsymbol{v}^{\mathsf{H}} \boldsymbol{S}\boldsymbol{h}_i \boldsymbol{h}_i^{\mathsf{H}} \boldsymbol{S}\boldsymbol{z}_\ell \right|^2 \leq \sum_{i\neq\ell}^{J} \big| \boldsymbol{v}^{\mathsf{H}} \boldsymbol{S}\boldsymbol{h}_i \big|^2 \big| \boldsymbol{h}_i^{\mathsf{H}} \boldsymbol{S}\boldsymbol{z}_\ell \big|^2 \leq (J-1)(m_2+\delta)^4. \tag{A.36}$$

We also have that

$$\begin{aligned}
I_7 &= \left| \sum_{i\neq\ell}^{J} \boldsymbol{v}^{\mathsf{H}} \boldsymbol{S}\boldsymbol{h}_i \boldsymbol{h}_i^{\mathsf{H}} \boldsymbol{S}\boldsymbol{h}_\ell \right|^2 \leq \sum_{i\neq\ell}^{J} \big| \boldsymbol{v}^{\mathsf{H}} \boldsymbol{S}\boldsymbol{h}_i \big|^2 \big| \boldsymbol{h}_i^{\mathsf{H}} \boldsymbol{S}\boldsymbol{h}_\ell \big|^2 \leq \|\boldsymbol{S}\|^2 \sum_{i\neq\ell}^{J} \big| \boldsymbol{h}_i^{\mathsf{H}} \boldsymbol{S}\boldsymbol{h}_\ell \big|^2 \\
&\leq (m_2+\delta)^2 \sum_{i\neq\ell}^{J} \big| \boldsymbol{h}_i^{\mathsf{H}} \boldsymbol{S}\boldsymbol{h}_\ell \big|^2.
\end{aligned}$$

By inkoving the same tools, we also have

$$I_8 = \Big(\sum_{i\neq\ell}^{J} \big|\boldsymbol{v}^{\mathsf{H}}\boldsymbol{S}\boldsymbol{h}_i\boldsymbol{z}_i^{\mathsf{H}}\boldsymbol{S}\boldsymbol{h}_\ell\big| \Big)^2 \leq \sum_{i\neq\ell}^{J} \big|\boldsymbol{v}^{\mathsf{H}}\boldsymbol{S}\boldsymbol{h}_i\big|^2 \big|\boldsymbol{z}_i^{\mathsf{H}}\boldsymbol{S}\boldsymbol{h}_\ell\big|^2 \leq \sum_{i\neq\ell}^{J} \big\|\boldsymbol{S}\big\|^4 \leq (J-1)(m_2+\delta)^4,$$

$$I_9 = \Big(\sum_{i\neq\ell}^{J} \big|\boldsymbol{v}^{\mathsf{H}}\boldsymbol{S}\boldsymbol{z}_i\boldsymbol{h}_i^{\mathsf{H}}\boldsymbol{S}\boldsymbol{h}_\ell\big| \Big)^2 \leq \sum_{i\neq\ell}^{J} \big|\boldsymbol{v}^{\mathsf{H}}\boldsymbol{S}\boldsymbol{z}_i\big|^2 \big|\boldsymbol{h}_i^{\mathsf{H}}\boldsymbol{S}\boldsymbol{h}_\ell\big|^2 \leq \|\boldsymbol{S}\|^2 \sum_{i\neq\ell}^{J} \big|\boldsymbol{h}_i^{\mathsf{H}}\boldsymbol{S}\boldsymbol{h}_\ell\big|^2$$
$$\leq (m_2+\delta)^2 \sum_{i\neq\ell}^{J} \big|\boldsymbol{h}_i^{\mathsf{H}}\boldsymbol{S}\boldsymbol{h}_\ell\big|^2.$$

Thanks to the Cauchy-Schwarz inequality and Corollary 17,

$$I_{10} \leq \Big(\sum_{i\neq\ell}^{J} \big|\boldsymbol{v}^{\mathsf{H}}\boldsymbol{S}\boldsymbol{h}_i\boldsymbol{z}_i^{\mathsf{H}}\boldsymbol{S}\boldsymbol{z}_\ell\big| \Big)^2 \leq \sum_{i\neq\ell}^{J} \big|\boldsymbol{v}^{\mathsf{H}}\boldsymbol{S}\boldsymbol{h}_i\big|^2 \big|\boldsymbol{z}_i^{\mathsf{H}}\boldsymbol{S}\boldsymbol{z}_\ell\big|^2 \leq (J-1)(m_2+\delta)^2\delta^2.$$

Finally, via Cauchy-Schwarz inequality and Corollary 18,

$$I_{11} \leq \Big(\sum_{i\neq\ell}^{J} \big|\boldsymbol{v}^{\mathsf{H}}\boldsymbol{S}\boldsymbol{z}_i\boldsymbol{h}_i^{\mathsf{H}}\boldsymbol{S}\boldsymbol{z}_\ell\big| \Big)^2 \leq \sum_{i\neq\ell}^{J} \big|\boldsymbol{v}^{\mathsf{H}}\boldsymbol{S}\boldsymbol{z}_i\boldsymbol{z}_\ell^{\mathsf{T}}\boldsymbol{S}^{\mathsf{T}}\overline{\boldsymbol{h}_i}\big|^2 \leq \sum_{i\neq\ell}^{J} \big\|\boldsymbol{F}_{\ell i}(\boldsymbol{z})\big\|^2 \ \leq (J-1)(m_2+\delta)^2.$$

Therefore, we obtain

$$\begin{aligned}
&\left| \sum_{i\neq\ell}^{J} \boldsymbol{u}^{\mathsf{H}}\Big(\boldsymbol{S}\boldsymbol{q}_i\boldsymbol{q}_i^{\mathsf{H}}\boldsymbol{S}\boldsymbol{q}_\ell - \mathrm{e}^{j\phi(\boldsymbol{q}_\ell)}\boldsymbol{S}\boldsymbol{z}_i\boldsymbol{z}_i^{\mathsf{H}}\boldsymbol{S}\boldsymbol{z}_\ell\Big) \right|^2 \\
&\quad \leq 7\xi^2\Big(\frac{K+J-1}{K}m_2^2 + \frac{\kappa}{K} + \delta\Big)^2 + 7\xi^4(J-1)(m_2+\delta)^4 \\
&\qquad + 7\xi^6(m_2+\delta)^2 \sum_{i\neq\ell}^{J} \big|\boldsymbol{h}_i^{\mathsf{H}}\boldsymbol{S}\boldsymbol{h}_\ell\big|^2 + 7\xi^4(J-1)(m_2+\delta)^4 \\
&\qquad + 7\xi^4(m_2+\delta)^2 \sum_{i\neq\ell}^{J} \big|\boldsymbol{h}_i^{\mathsf{H}}\boldsymbol{S}\boldsymbol{h}_\ell\big|^2 + 7\xi^2(J-1)(m_2+\delta)^2\delta^2 + 7\xi^2(J-1)(m_2+\delta)^2. \quad \text{(A.37)}
\end{aligned}$$

By substituting Eqs.(A.37) and (A.35) into Eq.(A.34), we have that

$$
\begin{aligned}
&\frac{1}{\beta}\Big|\boldsymbol{u}^{\mathsf{H}}\big(\nabla_\ell g(\boldsymbol{q}) - \mathrm{e}^{j\phi(\boldsymbol{q}_\ell)}\nabla_\ell g(\boldsymbol{z})\big)\Big|^2 \\
&\quad\le 2\Big|\boldsymbol{u}^{\mathsf{H}}\nabla f(\boldsymbol{q}_\ell) - \mathrm{e}^{j\phi(\boldsymbol{q}_\ell)}\nabla f(\boldsymbol{z}_\ell)\Big|^2 + 2\gamma_0^2\left|\sum_{i\neq\ell}^{J}\boldsymbol{u}^{\mathsf{H}}\Big(\boldsymbol{S}\boldsymbol{q}_i\boldsymbol{q}_i^{\mathsf{H}}\boldsymbol{S}\boldsymbol{q}_\ell - \mathrm{e}^{j\phi(\boldsymbol{q}_\ell)}\boldsymbol{S}\boldsymbol{z}_i\boldsymbol{z}_i^{\mathsf{H}}\boldsymbol{S}\boldsymbol{z}_\ell\Big)\right|^2 \\
&\quad\le 2\Bigg(4D(2m_2^2+\kappa+\delta)^2 + \big(m_2^2+\kappa+(1+R_2)\delta\big)^2\cdot\mathbf{1}[Q\neq 4] \\
&\qquad\quad + \frac{9D\xi^2(2m_2^2+\kappa+\delta) + DB^2L\xi^4(m_2+\delta)}{K}\sum_{k=1}^{K}|\boldsymbol{s}_k^{\mathsf{H}}\boldsymbol{h}_\ell|^4\Bigg) \\
&\qquad + 14\gamma_0^2\xi^2\Bigg(\Big(\frac{K+J-1}{K}m_2^2 + \frac{\kappa}{K} + \delta\Big)^2 + 2\xi^2(J-1)(m_2+\delta)^4 \\
&\qquad\quad + \xi^2(1+\xi^2)(m_2+\delta)^2\sum_{i\neq\ell}^{J}\big|\boldsymbol{h}_i^{\mathsf{H}}\boldsymbol{S}\boldsymbol{h}_\ell\big|^2 + (J-1)(m_2+\delta)^2(1+\delta^2)\Bigg) \\
&\quad\le \beta\Bigg(\frac{2m_2^2-R_2m_2-\delta}{19} + \frac{\xi^2}{20K}\sum_{k=1}^{K}|\boldsymbol{s}_k^{\mathsf{H}}\boldsymbol{h}_\ell|^4 + \gamma_0^2 r_1 + \gamma_0^2R_2\xi^2\sum_{i\neq\ell}^{J}\big|\boldsymbol{h}_i^{\mathsf{H}}\boldsymbol{S}\boldsymbol{h}_\ell\big|^2\Bigg).
\end{aligned}
$$

Hence, Lemma 7 holds under the following condition:

$$
\begin{aligned}
\beta \ge \max\Bigg\{&\frac{152D(2m_2^2+\kappa+\delta)^2}{2m_2^2-R_2m_2-\delta} + \frac{38\big(m_2^2+\kappa+(1+R_2)\delta\big)^2}{2m_2^2-R_2m_2-\delta}\cdot\mathbf{1}[Q\neq 4] \\
&+ \frac{266\gamma_0^2}{2m_2^2-R_2m_2-\delta}\Bigg(\Big(\frac{K+J-1}{K}m_2^2+\frac{\kappa}{K}+\delta\Big)^2 \\
&+ 2\epsilon^2(J-1)(m_2+\delta)^4 + (J-1)(m_2+\delta)^2(1+\delta^2)\Bigg), \\
&360D(2m_2^2+\kappa+\delta) + 40DB^2L\epsilon^2(m_2+\delta),\ 14\gamma_0^2(1+\epsilon^2)(m_2+\delta)^2\Bigg\}. \qquad \text{(A.38)}
\end{aligned}
$$

With $\epsilon = (10B\sqrt{JL})^{-1}$, $\gamma_0 = 1$ and $\delta \le 0.001$, Eq.(A.38) holds for

$$
\begin{aligned}
&\beta \ge 730 + 267(J-1) \quad \text{for} \quad Q = 4, \\
&\beta \ge 1964 + 394(J-1) \quad \text{for} \quad Q \neq 4.
\end{aligned}
$$

Appendix B

Alternative Proofs for Riemannian Orthogonal CMA

Here, we use an alternative approach to prove that the mean Riemannian Hessian of the CMA cost function (4.3a) is strictly positive definite in a neighborhood of an optimum. Equivalently, we prove that the quadratic form of the Riemannian Hessian is strictly positive at an optimum, and thanks to its continuity, we conclude that the Riemannian Hessian is strictly positive definite in a neighborhood of such optimum. By using concentration of measure inequalities (such as the ones used for theoretical convergence guarantees of WFCMA), we expect to translate this result to the finite-sample Riemannian Hessian of ROCMA in future work.

In the following, we assume the conditions of Theorem 9 hold. Recall that the Riemannian Hessian can be lifted to the ambient manifold as follows:

$$
\begin{aligned}
&\operatorname{lift}_{\boldsymbol{Y}}\big(\operatorname{Hess}_{\boldsymbol{Y}} g\big([\boldsymbol{Y}]\big)[\boldsymbol{\xi}]\big) = \operatorname{Proj}^{\mathrm{H}}_{\boldsymbol{Y}}\Big(\mathrm{D}\overline{\overline{r}}(\boldsymbol{Y})[\boldsymbol{E}]\Big) \\
&\quad = \operatorname{Proj}^{\mathrm{H}}_{\boldsymbol{Y}}\Big(\mathrm{D}\big(\nabla_{\boldsymbol{Y}}\overline{\overline{g}}(\boldsymbol{Y})\big)[\boldsymbol{E}] - \boldsymbol{U}\operatorname{herm}\Big(\boldsymbol{Y}^{\mathsf{H}}\nabla_{\boldsymbol{Y}}\overline{\overline{g}}(\boldsymbol{Y})\Big) - \boldsymbol{Y}\operatorname{herm}\Big(\mathrm{D}\big(\boldsymbol{Y}^{\mathsf{H}}\nabla_{\boldsymbol{Y}}\overline{\overline{g}}(\boldsymbol{Y})\big)[\boldsymbol{E}]\Big)\Big) \\
&\quad = \operatorname{Proj}^{\mathrm{H}}_{\boldsymbol{Y}}\Big(\mathrm{D}\big(\nabla_{\boldsymbol{Y}}\overline{\overline{g}}(\boldsymbol{Y})\big)[\boldsymbol{E}] - \boldsymbol{E}\operatorname{herm}\Big(\boldsymbol{Y}^{\mathsf{H}}\nabla_{\boldsymbol{Y}}\overline{\overline{g}}(\boldsymbol{Y})\Big)\Big)
\end{aligned}
$$

where the last term in the RHS of the first equality vanishes through the projection, as it belongs to normal space.

Let

$$\begin{aligned}\boldsymbol{A}_k &= \big(\boldsymbol{I} \circ (\boldsymbol{Y}^{\mathsf{H}}\boldsymbol{Z}_k\boldsymbol{Y}) - R_2\boldsymbol{I}\big),\\ \boldsymbol{B}_k &= \big(\boldsymbol{I} \circ (\boldsymbol{Y}^{\mathsf{H}}\boldsymbol{Z}_k\boldsymbol{E} + \boldsymbol{E}^{\mathsf{H}}\boldsymbol{Z}_k\boldsymbol{Y})\big)\end{aligned}$$

which are real, diagonal matrices. Hence,

$$\begin{aligned}\mathrm{lift}_{\boldsymbol{Y}}\big(\mathrm{Hess}_{\boldsymbol{Y}} g([\boldsymbol{Y}])[\boldsymbol{\xi}]\big) &= \mathrm{Proj}^{\mathrm{H}}_{\boldsymbol{Y}}\Big(\mathrm{D}\big(\nabla_{\boldsymbol{Y}}\overline{\overline{g}}(\boldsymbol{Y})\big)[\boldsymbol{E}]\Big) - \mathrm{Proj}^{\mathrm{H}}_{\boldsymbol{Y}}\Big(\boldsymbol{E}\mathrm{herm}\Big(\boldsymbol{Y}^{\mathsf{H}}\nabla_{\boldsymbol{Y}}\overline{\overline{g}}(\boldsymbol{Y})\Big)\Big)\\
&= \mathrm{Proj}^{\mathrm{H}}_{\boldsymbol{Y}}\Big(\frac{1}{K}\sum_{k=1}^{K}\boldsymbol{Z}_k\boldsymbol{Y}\boldsymbol{B} + \boldsymbol{Z}_k\boldsymbol{E}\boldsymbol{A}\Big) - \mathrm{Proj}^{\mathrm{H}}_{\boldsymbol{Y}}\Big(\boldsymbol{E}\mathrm{herm}\Big(\frac{1}{K}\sum_{k=1}^{K}\boldsymbol{Y}^{\mathsf{H}}\boldsymbol{Z}_k\boldsymbol{Y}\boldsymbol{A}\Big)\Big)\\
&= \frac{1}{K}\sum_{k=1}^{K}\Big(\boldsymbol{Z}_k\boldsymbol{Y}\boldsymbol{B} + \boldsymbol{Z}_k\boldsymbol{E}\boldsymbol{A} - \boldsymbol{Y}\mathrm{herm}(\boldsymbol{Y}^{\mathsf{H}}\boldsymbol{Z}_k\boldsymbol{Y}\boldsymbol{B} + \boldsymbol{Y}^{\mathsf{H}}\boldsymbol{Z}_k\boldsymbol{E}\boldsymbol{A})\\
&\qquad - \boldsymbol{Y}\big(\boldsymbol{I}\circ\mathrm{skew}(\boldsymbol{Y}^{\mathsf{H}}\boldsymbol{Z}_k\boldsymbol{Y}\boldsymbol{B} + \boldsymbol{Y}^{\mathsf{H}}\boldsymbol{Z}_k\boldsymbol{E}\boldsymbol{A})\big)\Big)\\
&\quad - \frac{1}{K}\sum_{k=1}^{K}\Big(\boldsymbol{E}\boldsymbol{Y}^{\mathsf{H}}\boldsymbol{Z}_k\boldsymbol{Y}\boldsymbol{A} - \boldsymbol{Y}\mathrm{herm}\big(\boldsymbol{Y}^{\mathsf{H}}\boldsymbol{E}\boldsymbol{Y}^{\mathsf{H}}\boldsymbol{Z}_k\boldsymbol{Y}\boldsymbol{A}\big)\\
&\qquad - \boldsymbol{Y}\big(\boldsymbol{I}\circ\mathrm{skew}\big(\boldsymbol{Y}^{\mathsf{H}}\boldsymbol{E}\boldsymbol{Y}^{\mathsf{H}}\boldsymbol{Z}_k\boldsymbol{Y}\boldsymbol{A}\big)\big)\Big).\end{aligned} \tag{B.1}$$

To verify whether the Hessian is positive definite, we compute its quadratic form with $\boldsymbol{E}$ a unit vector in horizontal space, i.e. $\boldsymbol{E}^{\mathsf{H}}\boldsymbol{Y}$ is skew-Hermitian with zero diagonal, and $\|\boldsymbol{E}\|_{\boldsymbol{Y}} = \mathrm{Tr}(\boldsymbol{E}^{\mathsf{H}}\boldsymbol{E}) = \|\boldsymbol{E}\|_F^2 = 1$. Using the real trace inner product $\langle \boldsymbol{U}, \boldsymbol{V}\rangle_{\boldsymbol{Y}} = \mathrm{ReTr}(\boldsymbol{U}^{\mathsf{H}}\boldsymbol{V})$

for $\boldsymbol{U}, \boldsymbol{V} \in \mathrm{H}_{\boldsymbol{Y}}\overline{\mathcal{M}}$, we have

$$
\begin{aligned}
\Big\langle \boldsymbol{\xi}, \mathrm{Hess}_{\boldsymbol{Y}} g\big([\boldsymbol{Y}]\big)[\boldsymbol{\xi}] \Big\rangle_{[\boldsymbol{Y}]} &= \Big\langle \boldsymbol{E}, \mathrm{lift}_{\boldsymbol{Y}}\big(\mathrm{Hess}_{\boldsymbol{Y}} g\big([\boldsymbol{Y}]\big)[\boldsymbol{\xi}]\big) \Big\rangle_{\boldsymbol{Y}} \\
&= \frac{1}{K}\sum_{k=1}^{K} \mathrm{ReTr}\Bigg(\boldsymbol{E}^{\mathsf{H}}\boldsymbol{Z}_k\boldsymbol{Y}\boldsymbol{B} + \boldsymbol{E}^{\mathsf{H}}\boldsymbol{Z}_k\boldsymbol{E}\boldsymbol{A} - \boldsymbol{E}^{\mathsf{H}}\boldsymbol{Y}\mathrm{herm}(\boldsymbol{Y}^{\mathsf{H}}\boldsymbol{Z}_k\boldsymbol{Y}\boldsymbol{B} + \boldsymbol{Y}^{\mathsf{H}}\boldsymbol{Z}_k\boldsymbol{E}\boldsymbol{A}) \\
&\qquad - \boldsymbol{E}^{\mathsf{H}}\boldsymbol{Y}\big(\boldsymbol{I} \circ \mathrm{skew}(\boldsymbol{Y}^{\mathsf{H}}\boldsymbol{Z}_k\boldsymbol{Y}\boldsymbol{B} + \boldsymbol{Y}^{\mathsf{H}}\boldsymbol{Z}_k\boldsymbol{E}\boldsymbol{A}) \\
&\quad - \Big(\boldsymbol{E}^{\mathsf{H}}\boldsymbol{E}\boldsymbol{Y}^{\mathsf{H}}\boldsymbol{Z}_k\boldsymbol{Y}\boldsymbol{A} - \boldsymbol{E}^{\mathsf{H}}\boldsymbol{Y}\mathrm{herm}\big(\boldsymbol{Y}^{\mathsf{H}}\boldsymbol{E}\boldsymbol{Y}^{\mathsf{H}}\boldsymbol{Z}_k\boldsymbol{Y}\boldsymbol{A}\big) \\
&\qquad - \boldsymbol{E}^{\mathsf{H}}\boldsymbol{Y}\big(\boldsymbol{I} \circ \mathrm{skew}\big(\boldsymbol{Y}^{\mathsf{H}}\boldsymbol{E}\boldsymbol{Y}^{\mathsf{H}}\boldsymbol{Z}_k\boldsymbol{Y}\boldsymbol{A}\big)\Big)\Big)\Bigg) \\
&= \frac{1}{K}\sum_{k=1}^{K} \mathrm{ReTr}\Bigg(\boldsymbol{E}^{\mathsf{H}}\boldsymbol{Z}_k\boldsymbol{Y}\boldsymbol{B} + \boldsymbol{E}^{\mathsf{H}}\boldsymbol{Z}_k\boldsymbol{E}\boldsymbol{A} - \boldsymbol{E}^{\mathsf{H}}\boldsymbol{E}\boldsymbol{Y}^{\mathsf{H}}\boldsymbol{Z}_k\boldsymbol{Y}\boldsymbol{A} \\
&\qquad - \boldsymbol{E}^{\mathsf{H}}\boldsymbol{Y}\mathrm{herm}(\boldsymbol{Y}^{\mathsf{H}}\boldsymbol{Z}_k\boldsymbol{Y}\boldsymbol{B} + \boldsymbol{Y}^{\mathsf{H}}\boldsymbol{Z}_k\boldsymbol{E}\boldsymbol{A}) + \boldsymbol{E}^{\mathsf{H}}\boldsymbol{Y}\mathrm{herm}\big(\boldsymbol{Y}^{\mathsf{H}}\boldsymbol{E}\boldsymbol{Y}^{\mathsf{H}}\boldsymbol{Z}_k\boldsymbol{Y}\boldsymbol{A}\big) \\
&\quad - \boldsymbol{E}^{\mathsf{H}}\boldsymbol{Y}\big(\boldsymbol{I} \circ \mathrm{skew}(\boldsymbol{Y}^{\mathsf{H}}\boldsymbol{Z}_k\boldsymbol{Y}\boldsymbol{B} + \boldsymbol{Y}^{\mathsf{H}}\boldsymbol{Z}_k\boldsymbol{E}\boldsymbol{A}) + \boldsymbol{E}^{\mathsf{H}}\boldsymbol{Y}\big(\boldsymbol{I} \circ \mathrm{skew}\big(\boldsymbol{Y}^{\mathsf{H}}\boldsymbol{E}\boldsymbol{Y}^{\mathsf{H}}\boldsymbol{Z}_k\boldsymbol{Y}\boldsymbol{A}\big)\Bigg) \\
&= \frac{1}{K}\sum_{k=1}^{K} \mathrm{ReTr}\Big(\boldsymbol{E}^{\mathsf{H}}\boldsymbol{Z}_k\boldsymbol{Y}\boldsymbol{B} + \boldsymbol{E}^{\mathsf{H}}\boldsymbol{Z}_k\boldsymbol{E}\boldsymbol{A} - \boldsymbol{E}^{\mathsf{H}}\boldsymbol{E}\boldsymbol{Y}^{\mathsf{H}}\boldsymbol{Z}_k\boldsymbol{Y}\boldsymbol{A}\Big), \qquad \text{(B.2)}
\end{aligned}
$$

where:

- the terms of the form $\mathrm{ReTr}(\boldsymbol{E}^{\mathsf{H}}\boldsymbol{Y}\mathrm{herm}(\cdot))$ vanish because $\boldsymbol{E}^{\mathsf{H}}\boldsymbol{Y}$ is skew-Hermitian, which are orthogonal to Hermitian matrices; and
- the terms of the form $\mathrm{ReTr}\big(\boldsymbol{E}^{\mathsf{H}}\boldsymbol{Y}(\boldsymbol{I} \circ \cdot)\big)$ vanish because $\boldsymbol{E}^{\mathsf{H}}\boldsymbol{Y}$ has zero diagonal, and its product with a diagonal matrix has zero diagonal as well.

We now take expectation in Eq.(B.2). Recall that the optimum demixers in combined parameter space are $\widehat{\boldsymbol{Q}} = \boldsymbol{P}\boldsymbol{D}$, with $\boldsymbol{P} \in \mathbb{R}^{L\times J}$ a tall permutation matrix and $\boldsymbol{D} \in \mathbb{C}^{J\times J}$ a diagonal unitary matrix, and thus $\widehat{\boldsymbol{Q}}^{\mathsf{H}}\widehat{\boldsymbol{Q}} = \boldsymbol{I}$. Using the right singular vectors of the channel matrix $\boldsymbol{H}$, collected in matrix $\boldsymbol{V}$, we have that $\boldsymbol{Y} = \boldsymbol{V}\boldsymbol{Q}$, and we also have that

$\boldsymbol{Z}_k = \boldsymbol{V}^{\mathsf{H}}\boldsymbol{s}_k\boldsymbol{s}_k^{\mathsf{H}}\boldsymbol{V}$. Let $\boldsymbol{C} = \boldsymbol{V}\boldsymbol{E}$, and thus $\|\boldsymbol{C}\|_F^2 = \|\boldsymbol{E}\|_F^2 = 1$. Moreover, we have that

$$\boldsymbol{E}^{\mathsf{H}}\widehat{\boldsymbol{Y}} = \boldsymbol{C}^{\mathsf{H}}\widehat{\boldsymbol{Q}} = \boldsymbol{C}^{\mathsf{H}}\boldsymbol{P}\boldsymbol{D} \tag{B.3}$$

also is skew-Hermitian with zero diagonal, i.e., $(\boldsymbol{C}^{\mathsf{H}}\boldsymbol{P}) \circ \boldsymbol{I} = \boldsymbol{0}$. Note that if $\boldsymbol{P}$ follows the permutation $\nu : \ell \to \nu(\ell) \in \{1, \cdots, L\}$, then

$$\boldsymbol{P} = \big[\boldsymbol{e}_{\nu(1)} \ \cdots \ \boldsymbol{e}_{\nu(L)}\big]\boldsymbol{I}_{L,J} \tag{B.4}$$

where $\boldsymbol{I}_{L,J}$ contains the first J columns of the identity matrix of size L. Hence, the diagonal elements of $\boldsymbol{C}^{\mathsf{H}}\boldsymbol{P}$ (equal to zero) correspond to

$$\big[\boldsymbol{C}^{\mathsf{H}}\boldsymbol{P}\big]_{\ell\ell} = \Big[\boldsymbol{C}^{\mathsf{H}}\big[\boldsymbol{e}_{\nu(1)} \ \cdots \ \boldsymbol{e}_{\nu(L)}\big]\boldsymbol{I}_{L,J}\Big]_{\ell\ell} = \big[\overline{\boldsymbol{C}}\big]_{\nu(\ell),\ell} = \overline{c}_{\nu(\ell),\ell} = 0. \tag{B.5}$$

Without loss of generality, we let $\boldsymbol{P} = \boldsymbol{I}_{L,J}$, i.e. $\nu(\ell) = \ell$, and thus $c_{\ell\ell} = 0$ for all ℓ. Then, we have that

$$\begin{aligned}\mathbb{E}\Big\{\big\langle\boldsymbol{\xi}, \mathrm{Hess}_{\boldsymbol{Y}}\, g\big([\boldsymbol{Y}]\big)[\boldsymbol{\xi}]\big\rangle_{[\boldsymbol{Y}]}\Big\} &= \mathrm{ReTr}\mathbb{E}\Big\{\boldsymbol{E}^{\mathsf{H}}\boldsymbol{Z}_k\boldsymbol{Y}\boldsymbol{B} + \boldsymbol{E}^{\mathsf{H}}\boldsymbol{Z}_k\boldsymbol{E}\boldsymbol{A} - \boldsymbol{E}^{\mathsf{H}}\boldsymbol{E}\boldsymbol{Y}^{\mathsf{H}}\boldsymbol{Z}_k\boldsymbol{Y}\boldsymbol{A}\Big\} \\ &= \mathrm{ReTr}\mathbb{E}\big\{\boldsymbol{E}^{\mathsf{H}}\boldsymbol{Z}_k\boldsymbol{Y}\boldsymbol{B}\big\} + \mathrm{ReTr}\mathbb{E}\big\{\boldsymbol{E}^{\mathsf{H}}\boldsymbol{Z}_k\boldsymbol{E}\boldsymbol{A}\big\} - \mathrm{ReTr}\Big(\boldsymbol{E}^{\mathsf{H}}\boldsymbol{E}\mathbb{E}\big\{\boldsymbol{Y}^{\mathsf{H}}\boldsymbol{Z}_k\boldsymbol{Y}\boldsymbol{A}\big\}\Big). \end{aligned} \tag{B.6}$$

Now we develop each expectation in the RHS of Eq.(B.6). The first term is

$$\begin{aligned}\mathrm{ReTr}\mathbb{E}\big\{\boldsymbol{E}^{\mathsf{H}}\boldsymbol{Z}_k\boldsymbol{Y}\boldsymbol{B}\big\} &= \mathrm{ReTr}\mathbb{E}\big\{\boldsymbol{C}^{\mathsf{H}}\boldsymbol{S}_k\boldsymbol{Q}\big(\boldsymbol{I} \circ (\boldsymbol{C}^{\mathsf{H}}\boldsymbol{S}_k\boldsymbol{Q} + \boldsymbol{Q}^{\mathsf{H}}\boldsymbol{S}_k\boldsymbol{C})\big\} \\ &= \sum_{\ell=1}^{J} \mathrm{Re}\mathbb{E}\Big\{\big[\boldsymbol{C}^{\mathsf{H}}\boldsymbol{S}_k\boldsymbol{Q}\big(\boldsymbol{I} \circ (\boldsymbol{C}^{\mathsf{H}}\boldsymbol{S}_k\boldsymbol{Q} + \boldsymbol{Q}^{\mathsf{H}}\boldsymbol{S}_k\boldsymbol{C})\big]_{\ell\ell}\Big\}\end{aligned}$$

where, because of the product with a diagonal matrix, each element is

$$\begin{aligned}
&\big[\boldsymbol{C}^{\mathsf{H}}\boldsymbol{S}_k\boldsymbol{Q}\big(\boldsymbol{I}\circ(\boldsymbol{C}^{\mathsf{H}}\boldsymbol{S}_k\boldsymbol{Q}+\boldsymbol{Q}^{\mathsf{H}}\boldsymbol{S}_k\boldsymbol{C})\big)\big]_{\ell\ell}\\
&\qquad=\big[\boldsymbol{C}^{\mathsf{H}}\boldsymbol{S}_k\boldsymbol{Q}\big]_{\ell\ell}\cdot\big[\boldsymbol{C}^{\mathsf{H}}\boldsymbol{S}_k\boldsymbol{Q}+\boldsymbol{Q}^{\mathsf{H}}\boldsymbol{S}_k\boldsymbol{C}\big]_{\ell\ell}\\
&\qquad=\big(\boldsymbol{c}_\ell^{\mathsf{H}}\boldsymbol{S}_k\boldsymbol{q}_\ell\big)\big(\boldsymbol{c}_\ell^{\mathsf{H}}\boldsymbol{S}_k\boldsymbol{q}_\ell+\boldsymbol{q}_\ell^{\mathsf{H}}\boldsymbol{S}_k\boldsymbol{c}_\ell\big)=\big(\boldsymbol{c}_\ell^{\mathsf{H}}\boldsymbol{S}_k\boldsymbol{q}_\ell\big)^2+\big|\boldsymbol{c}_\ell^{\mathsf{H}}\boldsymbol{S}_k\boldsymbol{q}_\ell\big|^2\\
&\qquad=\Big(\sum_{a=1}^{L}\overline{c}_{\ell,a}s_{k,a}\overline{s}_{k,\ell}\Big)^2+\Big(\sum_{a=1}^{L}\overline{c}_{\ell,a}s_{k,a}\overline{s}_{k,\ell}\Big)\overline{\Big(\sum_{a=1}^{L}\overline{c}_{\ell,a}s_{k,a}\overline{s}_{k,\ell}\Big)}\\
&\qquad=\sum_{a=1}^{L}\sum_{b=1}^{L}\overline{c}_{\ell,a}\overline{c}_{\ell,a}s_{k,a}s_{k,b}\overline{s}_{k,\ell}^2+\sum_{a=1}^{L}\sum_{b=1}^{L}\overline{c}_{\ell,a}c_{\ell,b}s_{k,a}\overline{s}_{k,b}|s_{k,\ell}|^2\\
&\qquad=\overline{c}_{\ell,\ell}^2|s_{k,\ell}|^4+\sum_{a=1}^{L}|c_{\ell,a}|^2|s_{k,a}|^2|s_{k,\ell}|^2
\end{aligned}$$

and hence,

$$\mathrm{ReTr}\mathbb{E}\big\{\boldsymbol{E}^{\mathsf{H}}\boldsymbol{Z}_k\boldsymbol{Y}\boldsymbol{B}\big\}=m_4\overline{c}_{\ell,\ell}^2+(m_4-m_2^2)|c_{\ell,\ell}|^2+m_2^2\|\boldsymbol{c}_\ell\|^2=m_2^2\|\boldsymbol{c}_\ell\|^2. \tag{B.7}$$

The second term develops as follows:

$$\begin{aligned}
\mathrm{ReTr}\mathbb{E}\big\{\boldsymbol{E}^{\mathsf{H}}\boldsymbol{Z}_k\boldsymbol{E}\boldsymbol{A}\big\}&=\mathrm{ReTr}\mathbb{E}\big\{\boldsymbol{C}^{\mathsf{H}}\boldsymbol{S}_k\boldsymbol{C}\big(\boldsymbol{I}\circ(\boldsymbol{Q}^{\mathsf{H}}\boldsymbol{S}_k\boldsymbol{Q})-R_2\boldsymbol{I}\big)\big\}\\
&=\sum_{\ell=1}^{J}\mathrm{Re}\mathbb{E}\Big\{\big[\boldsymbol{C}^{\mathsf{H}}\boldsymbol{S}_k\boldsymbol{C}\big(\boldsymbol{I}\circ(\boldsymbol{Q}^{\mathsf{H}}\boldsymbol{S}_k\boldsymbol{Q})-R_2\boldsymbol{I}\big)\big]_{\ell\ell}\Big\}
\end{aligned}$$

where, because of the product with a diagonal matrix,

$$\begin{aligned}
\big[\boldsymbol{C}^{\mathsf{H}}\boldsymbol{S}_k\boldsymbol{C}\big(\boldsymbol{I}\circ(\boldsymbol{Q}^{\mathsf{H}}\boldsymbol{S}_k\boldsymbol{Q})-R_2\boldsymbol{I}\big)\big]_{\ell\ell}&=\big[\boldsymbol{C}^{\mathsf{H}}\boldsymbol{S}_k\boldsymbol{C}\big]_{\ell\ell}\cdot\big[\boldsymbol{Q}^{\mathsf{H}}\boldsymbol{S}_k\boldsymbol{Q}-R_2\boldsymbol{I}\big]_{\ell\ell}\\
&=\big(\boldsymbol{c}_\ell^{\mathsf{H}}\boldsymbol{S}_k\boldsymbol{c}_\ell\big)\big(\boldsymbol{q}_\ell^{\mathsf{H}}\boldsymbol{S}_k\boldsymbol{q}_\ell-R_2\big)=\big|\boldsymbol{c}_\ell^{\mathsf{H}}\boldsymbol{S}_k\boldsymbol{c}_\ell\big|^2\big(|s_{k,\ell}|^2-R_2\big)\\
&=\sum_{a=1}^{L}\sum_{b=1}^{L}\overline{c}_{\ell,a}c_{\ell,b}s_{k,a}\overline{s}_{k,b}|s_{k,\ell}|^2-R_2\sum_{a=1}^{L}\sum_{b=1}^{L}\overline{c}_{\ell,a}c_{\ell,b}s_{k,a}\overline{s}_{k,b}\\
&=\sum_{a=1}^{L}|c_{\ell,a}|^2|s_{k,a}|^2|s_{k,\ell}|^2-R_2\sum_{a=1}^{L}|c_{\ell,a}|^2|s_{k,a}|^2
\end{aligned}$$

yielding

$$\mathrm{ReTr}\mathbb{E}\big\{\boldsymbol{E}^{\mathsf{H}}\boldsymbol{Z}_k\boldsymbol{E}\boldsymbol{A}\big\} = (m_4 - m_2^2)|c_{\ell,\ell}|^2 + m_2^2\|\boldsymbol{c}_\ell\|^2 - R_2 m_2\|\boldsymbol{c}_\ell\|^2 = m_2^2\|\boldsymbol{c}_\ell\|^2 - R_2 m_2\|\boldsymbol{c}_\ell\|^2. \tag{B.8}$$

For the last term, we have

$$\begin{aligned}
\mathbb{E}\big\{\boldsymbol{Y}^{\mathsf{H}}\boldsymbol{Z}_k\boldsymbol{Y}\boldsymbol{A}\big\} &= \mathbb{E}\Big\{\boldsymbol{Q}^{\mathsf{H}}\boldsymbol{S}_k\boldsymbol{Q}\big(\boldsymbol{I}\circ(\boldsymbol{Q}^{\mathsf{H}}\boldsymbol{S}_k\boldsymbol{Q}) - R_2\boldsymbol{I}\big)\Big\} \\
&= \mathbb{E}\Big\{\boldsymbol{Q}^{\mathsf{H}}\boldsymbol{S}_k\boldsymbol{Q}\big(\boldsymbol{I}\circ(\boldsymbol{Q}^{\mathsf{H}}\boldsymbol{S}_k\boldsymbol{Q})\big) - R_2\boldsymbol{Q}^{\mathsf{H}}\boldsymbol{S}_k\boldsymbol{Q}\Big\} \\
&= \mathbb{E}\Big\{\boldsymbol{Q}^{\mathsf{H}}\boldsymbol{S}_k\boldsymbol{Q}\big(\boldsymbol{I}\circ(\boldsymbol{Q}^{\mathsf{H}}\boldsymbol{S}_k\boldsymbol{Q})\big)\Big\} - R_2 m_2\boldsymbol{I}.
\end{aligned}$$

Now, let $\boldsymbol{M} = \boldsymbol{Q}^{\mathsf{H}}\boldsymbol{S}_k\boldsymbol{Q}\big(\boldsymbol{I}\circ(\boldsymbol{Q}^{\mathsf{H}}\boldsymbol{S}_k\boldsymbol{Q})\big)$. Then, thanks to the product with a diagonal matrix,

$$[\boldsymbol{M}]_{ij} = \boldsymbol{q}_i^{\mathsf{H}}\boldsymbol{S}_k\boldsymbol{q}_j\cdot(\boldsymbol{q}_j^{\mathsf{H}}\boldsymbol{S}_k\boldsymbol{q}_j) = \overline{s}_{k,i}s_{k,j}|s_{k,j}|^2 \Rightarrow \mathbb{E}\big\{[\boldsymbol{M}]_{ij}\big\} = m_4\delta_{ij}$$

and

$$\mathbb{E}\big\{\boldsymbol{Y}^{\mathsf{H}}\boldsymbol{Z}_k\boldsymbol{Y}\boldsymbol{A}\big\} = m_4\boldsymbol{I} - R_2 m_2\boldsymbol{I} = \boldsymbol{0}. \tag{B.9}$$

Replacing Eqs.(B.7), (B.8) and (B.9) in Eq.(B.6), we have

$$\begin{aligned}
\mathbb{E}\Big\{\big\langle\boldsymbol{\xi},\mathrm{Hess}_{\boldsymbol{Y}}g\big([\boldsymbol{Y}]\big)[\boldsymbol{\xi}]\big\rangle_{[\boldsymbol{Y}]}\Big\} &= \sum_{\ell=1}^{J}\mathrm{Re}\Big(m_2^2\|\boldsymbol{c}_\ell\|^2 + m_2^2\|\boldsymbol{c}_\ell\|^2 - R_2 m_2\|\boldsymbol{c}_\ell\|^2 - 0\Big) \\
&= (2m_2^2 - m_4)\sum_{\ell=1}^{J}\|\boldsymbol{c}_\ell\|^2 \\
&= (2m_2^2 - m_4)\|\boldsymbol{C}\|_F^2 \\
&= (2m_2^2 - m_4) > 0
\end{aligned}$$

which is strictly larger than zero for all regular QAM modulations.

References

[1] A. Al-Fuqaha, M. Guizani, M. Mohammadi, M. Aledhari, and M. Ayyash, "Internet of Things: A Survey on Enabling Technologies, Protocols, and Applications," *IEEE Communications Surveys Tutorials*, vol. 17, no. 4, pp. 2347–2376, 4th Quarter 2015.

[2] Qualcomm Technologies Inc., "The 5G unified air interface: Scalable to an extreme variation of requirements," Tech. Rep., November 2015.

[3] J. G. Andrews, S. Buzzi, W. Choi, S. V. Hanly, A. Lozano, A. C. K. Soong, and J. C. Zhang, "What will 5g be?" *IEEE Journal on Selected Areas in Communications*, vol. 32, no. 6, pp. 1065–1082, 2014.

[4] H. Holma and A. Toskala, *LTE Advanced: 3GPP Solution for IMT-Advanced*. New York, NY, USA: Wiley, 2012.

[5] S. Verdu, "Minimum probability of error for asynchronous Gaussian multiple-access channels," *IEEE Transactions on Information Theory*, vol. 32, no. 1, pp. 85–96, 1986.

[6] P. Vandenameele, L. Van Der Perre, M. Engels, B. Gyselinckx, and H. De Man, "A combined OFDM/SDMA approach," *IEEE Journal on Selected Areas in Communications*, vol. 18, no. 11, pp. 2312–2321, 2000.

[7] L. Hanzo, T. Keller, M. Muenster, and B.-J. Choi, *OFDM and MC-CDMA for Broadband Multi-User Communications, WLANs and Broadcasting*. USA: John Wiley & Sons, Inc., 2003.

[8] S. Verdu, "Optimum multiuser asymptotic efficiency," *IEEE Transactions on Communications*, vol. 34, no. 9, pp. 890–897, 1986.

[9] X. Zhu and R. Murch, "Performance analysis of maximum likelihood detection in a MIMO antenna system," *IEEE Transactions on Communications*, vol. 50, no. 2, pp. 187–191, 2002.

[10] R. Lupas and S. Verdu, "Linear multiuser detectors for synchronous code-division multiple-access channels," *IEEE Transactions on Information Theory*, vol. 35, no. 1, pp. 123–136, 1989.

[11] Z. Xie, R. Short, and C. Rushforth, "A family of suboptimum detectors for coherent multiuser communications," *IEEE Journal on Selected Areas in Communications*, vol. 8, no. 4, pp. 683–690, 1990.

[12] U. Madhow and M. Honig, "Mmse interference suppression for direct-sequence spread-spectrum cdma," *IEEE Transactions on Communications*, vol. 42, no. 12, pp. 3178–3188, 1994.

[13] R. Heath and D. Love, "Multimode antenna selection for spatial multiplexing systems with linear receivers," *IEEE Transactions on Signal Processing*, vol. 53, no. 8, pp. 3042–3056, 2005.

[14] L. Liu, R. Chen, S. Geirhofer, K. Sayana, Z. Shi, and Y. Zhou, "Downlink MIMO in LTE-advanced: SU-MIMO vs. MU-MIMO," *IEEE Communications Magazine*, vol. 50, no. 2, pp. 140–147, 2012.

[15] A. Azari, P. Popovski, G. Miao, and C. Stefanovic, "Grant-Free Radio Access for Short-Packet Communications over 5G Networks," in *Proc. IEEE Global Communications Conference*, Dec 2017, pp. 1–7.

[16] D. Ciuonzo, P. S. Rossi, and S. Dey, "Massive MIMO Channel-Aware Decision Fusion," *IEEE Transactions on Signal Processing*, vol. 63, no. 3, pp. 604–619, 2015.

[17] A. Shirazinia, S. Dey, D. Ciuonzo, and P. Salvo Rossi, "Massive MIMO for Decentralized Estimation of a Correlated Source," *IEEE Transactions on Signal Processing*, vol. 64, no. 10, pp. 2499–2512, May 2016.

[18] M. Masoudi, A. Azari, E. A. Yavuz, and C. Cavdar, "Grant-Free Radio Access IoT Networks: Scalability Analysis in Coexistence Scenarios," in *Proc. IEEE Int. Conf on Communications*, May 2018, pp. 1–7.

[19] A. Goldsmith, S. Jafar, N. Jindal, and S. Vishwanath, "Capacity limits of MIMO channels," *IEEE Journal on Selected Areas in Communications*, vol. 21, no. 5, pp. 684–702, 2003.

[20] E. Castañeda, A. Silva, A. Gameiro, and M. Kountouris, "An overview on resource allocation techniques for multi-user MIMO systems," *IEEE Communications Surveys Tutorials*, vol. 19, no. 1, pp. 239–284, 2017.

[21] T. F. Maciel and A. Klein, "On the performance, complexity, and fairness of suboptimal resource allocation for multiuser MIMO–ofdma systems," *IEEE Transactions on Vehicular Technology*, vol. 59, no. 1, pp. 406–419, 2010.

[22] Z. Hong, K. Liu, R. Heath, and A. Sayeed, "Spatial multiplexing in correlated fading via the virtual channel representation," *IEEE Journal on Selected Areas in Communications*, vol. 21, no. 5, pp. 856–866, 2003.

[23] D.-S. Shiu, G. Foschini, M. Gans, and J. Kahn, "Fading correlation and its effect on the capacity of multielement antenna systems," *IEEE Transactions on Communications*, vol. 48, no. 3, pp. 502–513, 2000.

[24] D. Godard, "Self-Recovering Equalization and Carrier Tracking in Two-Dimensional Data Communication Systems," *IEEE Transactions on Communications*, vol. 28, no. 11, pp. 1867–1875, November 1980.

[25] J. Treichler and M. Larimore, "New processing techniques based on the constant modulus adaptive algorithm," *IEEE Transactions on Acoustics, Speech, and Signal Processing*, vol. 33, no. 2, pp. 420–431, 1985.

[26] Z. Ding and Y. G. Li, *Blind Equalization and Identification*. Marcel Dekker, Inc., December 2000.

[27] *Evolved Universal Terrestrial Radio Access (E-UTRA); Multiplexing and channel coding*, 3GPP Tech. Specification TS 36.212 (v13.2.0), 2016.

[28] A. Jalali and Z. Ding, "Joint Detection and Decoding of Polar Coded 5G Control Channels," *IEEE Transactions on Wireless Communications*, vol. 19, no. 3, pp. 2066–2078, 2020.

[29] Ye Li and Zhi Ding, "Global Convergence of Fractionally Spaced Godard Equalizers," in *Proceedings of 1994 28th Asilomar Conference on Signals, Systems and Computers*, vol. 1, Oct 1994, pp. 617–621 vol.1.

[30] I. Fijalkow, C. Manlove, and C. Johnson, "Adaptive Fractionally Spaced Blind CMA Equalization: Excess MSE," *IEEE Transactions on Signal Processing*, vol. 46, no. 1, pp. 227–231, 1998.

[31] W. Chung and J. P. LeBlanc, "The Local Minima of Fractionally-Spaced CMA Blind Equalizer Cost Function in the Presence of Channel Noise," in *Proc. IEEE Int. Conf. on Acoustics, Speech and Signal Processing*, vol. 6. IEEE, 1998, pp. 3345–3348.

[32] H. H. Zeng, L. Tong, and C. R. Johnson, "An Analysis of Constant Modulus Receivers," *IEEE Transactions on Signal Processing*, vol. 47, no. 11, pp. 2990–2999, Nov 1999.

[33] O. Dabeer and E. Masry, "Convergence Analysis of the Constant Modulus Algorithm," *IEEE Transactions on Information Theory*, vol. 49, no. 6, pp. 1447–1464, June 2003.

[34] B. Mariere, Z.-Q. T. Luo, and T. N. Davidson, "Blind Constant Modulus Equalization via Convex Optimization," *IEEE Trans. Signal Processing*, vol. 51, pp. 805–818, 2003.

[35] Z. Luo, W. Ma, A. M. So, Y. Ye, and S. Zhang, "Semidefinite Relaxation of Quadratic Optimization Problems," *IEEE Signal Processing Magazine*, vol. 27, no. 3, pp. 20–34, May 2010.

[36] K. Wang, "Semidefinite Relaxation Based Blind Equalization using Constant Modulus Criterion," August 2018. [Online]. Available: arXiv:1808.07232v2[cs.IT]

[37] A. Adler and M. Wax, "Constant Modulus Algorithms via Low-Rank Approximation," *Signal Processing*, vol. 160, pp. 263 – 270, 2019. [Online]. Available: http://www.sciencedirect.com/science/article/pii/S0165168419300568

[38] B. Hassibi, A. Paulraj, and T. Kailath, "On a Closed Form Solution to the Constant Modulus Factorization Problem," in *Proc. 28th Asilomar Conf. on Signals, Systems and Computers*, vol. 2, Oct 1994, pp. 775–779.

[39] A.-J. van der Veen and A. Paulraj, "An Analytical Constant Modulus Algorithm," *IEEE Trans. on Signal Processing*, vol. 44, no. 5, pp. 1136–1155, May 1996.

[40] A.-J. van der Veen, "An Adaptive Version of the Algebraic Constant Modulus Algorithm [Blind Source Separation Applications]," in *Proc. IEEE Intl. Conf. on Acoustics, Speech, and Signal Processing*, vol. 4, March 2005, pp. iv/873–iv/876 Vol. 4.

[41] V. Zarzoso and P. Comon, "Optimal Step-Size Constant Modulus Algorithm," *IEEE Trans. Communications*, vol. 56, no. 1, pp. 10–13, Jan. 2008.

[42] J. J. Shynk and R. P. Gooch, "Performance Analysis of the Multistage CMA Adaptive Beamformer," in *Proceedings of MILCOM '94*, Oct 1994, pp. 316–320 vol.2.

[43] D. Liu and L. Tong, "An Analysis of Constant Modulus Algorithm for Array Signal Processing," *Signal Processing*, vol. 73, no. 1, pp. 81 – 104, 1999. [Online]. Available: http://www.sciencedirect.com/science/article/pii/S0165168498001868

[44] A. Bessios and C. Nikias, "Multichannel adaptive blind equalization with CRIMNO-MSE technique," in *MILCOM 92 Conference Record*, 1992, pp. 236–240 vol.1.

[45] Ye Li and K. J. R. Liu, "Adaptive Blind Source Separation and Equalization for Multiple-Input/Multiple-Output Systems," *IEEE Transactions on Information Theory*, vol. 44, no. 7, pp. 2864–2876, Nov 1998.

[46] A. Ikhlef and D. Le Guennec, "A Simplified Constant Modulus Algorithm for Blind Recovery of MIMO QAM and PSK Signals: A Criterion with Convergence Analysis," *EURASIP Journal on Wireless Communications and Networking*, vol. 56, no. 6, December 2007. [Online]. Available: https://doi.org/10.1155/2007/90401

[47] T. Nguyen and Z. Ding, "Cma beamforming for multipath correlated sources," in *1997 IEEE International Conference on Acoustics, Speech, and Signal Processing*, vol. 3, 1997, pp. 2521–2524 vol.3.

[48] E. J. Candès, X. Li, and M. Soltanolkotabi, "Phase Retrieval via Wirtinger Flow: Theory and Algorithms," *IEEE Transactions on Information Theory*, vol. 61, no. 4, pp. 1985–2007, April 2015.

[49] ——, "Phase Retrieval from Masked Fourier Transforms," October 2013. [Online]. Available: arXiv:1310.3240v2[cs.IT]

[50] R. H. Keshavan, A. Montanari, and S. Oh, "Matrix Completion from a Few Entries," *IEEE Trans. Inf. Theor.*, vol. 56, no. 6, pp. 2980–2998, Jun. 2010. [Online]. Available: http://dx.doi.org/10.1109/TIT.2010.2046205

[51] K. Yang, Y. Shi, and Z. Ding, "Low-Rank Matrix Completion for Mobile Edge Caching in Fog-RAN via Riemannian Optimization," in *2016 IEEE Global Communications Conference*, Dec 2016, pp. 1–6.

[52] J. Dong and Y. Shi, "Nonconvex Demixing From Bilinear Measurements," *IEEE Transactions on Signal Processing*, vol. 66, no. 19, pp. 5152–5166, Oct 2018.

[53] P.-A. Absil, R. Mahony, and R. Sepulchre, *Optimization Algorithms on Matrix Manifolds*. Princeton, NJ, USA: Princeton University Press, 2008.

[54] H. Sato, "Riemannian conjugate gradient method for complex singular value decomposition problem," in *53rd IEEE Conference on Decision and Control*, 2014, pp. 5849–5854.

[55] W. Huang, K. A. Gallivan, and X. Zhang, "Solving phaselift by low-rank riemannian optimization methods1," *Procedia Computer Science*, vol. 80, pp. 1125 – 1134, 2016, international Conference on Computational Science 2016, ICCS 2016, 6-8 June 2016, San Diego, California, USA.

[56] J. Dong, K. Yang, and Y. Shi, "Blind Demixing for Low-Latency Communication," *IEEE Transactions on Wireless Communications*, vol. 18, no. 2, pp. 897–911, Feb 2019.

[57] A. Cherian and S. Sra, "Riemannian dictionary learning and sparse coding for positive definite matrices," 2015.

[58] J. Sun, Q. Qu, and J. Wright, "Complete dictionary recovery over the sphere ii: Recovery by riemannian trust-region method," *IEEE Transactions on Information Theory*, vol. 63, no. 2, pp. 885–914, 2017.

[59] D. Tse and P. Viswanath, *Fundamentals of Wireless Communication*. Cambridge Univ. Press, 2005.

[60] E. Björnson and E. Jorswieck, "Optimal Resource Allocation in Coordinated Multi-Cell Systems," *Foundations and Trends® in Communications and Information Theory*, vol. 9, no. 2-3, pp. 113–381, 2013.

[61] T. Lo, "Maximum ratio transmission," *IEEE Transactions on Communications*, vol. 47, no. 10, pp. 1458–1461, 1999.

[62] N. Jindal, "MIMO Broadcast Channels With Finite-Rate Feedback," *IEEE Transactions on Information Theory*, vol. 52, no. 11, pp. 5045–5060, 2006.

[63] X. Chen, H. Hu, H. Wang, H.-h. Chen, and M. Guizani, "Double proportional fair user pairing algorithm for uplink virtual MIMO systems," *IEEE Transactions on Wireless Communications*, vol. 7, no. 7, pp. 2425–2429, 2008.

[64] H.-W. Chang and L.-C. Wang, "A low-complexity uplink multiuser scheduling for virtual MIMO systems," *IEEE Transactions on Vehicular Technology*, vol. 65, no. 1, pp. 463–466, 2016.

[65] S. Wang, F. Wang, Y. Wang, and D. Yang, "A novel scheduling scheme based on MU-MIMO in TD-LTE uplink," in *2011 IEEE Wireless Communications and Networking Conference, WCNC 2011, Proceedings, Cancun, Mexico, 28-31 March, 2011*. IEEE, 2011, pp. 915–919.

[66] Y. J. Zhang and K. Letaief, "An efficient resource-allocation scheme for spatial multiuser access in MIMO/OFDM systems," *IEEE Transactions on Communications*, vol. 53, no. 1, pp. 107–116, 2005.

[67] B. Kim, W. Chung, S. Lim, S. Suh, J. Kwun, S. Choi, and D. Hong, "Uplink NOMA with multi-antenna," in *2015 IEEE 81st Vehicular Technology Conference (VTC Spring)*, 2015, pp. 1–5.

[68] D. Kudathanthirige and G. A. A. Baduge, "NOMA-aided multicell downlink massive MIMO," *IEEE Journal of Selected Topics in Signal Processing*, vol. 13, no. 3, pp. 612–627, 2019.

[69] S. C. R. Gaddam, D. Kudathanthirige, and G. Amarasuriya, "Achievable rate analysis for NOMA-aided massive MIMO uplink," in *2019 IEEE International Conference on Communications (ICC)*, 2019, pp. 1–7.

[70] C. Jiang, H. Zhang, Y. Ren, Z. Han, K.-C. Chen, and L. Hanzo, "Machine learning paradigms for next-generation wireless networks," *IEEE Wireless Communications*, vol. 24, no. 2, pp. 98–105, 2017.

[71] M. E. Morocho-Cayamcela, H. Lee, and W. Lim, "Machine Learning for 5G/B5G Mobile and Wireless Communications: Potential, Limitations, and Future Directions," *IEEE Access*, vol. 7, pp. 137 184–137 206, 2019.

[72] Y. Xu, G. Yue, and S. Mao, "User grouping for massive MIMO in FDD systems: New design methods and analysis," *IEEE Access*, vol. 2, pp. 947–959, 2014.

[73] J. Cui, Z. Ding, P. Fan, and N. Al-Dhahir, "Unsupervised machine learning-based user clustering in millimeter-wave-NOMA systems," *IEEE Transactions on Wireless Communications*, vol. 17, no. 11, pp. 7425–7440, 2018.

[74] C. Feres and Z. Ding, " Wirtinger Flow Meets Constant Modulus Algorithm: Revisiting Signal Recovery for Grant-Free Access," *IEEE Transactions on Signal Processing*, pp. 1–1, 2021.

[75] Y. Chen, C. Nikias, and J. G. Proakis, "CRIMNO: Criterion with Memory Nonlinearity for Blind Equalization," in *Proc. 25th Asilomar Conf. on Signals, Systems Computers*, Nov 1991, pp. 694–698.

[76] Y. Chen and E. Candes, "Solving Random Quadratic Systems of Equations Is Nearly as Easy as Solving Linear Systems," in *Advances in Neural Information Processing Systems 28*, C. C. et al., Ed. Curran Associates, Inc., 2015, pp. 739–747.

[77] H. Zhang, Y. Liang, and Y. Chi, "A Nonconvex Approach for Phase Retrieval: Reshaped Wirtinger Flow and Incremental Algorithms," *Journal of Machine Learning Research*, vol. 18, no. 141, pp. 1–35, 2017.

[78] E. Bostan, M. Soltanolkotabi, D. Ren, and L. Waller, "Accelerated Wirtinger Flow for Multiplexed Fourier Ptychographic Microscopy," *Proc. 25th IEEE Int. Conf. on Image Processing*, pp. 3823–3827, 2018.

[79] J. Dong, Y. Shi, and Z. Ding, "Blind Over-the-Air Computation and Data Fusion via Provable Wirtinger Flow," *IEEE Transactions on Signal Processing*, vol. 68, pp. 1136–1151, 2020.

[80] K. Kreutz-Delgado, "The Complex Gradient Operator and the CR-Calculus," June 2009. [Online]. Available: arXiv:0906.4835v1[math.OC]

[81] L. Armijo, "Minimization of Functions having Lipschitz Continuous First Partial Derivatives," *Pacific J. Math.*, vol. 16, no. 1, pp. 1–3, 1966.

[82] D. L. Jones, "A Normalized Constant-Modulus Algorithm," in *Conference Record of The Twenty-Ninth Asilomar Conference on Signals, Systems and Computers*, vol. 1, Oct 1995, pp. 694–697 vol.1.

[83] O. Tanrikulu, A. G. Constantinides, and J. A. Chambers, "New Normalized Constant Modulus Algorithms with Relaxation," *IEEE Signal Processing Letters*, vol. 4, no. 9, pp. 256–258, Sep. 1997.

[84] K. Dogancay and O. Tanrikulu, "Normalised Constant Modulus Algorithm with Selective Partial Updates," in *2001 IEEE International Conference on Acoustics, Speech, and Signal Processing. Proceedings (Cat. No.01CH37221)*, vol. 4, May 2001, pp. 2181–2184 vol.4.

[85] Y. M. Lu and G. Li, "Spectral Initialization for Nonconvex Estimation: High-Dimensional Limit and Phase Transitions," in *Proc. IEEE Int. Symp. on Information Theory*, June 2017, pp. 3015–3019.

[86] H. H. Zeng, L. Tong, and C. R. Johnson, "An Analysis of Constant Modulus Receivers," *IEEE Transactions on Signal Processing*, vol. 47, no. 11, pp. 2990–2999, 1999.

[87] H. Akaike, "A New Look at the Statistical Model Identification," *IEEE Transactions on Automatic Control*, vol. 19, no. 6, pp. 716–723, 1974.

[88] M. Wax and T. Kailath, "Detection of Signals by Information Theoretic Criteria," *IEEE Transactions on Acoustics, Speech, and Signal Processing*, vol. 33, no. 2, pp. 387–392, 1985.

[89] B. Gao, H. Liu, and Y. Wang, "Phase retrieval for sub-Gaussian measurements," *Applied and Computational Harmonic Analysis*, vol. 53, pp. 95–115, 2021.

[90] R. Vershynin, "Introduction to the Non-Asymptotic Analysis of Random Matrices," in *Compressed Sensing: Theory and Applications*, Y. C. Eldar and G. Kutyniok, Eds. Cambridge University Press, 2012, ch. 5, pp. 210–268.

[91] ——, *High-Dimensional Probability: An Introduction with Applications in Data Science*, ser. Cambridge Series in Statistical and Probabilistic Mathematics. Cambridge University Press, September 2018.

[92] T. P. Minka, "Automatic choice of dimensionality for PCA," M.I.T. Media Laboratory, Cambridge, MA, Tech. Rep. 504, December 2000, (revised Sept. 2008).

[93] A. Edelman, T. A. Arias, and S. T. Smith, "The geometry of algorithms with orthogonality constraints," *SIAM J. Matrix Anal. Appl.*, vol. 20, no. 2, p. 303–353, Apr. 1999.

[94] R. Vidal, Y. Ma, and S. S. Sastry, *Generalized Principal Component Analysis*, 1st ed. Springer Publishing Company, Incorporated, 2016.

[95] N. Boumal, "An introduction to optimization on smooth manifolds," Available online, Nov 2020. [Online]. Available: http://www.nicolasboumal.net/book

[96] T. A. Palka and R. J. Vaccaro, "Asymptotically efficient estimators for multidimensional harmonic retrieval based on the geometry of the Stiefel manifold," in *2015 49th Asilomar Conference on Signals, Systems and Computers*, 2015, pp. 1691–1695.

[97] P. A. Absil, C. G. Baker, and K. A. Gallivan, "Trust-Region Methods on Riemannian Manifolds," *Found. Comput. Math.*, vol. 7, no. 3, pp. 303–330, Jul. 2007. [Online]. Available: https://doi.org/10.1007/s10208-005-0179-9

[98] N. Boumal, B. Mishra, P.-A. Absil, and R. Sepulchre, "Manopt, a Matlab Toolbox for Optimization on Manifolds," *Journal of Machine Learning Research*, vol. 15, pp. 1455–1459, 2014. [Online]. Available: http://jmlr.org/papers/v15/boumal14a.html

[99] Z. Ding, R. Kennedy, B. Anderson, and C. Johnson, "Ill-convergence of godard blind equalizers in data communication systems," *IEEE Transactions on Communications*, vol. 39, no. 9, pp. 1313–1327, 1991.

[100] K. Kreutz-Delgado and Y. Isukapalli, "Use of the Newton Method for Blind Adaptive Equalization Based on the Constant Modulus Algorithm," *IEEE Transactions on Signal Processing*, vol. 56, no. 8, pp. 3983–3995, Aug 2008.

[101] S. Mayrargue, "A Blind Spatio-temporal Equalizer for a Radio-mobile Channel Using the Constant Modulus Algorithm (CMA)," in *Proceedings of ICASSP '94. IEEE International Conference on Acoustics, Speech and Signal Processing*, vol. iii, April 1994, pp. III/317–III/320 vol.3.

[102] H. H. Zeng, L. Tong, and C. R. Johnson, "Relationships between the constant modulus and wiener receivers," *IEEE Transactions on Information Theory*, vol. 44, no. 4, pp. 1523–1538, 1998.

[103] H. H. Zeng, L. Tong, and C. Johnson, "An analysis of constant modulus receivers," *IEEE transactions on Signal Processing*, vol. 47, no. 11, pp. 2990–2999, 1999.

[104] C. Feres and Z. Ding, "Wirtinger Flow Meets Constant Modulus Algorithm: Revisiting Signal Recovery for Grant-Free Access," *IEEE Transactions on Signal Processing*, p. Accepted, 2020.

[105] F. J. Theis, T. P. Cason, and P. A. Absil, "Soft dimension reduction for ica by joint diagonalization on the stiefel manifold," in *Independent Component Analysis and Signal Separation*, T. Adali, C. Jutten, J. M. T. Romano, and A. K. Barros, Eds. Springer Berlin Heidelberg, 2009, pp. 354–361.

[106] T. Bendory, Y. C. Eldar, and N. Boumal, "Non-convex phase retrieval from stft measurements," *IEEE Transactions on Information Theory*, vol. 64, no. 1, pp. 467–484, 2018.

[107] M. Costa, "Writing on dirty paper (corresp.)," *IEEE Transactions on Information Theory*, vol. 29, no. 3, pp. 439–441, 1983.

[108] R. Mo and Y. H. Chew, "MMSE-based joint source and relay precoding design for amplify-and-forward MIMO relay networks," *IEEE Transactions on Wireless Communications*, vol. 8, no. 9, pp. 4668–4676, 2009.

[109] K. H. Lee and D. P. Petersen, "Optimal linear coding for vector channels," *IEEE Transactions on Communications*, vol. 24, pp. 1283–1290, Dec. 1976.

[110] H. Sampath, P. Stoica, and A. Paulraj, "Generalized linear precoder and decoder design for MIMO channels using the weighted MMSE criterion," *IEEE Transactions on Communications*, vol. 49, no. 12, pp. 2198–2206, 2001.

[111] A. Scaglione, G. Giannakis, and S. Barbarossa, "Redundant filterbank precoders and equalizers. i. unification and optimal designs," *IEEE Transactions on Signal Processing*, vol. 47, no. 7, pp. 1988–2006, 1999.

[112] D. Palomar, M. Bengtsson, and B. Ottersten, "Minimum BER linear transceivers for MIMO channels via primal decomposition," *IEEE Transactions on Signal Processing*, vol. 53, no. 8, pp. 2866–2882, 2005.

[113] L. Kaufman and P. J. Rousseeuw, *Finding Groups in Data: An Introduction to Cluster Analysis*. New York, NY, USA: Wiley, 1990.

[114] A. Goh and R. Vidal, "Clustering and dimensionality reduction on Riemannian manifolds," in *2008 IEEE Conference on Computer Vision and Pattern Recognition*, 2008, pp. 1–7.

[115] S. Stiverson, M. Kirby, and C. Peterson, "Subspace quantization on the grassmannian," in *Advances in Self-Organizing Maps, Learning Vector Quantization, Clustering and Data Visualization*, A. Vellido, K. Gibert, C. Angulo, and J. D. Martín Guerrero, Eds. Cham: Springer International Publishing, 2020, pp. 251–260.

[116] N. Boumal and P.-A. Absil, "Low-rank matrix completion via preconditioned optimization on the grassmann manifold," *Linear Algebra and its Applications*, vol. 475, pp. 200–239, 2015. [Online]. Available: https://www.sciencedirect.com/science/article/pii/S0024379515001342

[117] M. Usama, J. Qadir, A. Raza, H. Arif, K.-l. A. Yau, Y. Elkhatib, A. Hussain, and A. Al-Fuqaha, "Unsupervised machine learning for networking: Techniques, applications and research challenges," *IEEE Access*, vol. 7, pp. 65 579–65 615, 2019.

[118] D. Xu and Y. Tian, "A comprehensive survey of clustering algorithms," *Annals of Data Science*, vol. 2, pp. 165–193, 2015.

[119] D. Arthur and S. Vassilvitskii, "K-Means++: The Advantages of Careful Seeding," in *Proceedings of the Eighteenth Annual ACM-SIAM Symposium on Discrete Algorithms*, ser. SODA '07. USA: Society for Industrial and Applied Mathematics, 2007, p. 1027–1035.

[120] N. Jindal and A. Goldsmith, "Dirty-paper coding versus tdma for mimo broadcast channels," *IEEE Transactions on Information Theory*, vol. 51, no. 5, pp. 1783–1794, 2005.

[121] M. J. Zaki and W. M. Jr, *Data Mining and Analysis: Fundamental Concepts and Algorithms*. New York, NY, USA: Cambridge Univ. Press, 2014.

[122] R. Tibshirani, G. Walther, and T. Hastie, "Estimating the number of clusters in a data set via the gap statistic," *Journal of the Royal Statistical Society Series B*, vol. 63, no. 2, pp. 411–423, 2001.

[123] P. J. Rousseeuw, "Silhouettes: A graphical aid to the interpretation and validation of cluster analysis," *Journal of Computational and Applied Mathematics*, vol. 20, pp. 53–65, 1987.

[124] W. J. Krzanowski and Y. T. Lai, "A criterion for determining the number of groups in a data set using sum-of-squares clustering," *Biometrics*, vol. 44, no. 1, pp. 23–34, 1988.

[125] J. A. Hartigan, *Clustering Algorithms*. New York, NY, USA: John Wiley & Sons, 1975.

[126] H. Zhang, Y. Chi, and Y. Liang, "Provable Non-convex Phase Retrieval with Outliers: Median truncated Wirtinger Flow," in *33rd International Conference on Machine Learning, ICML 2016*, vol. 3. International Machine Learning Society (IMLS), 2016, pp. 1607–1627.

[127] T. T. Cai, X. Li, and Z. Ma, "Optimal Rates of Convergence for Noisy Sparse Phase Retrieval via Thresholded Wirtinger Flow," *Ann. Statist.*, vol. 44, no. 5, pp. 2221–2251, 10 2016. [Online]. Available: https://doi.org/10.1214/16-AOS1443

[128] M. B. Lazreg and R. Amara, "A Robust Sparse Wirtinger Flow Algorithm with Optimal Stepsize for Sparse Phase Retrieval," in *2018 15th International Multi-Conference on Systems, Signals Devices (SSD)*, March 2018, pp. 1–6.

[129] A. Benveniste, M. Goursat, and G. Ruget, "Robust Identification of a Nonminimum Phase System: Blind Adjustment of a Linear Equalizer in Data Communications," *IEEE Transactions on Automatic Control*, vol. 25, no. 3, pp. 385–399, June 1980.

[130] Y. Sato, "A Method of Self-Recovering Equalization for Multilevel Amplitude-Modulation Systems," *IEEE Transactions on Communications*, vol. 23, no. 6, pp. 679–682, June 1975.

[131] O. Shalvi and E. Weinstein, "New Criteria for Blind Deconvolution of Nonminimum Phase Systems (Channels)," *IEEE Transactions on Information Theory*, vol. 36, no. 2, pp. 312–321, March 1990.

[132] A. Kovnatsky, K. Glashoff, and M. M. Bronstein, "MADMM: A Generic Algorithm for Non-smooth Optimization on Manifolds," in *Computer Vision – ECCV 2016*, B. Leibe, J. Matas, N. Sebe, and M. Welling, Eds. Cham: Springer International Publishing, 2016, pp. 680–696.

[133] P.-A. Absil and S. Hosseini, *A Collection of Nonsmooth Riemannian Optimization Problems*. Cham: Springer International Publishing, 2019, pp. 1–15. [Online]. Available: https://doi.org/10.1007/978-3-030-11370-4_1

[134] G. H. Golub and C. F. Van Loan, *Matrix Computations*, 4th ed. The Johns Hopkins University Press, 2013.